

Molecular fossils as a tool for investigating Quaternary sea-level change in sediments

Martina Conti

PhD

University of York

Chemistry

February 2020

Abstract

Climate fluctuations affect environment and sea levels, understanding the drivers of past sea levels is key for predicting future scenarios. Studies of sea-level change are carried out conventionally by microfossil analyses, but these can occur in low numbers. In this work, Quaternary transgressions and palaeoenvironmental changes were studied using molecular fossils.

The widely used glycerol dialkyl glycerol tetraether (GDGTs) biomarkers can occur in sediments in trace amounts. To enhance their detection limits, lipids were derivatised with fluorescent groups. High yields were recorded for derivatisation of lipid standards but, surprisingly, derivatisation of GDGT samples from sediments indicated lower MS response than for the native lipids. Thus, GDGTs were analysed as native compounds.

Interpretation of the molecular fossil distributions from transgressions in a well-constrained Holocene core (Loch of Stenness, Orkney) and in five Middle Pleistocene cores (East Anglia) enabled corroboration of earlier results and recognition of characteristics that were not evident from microfossils. In the Loch of Stenness, these included the earlier detection of the onset and cessation of the transgression, the redox conditions of the water column, and the shift in vegetation from forest to grassland. Six different type distributions were recognised among the molecular fossils of four cores from the Nar Valley (Norfolk). The timing of the transgression was refined, marine influence was proposed for the first time in one core, and vegetation of the hinterland was reconstructed. The overall similarity in the types of molecular fossil distributions in the East Anglian cores may indicate that they were deposited under similar environmental conditions. Novel glycerol monoalkanediol diether (GMD) lipids with straight alkyl chains and methyl branches were identified from aquatic, marine and terrestrial sediments discussed here.

Molecular fossils have been shown to provide useful additional data on Quaternary sea-level change and it is recommended that they become an integral part of sea-level studies.

Table of contents

Abstract	2
Table of contents	3
List of tables	10
List of figures	13
Acknowledgments.....	24
Author's declaration	26
1. Introduction	27
1.1. Causes of sea-level change	28
1.2. Marine transgressions and regressions	31
1.3. Indicators of sea-level change	31
1.3.1. Lithological and regional features.....	31
1.3.2. Palaeontological evidence	32
1.3.3. Stable oxygen isotope evidence.....	34
1.3.4. Markers of changes of organic matter source	35
1.3.4.1 $\delta^{13}\text{C}$	35
1.3.4.2. Carbon and nitrogen ratio (C/N).....	36
1.4. Molecular fossils	37
1.4.1. Markers of aquatic production	37
1.4.2. Markers of marine organic matter.....	42
1.4.3. Markers of terrestrial organic matter	44
1.4.4. Proxies based on molecular fossils	46
1.4.4.1. CPI for fresh terrestrial and reworking / algal OM based on <i>n</i> -alkanes	46
1.4.4.2. P_{aq} to distinguish terrestrial and macrophyte OM based on <i>n</i> -alkanes.....	46
1.4.4.3. ACL index for inputs of plant OM.....	46
1.4.4.4. BIT index for discerning terrestrial and marine OM (brGDGTs and crenarchaeol)	47
1.4.4.5. TEX_{86} and $\text{TEX}_{86}^{\text{L}}$ for calculating sea-surface temperature based on iGDGTs	47

1.4.4.6. CBT index for soil pH and MBT index for mean annual air temperature based on brGDGTs	49
1.4.4.7. U_{37}^k and U_{37}^k sea-surface temperatures based on long chain alkenones	51
1.4.4.8. Proxies for pH and temperature based on 3-hydroxylated fatty acids	52
1.4.4.9. Diol index to distinguish freshwater and marine OM.....	53
1.4.4.10. Surface water temperature calculated with heterocyst glycolipids (HG).....	54
1.4.5. Analysis of molecular fossils	55
1.4.5.1. Analysis of steranes, sterols and alkan-es, -als, -ones, -ols, -oic acids, long chain diols, 3-OH fatty acids	55
1.4.5.2. Analysis of GDGTs and HG	55
1.4.5.3. Analysis of pigments	55
1.5. Transformation of molecular fossils in the natural environment.....	57
1.6. Molecular fossil applications to study sea-level change.....	62
1.7. Summary and aims.....	64
2. Application of a modified Steglich esterification to alcohol lipid standards and glycerol dialkyl glycerol tetraether (GDGT) lipids from sediments	65
2.1. Introduction	66
2.1.1. Potential application of Steglich esterification to glycerol dialkyl glycerol tetraether lipids (GDGT) from sediments.....	67
2.1.1.1. Steglich esterification.....	67
2.1.1.2. Use of microwaves to enhance rates of chemical reactions	70
2.1.2. Aims.....	71
2.2. Results and discussion	72
2.2.1. Derivatisation of standard alcohols 1,12-dodecanediol, 1-octadecanol and cholesterol with Fmoc-Gly and 1-octadecanol with Fmoc-Lys(Boc).....	72
2.2.1.1. Esterification of cholesterol with Fmoc-Gly.....	72
2.2.1.2. Esterification of 1-octadecanol with Fmoc-Gly.....	74
2.2.1.3. Esterification of 1-octadecanol with Fmoc-Lys(Boc).....	76
2.2.1.4. Esterification of 1,12-dodecanediol with Fmoc-Gly.....	77

2.2.2. HPLC-FLD and HPLC-UV quantification	82
2.2.3. Derivatisation of 1-octadecanol with Fmoc-Lys(Boc) with microwave irradiation.....	83
2.2.4. Evaluation of Fmoc-Lys(Boc)-1-octadecanol (FLB-o) HPLC-UV and HPLC-FLD yields of multiple derivatives in a plastic rack and a beaker	87
2.2.5. Derivatisation of GDGTs from sediments with Fmoc-Lys(Boc)	90
2.3. Conclusions	98
3. Molecular fossils as a tool for tracking Holocene sea-level change in the Loch of Stenness, Orkney.....	100
3.1. Introduction	101
3.1.1. Molecular fossils inferring sea-level changes	102
3.1.2. Aims.....	105
3.2. Materials and methods	108
3.2.1. Site description	108
3.2.2. Previous studies of the Loch of Stenness core 2014-1 (Bates <i>et al.</i> , 2016)	108
3.2.3. Separation of mollusc shells	110
3.2.4. Extraction and analysis of molecular fossils	110
3.3. Results and discussion	110
3.3.1. The freshwater lake (200-104 cm)	111
3.3.2. The marine transgression (102-81 cm)	113
3.3.3. The established brackish loch (80-0 cm).....	114
3.3.4. Signatures of terrestrial vegetation as markers of changing environment	117
3.3.5. Water temperature and pH from GDGT-based indices	120
3.3.6. Contextualising the transgression.....	121
3.4. Conclusions	123
4. Pleistocene transgression in East Anglia: the Nar Valley (Norfolk) and Woodston (Cambridgeshire)	124
4.1. Introduction	125
4.1.1. Geology of the Nar Valley Pleistocene deposits	126

4.1.2. Uncertainty in age of the Nar Valley Pleistocene deposits.....	126
4.1.3. Aims.....	127
4.2. Site description and previous work on the Nar Valley.....	128
4.2.1. Lithology of Nar Valley cores	128
4.2.2. Loss-on-ignition.....	129
4.2.3. Foraminifera.....	133
4.2.4. Pollen	134
4.2.5. AAR dating.....	135
4.2.6. Change in sea level.....	135
4.3. Materials and methods.....	136
4.4. Results and discussion	136
4.4.1. Molecular fossils common in all Nar Valley cores.....	139
4.4.2. Molecular distribution type A.....	141
4.4.3. Molecular distribution type B	146
4.4.4. Molecular distribution type C	151
4.4.5. Molecular distribution type D.....	152
4.4.6. Molecular distribution type E	154
4.4.7. Molecular distribution type F	159
4.4.8. Reconstructed soil pH and sea-surface temperatures.....	160
4.4.9. Summary of the Nar Valley palaeoenvironment	162
4.4.10. Transgression at Woodston	169
4.4.10.1. Previous work on Woodston core HiB 12-6.....	169
4.4.10.2. Molecular fossils at Woodston	170
4.5. Conclusions	175
5. Unknown glycerolipid structures found in sediments.....	176
5.1. Introduction	177
5.1.1. Aims.....	178
5.2. Materials and methods.....	179

5.3. Results and discussion	179
5.3.1. Elucidation of structures by HPLC-MS and HPLC-MS/MS	179
5.3.2. Distribution of GMD lipids in sediments	184
5.4. Conclusions	190
6. Conclusions and future work	191
6.1. Overall summary and conclusions	192
6.1.1. Optimisation of detection of glycerol dialkyl glycerol tetraether	192
6.1.2. Molecular fossils to study Quaternary transgressions	193
6.1.3. Structure and occurrence of unknown glycerolipids in sediments	194
6.2. Future work	195
7. Experimental and analytical procedures	197
7.1. General procedures	198
7.1.1. Solvents and reagents	198
7.1.2. Glassware	198
7.1.3. Sample collection	198
7.1.4. Sample storage and handling	199
7.1.5. Separation of shells	199
7.2. Extraction and isolation of organic compounds from sediments	199
7.2.1. Extraction of sediment	199
7.2.2. Preparation of diazomethane to methylate pigments	200
7.2.3. Fractionation of the lipid extracts	200
7.2.4. Methylation and silylation of polar fractions	200
7.2.5. Fractionation of GDGTs prior to acetylation	201
7.2.6. Acetylation of glycerolipids	201
7.3. Steglich esterification of lipids	201
7.3.1. Derivatisation and fractionation of alcohol standards 1,12-dodecanediol, 1-octadecanol and cholesterol with Fmoc-Gly and Fmoc-Lys(Boc)	201
7.3.2. Derivatisation of 1-octadecanol with Fmoc-Lys(Boc) by microwave	202

7.3.3. Steglich esterification of GDGTs.....	202
7.4. Analysis	202
7.4.1. Gas chromatography flame ionisation detection (GC-FID) of lipid fractions.....	202
7.4.2. Gas chromatography-mass spectrometry (GC-MS) of lipid fractions.....	203
7.4.3. Normal phase (NP) high-performance liquid chromatography (HPLC) of native GDGT lipid cores.....	203
7.4.4. Ultra-high performance liquid chromatography-diode array detector (UHPLC-DAD) of chlorophyll pigments	204
7.4.5. Reversed-phase (RP) high-performance liquid chromatography with ultraviolet detector (HPLC-UV) and HPLC with fluorescence detector (FLD) method for scanning of derivatised standard lipids.....	204
7.4.6. RP-HPLC-UV and HPLC-FLD analysis of native and derivatised GDGT lipids	205
7.4.7. Fraction collection of native GDGT lipids.....	205
7.4.8. RP-HPLC of acetylated glycerolipids	206
7.4.9. Atmospheric pressure chemical ionisation mass spectrometry (APCI-MS) detection of chlorophyll pigments	206
7.4.10 APCI-MS detection of derivatised lipid standards and derivatised GDGT lipids.....	206
7.4.11. APCI-MS detection of native and acetylated GDGT lipids	207
7.4.12. Tandem MS of native and derivatised lipids.....	207
7.5. Standard preparation and calculations.....	207
7.5.1. Standard pigments.....	207
7.5.2. Standard <i>n</i> -alkanes	209
Appendices	211
Appendix 1. Definitions of terms and additional information relevant to their application in this work	212
Appendix 2. Marine isotope stages and substages of the last 1.05 million years	228
Appendix 3. Appendices to Chapter 3	229
Appendix 4. Appendices to Chapter 4	233

Appendix 4.1. Chromatogram and table of peaks of chlorophyll pigments from Horse Fen 13-1	233
Appendix 4.2. Chromatogram and table of peaks of chlorophyll pigments from Railway Cottage.....	237
Appendix 4.3. Chromatogram and table of peaks of chlorophyll pigments from Tottenhill Quarry	242
Appendix 4.4. Chromatogram and table of peaks of chlorophyll pigments from Blackborough Quarry	246
Appendix 4.5. Chromatogram and table of peaks of chlorophyll pigments from Woodston HiB 12-6	250
Appendix 4.6. Chromatogram of an aromatic hydrocarbon fraction showing long chain alkenones.....	254
Appendix 5. GC-MS analysis of lipids and interpretation of data	254
Appendix 6. UHPLC-DAD and UHPLC-DAD-MS analysis of pigments and interpretation of data	254
Appendix 7. HPLC-MS analysis of GDGTs native lipids and interpretation of data	255
Appendix 8. HPLC-MS analysis of derivatised lipids and interpretation of data	255
Appendix 9. Appendix of structures	256
Abbreviations:	256
G: Glycerol dialkyl glycerol tetraether lipids (GDGTs).....	257
L: Lipid standards	260
A: Alkanes, alkanones, alkenones, alkanals, alkanoic acids, alkanols.....	261
T: Terpenoids	263
C: Chlorophyll pigments.....	267
B: Bacteriochlorophylls, bacterioviridin pigments.....	271
R: Carotenoids.....	273
Abbreviations	274
References.....	277

List of tables

Table 1.1. Summary of chemical derivatisation and analytical techniques to analyse the molecular fossils described in this section.....	57
Table 2.1. Percentage, mean and 1 standard deviation of HPLC-UV and HPLC-FLD yields for the three replicates of Fmoc-Lys(Boc)-1-octadecanol derivatives.	88
Table 2.2. Mean percentage of HPLC-UV, HPLC-FLD and weighed yields for synthesis of Fmoc-Lys(Boc)-1-octadecanol in a plastic rack and in a beaker.	90
Table 3.1. Proxies developed from biological markers of terrestrial, aquatic and marine organic matter (OM).	106
Table 3.2. Depth ranges of key environmental transitions identified by Bates <i>et al.</i> (2016) in the core from the Loch of Stenness, and the depths subsampled here for molecular fossil analysis.....	111
Table 3.3. CPI, P_{aq} , ACL and BIT indices, TEX_{86}^L values and sea surface temperatures (SST) calculated from TEX_{86}^L , and mean summer lake temperature for the Loch of Stenness sediments.	118
Table 4.1. Summary of the Hoxnian-type pollen assemblages and tentative assignments of Hoxnian stage to the Nar Valley cores (redrawn from Barlow <i>et al.</i> , 2017).	135
Table 4.2. Summary of lithology, foraminifera, pollen and palaeoenvironment of the Nar Valley cores after Barlow <i>et al.</i> (2017).	136
Table 4.3. Summary of the main environmental information for each molecular fossil type defined in this study from the Nar Valley: terrestrial and aquatic lipids, alkenones, BIT, pigments and interpretation of results.....	138
Table 4.4. Elevation, BIT, CPI, P_{aq} and ratio of chlorophylls / carotenoids of samples with molecular distributions of type A.	141
Table 4.5. Elevation, BIT, CPI, P_{aq} and ratio of chlorophylls / carotenoids of samples with molecular distributions of type B.....	149
Table 4.6. Elevation, BIT, CPI, P_{aq} and ratio of chlorophylls / carotenoids of samples with molecular distributions of type C.....	152

Table 4.7. Elevation, BIT, CPI, P_{aq} and ratio of chlorophylls / carotenoids of samples with molecular distributions of type D.	153
Table 4.8. Elevation, BIT, CPI, P_{aq} and ratio of chlorophylls / carotenoids of samples with molecular distributions of type E.	157
Table 4.9. Elevation, BIT, CPI, P_{aq} and ratio of chlorophylls / carotenoids of samples with molecular distributions of type F.	159
Table 4.10. Reconstructed sea-surface temperatures from TEX_{86} , TEX_{86}^L and $U^{k'}_{37}$ (calibration from Prahl and Wakeham, 1987) proxies and BIT values in the Nar Valley cores. BQ = Blackborough Quarry, TQ = Tottenhill Quarry, HF = Horse Fen, RC = Railway Cottage. Blank spaces indicate that key components were absent or were below the LOQ >10. Colours indicate: transgression, marine environment.	162
Table 4.11. Elevation, CPI, P_{aq} , BIT, ratio of chlorophylls and carotenoids, soil pH from CBT and SST from TEX_{86} and TEX_{86}^L for the Woodston core.	174
Table 5.1. Correlations between GMDs vs brGDGTs and GMDs vs iGDGTs in all the cores analysed in this work for all the samples in the core and after separation of samples depending on terrestrial / aquatic or marine / brackish environment.	189
Table 7.1. Coordinates of cores discussed in the thesis.	199
Table 7.2. UHPLC-DAD solvent gradient for elution of pigments (Saesaengseerung, 2013).	204
Table 7.3. HPLC method A, used for separation of cholesterol and 1,12-dodecanediol derivatives.	205
Table A3.1. Lithological and microfossil analysis from Loch of Stenness (Orkney, Scotland) core 2014-1.	229
Table A3.2. Equations for <i>n</i> -alkane-based proxies CPI P_{aq} and ACL, and GDGT-based proxies BIT, TEX_{86} , TEX_{86}^L , mean summer lake temperature and CBT. Structures of GDGTs discussed in the table are included.	230
Table A4.1. Assignments of pigments and carotenoids in Horse Fen 13-1 sediments (continued over).	234

Table A4.2. Assignments of pigments and carotenoids in Railway Cottage sediments (continued over).....	238
Table A4.3. Assignments of pigments and carotenoids in Tottenhill Quarry sediments (continued over).....	243
Table A4.4. Assignments of pigments and carotenoids in Blackborough Quarry sediments (continued over).	247
Table A4.5. Assignments of pigments and carotenoids in Woodston sediments (continued over).	251
Table A9.1. List of GDGT structure numbers, name of compounds and <i>m/z</i> . For structures, see Figure A9.1.	257
Table A9.2. List of lipid standard structure numbers, name of compounds and <i>m/z</i> . For structures, see Figure A9.2.....	260
Table A9.3. List of alkanes, alkanones, alkenones, alkanals, alkanolic acids, alkanols structure numbers and name of compounds. For structures, see Figure A9.3.....	261
Table A9.4. List of terpenoid structure numbers and name of compounds. For structures, see Figure A9.4.	263
Table A9.5. List of chlorophyll pigment structure numbers and name of compounds. For structures, see Figure A9.5.....	267
Table A9.6. List of bacteriochlorophyll and bacterioviridin pigment structure numbers and name of compounds. For structures, see Figure A9.6.	271
Table A9.7. List of carotenoid structure numbers and name of compounds. For structures, see Figure A9.7.	273

List of figures

Figure 1.1. Glacio-eustasy and its impact on sea-level change. At T1 the growing ice sheet locks seawater as ice resulting in low eustatic sea level (ESL-T1); at T2 the ice sheet is melting thus releasing water and increasing sea level (ESL-T2; from Rovere <i>et al.</i> , 2016).	29
Figure 1.2. a) (dotted line) Approximate maximum extent of the ice sheet over Britain and Ireland between 25 and 23 ka (from Shennan <i>et al.</i> , 2018); b) rate of isostatic change in Great Britain (in mm yr ⁻¹) since 4 ka: positive values indicate land uplift or sea-level fall (in yellow shaded areas) and negative values indicate subsistence or sea-level rise (in blue shaded areas; values in brackets include a correction for changes in tidal range; adapted from Shennan and Horton, 2002).	30
Figure 1.3. Sedimentological evidence of a marine transgression and a regression.	32
Figure 1.4. Generalised structure of sterol with the double bond in red (at C ₅); in stanols the double bond at C ₅ is absent.	38
Figure 1.5. Structure of a branched GDGT: a) intact polar lipid with (red) polar head groups (monohexose); (green) ether group; (orange) alkyl chain; (blue) glycerol group; (pink) methyl branches of brGDGT; b) lipid core with (black) OH groups.	38
Figure 1.6. Structure of isoprenoid GDGT-0.	39
Figure 1.7. Structures of porphyrin, chlorin and bacteriochlorin tetrapyrrole macrocycle.	40
Figure 1.8. Structure of chlorophyll <i>a</i> : (green) tetrapyrrole chlorin macrocycle; (blue) substituents in the periphery of the ring showing the carbon number; (pink) chelating magnesium ion; (red) 5-membered exocyclic ring E.	40
Figure 1.9. Structures of a) β -carotene (hydrocarbon carotenoid) and b) lutein (xanthophyll).	41
Figure 1.10. General structure of heterocyst glycolipid, showing the range of the carbon chain and the possible substituents; here the sugar group is hexose.	42
Figure 1.11. Structure of alkenone C _{37:2} methyl.	43
Figure 1.12. Structures of a) crenarchaeol, b) crenarchaeol regiosomer (after Damsté <i>et al.</i> , 2002), and c) crenarchaeol stereoisomer (after Damsté <i>et al.</i> , 2018).	44

Figure 1.13. Biosynthetic pathway of formation of fatty acids in plant waxes and their microbial decarboxylation to form <i>n</i> -alkanes and reduction to form <i>n</i> -alkanols, <i>n</i> -alkanones and <i>n</i> -alkanals.	45
Figure 1.14. a) General structure of 3-hydroxy fatty acid (3-OH FA) showing the β carbon; b) normal carbon chain; c) iso carbon chain; d) anteiso carbon chain.....	52
Figure 1.15. Structures of 1,15 C ₃₀ and 1,15-C ₃₂ diols.....	53
Figure 1.16. Representation of three sedimentary environments: A) oxic water column with oxic-anoxic transition in the sediment; B) oxic water column with anoxia in the bottom waters; C) oxic surface waters and extensive anoxia in the water column (redrawn from Didyk <i>et al.</i> , 1978).....	59
Figure 1.17. Degradation of chlorophyll <i>a</i> showing the modifications that occur in the early and later stages of diagenesis (adapted from Keely <i>et al.</i> , 1990).	60
Figure 1.18. Degradation of sterols (here cholesterol shown) to stanols (cholestanol) with sterones (cholestanone) as intermediate.	61
Figure 2.1. Mechanism of the Steglich esterification showing the ester product in the red square (Neises and Steglich, 1985).	68
Figure 2.2. Mechanism of transformation of <i>O</i> -acylisourea to <i>N</i> -acylisourea, by-product of the Steglich esterification (Eyley and Thielemans, 2014).	69
Figure 2.3. Esterification reaction of alcohol lipid with Fmoc-Lys(Boc) (Fmoc-lysine(tert-butoxycarbonyl) showing reagents and conditions (Poplawski, 2017).	69
Figure 2.4. Diagram of the working principle of microwave heating (from Vollmer, 2004).....	70
Figure 2.5. The temperature profile of a liquid in a test tube after 60 s affected by (left) microwave irradiation compared to (right) treatment in an oil-bath. Microwave irradiation raises the temperature (in red) of the whole reaction volume simultaneously, whereas in the oil heated tube, the reaction mixture in contact with the vessel wall is heated first (reproduced from Schanche, 2003).	71
Figure 2.6. (Top) HPLC-MS base peak chromatogram (BPC) <i>m/z</i> 220-1000 of Fmoc-Gly-cholesterol; (middle) (+)APCI-MS spectrum of Fmoc-Gly-cholesterol with inset of the protonated molecule and (bottom) structure of derivative showing the main fragment formed.	73

Figure 2.7. (+)APCI-MS ² spectrum of the product ion at <i>m/z</i> 369.2 of Fmoc-Gly-cholesterol.	73
Figure 2.8. (Top) HPLC-MS BPC <i>m/z</i> 220-1000 of Fmoc-Gly-1-octadecanol; (middle) (+)APCI-MS spectrum of Fmoc-Gly-1-octadecanol and (bottom) structure of derivative showing the main fragments formed.	75
Figure 2.9. (+)APCI-MS ² spectrum of the product ions at <i>m/z</i> 328.2, <i>m/z</i> 369.2 and <i>m/z</i> 550.2 of Fmoc-Gly-1-octadecanol.	76
Figure 2.10. (Top) HPLC-MS BPC <i>m/z</i> 220-1000 of Fmoc-Lys(Boc)-1-octadecanol; (middle) (+)APCI-MS spectrum of Fmoc-Lys(Boc)-1-octadecanol and (bottom) structure of derivative showing the main fragment formed.	77
Figure 2.11. HPLC-MS BPC <i>m/z</i> 220-1000 of Fmoc-Gly-1,12-dodecanediol.	78
Figure 2.12. (Top) (+)APCI-MS spectrum of the monoester of the Fmoc-Gly-1,12-dodecanediol derivative and (bottom) structure of derivative showing the main fragments formed.	79
Figure 2.13. (+)APCI-MS ² spectrum of the monoester of Fmoc-Gly-1,12-dodecanediol derivative.	79
Figure 2.14. (Top) (+)APCI-MS spectrum of the diester of Fmoc-Gly-1,12-dodecanediol derivative and (bottom) structure of derivative showing the main fragments formed.	80
Figure 2.15. (+)APCI-MS ² spectrum of the diester of Fmoc-Gly-1,12-dodecanediol derivative.	81
Figure 2.16. Calibration curve of Fmoc-Lys(Boc)-1-octadecanol (FLB-o): (left) concentration vs HPLC-UV area; (right) concentration vs HPLC-FLD area.	83
Figure 2.17. HPLC-FLD and HPLC-UV yields for the microwave synthesis of FLB-o heating for 30 s at increasing temperatures.	84
Figure 2.18. HPLC-FLD yields for the microwave synthesis of FLB-o heating at 80°C for an increasing amount of time. ✖ Indicates signal below limit of detection	85
Figure 2.19. HPLC-FLD yields for the microwave synthesis of FLB-o heating at 100°C (in grey), 90°C (in black) and 60°C (in white) for an increasing amount of time. ✖ Indicates signal below limit of detection.	85

Figure 2.20. HPLC-FLD and HPLC-UV yields for the microwave synthesis of FLB-o heating at varying powers, time and temperatures.	86
Figure 2.21. Grid representing the positions in the plastic rack for derivatisation of 10 samples (red cells).	87
Figure 2.22. Mean HPLC-UV (in blue) and HPLC-FLD (in orange) percentage yields for the esterification product Fmoc-Lys(Boc)-1-octadecanol. The error bars represent one standard deviation, $n = 3$	88
Figure 2.23. Yields by weight, HPLC-UV, HPLC-FLD for the esterification reaction of Fmoc-Lys(Boc) with 1-octadecanol in a plastic rack (in yellow) and in a beaker (in purple). The error bars represent one standard deviation, $n = 5$	89
Figure 2.24. Reversed-phase HPLC-MS of the native GDGTs in the polar lipid fraction from a sample from Loch of Stenness: BPC m/z 1000-1350.	90
Figure 2.25. Reversed-phase HPLC-MS of the Fmoc-Lys(Boc) derivatives of GDGTs in the polar lipid fraction from a sample from Loch of Stenness: a) BPC m/z 1810-2110, b) extracted ion chromatogram (EIC) for FLB-caldarchaeol m/z 2103, c) EIC for FLB-GDGT IIIa m/z 1851, d) EIC for FLB-GDGT IIa m/z 1837, e) EIC for FLB-GDGT Ia m/z 1823. Note: the MS intensity scale is the same for all chromatograms.	91
Figure 2.26. (Top) structure of FLB-Ia and (bottom) structure of FLB-caldarchaeol.	92
Figure 2.27. Reversed-phase HPLC-MS of the native GDGTs in the polar lipid fraction from Willershausen 1.2 m above the fossil band: BPC m/z 1000-1350.	92
Figure 2.28. Reversed-phase HPLC-MS of the Fmoc-Lys(Boc) derivatives of GDGTs in the polar lipid fraction from Willershausen 1.2 m above the fossil band: a) BPC m/z 1810-2110; b) EIC for FLB-caldarchaeol m/z 2103, c) EIC for FLB-crenarchaeol m/z 2093; d) EIC for FLB-IIIa m/z 1851; e) EIC for FLB-IIa m/z 1837; f) EIC for FLB-IIb m/z 1835; g) EIC for FLB-Ia m/z 1823; h) EIC for FLB-Ib m/z 1821. Note: the MS intensity scale is the same for all chromatograms.	93
Figure 2.29. Reversed-phase HPLC analysis of the Fmoc-Lys(Boc) derivatives of GDGTs in the polar lipids from Willershausen 1.2 m above the fossil band: a) HPLC-UV analysis λ_{max} 263 nm and detail of FLB-GDGTs in the inset; b) HPLC-FLD analysis λ_{ex} 263 nm, λ_{em} 309 nm. Derivatives of branched and isoprenoid GDGTs are indicated.	94

Figure 2.30. Comparison of HPLC-MS signal of native and FLB derivatives of: a) <i>r</i> -dOG and cholesterol (reproduced from Poplawski, 2017); b) GDGT lipids from Loch of Stenness sediments; c) GDGT lipids from Willershausen sediments 1.2 m above the fossil band.	95
Figure 2.31. Reversed-phase HPLC-MS of native and Fmoc-Lys(Boc) derivatives of GDGTs in the polar lipids from Willershausen 1.2 m above the fossil band: a) native brGDGTs BPC <i>m/z</i> 1000-1060; b) native iGDGTs BPC <i>m/z</i> 1290-1305.	97
Figure 3.1. Summary of key biological markers employed in this study and their association with particular organic matter sources. Abbreviations: OM = organic matter; iGDGTs = isoprenoid glycerol dialkyl glycerol tetraethers; Chl = chlorophyll pigments; Bchl = bacteriochlorophyll pigments; brGDGTs = branched glycerol dialkyl glycerol tetraethers.	102
Figure 3.2. a) Map of the British Isles showing the Orkney archipelago (white square) and the Loch of Stenness (green square, adapted from Google Maps); b) map of the Loch of Stenness showing the location of core 2014-1 in the red rectangle. Bathymetry only shown for the Loch of Stenness (adapted from Bates <i>et al.</i> , 2016).	108
Figure 3.3. Stenness core 2014-1 showing the main lithological zones, the loss-on-ignition results (sampled every 5 cm) and the dates of the beginning and end of transgression according to Bates <i>et al.</i> (2016); sampling depths analysed in this study are marked with arrows.	109
Figure 3.4. HPLC-MS chromatograms <i>m/z</i> 950-1500 of GDGTs from the Loch of Stenness from depths of 38 cm (top) and 118 cm (bottom). The boxes indicate iGDGTs (solid line), brGDGTs (dashed line) and crenarchaeol (dotted line). Note the presence of marine marker crenarchaeol at 38 cm.	112
Figure 3.5. Lithology and radiocarbon dating from Bates <i>et al.</i> (2016), and a) Concentrations of <i>n</i> -alkanes <i>n</i> -C ₂₃₋₃₅ ; b) concentrations of <i>n</i> -C ₁₆ , <i>n</i> -C ₁₈ and <i>n</i> -C ₂₂₋₃₀ <i>n</i> -alkanols, and <i>n</i> -C ₁₆ , <i>n</i> -C ₁₈ and <i>n</i> -C ₂₂₋₂₈ <i>n</i> -alkanoic acids; c) concentrations of sterols; d) concentrations of chlorophyll <i>a+b</i> , bacteriochlorophyll <i>a</i> pigments and bacterioviridin <i>a</i> in the Loch of Stenness sediments. The arrows indicate sample depths where lipids or pigments were not detected.	115
Figure 3.6. (Left to right) Lithology and radiocarbon dating from Bates <i>et al.</i> (2016), and proxies applied to the Loch of Stenness sediments: BIT (branched and isoprenoid tetraether lipids), CPI (carbon preference index based on <i>n</i> -alkanes), P _{aq} (proxy of aquatic macrophytes based on <i>n</i> -alkanes), ACL (average chain length based on <i>n</i> -alkanes), pH calculated from CBT (cyclisation of	

branched tetraether lipids) and TEX ₈₆ ^L values (tetraether index of 86 carbons – low) for sea-surface temperature calculations.....	116
Figure 3.7. Scheme summarising the main findings from the core from the Loch of Stenness, Orkney: lithology, microscopy, <i>n</i> -alkanes, polar lipids, pigments and BIT index.	122
Figure 4.1. a) Map of south-east England showing Norfolk and the locations of the Nar Valley cores (red) and Woodston (black); b) map showing the location of the Nar Valley cores; c) map showing the location of Woodston HiB 12-6 core (maps adapted from Google Maps).	125
Figure 4.2. Cross section of the lower Nar Valley showing the sedimentation zones (adapted from Ventris, 1996; not to scale).	126
Figure 4.3. Borehole lithology of Nar Valley cores redrawn from Barlow <i>et al.</i> , 2017 and Woodston HiB 12-6.....	128
Figure 4.4. Scheme of lithology, loss-on-ignition (showing the percentage of organic carbon), foraminifera, pollen and interpretation of the palaeoenvironment of Tottenhill Quarry samples (redrawn from Barlow <i>et al.</i> , 2017).	130
Figure 4.5. Scheme of lithology, loss-on-ignition (showing the percentage of organic carbon), foraminifera, pollen and interpretation of the palaeoenvironment of Horse Fen 13-1 samples (redrawn from Barlow <i>et al.</i> , 2017).	131
Figure 4.6. Scheme of lithology, loss-on-ignition (showing the percentage of organic carbon), foraminifera, pollen and interpretation of the palaeoenvironment of Blackborough Quarry samples (redrawn from Barlow <i>et al.</i> , 2017).	132
Figure 4.7. Scheme of lithology, loss-on-ignition (showing the percentage of organic carbon), foraminifera, pollen and interpretation of the palaeoenvironment of Railway Cottage samples (redrawn from Barlow <i>et al.</i> , 2017).	133
Figure 4.8. Nar Valley borehole lithology from Barlow <i>et al.</i> , 2017 and separation of the six types of sediment reflecting the molecular fossil distributions from this study.....	137
Figure 4.9. UV/vis spectrum of unidentified carotenoid peak 7 (P7).	140
Figure 4.10. Concentrations of <i>n</i> -alkanes, kaur-15-ene, kaur-16-ene, and kaurane, <i>n</i> -alkanones and <i>n</i> -alkanals in the Tottenhill Quarry samples.	142

Figure 4.11. Concentrations of <i>n</i> -alkanoic acids, <i>n</i> -alkanols and terpenoids in the Tottenhill Quarry samples.	142
Figure 4.12. Concentrations of chlorophyll and bacteriochlorophyll pigments in the Tottenhill Quarry core.	143
Figure 4.13. Concentrations of <i>n</i> -alkanes, kaur-15-ene, kaur-16-ene, and kaurane, <i>n</i> -alkanones, lupenone, lupanone, friedelan-3-one and <i>n</i> -alkanals in the Blackborough Quarry samples.	144
Figure 4.14. Concentrations of <i>n</i> -alkanoic acids, <i>n</i> -alkanols and terpenoids in the Blackborough Quarry samples.	145
Figure 4.15. Concentrations of chlorophyll and bacteriochlorophyll pigments in the Blackborough Quarry core.	146
Figure 4.16. Concentrations of <i>n</i> -alkanes, kaur-15-ene, kaur-16-ene, and kaurane, <i>n</i> -alkanones, alkenones C _{37:2} and C _{37:3} , γ -sitostenone, friedelan-3-one and <i>n</i> -alkanals in the Horse Fen samples.	149
Figure 4.17. Concentrations of <i>n</i> -alkanoic acids, <i>n</i> -alkanols and terpenoids in the Horse Fen samples.	150
Figure 4.18. Concentrations of chlorophyll and bacteriochlorophyll pigments in the Horse Fen core.	150
Figure 4.19. GC-EI-MS spectrum and structure of the alkenone C _{37:3Me} showing the most prominent fragments.	151
Figure 4.20. GC-EI-MS spectra of long chain alkenones: C _{37:2 Me} and C _{38:2 Et} and structures showing the most prominent fragments.	155
Figure 4.21. Concentrations of <i>n</i> -alkanes, alkenones C _{37:2} , C _{37:3} and C _{38:2} and friedelan-3-one in the Railway Cottage samples.	158
Figure 4.22. Concentrations of <i>n</i> -alkanoic acids, <i>n</i> -alkanols and terpenoids in the Railway Cottage samples.	158
Figure 4.23. Concentrations of chlorophyll and bacteriochlorophyll pigments in the Railway Cottage core.	159

Figure 4.24. Summary of the key environmental conditions in the Tottenhill Quarry core; on the left of each core is the evidence from the lithology & microfossils (Barlow <i>et al.</i> , 2017); on the right is the evidence from the molecular fossils from this study.	164
Figure 4.25. Summary of the key environmental conditions in the Blackborough Quarry core; on the left of each core is the evidence from the lithology & microfossils (Barlow <i>et al.</i> , 2017); on the right is the evidence from the molecular fossils from this study.	165
Figure 4.26. Summary of the key environmental conditions in the Horse Fen core; on the left of each core is the evidence from the lithology & microfossils (Barlow <i>et al.</i> , 2017); on the right is the evidence from the molecular fossils from this study.	166
Figure 4.27. Summary of the key environmental conditions in the Railway Cottage core; on the left of each core is the evidence from the lithology & microfossils (Barlow <i>et al.</i> , 2017); on the right is the evidence from the molecular fossils from this study.	167
Figure 4.28. Summary of the key environmental conditions in the Nar Valley cores; on the left of each core is the evidence from the lithology & microfossils (Barlow <i>et al.</i> , 2017); on the right is the evidence from the molecular fossils from this study.	168
Figure 4.29. Lithology and magnetic susceptibility data from the core at Woodston (redrawn from Barlow, pers. comm.).	170
Figure 4.30. Concentrations of <i>n</i> -alkanes, <i>n</i> -alkanones, <i>n</i> -alkanals and terpenoids in the Woodston samples with inset from -18.22 to -17.53 m OD.	172
Figure 4.31. Concentrations of <i>n</i> -alkanoic acids, <i>n</i> -alkanols and terpenoids in the Woodston samples.	173
Figure 4.32. Concentrations of chlorophyll and bacteriochlorophyll pigments in the Woodston core.	173
Figure 5.1. Structures of a) GDD archaeol, b) GMGD-0, c) GTGT-0, d) OH-GDGT-0 and e) GMD-0 (note that the position of the covalent bond between the isoprenoidal chains is tentative and based on the position in GMGT-0).	178
Figure 5.2. (+)APCI-MS extracted ion chromatograms (EIC) <i>m/z</i> 1047.5-1048.5, 1033.5-1034.5 and 1019.5-1020.5 of the polar fraction from sediments showing the brGDGTs and the peaks for the unknown glycerolipids. Note that the intensity scale is the same for the three EICs.	180

Figure 5.3. (Top) (+)APCI-MS ² spectrum of glycerolipid <i>m/z</i> 1048.3, (middle) inset of the MS ² <i>m/z</i> range 825-1100 and (bottom) suggested structure of glycerolipid <i>m/z</i> 1048.3 showing the most prominent losses. Note that the order of loss of each OH group, the position of the covalent bond between the alkyl chains and of the methyl branches are only suggested.....	181
Figure 5.4. (Top) (+)APCI-MS ² spectrum of glycerolipid <i>m/z</i> 1034.3 and (bottom) suggested structure of glycerolipid <i>m/z</i> 1034.3 showing the most prominent losses. Note that the order of loss of each OH group, the position of the covalent bond between the alkyl chains and of the methyl branch are only suggested.	181
Figure 5.5. (Top) (+)APCI-MS ² spectrum of glycerolipid <i>m/z</i> 1020.3 and (bottom) suggested structure of glycerolipid <i>m/z</i> 1020.3 showing the most prominent fragment ions. Note that the order of loss of each OH group and the position of the covalent bond between the alkyl chains are only suggested.	182
Figure 5.6. (Top) (+)APCI-MS ² spectrum of the diacetate glycerolipid <i>m/z</i> 1104.0 and suggested structure of the acetate derivative showing the main losses. Note that the positions of the covalent bond between the alkyl chains and of the acetylated alcohol groups are only suggested.....	183
Figure 5.7. (continued) Peak areas of GMD lipids <i>m/z</i> 1048.3, 1034.3 and 1020.3 in the type sediments from the Nar Valley, in the Woodston and Loch of Stenness sediments. Abbreviations: BQ = Blackborough Quarry, TQ = Tottenhill Quarry, HF = Horse Fen, RC = Railway Cottage. The cross indicates absence of GMDs.....	187
Figure 5.8. Example of correlation between peak areas of GMDs vs brGDGTs (in blue) and GMDs vs iGDGTs (in red) in Blackborough Quarry from -1.19 to -0.95 m OD.	188
Figure 7.1. Calibration curves used for calculating chlorophyll pigment amount. From left to right: phaeophorbide <i>a</i> , chlorophyll <i>a</i> and phaeophytin <i>a</i>	208
Figure 7.2. Calibration curve for calculating the concentration of lipids: <i>n</i> -C ₂₄ , <i>n</i> -C ₂₈ , <i>n</i> -C ₃₄ , <i>n</i> -C ₃₆ , <i>n</i> -C ₃₈	209
Figure A1.1. Phylogenetic tree of living organisms: the three main domains, Eubacteria, Eukaryota and Archaea; the separation of the Archaea into the major phyla, Korarchaeota, Euryarchaeota and Crenarchaeota showing the Thaumarchaeota strain (adapted from Raymann <i>et al.</i> , 2015).....	213
Figure A1.2. Ionisation of the sample in APCI (redrawn from Chromacademy_APCI).	213

Figure A1.3. Depiction of the three factors that control Quaternary glacial-interglacial cycles according to the Croll-Milankovitch Hypothesis: a) eccentricity; b) obliquity; c) precession (from Maslin, 2016).	215
Figure A1.4. Schematic diagram of a diode array detector (redrawn from Chromacademy_HPLC detectors).....	216
Figure A1.5. HPLC-DAD chromatogram of a sample containing compounds that absorb in the UV-vis range. Each peak has a specific UV-vis spectrum (right).	216
Figure A1.6. Schematic representation of the electrospray ionisation process (redrawn from Banerjee and Muzumdar, 2012).	217
Figure A1.7. Schematic of the flame ionisation detection process	217
Figure A1.8. Scheme of the general principles of fluorescent detector.	218
Figure A1.9. Schematic representation of gas chromatograph.	219
Figure A1.10. Schematic diagram of high-performance liquid chromatography.	220
Figure A1.11. Diagram of the taxonomic rank for organisms.....	225
Figure A1.12. Diagram of TLC sequence to separate multiple analytes.	225
Figure A1.13. Schematic diagram of a UV-vis detector.	226
Figure A2.1. Marine isotope stages and substages for the last 1.05 Ma (from Railsback <i>et al.</i> , 2015).	228
Figure A3.1. Concentrations of chlorophyll pigments in the Loch of Stenness core 2014-1: chlorophyllone (chlone), phaeophytin <i>a</i> (phe <i>a</i>), pyropheophytin <i>a</i> (pphe <i>a</i>), pyropheophorbide <i>a</i> (pphorb <i>a</i>), hydroxyphaeophytin <i>a</i> (hphe <i>a</i>), purpurin-7 trimethyl ester, chlorin e6, phaeophytin <i>b</i> (phe <i>b</i>), bacteriochlorophyll <i>a</i> (bchl <i>a</i>), bacteriopheophytin <i>a</i> (bphe <i>a</i>), pyrobacteriopheophytin <i>a</i> (bpphe <i>a</i>), and bacterioviridin <i>a</i> (bvir <i>a</i>).....	231
Figure A3.2. Comparison of vegetation changes in three cores from Orkney: a) Crudale Meadow (Bunting, 1994); b) Blows Moss (Farrell <i>et al.</i> , 2014); c) Loch of Stenness (this study).....	232

Figure A4.1. UHPLC-DAD chromatogram (300-800 nm) of Horse Fen 13-1 pigments sample -2.26 m OD (9.96 m depth). For peak assignments see Table A4.1	233
Figure A4.2. UHPLC-DAD chromatogram (300-800 nm) of Railway Cottage pigments sample 9.46 m OD (5.56 m depth) and 9.93 m OD (5.09 m depth). For peak assignments see Table A4.2.	237
Figure A4.3. UHPLC-DAD chromatogram (300-800 nm) of Tottenhill Quarry pigments sample 2.08 m OD (0.90 m depth) and 2.63 m OD (0.35 m depth). For peak assignments see Table A4.3.	242
Figure A4.4. UHPLC-DAD chromatogram (300-800 nm) of Blackborough Quarry pigments sample - 0.74 m OD. For peak assignments see Table A4.4.	246
Figure A4.5. UHPLC-DAD chromatogram (300-800 nm) of Woodston pigments sample -18.42 m OD. For peak assignments see Table A4.5.	250
Figure A4.6. GC-FID chromatogram of the aromatic hydrocarbon fraction from Horse Fen 13-1 sample -2.20 m OD showing the retention time of alkenones after long chain <i>n</i> -alkanones and <i>n</i> -alkanals.	254
Figure A9.1. Structure of GDGTs (continued over).	258
Figure A9.2. Structures of lipid standards.....	260
Figure A9.3. Structures of alkanes, alkanones, alkenones, alkanals, alkanoic acids, alkanols (continued over).	261
Figure A9.4. Structures of terpenoids (continued over).	264
Figure A9.5. Structures of chlorophyll pigments (continued over).	268
Table A9.6. List of bacteriochlorophyll and bacterioviridin pigment structure numbers and name of compounds. For structures, see Figure A9.6.	271
Figure A9.6. Structures of bacteriochlorophyll and bacterioviridin pigments (continued over)....	271
Figure A9.7. Structures of carotenoids.	273

Acknowledgments

I would like to express my gratitude to my research supervisors Prof. Brendan Keely and Dr. Kirsty Penkman for providing me with the opportunity to do a PhD in a most interesting subject that gave me the opportunity to learn a lot and meet a wide variety of scientists. I would like to thank my supervisors for their invaluable advice, support, critical comments, guidance and patience during the research project and the writing of this thesis. I feel I have developed as a scientist and as a person over the past 3.5 years, and I have my supervisors to thank for this. I am thankful to Dr. Caroline Dessent for all the stimulating scientific discussions and professional advice during our TAP meetings.

A big thank you goes to my collaborators, Dr. Martin Bates, Dr. Natasha Barlow and Dr. Richard Preece, for providing the cores I analysed for my project and identifying shell species, and for the valuable discussions that improved my research.

I would like to thank Dr. Scott Hicks for providing training and the possibility of using the Trace GC-FID, Karl Heaton for accommodating hundreds of my GC-MS samples, Dr. Ed Bergström for providing training on ion trap and orbitrap and Dr. Graeme McAllister and Dr. John Liddon for use of the microwave. I would like to thank the Department of Chemistry of the University of York for funding my PhD through a teaching studentship. Much appreciation to the teaching laboratories technicians, Scott, Helen, Phil, Charlotte, Liza and Sofia, for the random chats and support in teaching labs. Thank you to the departmental staff, Rachel, Sharon, Alice, Leonie and Cristina for your help during my PhD.

I had the pleasure of working with an amazing group of people in both Brendan's and Kirsty's groups, you helped me going through this PhD remaining (almost) sane! Thank you Natta, Jan, Marianna and Marina for your friendship and tea breaks. Thank you Scott, Matt and Cezary for interesting discussions and initial training in the lab. Thank you Sheila for always taking the time for a quick chat and training me on AAR, and thank you Kirsty, Lucy, Marc, Eden, Sam and Chloë for your support, enthusiasm and help during outreach activities. I also would like to thank the Postgraduate sea level discussion group, Lucy W, Sophie, Graham, Lucy M, Ed, Fiona, Luke, Alex and Glenn, for cake breaks, chats and sharing the wide variety of sea-level science going around in the University.

Massive appreciation to Rosaria for always being available for a chat and food, for being my gym buddy and for being a supporting and caring friend. I've missed you so much in the past few

months. And thank you to my friends, Manuela, Marco, Chiara, Antonella and Angelo, for bringing a bit of “italianità” every time we meet and making me feel more at home. During my years in York, I have met some fantastic people so thank you Claudia, Sofia, Chiara, Silvia, Megan, Abby, Zoë, Amy, Sophie, Stefan, Huda and Andrea. I’m grateful to Denise, Tony and Liam for their support and to Poppy and Finn for relaxing cuddles.

I would like to thank my wonderful Mum and Dad for their unconditional love, support and encouragement during all my life and especially since I have been in York even if we are 2000 km away! I’m thankful to have you as my parents.

A final thank you to my special man who always encouraged me, picked me up and put up with my craziness, stress and tears during my PhD, thank you my love.

Author's declaration

I declare that this thesis is a presentation of original work and I am the sole author. This work has not previously been presented for an award at this, or any other, University. All sources are acknowledged as References.

Martina Conti

Chapter 3 was submitted for publication to the Journal of Quaternary Science and is currently under review. The format was adapted to the thesis but the content is similar to the submitted publication.

Authors: Conti, M.L.G., Bates, M.R., Preece, R.C., Penkman, K.E.H., Keely, B.J.

Collection of samples, molecular fossils analysis and interpretation was carried out by Conti. The manuscript was written by Conti with inputs from Bates, Preece, Penkman and Keely.

1. Introduction

Over its long history, the Earth has experienced changes in climate that have affected ocean and sea levels. These fluctuations have occurred over a wide range of timescales, extents of inundations and for a variety of causes. Through studying past fluctuations, the reasons behind sea-level changes are progressively recognised. Studies of the geological record have been able to estimate global sea-level changes in the last 250 million years (Ma) showing both long term and short term fluctuations (Miller, 2009). For example, during the Cretaceous period (145-66 Ma), sea level was estimated to be 100-250 m higher than today causing most of the present continents to be submerged (Miller, 2009), whereas during the Last Glacial Maximum (LGM, underlined words are explained in more detail in Appendix 1; 26,000-20,000 years ago (26-20 ka)) reconstructions estimated sea levels to be 130 m lower than present (Lambeck *et al.*, 2014). Interpreting the past sea-level record also allowed the reconstruction of past climatic conditions and interpretation of how such changes affected coastlines, ecosystems and human settlements (Devoy, 1977; Rollins *et al.*, 1979; Jablonski, 1980; Gaffney *et al.*, 2009; Hodgson *et al.*, 2009; Bates *et al.*, 2016; Benjamin *et al.*, 2017; Shennan *et al.*, 2018; Brendryen *et al.*, 2020). By understanding the main drivers, causes and consequences of past sea-level changes, this knowledge can be applied to understanding future climate and sea-level change scenarios (Nicholls and Cazenave, 2010; Woodroffe and Murray-Wallace, 2012; Murray-Wallace and Woodroffe, 2014). The present increasing sea-level trend (3.3 mm yr⁻¹; NASA) and a multitude of other studies on past and present climate have underpinned predictions of future climate and sea-level scenarios (IPCC, 2014; SROCC, 2019) from which actions are taken and policies are implemented.

1.1. Causes of sea-level change

Worldwide sea-level fluctuations affected by the volume of ocean water are termed eustatic fluctuations. Glacio-eustatic sea-level changes are caused by the growth / contraction of continental ice sheets locking / releasing ice from ocean water (Figure 1.1; Maclaren, 1842; Murray-Wallace and Woodroffe, 2014).

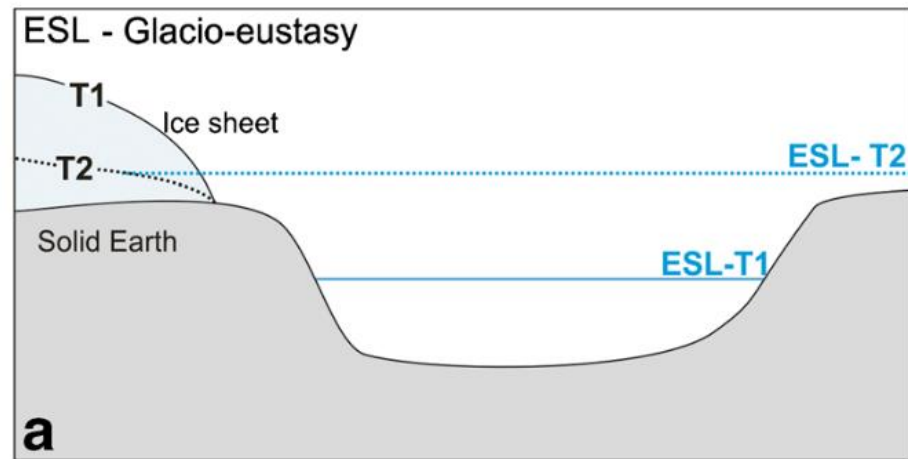


Figure 1.1. Glacio-eustasy and its impact on sea-level change. At T1 the growing ice sheet locks seawater as ice resulting in low eustatic sea level (ESL-T1); at T2 the ice sheet is melting thus releasing water and increasing sea level (ESL-T2; from Rovere *et al.*, 2016).

The viscosity of the Earth's mantle keeps the crust in isostatic equilibrium, the balance between the depression of the crust in one location and the uplift in another location (Airy, 1855; Pratt, 1855; Peltier, 2004; Teixell *et al.*, 2009; Lowe and Walker, 2015). Isostasy controls sea level on a local scale. The weight of the ice sheets depresses the Earth's crust increasing sea levels; as the ice sheet melts, the crust rebounds lowering sea levels relative to the land. For example, during the LGM in UK the ice sheet depressed the Earth's crust in northern parts of the country while southern areas were uplifting (Figure 1.2a). Following the LGM, deglaciation occurred from the end of the Pleistocene to the early Holocene (20-6 ka; Shennan *et al.*, 2006). The loss of ice sheets in northern UK resulted in a rebound of the crust and decrease in sea levels, while in southern UK crustal subsiding occurred and sea level increased (Figure 1.2b); these processes are still occurring today (Shennan, 1989; Shennan and Horton, 2002; Shennan *et al.*, 2018).

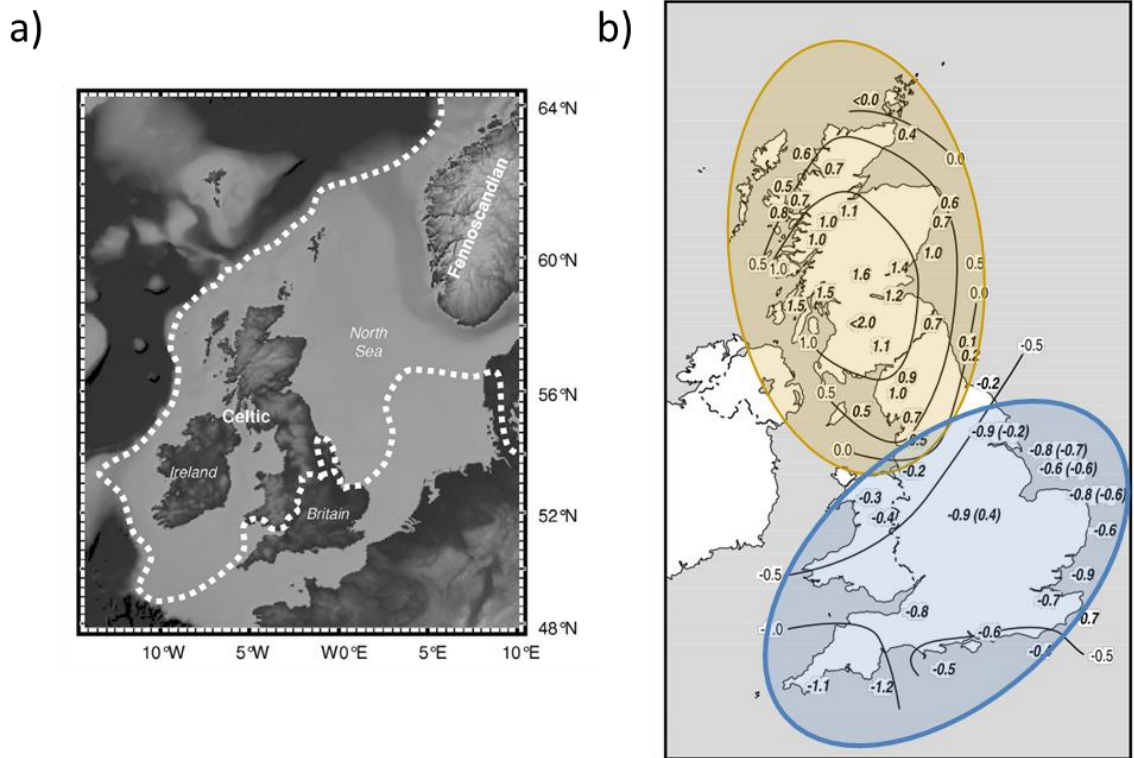


Figure 1.2. a) (dotted line) Approximate maximum extent of the ice sheet over Britain and Ireland between 25 and 23 ka (from Shennan *et al.*, 2018); b) rate of isostatic change in Great Britain (in mm yr^{-1}) since 4 ka: positive values indicate land uplift or sea-level fall (in yellow shaded areas) and negative values indicate subsistence or sea-level rise (in blue shaded areas; values in brackets include a correction for changes in tidal range; adapted from Shennan and Horton, 2002).

Glacio-eustasy and isostasy are the main drivers of global and local sea-level change. At a regional scale, several additional processes can occur such as hydro-isostasy – the response of Earth’s crust to both ice and water loading – affecting mostly coastal locations. Geoid configuration anomalies, ocean thermal expansion, ocean water siphoning to far-field regions, tectonic movements, tidal ranges and volcanism are all mechanisms that can drive smaller-scale sea-level changes (Mitrovica and Peltier, 1991; McGuire *et al.*, 1997; Peltier, 2004; Schellmann and Radtke, 2004; Lambeck *et al.*, 2014; Murray-Wallace and Woodroffe, 2014; Rovere *et al.*, 2016; Gehrels *et al.*, 2020). The net result of a combination of these processes is that global, regional and local sea levels have fluctuated significantly in the past. This thesis studies transgressions that occurred in coastal locations in the UK, where tectonic and volcanic factors are absent and isostatic and eustatic factors have been identified as the main drivers of sea-level change.

1.2. Marine transgressions and regressions

Conventionally, an increase in sea level relative to the land surface is termed marine transgression, resulting in the shoreline moving inland, while a sea-level decrease is called a marine regression. The nature and extent of the transgression / regression dictates rates of sediment supply / erosion (Swift, 1968; Muto and Steel, 1997; Murray-Wallace and Woodroffe, 2014), thus affecting organic matter (OM) origin, reworking, preservation and sedimentation (Killops and Killops, 1993; Cattaneo and Steel, 2003). Transgressions increase the volume of water in the basin and may result in additional nutrient discharge, enhanced primary productivity, development of anoxic water and, in low erosion environments, OM deposition (Killops and Killops, 1993; Cattaneo and Steel, 2003; Talbot *et al.*, 2006). In high erosion and low deposition transgressions the sediment supply and thus OM input is sporadic (Cattaneo and Steel, 2003; Murray-Wallace and Woodroffe, 2014). During a regression, oceans are well mixed and oxygenated resulting in preservation of OM being limited (Arthur *et al.*, 1987; Killops and Killops, 1993). Nutrient input decreases, thus reducing productivity and sedimentation of OM (Arthur *et al.*, 1987; Killops and Killops, 1993).

1.3. Indicators of sea-level change

Transgressions and regressions are represented by fluctuations between terrestrial and marine environments (and vice versa). Studies of transgressions can be inferred from recognising an increase in the volume of seawater and flooding inland. In a regression the volume of ocean water decreases, thus moving the coast seaward (Cattaneo and Steel, 2003). This horizontal movement of the land-sea system affects the environment and the organisms living in it. Therefore, transgressions and regressions are recorded in the sediment, where variations in the nature of the sediments, macrofossil, microfossil and biomarker assemblages can provide evidence of sea-level changes (Kjemperud, 1981; Horton *et al.*, 1992; Shennan *et al.*, 1993; Ficken and Farrimond, 1995; Squier *et al.*, 2002; Cattaneo and Steel, 2003; Bendle *et al.*, 2009; van Soelen *et al.*, 2010; Lowe and Walker, 2015; De Jonge *et al.*, 2016; Li *et al.*, 2017; Smith *et al.*, 2017; Gehrels *et al.*, 2020). The methodology used in this thesis for studying transgressions is based on biomarkers.

1.3.1. Lithological and regional features

Studies of the stratification of different horizons by visual and lithological analyses can recognise changes in sea level. During a transgressive event, marine sediments (sands, silts) are deposited over terrestrial sediment, such as peat or clay, resulting in the sediment fining towards the surface (Figure 1.3). In a regression the opposite is observed: with sea-level decrease, the sand-silt system

will be deposited further from the coast, thus forming a core with marine silts and sands at the base overlain by terrestrial deposits, coarsening upwards (Figure 1.3; Cattaneo and Steel, 2003; Lowe and Walker, 2015). Fieldwork surveys through geomorphological, geographical, global positioning system (GPS) and mapping can identify areas that exhibit sea-level changes (e.g. West, 1956; Bates and Bates, 2000; Hein *et al.*, 2016; Rovere *et al.*, 2016; Benjamin *et al.*, 2017). Fieldwork observations of specific landforms (such as coral reefs, coastal caves, speleothems, sinkholes, terraces and peat deposits) can be indicators of past sea-level oscillations (Chappell, 1980; Bull and Cooper, 1986; Richards *et al.*, 1994; Bates *et al.*, 2003; Antonioli *et al.*, 2004; Lane *et al.*, 2011; Shennan *et al.*, 2015).

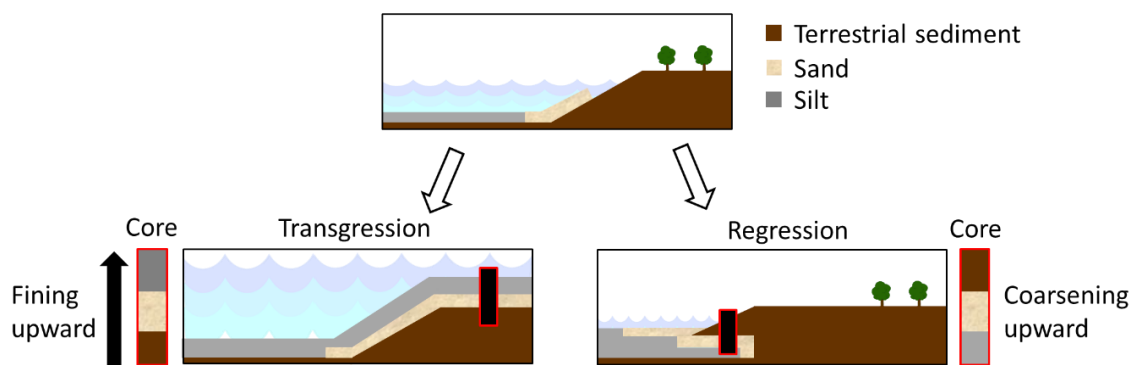


Figure 1.3. Sedimentological evidence of a marine transgression and a regression.

1.3.2. Palaeontological evidence

Sea-level fluctuations impact on the flora and fauna (e.g. Rollins *et al.*, 1979; Jablonski, 1980; Fürsich *et al.*, 1991; Hodgson *et al.*, 2009; Roe *et al.*, 2009; Bates *et al.*, 2016; Barlow *et al.*, 2017), enabling biological indicators, such as macrofossils and microfossils including plant leaves, pollen, spores, foraminifera, diatoms, molluscs and ostracods, to be used as markers of sea-level change (Kjemperud, 1981; Horton *et al.*, 1992; Mitlehner, 1992; Shennan *et al.*, 1993; Gehrels *et al.*, 2001; Barlow *et al.*, 2017; Smith *et al.*, 2017; Gehrels *et al.*, 2020). Other markers (including corals, microatolls and mangroves) are specific to warm tropical regions (Chappell, 1980; Woodroffe, 1990; Ellison and Stoddart, 1991; Schellmann and Radtke, 2004; Murray-Wallace and Woodroffe, 2014) and so are not discussed here.

Plant macrofossils including wood, leaves, fruits, seeds and mosses represent autochthonous and / or transported sources of OM depending on the type of sediments (Shennan *et al.*, 2015). For example, in fens or bogs plant macrofossils have almost exclusively in situ origin, whereas in lake sediments plant macrofossils transported by wind, water or animals dominate the assemblage (Greenwood, 1991; Hughes *et al.*, 2000; Lowe and Walker, 2015). Identification of plant macrofossil

taxa provides evidence for reconstructing past environments and infer relative sea-level movements (Horton *et al.*, 1992; Hughes *et al.*, 2000; Behre, 2004; Shennan *et al.*, 2015). Plant remains are often used for radiocarbon dating of sediments, provided that bioturbation and mixing of old and new OM are excluded, thereby giving accurate results (Hillman *et al.*, 2001; Lowe and Walker, 2015). Due to the size of the macrofossil, large volumes of sediment are necessary to ensure correct assignments of the macrofossil assemblage, reducing the sampling resolution possible.

Microfossils, such as pollen and spores, are ubiquitous in most sediment records and have higher frequency and durability than plant macrofossils. As pollen and spores are very small (25-100 µm in diameter) and light, they are regularly transported by wind, water and animals. Thus, pollen represents allochthonous OM, with different pollen grains being able to travel a range of distances due to their specific surface features (Jackson and Lyford, 1999; Shennan *et al.*, 2015). Identification of pollen taxa is usually to the genus level, however some can only be discerned to the family level (Lowe and Walker, 2015). Pollen analysis enables reconstruction of vegetation history of local and regional areas (Horton *et al.*, 1992; Bunting, 1994; Roe and van de Plassche, 2005; Farrell *et al.*, 2014; Lowe and Walker, 2015) and differentiation between vegetation zones, including peat types, upland and lowland vegetation, and can imply aridity (Van Campo *et al.*, 1982).

Siliceous diatoms, aquatic unicellular algae, represent populations living in the photic zone and performing oxygenic photosynthesis (Kuczyńska *et al.*, 2015). Diatom microfossils have the potential to be well preserved in sediments and have widespread applications in sea-level studies due to the sensitivity of diatoms to salinity, substrate and pH (Kjemperud, 1981; Gehrels *et al.*, 2001). They have proved valuable in identifying transgressions and regressions, durations of tidal inundations, changes in pH and in nutrient availability (Kjemperud, 1981; Gehrels *et al.*, 2001; Lowe and Walker, 2015; Kuczyńska *et al.*, 2015; Shennan *et al.*, 2015).

Calcitic microfossils, including foraminifera, ostracods and molluscs, are also represented in sediments. Specific gastropod, crustacean and mollusc species / genus are correlated with marine, brackish, freshwater or terrestrial conditions, aiding in the understanding of sea-level changes (Fürsich *et al.*, 1991; Mazzini *et al.*, 1999; Bates *et al.*, 2016; Benjamin *et al.*, 2017). Foraminifera are shelled animals and the vast majority lives in marine environments (Gehrels *et al.*, 2001; Lane *et al.*, 2011; Barlow *et al.*, 2017). As in the case of pollen, some uncertainties in taxon identification can occur. In order to describe accurately past ocean conditions, affinity between fossil and modern species must converge and spatial and temporal variabilities need to be accounted for (Shennan *et al.*, 2015).

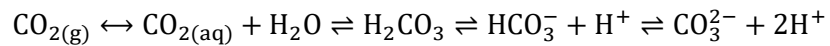
1.3.3. Stable oxygen isotope evidence

Oxygen isotopes ^{16}O and ^{18}O occur naturally in water with abundances of 99.759% and 0.204%, respectively. At first, the ratio of the relative abundances of the two isotopes in marine foraminifera, expressed as $\delta^{18}\text{O}$ (Equation 1.1), was postulated to change with temperature due to isotopic fractionation (Emiliani, 1955). Shackleton and Opdyke (1973) showed that the majority of the fractionation in foraminifera depended on changes in ice volume. As seawater evaporates and precipitates in the polar regions where it is incorporated into forming ice sheets, the lighter isotope, ^{16}O , is preferentially removed, leaving seawater enriched in the heavier isotope, ^{18}O . With ice sheets melting the ^{16}O -enriched ice is released into the ocean, thus seawater will be enriched in ^{16}O (Shackleton and Opdyke, 1973; Hays *et al.*, 1976; Zachos *et al.*, 1992; Murray-Wallace and Woodroffe, 2014).

$$\delta^{18}\text{O} = \left(\frac{\frac{^{18}\text{O}}{^{16}\text{O}} \text{ in sample}}{\frac{^{18}\text{O}}{^{16}\text{O}} \text{ in standard}} - 1 \right) \times 1000$$

(Equation 1.1, standard is PDB belemnite)

Marine organisms, such as foraminifera, reflect the isotope chemistry of the seawater in which they live. As carbon dioxide (CO_2) is absorbed in the ocean, hydration occurs forming carbonic acid (H_2CO_3 ; Equation 1.2). In seawater, pH is mildly alkaline, thus shifting the dynamic equilibrium of carbonic acid resulting in its dissociation (Equation 1.2). Organisms that secrete calcium carbonate shells reflect the source and the isotopic composition of seawater (Killops and Killops, 1993). Shackleton and Opdyke (1973) identified 22 periodic fluctuations in temperatures and in ice accumulation by measuring the $\delta^{18}\text{O}$ in foraminifera from marine sediments.



(Equation 1.2)

Changing ice volume affects the isotopic composition of seawater, thus $\delta^{18}\text{O}$ can indirectly infer glacio-eustatic changes in sea level (Shackleton and Opdyke, 1973). Notably, the direct use of the $\delta^{18}\text{O}$ record to infer sea-level changes is complicated by regional and local deep-water temperature and hydrographic effects, samples containing microfossils from contrasting water depths, foraminifera dissolution and presence of foraminifera genera that are not in isotopic equilibrium with seawater (Murray-Wallace and Woodroffe, 2014; PAGES, 2016). Nevertheless, oxygen

isotopes provide a valuable record of ice fluctuations in sediments from at least 65 Ma to the present (Zachos *et al.*, 2001; Miller, 2009). These fluctuations are formally called Marine Isotope Stages (MIS) assigning numbers working back from the present (MIS 1; Appendix 2) to the oldest recognised to date (Lisiecki and Raymo, 2005).

During the Quaternary (from 2.58 Ma to today; Gibbard and Head, 2009), fluctuations in $\delta^{18}\text{O}$ have become more cyclical and more intense than in the Pliocene (5.33-2.58 Ma) and have been characterised by expansion and retraction of ice sheets (PAGES, 2016). The cyclicity in the Quaternary ice ages can be partially explained by the Croll-Milankovitch Hypothesis. According to this theory, fluctuations in the geometry of the Earth's orbit (eccentricity, obliquity and precession) affect the amount of insolation received on the Earth's surface and the seasonality, leading to long-term cooling and warming cycles (Appendix 1, Figure A1.3). As a result of these cycles, the extent of ice sheet cover dramatically increases or decreases, thus affecting global sea levels (Hays *et al.*, 1976). However, not all Quaternary glacials (lasting approx. 100 ka) and interglacials (lasting approx. 10-15 ka) can be explained by Milankovitch cycles and further work is still needed to explain fully the periodicity of these cycles (PAGES, 2016 and references therein). Nevertheless, the periodic cycles of glaciation and deglaciation during the Quaternary markedly impacted sea levels and global palaeoenvironments. These Quaternary fluctuations are studied to understand the drivers of these changes and to inform ideas of future climate scenarios.

1.3.4. Markers of changes of organic matter source

$\delta^{13}\text{C}$ and carbon to nitrogen (C/N) ratios can indicate changes in source of bulk OM, such as terrestrial, freshwater or marine origin. Such changes are also associated with environments affected by changes in relative sea level. Although it is possible to differentiate sources of OM in coastal deposits, the signal can be affected by contributions from allochthonous and degraded OM, weakening the interpretative capability. Hence, $\delta^{13}\text{C}$ and carbon and nitrogen ratios (C/N) should be used with caution and only in support to other markers of sea-level change, such as foraminifera or diatoms (Müller and Mathesius, 1999; Mackie *et al.*, 2005).

1.3.4.1 $\delta^{13}\text{C}$

Carbon is the primary element of all known life on Earth. ^{12}C accounts for c. 98.9% of total carbon, with c. 1% of ^{13}C . The isotope ratio of the carbon that is fixed during photosynthesis in higher plants, algae and cyanobacteria is depleted compared to the CO_2 source from the atmosphere. The different mechanisms and extent of carbon isotope absorption from photosynthesis gives rise to differences in $\delta^{13}\text{C}$ according to primary producers (Equation 1.3; O'Leary, 1988; Hayes, 1993;

Killops and Killops, 1993). According to the pathway of photosynthetic fixation and resulting isotopic fractionation, plants can be distinguished as: C₄ plants (aquatic plants and tropical grasses), having $\delta^{13}\text{C}$ values between -12 and -17‰, C₃ plants (most higher plants), showing $\delta^{13}\text{C}$ values between -20 and -34‰, and CAM plants (desert plants and some algae), with $\delta^{13}\text{C}$ values from -10 to -22‰ (O’Leary, 1988; Meyers, 1997; Chikaraishi *et al.*, 2004; Mackie *et al.*, 2005). Measurements of $\delta^{13}\text{C}$ in marine organic matter have shown values from -10 to -25‰ (Ishiwatari *et al.*, 1994; Meyers, 1997; Mackie *et al.*, 2005). Thus, the isotopic composition of photosynthetic organisms differs and $\delta^{13}\text{C}$ can broadly distinguish between terrestrial plants and algal OM (O’Leary, 1988; Mackie *et al.*, 2005; Zhang *et al.*, 2010; Carr *et al.*, 2015; Shennan *et al.*, 2015). In environments where C₄ and marine contributions are present, the similarity in the isotopic values of the sources would preclude their discrimination (Chikaraishi *et al.*, 2004). Thus, $\delta^{13}\text{C}$ values can only distinguish marine and terrestrial OM in mid-latitudes environments where C₃ plants are dominant.

$$\delta^{13}\text{C} = \left(\frac{\frac{^{13}\text{C}}{^{12}\text{C}} \text{ in sample}}{\frac{^{13}\text{C}}{^{12}\text{C}} \text{ in standard}} - 1 \right) \times 1000$$

(Equation 1.3; standard is PDB belemnite)

1.3.4.2. Carbon and nitrogen ratio (C/N)

Aquatic and terrestrial plants show different ratios of C/N, due to differences in the nature of the biopolymer compositions of terrestrial and aquatic plants. Terrestrial plants are made up of carbon-rich hemicellulose, cellulose and lignin, whereas marine and aquatic plants are generally richer in protein and so have higher N contents. This distinction results in very high C/N ratios (20-500) for terrestrial plants and lower values (3-50) for aquatic plants (Ishiwatari *et al.*, 1994; Meyers, 1997; Müller and Mathesius, 1999; Mackie *et al.*, 2005; Bendle *et al.*, 2009; Carr *et al.*, 2015; Shennan *et al.*, 2015). Preferential degradation of protein over lipids (Müller and Mathesius, 1999) means that care needs to be taken when comparing C/N ratios over long timescales. Moreover, in mixed-source environments, evidence from the C/N ratio should be supported by other lines of evidence such as biomarkers and $\delta^{13}\text{C}$ (Müller and Mathesius, 1999; Mackie *et al.*, 2005).

1.4. Molecular fossils

A great wealth of palaeoenvironmental information can be gathered from the sediment geomorphology, macro and microfossil evidence. The sediment matrix also contains molecular fossils that represent OM produced by organisms, such as algae (e.g. **C1**; text in bold denotes structures in Appendix 9), bacteria (e.g. **B1**, **C6**) and terrestrial plants (e.g. **A1-A5**, **T11**). The molecular fossils that are unambiguously linked to organisms or to a particular process are termed biomarkers. Ideal biomarkers are resistant to transformations or it is possible to associate their transformation products to the original components (Poynter and Eglinton, 1991). Using molecular fossils, it is possible to identify *in situ* production of OM as well as transported OM from the hinterland (Killops and Killops, 1993).

1.4.1. Markers of aquatic production

The n -C₁₆ and n -C₁₈ n -alkanoic acids (**A4**) occur in terrestrial and algal material (Cranwell, 1973; Chikaraishi *et al.*, 2004; Wang and Liu, 2012; Fang *et al.*, 2014; Liu and Liu, 2017; Wang *et al.*, 2019) and can be inferred to be derived from aquatic OM when supported by the presence of other biomarkers (Cranwell, 1973). Short chain n -alkanes (n -C₁₇₋₂₄; **A1**) without odd-over-even carbon chain predominance can represent algal OM (Cranwell, 1973; Ficken and Farrimond, 1995).

Sterols are terpenoid membrane lipids of plants and aquatic organisms. Structural differences among sterols include C₂₀ side-chain lengths, and stereochemistry and substituents (at C₃, C₄, C₁₀, C₁₃, C₁₄, C₁₇) that differ according to the producers (Figure 1.4). Sterols are characterised by a double bond on carbon 5 (Figure 1.4), while in stanols the double bond is absent. A limited number of sterols are specific to particular source organisms such as dinoflagellates (dinosterol; **T10**) and diatoms (diatomsterol; **T13**), representing aquatic production (Volkman, 1986; Ficken and Farrimond, 1995; Thiel *et al.*, 1997; van Soelen *et al.*, 2010; Chagué-Goff *et al.*, 2017).

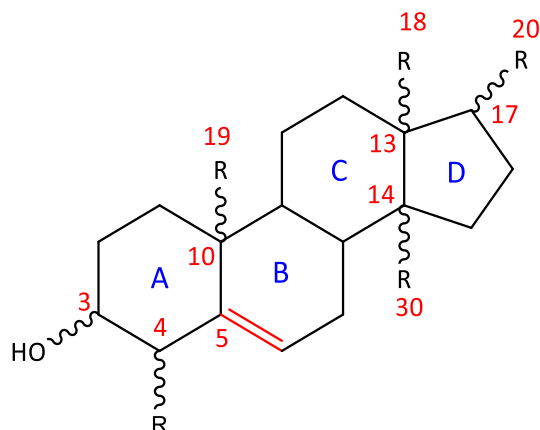


Figure 1.4. Generalised structure of sterol with the double bond in red (at C_5); in stanols the double bond at C_5 is absent.

Glycerol dialkyl glycerol tetraether (GDGT) lipids are component structures of membranes produced by *Archaea* and some bacteria and they can be preserved in terrestrial soils, lake sediments, and sediments of open and coastal marine environments (Schouten *et al.*, 2013). The GDGT structures comprise dialkyl chains connected to two glycerol moieties by four ether groups (Figure 1.5). The alcohol groups on the glycerol moieties are bonded to two polar head groups in the intact polar lipids (Figure 1.5a). The head groups tend to hydrolyse to OH during senescence (Sturt *et al.*, 2004), thus forming the tetraether lipid cores (Figure 1.5b).

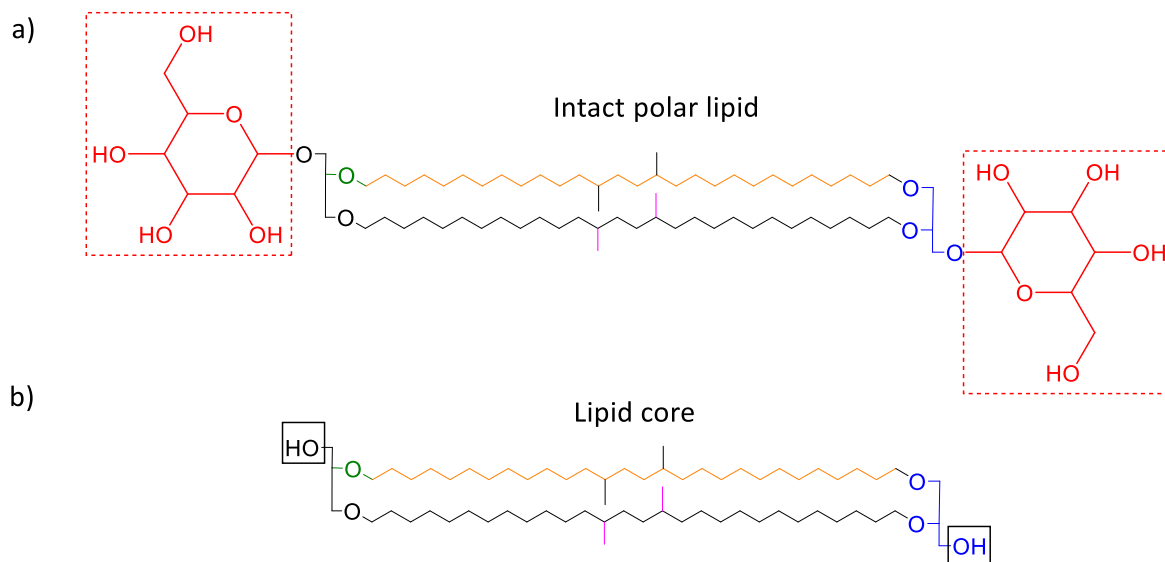


Figure 1.5. Structure of a branched GDGT: a) intact polar lipid with (red) polar head groups (monohexose); (green) ether group; (orange) alkyl chain; (blue) glycerol group; (pink) methyl branches of brGDGT; b) lipid core with (black) OH groups.

The archaeal GDGT structure presents two isoprenoid alkyl chains attached to the glycerol groups (called isoprenoid GDGTs or iGDGTs; **G1**; Figure 1.6). Archaea can incorporate five-membered rings in the alkyl chains of the GDGT lipids, denoted GDGT-1 to 8 according to the number of cyclopentane rings; GDGT-1 to GDGT-4 are the most common (**G2-G4**; Schouten *et al.*, 2007b). The introduction of rings is believed to be an adaptation to increasing temperatures experienced by the primary producers, making the membrane more rigid and hence more resistant to harsh conditions (Hanford and Peeples, 2002; Uda *et al.*, 2004). This correlation gave rise to proxies to reconstruct sea-surface temperature (Section 1.4.4.5; Schouten *et al.*, 2002). Tetraether lipids with 5-8 cyclopentane moieties have the most restricted occurrence, being present in Archaea thriving at low pH (<4), indicating that higher numbers of cyclopentane rings are essential for Archaea to survive in hot acidic environments (Schouten *et al.*, 2007b; Kaur *et al.*, 2015). The iGDGTs have been found in culture studies of hyperthermophilic and mesophilic Archaea (Thaumarchaeota, Crenarchaeota and Euryarchaeota; Schouten *et al.*, 2000; 2007b; 2008; Knappy *et al.*, 2012) and in sediments with aquatic and marine input (Schouten *et al.*, 2000; Weijers *et al.*, 2006a; Knappy, 2010). Therefore, iGDGTs represent production in aquatic conditions, although low-level production of iGDGTs in soils has been observed (DeLong, 1992; DeLong *et al.*, 1994; Hershberger *et al.*, 1996; Tierney and Russell, 2009; Fietz *et al.*, 2012; Li *et al.*, 2015).

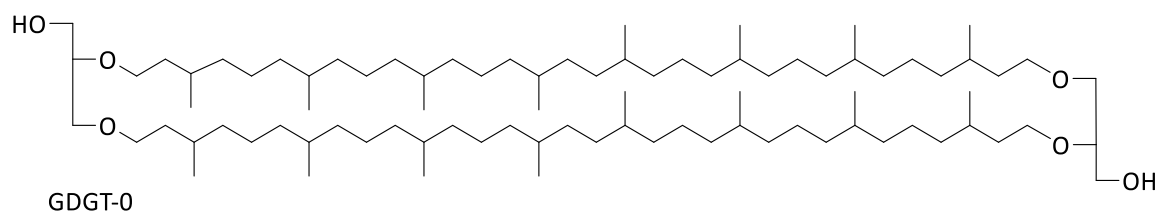


Figure 1.6. Structure of isoprenoid GDGT-0.

Chlorophyll pigments produced by photosynthetic organisms are another useful set of markers for aquatic conditions. Pigments can be markers for specific producers but also for the conditions of the water body at the time of deposition (Castañeda and Schouten, 2011). Chlorophylls comprise a tetrapyrrole macrocycle that has 18 π -electron system with porphyrin, chlorin and bacteriochlorin as basic structures (Figure 1.7). The macrocycle bears a unique 5-membered exocyclic ring (ring E; Figure 1.8). Various chlorophyll structures occur among photoautotrophs with differences in the structure of the tetrapyrrole macrocycle (Figure 1.7) and in the substituents in the periphery of the macrocycle (Figure 1.8; Scheer, 1991).

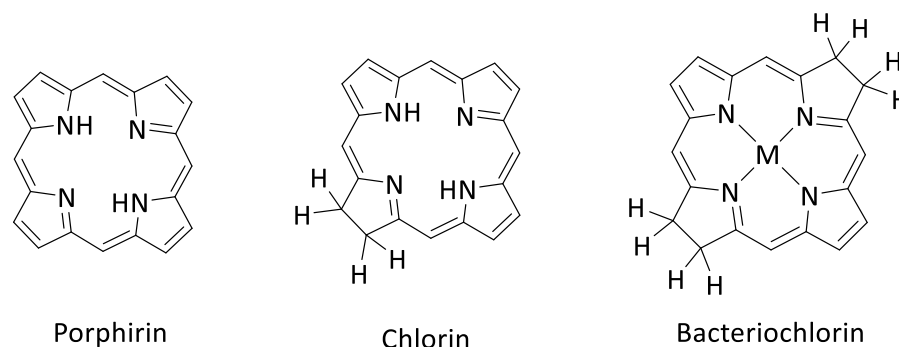


Figure 1.7. Structures of porphyrin, chlorin and bacteriochlorin tetrapyrrole macrocycle.

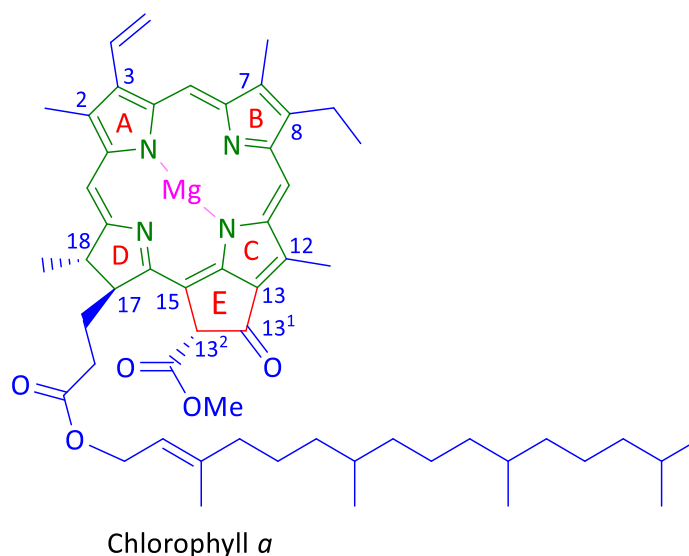


Figure 1.8. Structure of chlorophyll a: (green) tetrapyrrole chlorin macrocycle; (blue) substituents in the periphery of the ring showing the carbon number; (pink) chelating magnesium ion; (red) 5-membered exocyclic ring E.

Chlorophylls are present in all organisms carrying out oxygenic photosynthesis, while bacteriochlorophylls are used in anoxygenic photosynthesis. Chlorophyll *a* (Figure 1.8; **C1**) is present in all oxygenic photoautotrophs (*in vitro* chl *a* λ_{\max} 430, 662 nm; Scheer, 1991). Chl *b* (**C2**) is an accessory pigment in “green” organisms (i.e. prochlorophytes, green algae, green plants), the *in vitro* absorption spectra of chl *b* (λ_{\max} 456.9, 645.5 nm) reflecting the capability of the accessory pigment to broaden the light capture *in vivo* (Scheer, 1991). Chl *c* (**C13**) also exists as a common accessory pigment in brown algae, dinoflagellates, diatoms, cryptophytes and chrysophyta, in addition to chl *a* (Scheer, 1991). Chl *d* (**C14**) has been reported as the main pigment (>90%) in the cyanobacterium *Acaryochloris marina* (Miyashita *et al.*, 1996) and, with chl *f* (**C15**), in the cyanobacterium *Chlorogloeopsis fritschii* (Airs *et al.*, 2014), thus representing a good marker for these organisms. Bacteriochlorophyll (bchl) *a* (**B1**) is dominant in purple sulfur bacteria (Pfennig,

1977). Bacteriochlorophylls *c*, *d* and *e* (**B5-B7**) are dominant in green and brown sulfur bacteria (*chlorobiaceae*; Pfennig, 1977; Scheer, 1991). Purple bacteria tend to inhabit water bodies with sufficient light and in the presence of sulfide from OM fermentation processes. Such environments include stratified lakes, microbial mats in marine or hypersaline environments and extreme environments (for their temperature, pH, salinity; Madigan and Jung, 2009). Green sulfur bacteria possess pigments that allow them to live at low light intensities, so they can exist below a layer of purple bacteria (Pfennig, 1977). In stratified water columns, a microbial mat can consist of cyanobacteria carrying out oxygenic photosynthesis, as well as anoxygenic photoautotrophs such as purple bacteria above green bacteria (Pfennig, 1977; Squier *et al.*, 2002; Madigan and Jung, 2009).

Carotenoids are also photoreceptors and photoprotective pigments, extending the spectrum light absorption (Young, 1991). They are categorised in two groups: the carotenes or hydrocarbon carotenoids, such as β -carotene (Figure 1.9a; **R2**), and the xanthophylls, oxygenated carotenoids derived from carotenes, such as lutein (Figure 1.9b; **R3**; Rodriguez-Amaya and Kimura, 2004). Carotenoids are reported in plants, algae and bacteria; some structures are common in plants – α - and β -carotene (**R1-2**), violaxanthin (**R4**) and lutein (**R3**) – but others are more organism-specific, such as diadinoxanthin (**R5**) for dinoflagellates, and diatoxanthin (**R6**) for dinoflagellates and diatoms (Czeczuga, 1980; Leavitt, 1993; Takaichi, 2011).

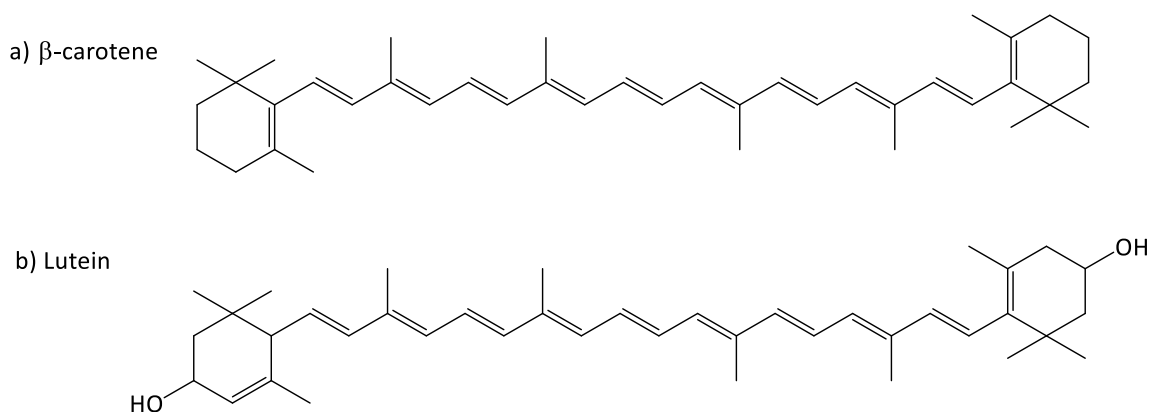


Figure 1.9. Structures of a) β -carotene (hydrocarbon carotenoid) and b) lutein (xanthophyll).

Heterocyst glycolipids (HG) are a class of compounds derived from the cell envelope of nitrogen-fixing cyanobacteria living in freshwater and brackish environments (Bauersachs *et al.*, 2009a). Structural modifications of the carbon chain length (C_{26-32}) and the nature and the position of the functional groups have shown correlation to specific orders of cyanobacteria (Figure 1.10): HG_{26} diols and keto-ols for Nostocaceae; HG_{28} triols and keto-diols for Rivulariaceae and some

Nostocaceae; HG₃₀ triols and keto-diols for Scytonemataceae and HG₃₂ triols and keto-ols for Stigonematales (Bauersachs *et al.*, 2009a; 2014; 2015a; Weber *et al.*, 2020). Linear correlation between surface water temperatures and the distribution of HG₂₆ diol and keto-ol, and HG₂₈, diol, keto-ol, triol and keto-diol prompted consideration of these markers for palaeothermometry (Section 1.4.4.10; Bauersachs *et al.*, 2015a).

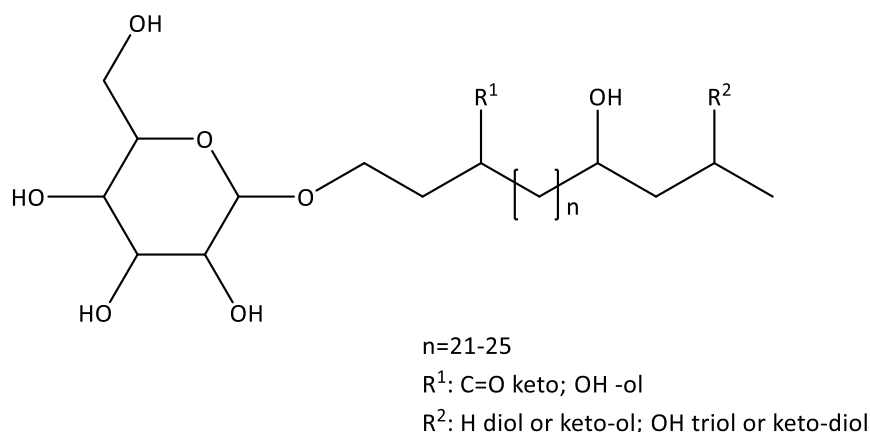


Figure 1.10. General structure of heterocyst glycolipid, showing the range of the carbon chain and the possible substituents; here the sugar group is hexose.

1.4.2. Markers of marine organic matter

Long chain unsaturated alkenones (n -C₃₇₋₃₉; Figure 1.11; **A6-A9**) are common markers of haptophyte algae in marine sediments (Marlowe *et al.*, 1984). Haptophytes *Emiliania huxleyi* showed the predominance of di- and tri-unsaturated C₃₇₋₃₈ alkenones (Volkman *et al.*, 1980) and *Isochrysis* sp. of C_{37:3} Me (**A7**) followed by C_{37:2} Me (**A6**) in lower amounts (Marlowe *et al.*, 1984). The unsaturation of C₃₇ alkenones (C_{37:2}, C_{37:3}, C_{37:4}) was correlated to growth temperature from culture studies, surface sediments and water columns and they have been used extensively as markers of sea-surface temperature (Section 1.4.4.7; Brassell *et al.*, 1986; Prahl and Wakeham, 1987; Müller *et al.*, 1998).

Long chain unsaturated alkenones have also been found in lakes generally (but not strictly) with high carbonate, sulfate, alkalinity and low salinity (Zink *et al.*, 2001; Sun *et al.*, 2004; D'Andrea and Huang, 2005; Pearson *et al.*, 2008; Toney *et al.*, 2010; Plancq *et al.*, 2018). In limnetic systems, the concentration of alkenone C_{37:4} (**A9**) had greater relative abundance to C_{37:3} and C_{37:2} than in marine environments, suggesting different source of alkenones and / or different mechanism(s) of controlling unsaturation in lacustrine and marine environments (Cranwell, 1985; Ficken and

Farrimond, 1995; Thiel *et al.*, 1997; Zink *et al.*, 2001; Sun *et al.*, 2004; D'Andrea and Huang, 2005; Bendle *et al.*, 2009).

A6 Alkenone C_{37:2} methyl

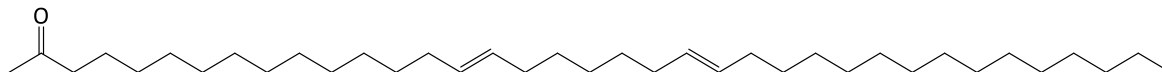
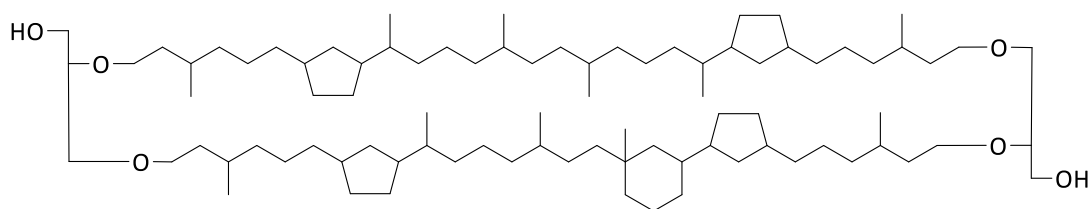


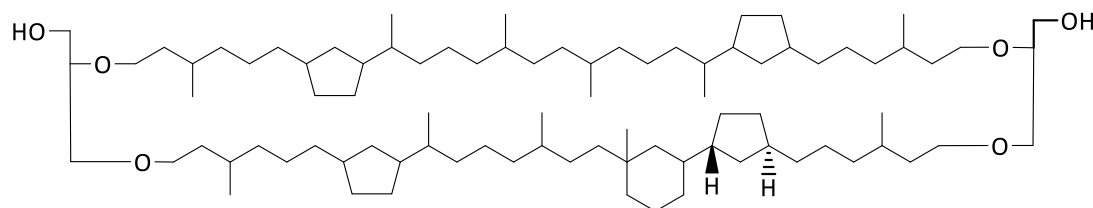
Figure 1.11. Structure of alkenone C_{37:2} methyl.

One specific marker of marine Archaea, Thaumarchaeota, is crenarchaeol, with a unique structure including four pentacyclic and one hexacyclic ring (Figure 1.12a; **G5**; Damsté *et al.*, 2002). Another component with the same molecular mass, eluting straight after crenarchaeol in normal phase high-performance liquid chromatography (NP-HPLC), and always in lower amounts compared to crenarchaeol (up to 5%) was detected in sediments (Damsté *et al.*, 2018). It was initially thought that this component was a regioisomer of crenarchaeol (cren'), presenting the OH groups in anti-parallel positions (Figure 1.12b; Damsté *et al.*, 2002). Further gas chromatography – mass spectrometry (GC-MS) and nuclear magnetic resonance (NMR) analyses concluded that the component was a stereoisomer of crenarchaeol with the pentacyclic ring adjacent to the hexacyclic ring with *cis* stereochemistry, compared to the *trans* stereochemistry in crenarchaeol (Figure 1.12c; **G5'**; Damsté *et al.*, 2018). Thaumarchaeota have also been detected in soils, although crenarchaeol occurred in low concentration compared to other soil markers (brGDGTs, see Section 1.4.3; Weijers *et al.*, 2006a).

a) Crenarchaeol



b) Crenarchaeol regioisomer



c) Crenarchaeol stereoisomer

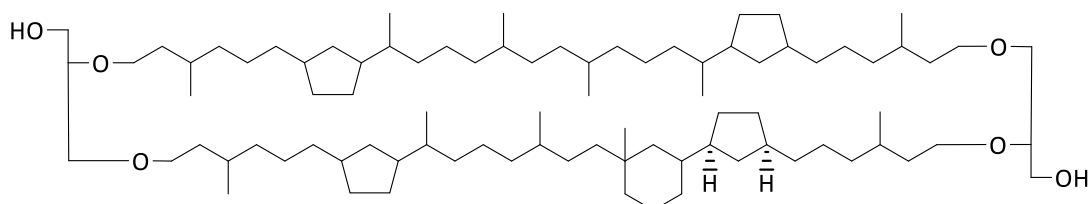


Figure 1.12. Structures of a) crenarchaeol, b) crenarchaeol regioisomer (after Damsté *et al.*, 2002), and c) crenarchaeol stereoisomer (after Damsté *et al.*, 2018).

1.4.3. Markers of terrestrial organic matter

While the main accumulations of terrestrial OM occur in soils and peats, transport of this OM to aquatic environments can occur, thus providing information about the hinterland. Plant waxes contain long chain fatty acids of even carbon number, resulting in an even carbon chain predominance that can be preserved in sediments (n -C₂₀₋₃₀; **A4**; Eglinton and Hamilton, 1967). Microbial decarboxylation of the fatty acids can occur, forming odd carbon number n -alkanes (n -1 rule, n -C₂₅₋₃₅; Figure 1.13; **A1**; Cranwell, 1973; Schirmer *et al.*, 2010). Reduction of the fatty acids produces less functionalised components such as long chain n -alkanones with odd carbon numbers (n -C₂₀₋₃₀; **A2**), n -alkanals (**A3**) and n -alkanols with even carbon numbers (n -C₂₀₋₃₀; **A5**; Figure 1.13; Eglinton and Hamilton, 1967). In plants n -alkanes, n -alkanones, n -alkanals, n -alkanols and n -alkanoic acids represent 70-80% of the total plant wax content, with n -alkanes as the most abundant components, followed by n -alkanols and n -alkanoic acids, and n -alkanones and n -alkanals in trace levels (Jetter *et al.*, 2000; Diefendorf *et al.*, 2015).

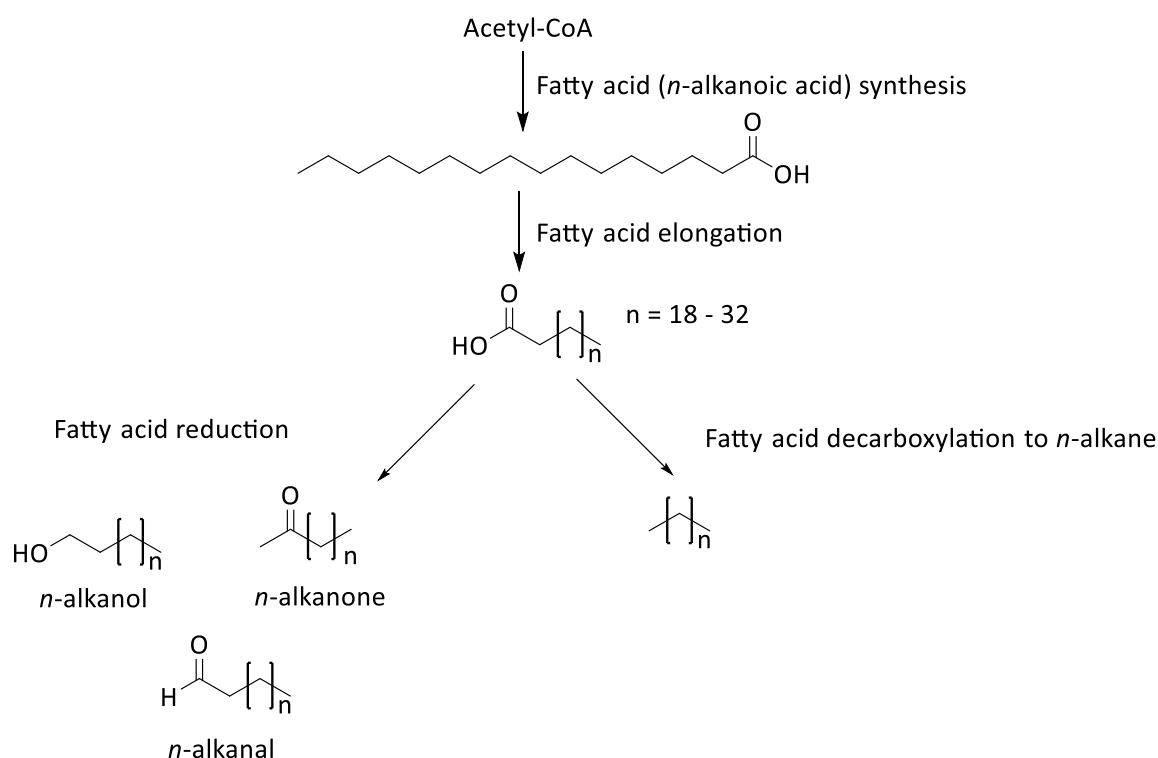


Figure 1.13. Biosynthetic pathway of formation of fatty acids in plant waxes and their microbial decarboxylation to form *n*-alkanes and reduction to form *n*-alkanols, *n*-alkanones and *n*-alkanals.

A wide range of sterols occur in terrestrial plants, examples include β -sitosterol (**T11**) and stigmasterol (**T12**; Volkman, 1986; Ficken and Farrimond, 1995; Thiel *et al.*, 1997; van Soelen *et al.*, 2010; Ronkainen *et al.*, 2013). It is not always possible to attribute a sterol to a specific plant source as particular structures occur in more than one species. The profile of leaf wax and membrane lipids can be used to distinguish terrestrial, reworked or aquatic OM input, but the specific vegetation origin cannot be reliably characterised (Volkman, 1986).

Branched GDGTs (brGDGTs; **G7**) have been attributed to soil bacteria (Schouten *et al.*, 2007b). The structures incorporate straight alkyl chains with increasing numbers of methyl branches and pentacyclic rings to maintain membrane integrity with changing temperature and pH, respectively (**G6-G14**; Figure 1.5; Damsté *et al.*, 2002; Schouten *et al.*, 2007b; Weijers *et al.*, 2007; Pei *et al.*, 2019). Correlation between increasing number of rings and soil pH and between methyl branches and soil temperature gave rise to proxies for reconstruction of soil pH and soil temperature (Section 1.4.4.6; Weijers *et al.*, 2007). Recent studies have shown that these are also produced (but in lower amounts) in aquatic environments (Tierney and Russell, 2009; Fietz *et al.*, 2012; Li *et al.*, 2015), although the distinction between the production of iGDGTs in aquatic environments and of brGDGTs in terrestrial settings is generally accepted.

1.4.4. Proxies based on molecular fossils

Culture and sediment studies of molecular fossils have shown correlations between certain structures and environmental parameters such as temperature and pH.

1.4.4.1. CPI for fresh terrestrial and reworking / algal OM based on *n*-alkanes

In ancient sediments, the carbon preference index (CPI, Equation 1.4), a ratio of odd over even long chain *n*-alkanes, can distinguish higher plant *n*-alkanes dominated inputs (CPI >5) from those containing reworked *n*-alkanes which lack the odd-over-even chain predominance (Bray and Evans, 1961). In immature sediments, CPI values <5 can reflect predominance of algal OM, especially when supported by other lines of evidence such as $\delta^{13}\text{C}$ and elemental analysis (Clark and Blumer, 1967; Ortiz *et al.*, 2004). Ratios of terrestrial to algal / reworked OM have been derived for *n*-alkanols, *n*-alkan-2-ols, *n*-alkanoic acids, *n*-alkanones and *n*-alkanals to study microbial degradation of the markers (Del Rio *et al.*, 1992; Xie *et al.*, 2004).

$$\text{CPI} = \frac{1}{2} \left(\frac{\text{C}_{25} + \text{C}_{27} + \text{C}_{29} + \text{C}_{31} + \text{C}_{33}}{\text{C}_{24} + \text{C}_{26} + \text{C}_{28} + \text{C}_{30} + \text{C}_{32}} + \frac{\text{C}_{25} + \text{C}_{27} + \text{C}_{29} + \text{C}_{31} + \text{C}_{33}}{\text{C}_{26} + \text{C}_{28} + \text{C}_{30} + \text{C}_{32} + \text{C}_{34}} \right)$$

(Equation 1.4)

1.4.4.2. P_{aq} to distinguish terrestrial and macrophyte OM based on *n*-alkanes

The proxy for aquatic macrophytes (P_{aq}) is based on the ratio of mid chain *n*-alkanes (*n*-C₂₃ and *n*-C₂₅) to long chain *n*-alkanes (*n*-C₂₉ and *n*-C₃₁). The former *n*-alkanes represent aquatic macrophyte OM and the latter represent plant waxes (Equation 1.5; Ficken *et al.*, 2000). A ratio below 0.1 suggests a dominant terrestrial OM input, 0.1-0.4 suggests emergent macrophyte OM, while values above 0.4 indicate dominance of submerged / floating macrophytes (Ficken *et al.*, 2000).

$$P_{aq} = \frac{[\text{C}_{23}] + [\text{C}_{25}]}{[\text{C}_{23}] + [\text{C}_{25}] + [\text{C}_{29}] + [\text{C}_{31}]}$$

(Equation 1.5)

1.4.4.3. ACL index for inputs of plant OM

The average chain length (ACL) proxy of *n*-alkanes describes the average number of carbon atoms based on higher plant markers *n*-C₂₇, *n*-C₂₉ and *n*-C₃₁ (Equation 1.6; Poynter and Eglinton, 1990). Variations in the proxy values have been correlated to vegetation (Cranwell, 1973), latitude, temperature and moisture availability (Gagosian *et al.*, 1987; Poynter and Eglinton, 1990). Cranwell

(1973) suggested that forest trees showed dominance of n -C₂₇, whereas the n -C₃₁ component dominated among grasses, resulting variable ACL values depending on the major source. More recent studies contest the distinction between woody and non-woody plant n -alkanes based solely on ACL values (Wang *et al.*, 2015) and the correlation between ACL and temperature (Wang *et al.*, 2018b). Therefore, it is imperative to use multiple biomarkers and proxies to validate changes in ACL in palaeoenvironmental assessments (Schemmel *et al.*, 2017; Wang *et al.*, 2018b).

$$ACL = \frac{(27 \times [C_{27}]) + (29 \times [C_{29}]) + (31 \times [C_{31}])}{[C_{27}] + [C_{29}] + [C_{31}]}$$

(Equation 1.6)

1.4.4.4. BIT index for discerning terrestrial and marine OM (brGDGTs and crenarchaeol)

Branched tetraether lipids (brGDGTs) are synthesised mainly by soil bacteria living in terrestrial soils; brGDGTs are also found in coastal marine sediments as a result of river transportation of sediment (Peterse *et al.*, 2009). Crenarchaeol (**G5**) is conventionally considered a marker of marine Archaea, although low level production was observed in soils (Weijers *et al.*, 2006a). The branched and isoprenoid tetraether (BIT) index (Equation 1.7) describes the ratio of brGDGTs (**G6**, **G9**, **G12**) and crenarchaeol (**G5**; Hopmans *et al.*, 2004). The BIT ratio can be used to trace terrestrial organic matter from erosion in water bodies. BIT values can go from 0.01, indicating a marine environment, to 1, which implies terrestrial OM origin (Hopmans *et al.*, 2004). Although low concentrations of crenarchaeol occur in some soils and brGDGTs can be produced in low amounts in aquatic environments, the BIT ratio is not largely affected by these biases as brGDGTs and crenarchaeol are dominant components in soils and marine environments, respectively (Weijers *et al.*, 2006a).

$$BIT = \frac{[Ia] + [IIa] + [IIIa]}{[Crenarchaeol] + [Ia] + [IIa] + [IIIa]}$$

(Equation 1.7)

1.4.4.5. TEX_{86} and TEX_{86}^L for calculating sea-surface temperature based on iGDGTs

As discussed in Section 1.4.1, increase in number of rings in iGDGTs is an adaptation to increasing temperatures experience by Archaea (Hanford and Peebles, 2002; Uda *et al.*, 2004). These differences among archaeal membrane lipid cores have been expressed by the TetraEther index of 86 carbons (TEX_{86}), which, through Equation 1.8, quantifies the relative abundances of particular iGDGTs (**G2-G4**) and the crenarchaeol stereoisomer (cren'; **G5'**; Damsté *et al.*, 2018). The TEX_{86} index value shows a correlation with sea-surface temperature (Equation 1.9; Schouten *et al.*, 2002).

$$\text{TEX}_{86} = \frac{[\text{GDGT 2} + \text{GDGT 3} + \text{cren'}]}{[\text{GDGT 1} + \text{GDGT 2} + \text{GDGT 3} + \text{cren'}]}$$

(Equation 1.8)

$$\text{TEX}_{86} = 0.015T + 0.28 \quad (\text{error } \pm 2.0^{\circ}\text{C})$$

(Equation 1.9)

In marine settings TEX_{86} can be influenced by pH, salinity and growth phase, thus potentially compromising the results (Elling *et al.*, 2014). Similarly, the index can be applied to lake systems, though factors such as pH, seasonality changes and terrestrial production of GDGTs need to be considered in its interpretation (Castañeda and Schouten, 2011). A comprehensive study of 46 globally distributed lakes showed that cren' was not always detected, and that there was a high variation in terrestrial input to lake sediments (BIT values from 0 to 1; Section 1.4.3.3; Powers *et al.*, 2010). Excluding the lakes with high terrestrial OM (BIT >0.5), the new calibration curve exhibited a much higher R^2 , showing that soil-derived iGDGTs have a high impact on TEX_{86} for temperature calculations in lakes (Powers *et al.*, 2010).

To obviate the lack of detection of cren' due to its low abundance in sediments, Kim *et al.* (2010) proposed two modified indices that include logarithmic formulae for calculating $\text{TEX}_{86}^{\text{L}}$ (L for low temperature) and $\text{TEX}_{86}^{\text{H}}$ (H for high temperature) and their linear correlation to sea-surface temperature (SST; Equations 1.10, 1.11; Kim *et al.*, 2010). $\text{TEX}_{86}^{\text{L}}$ performs best for temperatures falling below 15°C , whereas $\text{TEX}_{86}^{\text{H}}$ is more reliable above 15°C ; in sediments where SSTs may fall below and above 15°C , $\text{TEX}_{86}^{\text{L}}$ shows a more reliable temperature estimate (Kim *et al.*, 2010). Both crenarchaeol (**G5**) and GDGT-0 (**G1**) are excluded from TEX_{86} , $\text{TEX}_{86}^{\text{L}}$ and $\text{TEX}_{86}^{\text{H}}$ because their high abundance in sediments can overpower the results.

$$\text{TEX}_{86}^{\text{L}} = \log\left(\frac{[\text{GDGT 2}]}{[\text{GDGT 1}] + [\text{GDGT 2}] + [\text{GDGT 3}]}\right)$$

$$\text{SST} = (67.5 \times \text{TEX}_{86}^{\text{L}}) + 46.9 \quad (\text{error } \pm 4.0^{\circ}\text{C})$$

(Equation 1.10)

$$\text{TEX}_{86}^{\text{H}} = \log \left(\frac{[\text{GDGT 2}] + [\text{GDGT 3}] + [\text{cren'}]}{[\text{GDGT 1}] + [\text{GDGT 2}] + [\text{GDGT 3}] + [\text{cren'}]} \right)$$

$$\text{SST} = (68.4 \times \text{TEX}_{86}^{\text{H}}) + 38.6 \quad (\text{error} \pm 2.5^{\circ}\text{C})$$

(Equation 1.11)

In order to test and prove the robustness of TEX_{86} calibrations, recent models have employed statistical approaches (Bayesian, Spatially-Varying Regression – BAYSPAR; Tierney and Tingley, 2014; 2015) and considered uncertainties and deviations between ancient and modern global GDGT distributions (Optimized Palaeothermometry from Tetraethers via Machine Learning model – OPTiMAL; Eley *et al.*, under review). The models consider TEX_{86} variations with temperature, but it is likely that ecological and sedimentary factors, still poorly understood, may also impact on GDGT distributions (Tierney and Tingley, 2014).

1.4.4.6. CBT index for soil pH and MBT index for mean annual air temperature based on brGDGTs

The cyclisation of branched tetraether (CBT) index is used to reconstruct soil pH (Equation 1.12; Weijers *et al.*, 2007; De Jonge *et al.*, 2014). It is based on the relative abundance of cyclopentane rings in brGDGTs (**G9**, **G10**, **G12**, **G13**).

$$\text{CBT} = -\log \frac{[\text{Ib}] + [\text{IIb}]}{[\text{Ia}] + [\text{IIa}]}$$

$$\text{CBT} = 3.33 - 0.38 \text{ pH} \quad (\text{error} \pm 0.7)$$

(Equation 1.12)

The MBT (methylation of branched tetraethers) index depends on the relative abundance of methylated brGDGTs in soil (**G6**, **G9-14**; Equation 1.13). A higher number of methyl groups were observed with increasing temperature, thus the MBT index can be used to reconstruct mean annual air temperature (MAAT; Weijers *et al.*, 2007). A significant correlation between MBT and CBT resulted in the use of both proxies to calculate MAAT (Equation 1.14).

$$MBT = \frac{[Ia] + [Ib] + [Ic]}{[Ia] + [Ib] + [Ic] + [IIa] + [IIb] + [IIc] + [IIIa]}$$

(Equation 1.13)

$$MBT = 0.122 + 0.187 \text{ CBT} + 0.020 \text{ MAAT} \quad (\text{error} \pm 4.8^{\circ}\text{C})$$

(Equation 1.14)

Further research on lake sediments, surface soils and peats resulted in modified MBT and CBT proxies, due to differences in brGDGT distributions according to environmental conditions and bacterial production (Tierney *et al.*, 2010; Peterse *et al.*, 2012; Foster *et al.*, 2016; Naafs *et al.*, 2017; Dang *et al.*, 2018). For example, the original MBT index has been modified due to poor MAAT agreement with data from lake sediments in polar locations and at high latitudes (Foster *et al.*, 2016). Application of the calibration for high latitudes to a thermokarst lake in Arctic Alaska showed a good correlation between MBT temperatures, alkenone sea surface temperature (Section 1.4.3.7), fossil midges and the presence of *Populus* tree species (Elvert *et al.*, 2016). This study confirmed Foster's assumption that the new calibration could be applied to other high latitude samples, with good results. New CBT and MBT calibrations were developed for application to peats globally due to the chemical differences of peat compared to mineral soils (Equations 1.15-1.18; Naafs *et al.*, 2017). Given the similarity in slope between the peat and mineral soil calibrations, brGDGTs production in peats responds to temperature changes similarly to brGDGTs from mineral soils (Equation 1.18; Naafs *et al.*, 2019). The relatively high errors related to CBT_{peat} and MBT_{peat} calibrations mean that these proxies are more suitable to reconstruct large environmental changes, such as rapid warming-cooling like Bølling-Allerød, Younger Dryas or glacial-interglacial cycles (Naafs *et al.*, 2019 and references therein), rather than small temperature oscillations.

$$CBT_{\text{peat}} = \log \frac{[Ib] + [IIa'] + [IIb] + [IIb'] + [IIIa']}{[Ia] + [IIa] + [IIIa]}$$

(Equation 1.15)

$$pH = 2.49 \text{ CBT}_{\text{peat}} + 8.07 \quad (\text{error} \pm 0.8)$$

(Equation 1.16)

$$MBT_{\text{peat}} = \frac{[Ia] + [Ib] + [Ic]}{[Ia] + [Ib] + [Ic] + [IIa] + [IIb] + [IIc] + [IIIa]}$$

(Equation 1.17)

$$MBT_{\text{peat}} = 0.44 + 0.02 \text{ MAAT} \quad (\text{error} \pm 4.7^{\circ}\text{C})$$

(Equation 1.18)

1.4.4.7. U_{37}^k and $U_{37}^{k'}$ sea-surface temperatures based on long chain alkenones

The first biomarker-based calibration to calculate past sea-surface temperature was established using the U_{37}^k index based on di-, tri- and tetra-unsaturated long chain alkenones C_{37} originating from the marine coccolithophore *Emiliania huxleyi* (Equation 1.19; Brassell *et al.* 1986) and applicable to oceanic particulate matter (Prahl and Wakeham, 1987). Further experiments excluded the tetraunsaturated alkenone because it is rarely detected in marine sediments and because it affects the index only when growth temperature is $<15^{\circ}\text{C}$ (Prahl and Wakeham, 1987). The later $U_{37}^{k'}$ index resulted in a linear calibration (Equation 1.20; Prahl and Wakeham, 1987). Subsequent studies, widening the range of surface sediments studied, resulted in calibrations remarkably similar to the one from Prahl and Wakeham (1987; Müller *et al.*, 1998; Conte *et al.*, 2006). Application of the marine calibration to lacustrine settings has been suggested (Zink *et al.*, 2001), but uncertainties remain due to the high variety in haptophyte species and general predominance of $C_{37:4}$ over $C_{37:2}$ resulting in unrealistic temperatures. Nevertheless, relative temperature changes can be suggested from alkenone calibrations in lake sediments (Castañeda and Schouten, 2011).

$$U_{37}^k = \frac{[C_{37:2}] - [C_{37:4}]}{[C_{37:2}] + [C_{37:3}] + [C_{37:4}]}$$

(Equation 1.19)

$$U_{37}^{k'} = \frac{[C_{37:2}]}{[C_{37:2}] + [C_{37:3}]}$$

$$U_{37}^{k'} = 0.033 T + 0.044 \quad (\text{error} \pm 1.5^{\circ}\text{C})$$

(Equation 1.20)

1.4.4.8. Proxies for pH and temperature based on 3-hydroxylated fatty acids

In addition to the linear fatty acids described in sections 1.4.1 and 1.4.3, hydroxylated fatty acids (FA) have been reported in sediments. 3-hydroxy FA (3-OH-FA or β -FA; Figure 1.14a) have been reported in aquatic and terrestrial settings as the main constituents of the cell wall of Gram-negative bacteria (Cranwell, 1982; Parker *et al.*, 1982; Wollenweber and Rietschel, 1990; Keinänen *et al.*, 2003; Wakeham *et al.*, 2003; Wang *et al.*, 2016; Huguet *et al.*, 2019; Yang *et al.*, 2020).

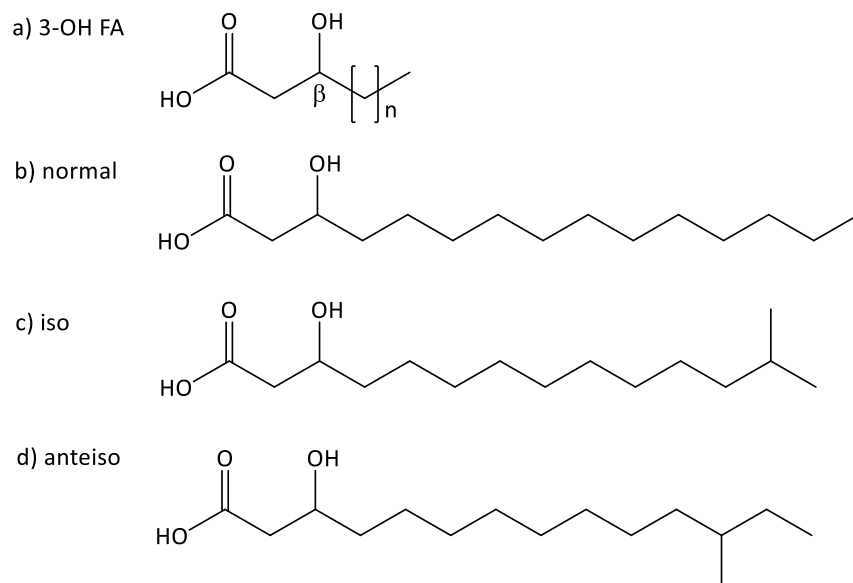


Figure 1.14. a) General structure of 3-hydroxy fatty acid (3-OH FA) showing the β carbon; b) normal carbon chain; c) iso carbon chain; d) anteiso carbon chain.

Soil pH showed a moderate correlation with the ratio of *iso* (Figure 1.14c) and *anteiso* (Figure 1.14d) to *normal* (Figure 1.14b) 3-OH fatty acids (RIAN; equation 1.21; Wang *et al.*, 2016). Thus, a method for pH estimation was proposed based on calibrations using regional mountain soils (Wang *et al.*, 2016; Huguet *et al.*, 2019).

$$\text{RIAN} = -\log \frac{[\text{iso}] + [\text{anteiso}]}{[\text{normal}]}$$

(Equation 1.21)

Weak correlations between the ratio of *anteiso* to *normal* (RAN) 3-OH fatty acids (with chain lengths C_{15} and C_{17}) and mean annual air temperatures, and strong correlation between 3-OH FA C_{13} and sea-surface temperature, led to the proxies RAN_{13} , RAN_{15} and RAN_{17} (equations 1.22-1.24) being proposed, with calibration being based on temperate and tropical soils (Wang *et al.*, 2016; Huguet *et al.*, 2019; Wang *et al.*, 2020). Initial applications of the proxies show the need for further research

to study the distribution of 3-OH FA under widely different environmental conditions and timescales (Wang *et al.*, 2018a; Li *et al.*, 2019; Pei *et al.*, 2019). Ultimately, the applicability of these temperature and pH proxies need to be assessed on a global scale and their applicability to palaeoenvironmental studies tested.

$$\text{RAN}_{13} = \frac{\text{anteiso } C_{13}}{\text{normal } C_{13}}$$

$$\text{SST} = e^{3.75 - (0.47 \times \text{RAN}_{13})} \text{ (error } \pm 2.55^\circ\text{C)}$$

(Equation 1.22)

$$\text{RAN}_{15} = \frac{\text{anteiso } C_{15}}{\text{normal } C_{15}}$$

(Equation 1.23)

$$\text{RAN}_{17} = \frac{\text{anteiso } C_{17}}{\text{normal } C_{17}}$$

(Equation 1.24)

1.4.4.9. Diol index to distinguish freshwater and marine OM

Long chain diols (C_{24-36}) have been reported in aquatic sediments and are thought to be produced by Eustigmatophyceae (Versteegh *et al.*, 1997; Volkman *et al.*, 1998; 1999). A distinctive difference in the proportions of the 1,15- C_{30} and 1,15- C_{32} diols (Figure 1.15) in freshwater and marine settings was observed, giving rise to formulation of the diol index (DI; Equation 1.25). Freshwater samples and algal cultures showed lower DI values (1-67) than open marine environments (DI above 79), suggesting applicability in distinguishing freshwater and marine OM sources (Versteeg *et al.*, 1997; 2000; van Soelen *et al.*, 2010).

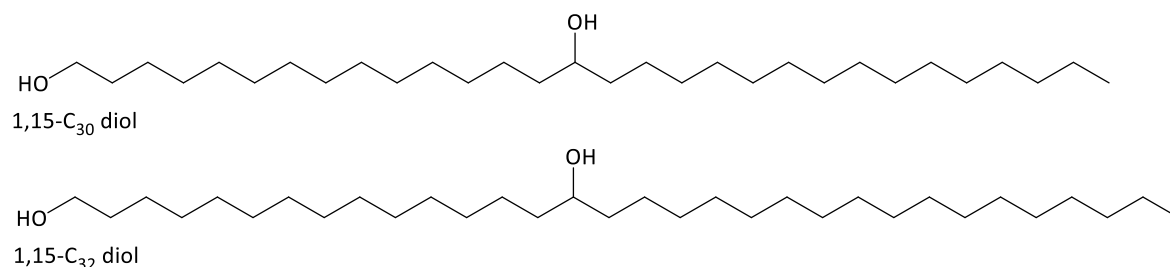


Figure 1.15. Structures of 1,15- C_{30} and 1,15- C_{32} diols.

$$\text{Diol index} = 100 \times \frac{[1,15 \text{ C}_{30} \text{ diol}]}{[1,15 \text{ C}_{30} \text{ diol}] + [1,15 \text{ C}_{32} \text{ diol}]}$$

(Equation 1.25)

1.4.4.10. Surface water temperature calculated with heterocyst glycolipids (HG)

Culture studies of three heterocystous cyanobacteria showed a decrease in the relative amount of the ketone HG compared to the diol component with higher temperatures (Figure 1.10; Bauersachs *et al.*, 2009a). This resulted in the definition of the HG₂₆ index (Equation 1.26), with values inversely proportional to temperature. Positive correlations of heterocyst diol index of 26 and 28 carbons (HDI₂₆ and HDI₂₈, respectively) and heterocyst triol index of 28 carbons (HTI₂₈) with surface water temperature were reported for Lake Schreventeich (Germany) and appropriate equations derived (Equations 1.27-1.29; Bauersachs *et al.*, 2015a). Although the HG proxies for surface water temperature showed consensus with other biomarker-derived temperatures (Sollai *et al.*, 2017; Klages *et al.*, 2020; Weber *et al.*, 2020), deviations indicate that further culture studies are needed to provide accurate temperatures (Sollai *et al.*, 2017).

$$\text{HG}_{26} = \frac{\text{HG}_{26}\text{keto ol}}{\text{HG}_{26}\text{diol} + \text{HG}_{26}\text{keto ol}}$$

(Equation 1.26)

$$\text{HDI}_{26} = \frac{\text{HG}_{26}\text{diol}}{\text{HG}_{26}\text{diol} + \text{HG}_{26}\text{keto ol}}$$

$$\text{HDI}_{26} = (0.0224 \times \text{SWT}) + 0.4381 \quad \text{error} \pm 0.27^\circ\text{C}$$

(Equation 1.27)

$$\text{HDI}_{28} = \frac{\text{HG}_{28}\text{diol}}{\text{HG}_{28}\text{diol} + \text{HG}_{28}\text{keto ol}}$$

$$\text{HDI}_{28} = (0.0405 \times \text{SWT}) + 0.0401 \quad \text{error} \pm 0.30^\circ\text{C}$$

(Equation 1.28)

$$\text{HTI}_{28} = \frac{\text{HG}_{28}\text{triol}}{\text{HG}_{28}\text{triol} + \text{HG}_{28}\text{keto diol}}$$

$$\text{HTI}_{28} = (0.0288 \times \text{SWT}) + 0.2292 \quad \text{error} \pm 0.34^\circ\text{C}$$

(Equation 1.29)

1.4.5. Analysis of molecular fossils

Molecular fossils extracted from sediments and soils are routinely analysed by chromatographic separation with detection by mass spectrometry (MS) or diode array detection (DAD; Table 1.1) for components having a chromophore.

1.4.5.1. Analysis of steranes, sterols and alkan-es, -als, -ones, -ols, -oic acids, long chain diols, 3-OH fatty acids

Apolar lipid components (*n*-alkanes, *n*-alkanones, alkenones, *n*-alkanals, steranes) can be readily analysed by gas chromatography-flame ionisation detection (GC-FID) and gas chromatography-mass spectrometry (GC-MS; Table 1.1; Marlowe *et al.*, 1984; Poynter and Eglinton, 1990). The alcohol groups on *n*-alkanols, sterols, diols and the acid groups on *n*-alkanoic acids and 3-OH fatty acids are typically derivatised to introduce silyl and methyl groups, respectively, before GC analysis (Table 1.1; Eglinton and Hamilton, 1967; Volkman, 1986; van Soelen *et al.*, 2010; Wang *et al.*, 2016).

1.4.5.2. Analysis of GDGTs and HG

The most common method for separation of both core and intact polar GDGTs is by normal phase high-performance liquid chromatography hyphenated with atmospheric pressure chemical ionisation mass spectrometry (NP HPLC-APCI-MS; Table 1.1; Hopmans *et al.*, 2000; Sturt *et al.*, 2004). To elucidate the structures of the dialkyl chains, ether cleavage of the glycerol moiety is carried out and the remaining apolar alkyl chains are analysed by GC-MS (Table 1.1; Morii *et al.*, 1998; Pearson *et al.*, 2004; Weijers *et al.*, 2006b; Zhu *et al.*, 2014). Like all molecular fossils, GDGTs occur in trace amounts in sediments, thus detection is challenging and places limits on their use as specific proxies in palaeoenvironmental studies. Although recent advances in MS have improved analytical capabilities, detection limits are still an issue (Schouten *et al.*, 2007a; Basse *et al.*, 2014; Elling *et al.*, 2014; Zhu *et al.*, 2014; Naafs *et al.*, 2017).

Heterocyst glycolipids (HG) are analysed using normal phase HPLC coupled with electrospray ionisation mass spectrometry (HPLC-ESI-MS; Bauersachs *et al.*, 2009b). Similarly to GDGTs, elucidation of the carbon chain is carried out by derivatising the alcohol groups prior to GC-MS analysis (Bauersachs *et al.*, 2009b).

1.4.5.3. Analysis of pigments

Prior to analysis, methylation of free acid groups on chls and bchls is carried out to improve chromatography peak shape and prolong sample storage life (Table 1.1; Naylor and Keely, 1998).

Pigments and carotenoids are routinely analysed by reversed-phase HPLC with diode array detection (DAD) and MS (Airs *et al.*, 2001). The relative retention time, HPLC-DAD absorption in the UV-vis region (350-800 nm) and MS spectra can confirm the identification of chlorophylls (Airs *et al.*, 2001). Chlorophylls present the main absorption band (Soret band) at around 400 nm and a second absorption (Q_y band) at around 660 nm in the absorption spectrum; bacteriochlorophylls, due to their macrocyclic structure (bacteriochlorin), absorb at around 360 nm (Soret band) and 770 nm (Q_y band; Hendry *et al.*, 1987). The intensity of the bands, the ratio of the Soret and Q_y bands and the wavelengths of their maximal absorbance depend on the structure of tetrapyrrole macrocycle and the substituents in the periphery of this, thus the UV-vis absorption is diagnostic of chlorophyll and bacteriochlorophyll pigments.

Most carotenoids show three absorption bands at wavelengths in the violet-to-green region of the visible spectrum (350-500 nm). The absorption is dependent on the degree of double bond conjugation, with higher maximum absorbance with greater conjugation (Rodriguez-Amaya and Kimura, 2004). In addition to identifying carotenoids by UV-vis absorption wavelengths, the shape of the fine structure of the spectrum is characteristic of the molecular structure of carotenoids. Increasing double bond conjugation results in more defined absorption peaks, i.e. more defined fine structure and marked difference in the relative intensities of absorption bands. The presence of hydroxy groups on the structure does not affect the UV-vis spectrum, but has an impact on the polarity of the pigments, thus evident in the retention time from the HPLC chromatogram (Rodriguez, 2001). Mass spectrometric data can also help in identifying chlorophylls and carotenoids, though most carotenoids ionise poorly under APCI conditions (Airs *et al.*, 2001). NMR analysis of individual pigments may enable elucidation of their structures; however, each compound needs to be separated from the rest of the pigments and purified (Rodriguez, 2001).

Table 1.1. Summary of chemical derivatisation and analytical techniques to analyse the molecular fossils described in this section.

Molecular fossil	Derivatisation	Analysis	Reference
<i>n</i> -alkanes, <i>n</i> -alkanones, alkenones, <i>n</i> -alkanals	No	GC-FID, GC-MS	Marlowe <i>et al.</i> , 1984; Poynter and Eglinton, 1990
<i>n</i> -alkanols, sterols, long chain diols <i>n</i> -alkanoic acids, 3-OH fatty acids	Silylation of alcohol groups. Methylation of acid groups	GC-FID, GC-MS	Eglinton and Hamilton, 1967; Volkman, 1986; van Soelen <i>et al.</i> , 2010; Wang <i>et al.</i> , 2016
Chlorophyll pigments	Methylation of acid groups	HPLC-UV, HPLC-DAD, HPLC-MS	Airs <i>et al.</i> , 2001
Carotenoids	No	HPLC-UV, HPLC-DAD	Airs <i>et al.</i> , 2001
GDGTs	No (Yes, in dialkyl chain studies)	HPLC-MS (GC-MS)	Hopmans <i>et al.</i> , 2000; Sturt <i>et al.</i> , 2004
Heterocyst glycolipids	No (Yes, in alkyl chain studies)	HPLC-ESI-MS (GC-MS)	Bauersachs <i>et al.</i> , 2009b

1.5. Transformation of molecular fossils in the natural environment

Section 1.4 highlighted the characteristics of molecular fossils and their proxies. As with traditional microfossils, molecular fossils are prone to transformations in the natural environment. Transformation processes have been well studied and corroborate the valuable information that molecular fossils can contribute to palaeoenvironmental and past sea-level studies, establishing links between sedimentary molecular fossils and the original precursor (Poynter and Eglinton, 1991).

Transformations can begin during senescence of the producer organisms, during transport and settling of debris, after reaching the sediment-water interface, and after lithification (Killops and Killops, 1993). With increasing depth of burial, biological markers can become heavily transformed largely from increasing temperatures (Killops and Killops, 1993). Such thermal transformations are

not relevant to the processes that affect the unconsolidated sediment studied in this project. Thus, OM is expected to have experienced initial transformations during transport, sinking and early deposition, primarily from autolytic enzyme activity, microbial attack and heterotrophic activity (Cranwell, 1976; 1982; Hendry *et al.*, 1987; Poynter and Eglinton, 1991; Killops and Killops, 1993; Meyers and Ishiwatari, 1993; Meyers, 1997; Volkman *et al.*, 2000; Castañeda and Schouten, 2011; Schouten *et al.*, 2013). Preservation of OM in sediments can depend on the extent of primary productivity, the sinking rate, the position of the oxic-anoxic interface and the nature and extent of microbial reworking (Didyk *et al.*, 1978). Figure 1.16 represents a simplified version of three sedimentary environments with variable depths of the oxic-anoxic interface. In scenario A, the water column is oxic and the oxic-anoxic interface is at the sediment-water interface (Figure 1.16). In this setting, the molecular fossils (from *in situ* production and allochthonous contributions through runoff) are subject to transformation by herbivores and / or oxidation in the oxic zone. Detritus reaching the sediment is further degraded by soil aerobic and anaerobic bacteria (Killops and Killops, 1993). Under these conditions extensive transformation may occur, aided by high oxygen levels, resulting in very low amounts of organic material being preserved in the sediments (Didyk *et al.*, 1978). If the oxic-anoxic boundary is above the sediment-water interface (scenario B), preservation of OM is higher than for scenario A due to the more limited extent of oxidation and lower extent of heterotrophic activity (Figure 1.16; Didyk *et al.*, 1978). Anaerobic bacteria can degrade OM in absence of oxygen though these processes are not as efficient as their aerobic counterparts (Killops and Killops, 1993). Optimal preservation is obtained in highly anoxic environments where OM is minimally altered during transport through the water column and after deposition (scenario C; Figure 1.16; Didyk *et al.*, 1978; Killops and Killops, 1993). The Black Sea represents a basin largely under anoxic conditions, where the chemocline occurs around 100-150 m depth (van der Meer *et al.*, 2008). Organic carbon concentrations and hydrogen index were employed as a measure of hydrogen richness and degree of preservation of OM (Arthur and Dean, 1998). Arthur and Dean (1998) identified enhanced preservation of organic matter that can be found only in low-energy and anoxic environments in Holocene sediments from the Black Sea.

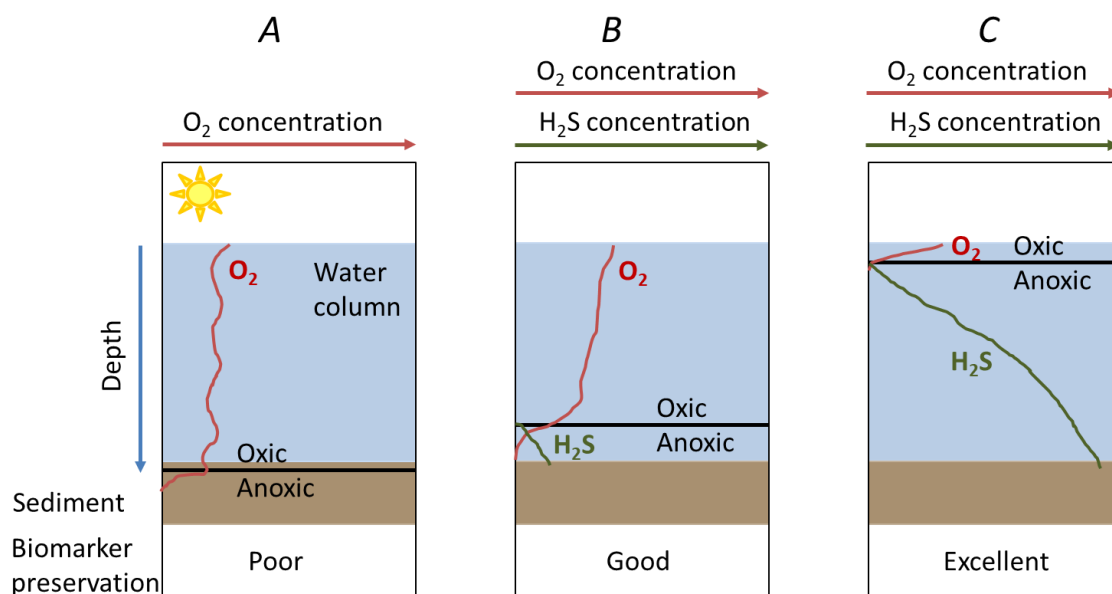


Figure 1.16. Representation of three sedimentary environments: A) oxic water column with oxic-anoxic transition in the sediment; B) oxic water column with anoxia in the bottom waters; C) oxic surface waters and extensive anoxia in the water column (redrawn from Didyk *et al.*, 1978).

The structure and the nature of different classes of molecular fossil contribute to their preservation potential. The molecules discussed in Section 1.4 are preserved and widespread in almost all sediments worldwide and spanning many geological eras. Alkanes are among the most refractive biomarkers, and hence largely remain unaffected by early diagenetic processes. Initial, biologically-mediated, transformation processes of chemical biomarkers include defunctionalisation, such as loss of functional groups on the periphery of the tetrapyrrole ring in chlorophyll pigments (Figure 1.17; Keely, 2006) and loss of the polar head groups in GDGTs (Figure 1.5; Sturt *et al.*, 2004).

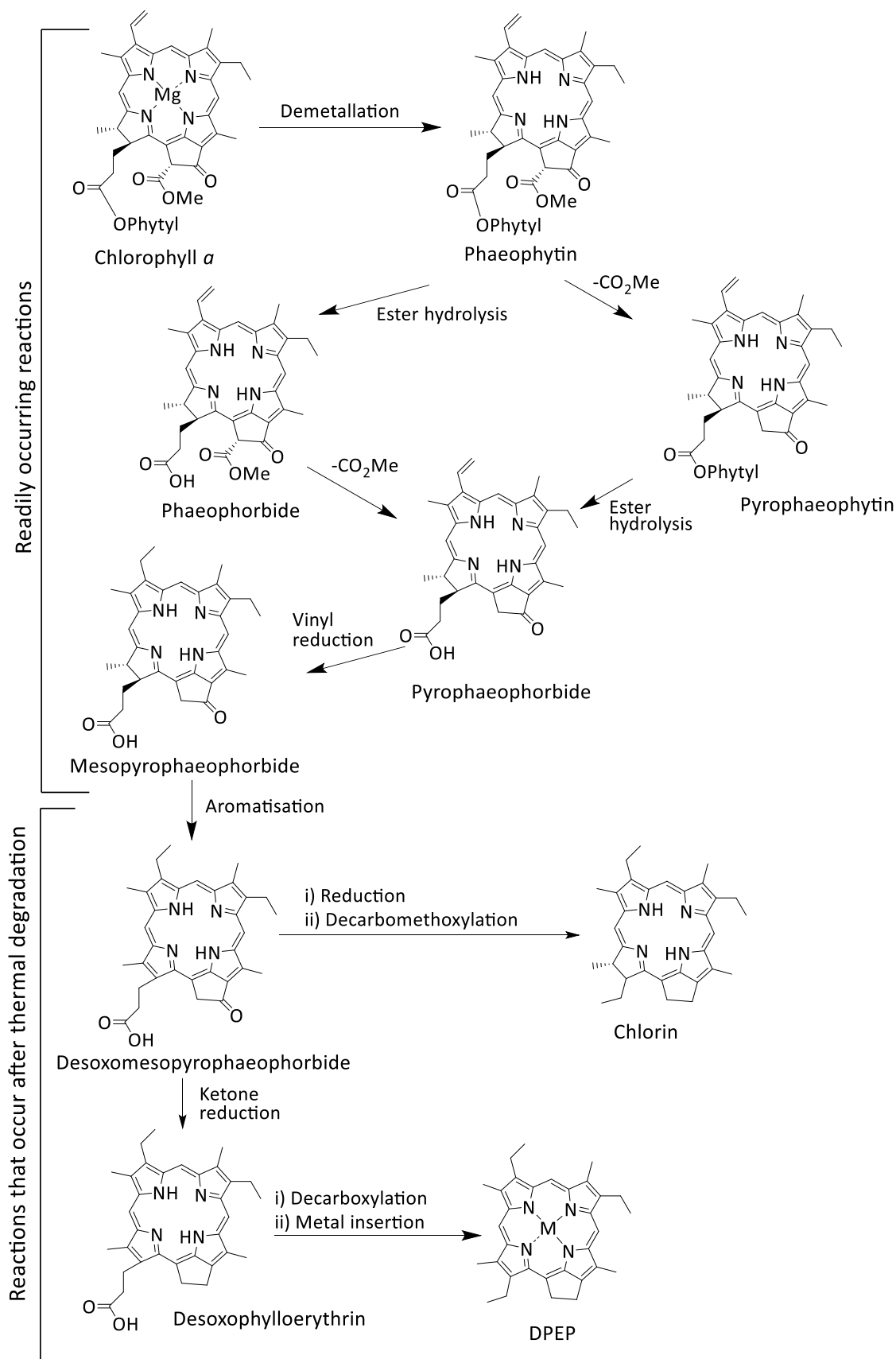


Figure 1.17. Degradation of chlorophyll *a* showing the modifications that occur in the early and later stages of diagenesis (adapted from Keely et al., 1990).

Chlorophyll pigments of terrestrial origin are almost completely degraded by autolytic oxidative transformations that take place in leaves during leaf senescence. Thus, sedimentary pigments can be regarded as representative of autochthonous algal and bacterial sources of OM (Gorham and Sanger, 1967; Keely, 2006). Photo-oxidative conditions in the water column can destroy the chlorophyll macrocycle and destroy most of the pigment prior to sedimentation (Hendry *et al.*, 1987; Keely, 2006). Studies of the transformations of tetrapyrrole pigments and carotenoids showed that the former are more susceptible to modification (Cranwell, 1976; Leavitt, 1988). Carotenoids are destroyed under aerobic conditions and enhanced microbial activity but are unaffected by illuminated anoxic conditions (Moss, 1968; Leavitt, 1988). Leavitt (1988) noted that xanthophylls are more susceptible to degradation than hydrocarbon carotenes (Figure 1.9) owing to their structural differences. Thus, rapid sinking under anaerobic conditions enhances preservation of chlorophyll pigments and carotenoids. Steryl chlorin esters (SCE), pigments comprising sterols esterified to pyropheophorbide (**C12**), are markers of herbivore grazing. Evidence for the incorporation of phytoplankton chlorophyll *a* and *b* into SCEs during zooplankton herbivory has been presented from studies of marine and lake sediments, plankton blooms and sediment trap material (Pearce *et al.*, 1993; Harradine *et al.*, 1996).

Microbially-mediated reduction of double bonds in sterols to form stanols (Figure 1.18) has been observed in the water column and in sediments, particularly in suboxic and anoxic waters (Gaskell and Eglinton, 1975; Wakeham, 1989; Nakakuni *et al.*, 2017). An intermediate product of microbial reduction from sterols to stanols are stanones (ketone steroids), although both stanols and sterones can also occur *in vivo* in biological organisms (Figure 1.18; Mackenzie *et al.*, 1982; Del Rio *et al.*, 1992; Rontani and Volkman, 2005).

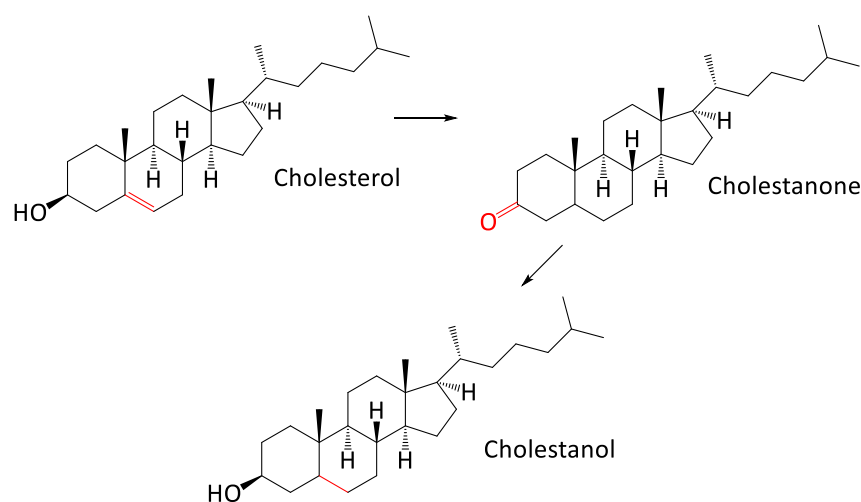


Figure 1.18. Degradation of sterols (here cholesterol shown) to stanols (cholestanol) with sterones (cholestanone) as intermediate.

1.6. Molecular fossil applications to study sea-level change

Microfossil analyses dominate the research on past sea level, but these markers are sometimes absent or in low numbers. These factors can preclude the reliability and accuracy of certain sea-level studies. For example, diatoms were poorly preserved in certain Holocene sediments from the Isle of Man, providing only a tentative interpretation to palaeoenvironmental changes (Gonzalez *et al.*, 2000). A record of sea level was established in selected horizons based on interpretation of the better-preserved pollen evidence (Gonzalez *et al.*, 2000). Molecular fossils, some of which are discussed in this chapter (Section 1.4), are routinely employed to reconstruct palaeoenvironmental conditions. Their application to determining sea-level change has, however, largely been overlooked. The ubiquitous, refractory and often abundant nature of molecular fossils means that they have the potential to contribute in reconstructing past sea-level change, including in situations where microfossils are not well preserved. Few studies report the use of molecular fossils to investigate transgressive and regressive events.

Zhang *et al.* (2010) noted that a decrease in $\delta^{13}\text{C}$ values coincided with decreasing *n*-alkane CPI values (<5) meaning that there was a noticeable increase in marine algal OM deposition in the Okinawa Trough (East China Sea) during the Holocene. The study suggested the occurrence of a transgressive event, considered to have happened rapidly due to increasing sediment grain size (Zhang *et al.*, 2010).

Increasing P_{aq} values above 0.2 were correlated with an increase in aquatic OM input and variable height of the water table. For example, higher water levels in peats and in sediments were observed as a result of Holocene climate changes (Schemmel *et al.*, 2017) and deglaciation events (Seki *et al.*, 2009). Another study in the Taiwan Strait observed two periods with a decrease in $\delta^{13}\text{C}$ values, an increase in the P_{aq} ratio and high concentration of long chain alkenones indicative of marine conditions from rising sea level (Li *et al.*, 2017). Radiocarbon and OSL dating confirmed that the two transgressions occurred in MIS 5e (Late Pleistocene; Appendix 2) and MIS 1 (Mid-Late Holocene; Li *et al.*, 2017).

Sea-level fluctuations on the west coast of South Africa were identified by *n*-alkanes, stable carbon isotopes and pollen (Carr *et al.*, 2015). High P_{aq} and low $\delta^{13}\text{C}$ values identified marine conditions (8.5-4.0 ka), followed by the establishment of a freshwater environment (4.0-2.5 ka). In the Late Holocene (2.5-0.9 ka), a decrease in P_{aq} , TOC and $\delta^{13}\text{C}$ values was indicative of drier conditions, with an increase in higher plant *n*-alkanes, CPI and ACL values. Subsequent increase in TOC, P_{aq} and $\delta^{13}\text{C}$

values and decrease in CPI, ACL and C/N ratios pointed towards wetter conditions and freshwater inundations in the last 700 years (Carr *et al.*, 2015).

Alkenone concentrations and chain length distributions reliably suggested a distinction between marine / brackish and lacustrine sediments in shallow coastal environments in Scotland (Bendle *et al.*, 2009). The study concluded that the percentage of alkenone C_{37:4} (**A9**) is an efficient marker for recognising the origins of sedimentary OM, with higher values (15-17%) reported in freshwater conditions (Ficken and Farrimond, 1995; Bendle *et al.*, 2009). Low TOC and C/N values during marine phases can support information gathered from alkenones and microfossil evidence (Ficken and Farrimond, 1995; Bendle *et al.*, 2009).

A Late Holocene transgression in Tampa Bay (United States) was identified by pollen, diatoms and molecular fossils (van Soelen *et al.*, 2010). In this research, the increase in diol index (Section 1.4.3.9) and in concentration of certain long chain alkenones, markers of exclusively haptophyte algae, identified the sea-level increase. The agreement between microfossil and molecular fossils provided a more detailed and robust interpretation of the palaeoenvironment (van Soelen *et al.*, 2010).

An increase in the concentration of marine crenarchaeol (**G5**) and decrease in soil brGDGTs (**G6-14**) resulted in a decrease in BIT from >0.8 – in the terrestrial part of a core from the Kara Sea (Arctic Ocean) – to <0.2 after the Holocene transgression in the Kara Sea (De Jonge *et al.*, 2016). *In situ* production of brGDGTs and erosion could also explain the variation in BIT, but when taken in conjunction with an increase in the absolute concentration of crenarchaeol (**G5**), the decrease in BIT values indicates sea-level rise (De Jonge *et al.*, 2016).

Pigment analysis from Holocene sediments from the Antarctic lake Kirisjes Pond identified a transgression based on the distribution of chlorophylls and bacteriochlorophylls (Squier *et al.*, 2002). Following a Holocene transgression, the freshwater lake, inhabited by oxygenic photosynthetic organisms, became a marine environment dominated by photic zone anoxia, recognised by high concentrations of bacteriochlorophyll *c* and *d* derivatives. Eutrophication as a result of increasing nutrient input from the transgression was likely the cause of the development of photic zone anoxia in the marine sediments (Squier *et al.*, 2002). A subsequent return of chlorophyll pigments and freshwater diatoms in the sediments suggests a regression and return to freshwater conditions in Kirisjes Pond (Squier *et al.*, 2002).

1.7. Summary and aims

The study of Quaternary sea-level change has been dominated by geophysical and palaeoecological proxies (Section 1.3), but more recently, interdisciplinary studies have coupled “traditional” methods with organic geochemical proxies, such as $\delta^{18}\text{O}$, $\delta^{13}\text{C}$ and C/N. In this chapter, the molecular fossils commonly used for studying palaeoclimatic changes have been discussed (Sections 1.4, 1.5) and few examples of their application to sea-level changes have been reported (Section 1.6). These refractory molecular fossils and proxies can reflect changes in origin of OM and represent terrestrial, aquatic and marine OM. Fluctuations in sea-surface and soil temperatures can provide estimates of a relative change in temperature from sea-level changes.

The main aim of this study was to develop an understanding of the changes in molecular fossil distributions during Quaternary transgressions, in order to assess the potential of the biomarker record for increasing our understanding of environmental responses to sea-level change. Multiple biomarker analysis, including sterols, long chain alkenones, GDGTs, chlorophyll pigments and *n*-alkanes, would be a powerful tool to help in the identification of these processes to reliably study sea level and palaeoenvironmental changes. To this end, the main objectives of this study were:

- To examine strategies to improve limits of detection and improve resolution of GDGTs when these markers are in low concentrations. Derivatisation of the alcohol groups with fluorescent tags was considered (Chapter 2);
- To study a Holocene transgression in a well-constrained core from the Loch of Stenness using the molecular fossils and proxies discussed in this chapter (Chapter 3);
- To apply molecular fossil studies to Pleistocene sediments from the Nar Valley (MIS 11 and / or MIS 9) and Woodston (near Peterborough, MIS 11) to test the applicability of molecular fossils for studying sea-level changes in older sediments, some of which have poor preservation of microfossils (Chapter 4);
- To elucidate the structure and suggest origins of unknown glycerolipids found in all of the sediments discussed in this thesis (Chapter 5).

Through this systematic approach, this thesis assesses the potential for the molecular fossil approach to provide a more detailed study of transgressive events.

2. Application of a modified Steglich esterification to alcohol lipid standards and glycerol dialkyl glycerol tetraether (GDGT) lipids from sediments

2.1. Introduction

Analysis of targeted biomarkers in soil is widely applied for reconstructing palaeoenvironments (Meyers, 1997; Castañeda and Schouten, 2011). Markers such as the glycerol dialkyl glycerol tetraether lipids (GDGTs; Sections 1.4.1-1.4.3) occur in complex sediment mixtures in trace amounts, presenting challenges for their detection and quantification (Schouten *et al.*, 2007a; Basse *et al.*, 2014; Elling *et al.*, 2014; Zhu *et al.*, 2014; Naafs *et al.*, 2017). The commonly used method to analyse GDGTs is normal phase (NP) high-performance liquid chromatography with mass spectrometry (HPLC-MS) with atmospheric pressure chemical ionisation (APCI; Hopmans *et al.*, 2000). APCI is preferred to the atmospheric pressure ionisation method of electrospray (ESI), due to APCI's higher ionisation efficiencies for GDGTs. However, the normal phase conditions for the separation require long equilibration times and frequent column back flushing during routine analysis of sediment extracts (Hopmans *et al.*, 2000).

The current challenges with detection and MS quantification of GDGTs (including the many low-abundant isomers such as crenarchaeol stereoisomer) mean that there is potential benefit from derivatisation of the GDGT hydroxyl groups with fluorescent head groups. This would allow a more accurate quantification method through HPLC with ultraviolet (UV) and fluorescence (FLD) detectors, as well as HPLC-MS, potentially increasing detection limits. Moreover, the fluorescent derivatives would have a higher degree of selectivity with only the fluorescing derivatives giving a response in a FLD. Analysis by HPLC-FLD would enable a relatively straightforward and lower-cost approach compared with MS. The derivatised GDGTs could benefit from lower equilibration time from reversed-phase (RP) HPLC, thereby also reducing the analysis time.

Derivatisation with fluorescent groups has been successfully applied to clinical samples containing lipophilic primary, secondary, tertiary and aromatic alcohols (Nelson, 2011) and to highly complex environmental samples, containing archaeal ether glycerolipids including GDGTs (Bai and Zelles, 1997), increasing the specificity and limit of detection. Previous studies on glycerolipids, lipophilic alcohols, hydrosteroids, amino acids and peptides showed lower limits of detection of derivative as opposed to native components (Goto *et al.*, 1983; Ohtsubo *et al.*, 1993; Bai and Zelles, 1997; Shangguan *et al.*, 2001). Following more recent developments in mass spectrometry, similar or higher response for HPLC-FLD than for MS were observed (Nelson, 2011; Poplawski, 2017), highlighting the potential of chemical modification by attaching fluorescent groups to hydroxyl moieties. Therefore, it was important to establish a rapid and straightforward method for attaching fluorescent groups to GDGTs in order to improve the limits of detection of HPLC-MS analyses of

GDGTs from sediments. Previous research by Neises and Steglich (1978) developed a mild and effective protocol for the esterification of carboxylic acids resulting in improved yields and facile reaction by stirring the mixture for just over 3 h at room temperature followed by isolation of the product from the reactants (Section 2.1.1). This straightforward protocol could be appropriate for derivatisation by sonication of GDGTs from sediments (Section 2.1.1.1). To improve reaction time and potentially yields, derivatisation carried out in a microwave oven was also explored (Section 2.1.1.2).

2.1.1. Potential application of Steglich esterification to glycerol dialkyl glycerol tetraether lipids (GDGT) from sediments

2.1.1.1. Steglich esterification

Neises and Steglich (1978) demonstrated improved yields and more facile base catalysed reaction between alcohols and amino acids when using carbodiimide and 4-dimethylaminopyridine (DMAP) to activate the amino acids compared to the use of only carbodiimide dicyclohexylcarbodiimide (DCC). The mechanism for the Steglich esterification is well-established (Figure 2.1); the carbodiimide (*N*'-ethylcarbodiimide hydrochloride, EDC) deprotonates the amino acid, enabling it to act as a nucleophile, reacting with the imide to give an *O*-acylisourea intermediate. One of the nitrogen atoms of this intermediate deprotonates another molecule of the acid, enabling the base catalyst, DMAP, to add to the carbonyl carbon of the activated ester to form an acyl pyridinium ion. The latter reacts rapidly with the alcohol to form the ester product and the deactivated DMAP. The addition of small molar equivalents of DMAP acts as a base catalyst that accelerates the activation of the carbodiimide, facilitating the esterification (Neises and Steglich, 1978).

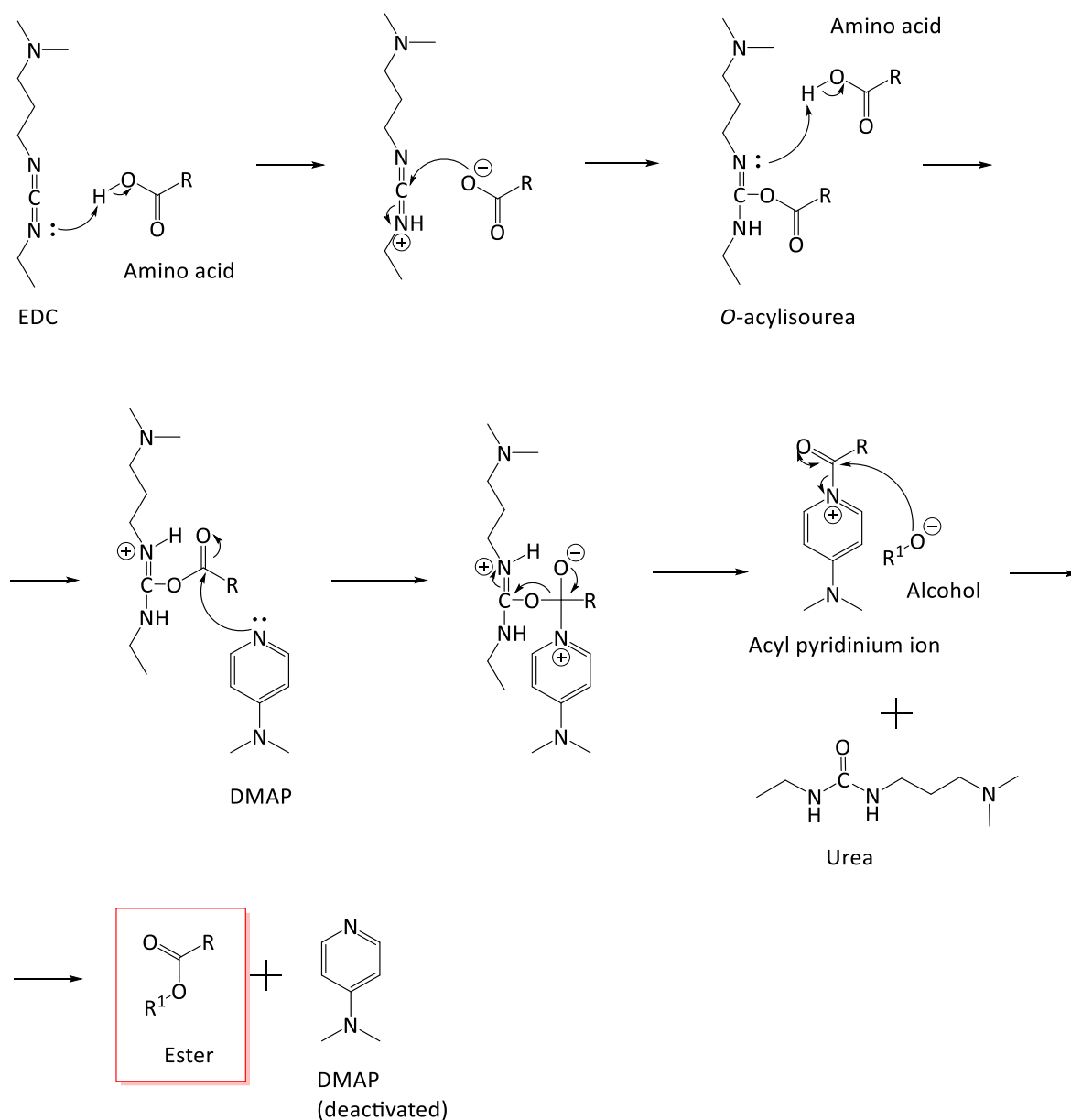


Figure 2.1. Mechanism of the Steglich esterification showing the ester product in the red square (Neises and Steglich, 1985).

A drawback of the Steglich esterification reaction is the formation of the unreactive *N*-acylisourea by intramolecular rearrangement of the intermediate *O*-acylisourea (Figure 2.2; Neises and Steglich, 1978). *N*-acylisourea reacts with the carboxylate, consuming it and preventing complete conversion to the ester (Tsakos *et al.*, 2015). Temperature is thought to catalyse the formation of the *N*-acylisourea, thus initial cooling of the reaction followed by stirring at room temperature are advised, to ensure high yields (Neises and Steglich, 1978). However, some authors report that higher temperatures were necessary to allow esterification of more hindered structures (Tsakos *et al.*, 2015 and references therein). The addition of catalytic amounts of DMAP can reduce the

formation of the *N*-acylisourea by rapidly reacting with the *O*-acylisourea to form the ester (Tsakos *et al.*, 2015). The addition of DMAP also increases the rate of reaction and allows esterification of even sterically hindered molecules (Neises and Steglich, 1978). Moreover, the urea is water soluble and can be readily separated from the ester product.

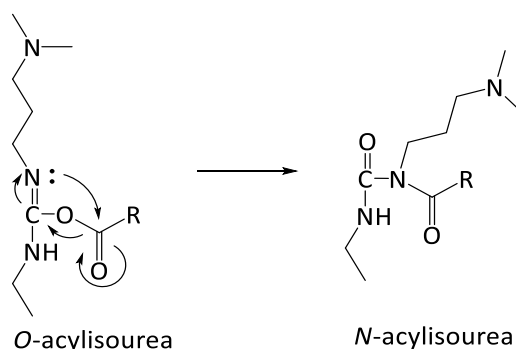


Figure 2.2. Mechanism of transformation of *O*-acylisourea to *N*-acylisourea, by-product of the Steglich esterification (Eyley and Thielemans, 2014).

Given the potential for Steglich esterification (Neises and Steglich, 1978) of GDGTs, a method to exploit the fluorescence of alcohols derivatised with fluorenylmethoxycarbonyl (Fmoc)-protected amino acids (Fmoc-AA) – the Fmoc being the fluorescent group – was developed by Poplawski (2017; Figure 2.3). The derivatives of the mono-alcohols 1-octadecanol (**L1**), cholesterol (**L2**) and 1,2-di-*O*-octadecyl-*rac*-glycerol (*r*-dOG; **L3**), selected as representative lipid standards, gave weighed yields of >90%, indicating that the reaction was very efficient. Similar limits of detection were observed for fluorescence and MS detection (Fmoc-AA of 1-octadecanol MS: 0.2 pmol on injection; UV: 6 pmol on injection; FLD: 9 pmol on injection; Poplawski, 2017). The lipid derivatives also exhibited higher HPLC-MS signal intensity than the native lipids by at least one order of magnitude, and it was suggested that multiple alcohol groups may enhance the MS and fluorescence signals, further improving the limit of detection (Poplawski, 2017).

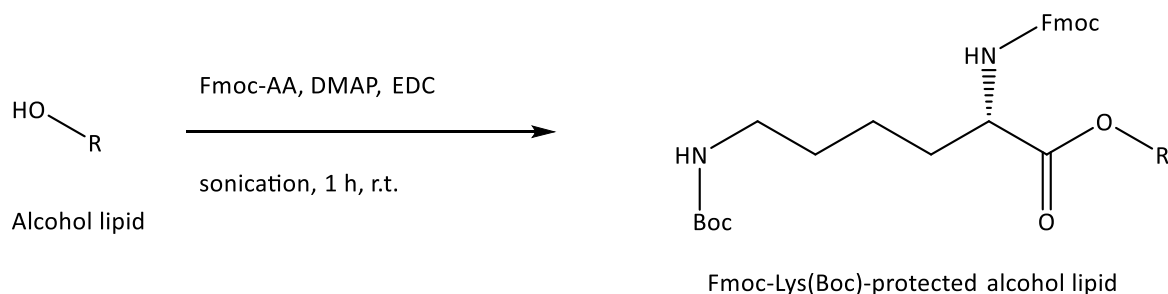


Figure 2.3. Esterification reaction of alcohol lipid with Fmoc-Lys(Boc) (Fmoc-lysine(*tert*-butoxycarbonyl)) showing reagents and conditions (Poplawski, 2017).

The success of the Steglich esterification applied to lipid standards cholesterol and 1-octadecanol (Poplawski, 2017) showed the potential for applying the Steglich esterification to GDGTs from sediments, not only to improve their detection by MS but also to enable detection by fluorescence. The application of this approach to sediment analysis would benefit greatly from a high throughput format capable of handling large batches of samples. Strategies to realise this goal could include increasing the number of samples handled simultaneously during ultrasonic-assisted derivatisation or using microwaves, which are known to shorten reaction times.

2.1.1.2. Use of microwaves to enhance rates of chemical reactions

Microwave heating was invented by Percy Spencer in 1945, with the first domestic oven being introduced by Raytheon in 1967. Microwave radiation extends over the wavelength range 0.01 to 1 m (0.3 to 300 GHz) of the electromagnetic spectrum. The radiation is produced by a magnetron, comprising a diode with heated cathodes that act as an electron source. Microwaves are directed to a target using microwave guides made of sheets of metal. A stirrer homogenises the microwaves to enable their even distribution (Figure 2.4; Rao *et al.*, 1999).

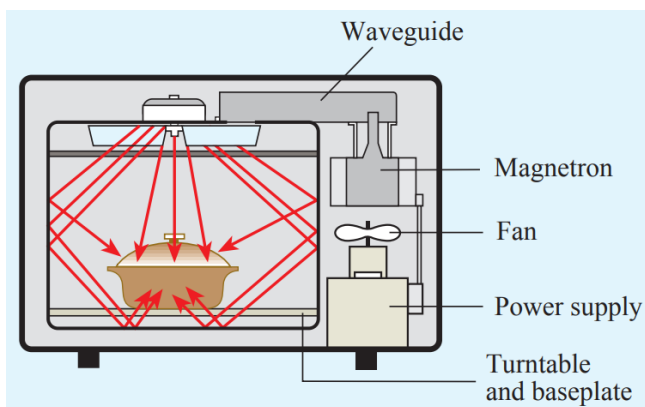


Figure 2.4. Diagram of the working principle of microwave heating (from Vollmer, 2004).

Microwave heating requires at least one component, i.e. a solvent or substrate, that is polar, ionic or polarisable, to absorb radiation. In the presence of an oscillating electromagnetic field, microwave active molecules are induced to align with the oscillating field, against resistive forces such as intermolecular forces and electric resistance; dielectric microwave heating results as a consequence of the resistance. The thermal energy can be transferred to other components of a mixture by conduction (Smart and Moore, 1995; Gaba and Dhingra, 2011).

The applications of microwave heating to aid chemical reactions started not long after its discovery, but the approach garnered increasing interest after Gedye and co-workers (1986) reported

decreased reaction times and increased yields in organic synthesis via the high pressures and temperatures achieved in the sealed container through microwave heating in place of reflux. Since then, microwave heating has been widely used to increase the rate of organic and inorganic syntheses, in both solid and solution state reactions (Gedye *et al.*, 1986; 1988; Rao *et al.*, 1999; Donati *et al.*, 2005; Matloubi Moghaddam *et al.*, 2012; Olariu *et al.*, 2014; Vekariya, 2017; da Silva Abranches *et al.*, 2018). Microwave irradiation heats the entire reaction volume, whereas traditional heating in an oil bath causes the vessel walls to be heated first and subsequently the heat is transferred to the substance inside (Figure 2.5; Schanche, 2003). The main advantages of microwave-assisted synthesis include shorter reaction times, mild experimental conditions, purer products, higher yields, uniform and selective heating of only polarisable compounds, therefore greater reproducibility (Gedye *et al.*, 1986; 1988). Based on the potential advantages over sonic-assisted reaction, the application of microwave-assisted Steglich esterification was also considered in this study.

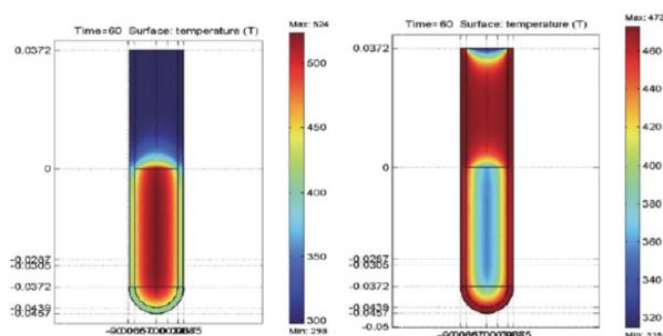


Figure 2.5. The temperature profile of a liquid in a test tube after 60 s affected by (left) microwave irradiation compared to (right) treatment in an oil-bath. Microwave irradiation raises the temperature (in red) of the whole reaction volume simultaneously, whereas in the oil heated tube, the reaction mixture in contact with the vessel wall is heated first (reproduced from Schanche, 2003).

2.1.2. Aims

The current analytical methodology for the detection and quantification of GDGTs has limitations arising from the use of normal phase chromatography, MS-only detection and moderate to high sample size requirements. Derivatisation of GDGTs with fluorescent compounds could give improved ionisation efficiencies, enable chromatographic separation using reversed-phase HPLC and take advantage of the excellent detection limits of FLD and UV as well as MS. The aims of the research described in this chapter were therefore:

- To apply the modified Steglich esterification method to mono- and di-alcohol lipid standards to evaluate the HPLC-MS signal and fragmentation of Fmoc-glycine (Fmoc-Gly) and Fmoc-Lys(Boc) derivatives (Section 2.2.1);
- To evaluate the potential of microwave-aided esterification of 1-octadecanol with Fmoc-Lys(Boc) (Section 2.2.3);
- To test the efficiency of the esterification with multiple samples of Fmoc-Lys(Boc)-1-octadecanol by sonicating 10 samples suspended in a rack (Sections 2.2.2, 2.2.4);
- To appraise the potential of esterification of GDGT lipid cores from sediments, in particular aiming to observe improved limits of detection (Section 2.2.5).

2.2. Results and discussion

2.2.1. Derivatisation of standard alcohols 1,12-dodecanediol, 1-octadecanol and cholesterol with Fmoc-Gly and 1-octadecanol with Fmoc-Lys(Boc)

Esterification of cholesterol, 1-octadecanol and 1,12-dodecanediol (**L4**) with Fmoc-Gly and Fmoc-Lys(Boc) was performed in order to determine the mass spectrometric response and the chromatographic and spectral characteristics of the derivatives. As described in detail in Section 7.3.1, the lipid standards were sonicated in 2 mL of DCM with DMAP, EDC and the Fmoc-protected amino acid for 1-2 h after which flash column chromatography with 1:1 hexane:ethyl acetate on silica was performed to isolate the products. The products were analysed by reversed-phase HPLC-UV, HPLC-FLD, HPLC-MS, and tandem MS (Sections 7.4.5, 7.4.10, 7.4.12).

2.2.1.1. Esterification of cholesterol with Fmoc-Gly

The esterified Fmoc-Gly-cholesterol eluted at 13.3 min under the reversed-phase HPLC-MS conditions (Figure 2.6), with the base peak ion representing the cholesteryl cation formed by loss of the Fmoc-Gly-OH group at m/z 369.3. A minor ion at m/z 666.2 (0.6% abundance) corresponds to the protonated molecule (Figure 2.6). Tandem MS of the base peak ion at m/z 369.3 shows groups of relatively low abundance product ions from fragmentation of the steroidal structure; Figure 2.7 shows the highest abundance ion of the group resembling the fragmentation of cholesterol under EI conditions (NIST), indicating similar stabilities of the product ions formed by dissociation. A second minor peak eluted at 12.2 min with peak area 18 times lower than the Fmoc-Gly-cholesterol. The MS showed a base peak at m/z 367.3 and protonated molecule at m/z 664.3; this minor compound is an impurity of the cholesterol standard, probably a sterol exhibiting an additional saturation. MS² of the base peak ion at m/z 367.3 showed a similar pattern to the MS²

of Fmoc-Gly-cholesterol but with an offset of m/z 2 lower. The fragmentation pathway of Fmoc-Gly-cholesterol favours alkyl cleavage of the ester. The favourability of this fragmentation accounts for the lower abundance of the protonated molecule of the cholesterol derivative.

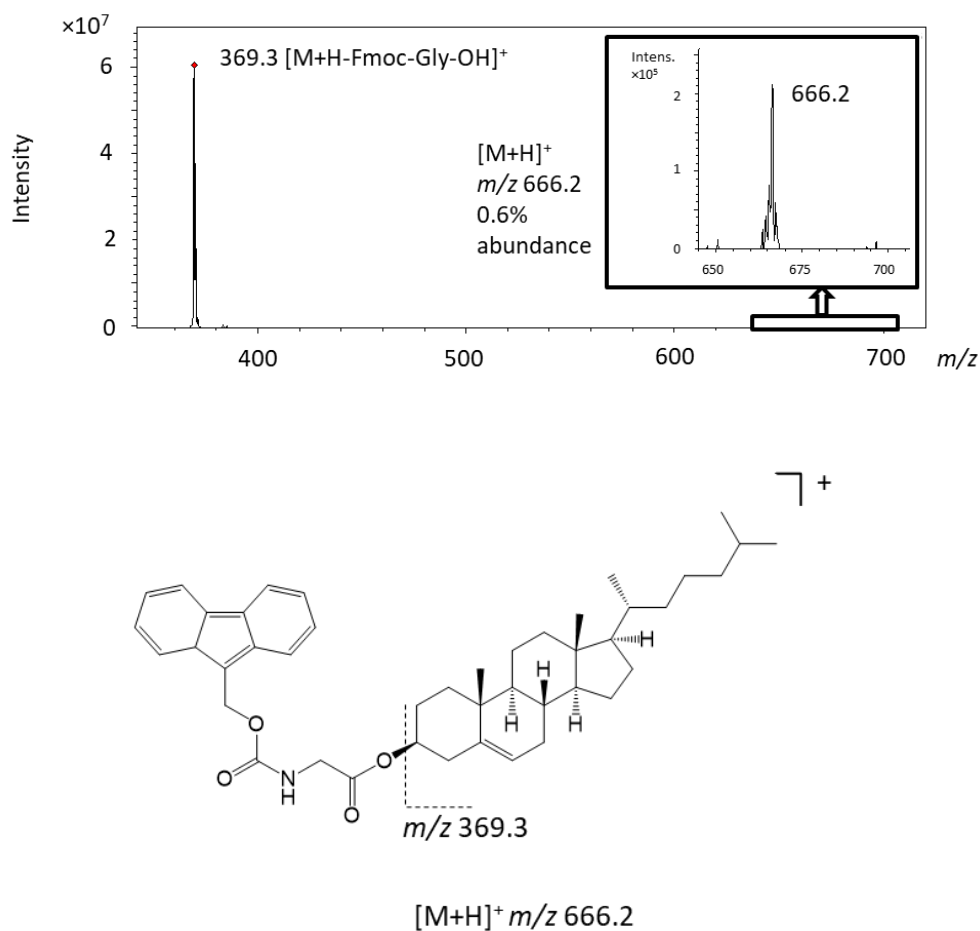


Figure 2.6. (Top) HPLC-MS base peak chromatogram (BPC) m/z 220-1000 of Fmoc-Gly-cholesterol; (middle) (+)APCI-MS spectrum of Fmoc-Gly-cholesterol with inset of the protonated molecule and (bottom) structure of derivative showing the main fragment formed.

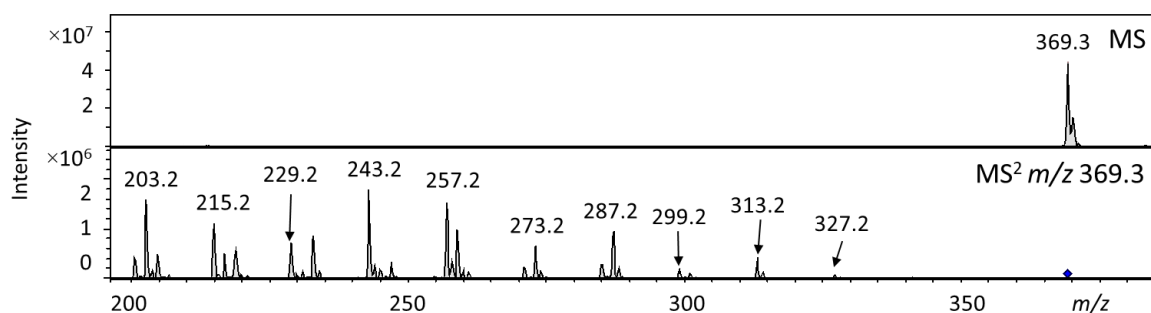


Figure 2.7. (+)APCI-MS² spectrum of the product ion at m/z 369.2 of Fmoc-Gly-cholesterol.

2.2.1.2. Esterification of 1-octadecanol with Fmoc-Gly

The product Fmoc-Gly-1-octadecanol exhibited a single peak eluting at 9.5 min (Figure 2.8). From the APCI-MS spectrum, the intact protonated molecule was observed at m/z 550.3, with an abundance of 0.5%. The base peak was at m/z 328.2, representing the 1-octadecanol derivative after loss of the Fmoc group. The other main fragment ion at m/z 372.2 resulted from the loss of the fluorenylmethyl group (6.4% abundance; Figure 2.8). MS² of the protonated molecule showed two product ions in the spectrum: m/z 372.2 and m/z 328.2 and tandem MS of m/z 372.2 showed m/z 328.2 as a prominent ion (Figure 2.9), demonstrating that the two ions in the MS spectrum are indeed the main fragment ions from Fmoc-Gly-1-octadecanol. Tandem MS of m/z 328.2 shows a very low abundance ion at m/z 282.2, 46 Da lower than the precursor ion that could potentially arise from concerted loss of a molecule of water from the amino acid and ethane from the alkyl chain.

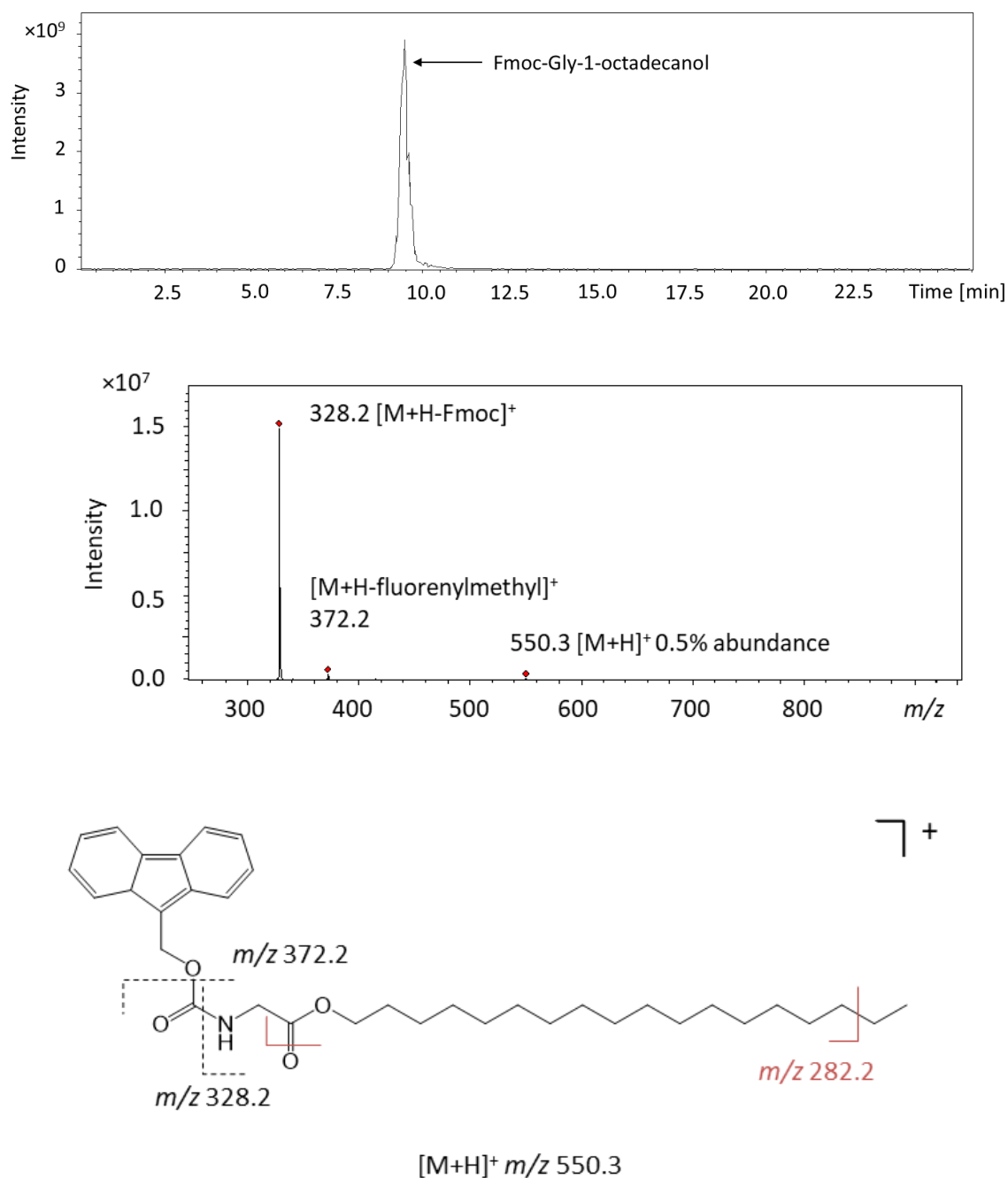


Figure 2.8. (Top) HPLC-MS BPC m/z 220-1000 of Fmoc-Gly-1-octadecanol; (middle) (+)APCI-MS spectrum of Fmoc-Gly-1-octadecanol and (bottom) structure of derivative showing the main fragments formed.

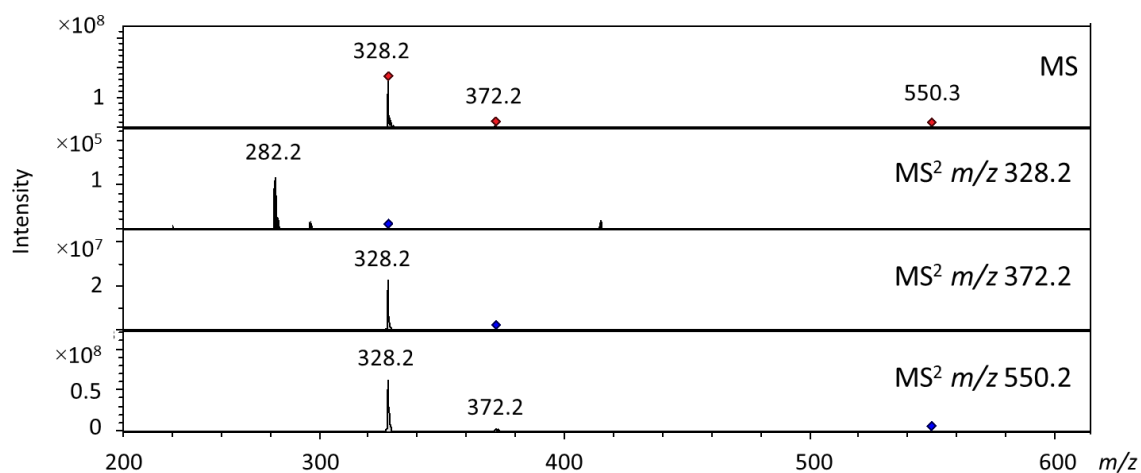


Figure 2.9. (+)APCI-MS² spectrum of the product ions at m/z 328.2, m/z 369.2 and m/z 550.2 of *Fmoc-Gly-1-octadecanol*.

2.2.1.3. Esterification of 1-octadecanol with *Fmoc-Lys(Boc)*

The esterification product *Fmoc-Lys(Boc)-1-octadecanol* eluted at 5.6 min as a single peak (Figure 2.10). The derivative showed two prominent ions: the protonated molecule at m/z 721.4, and a base peak ion at m/z 621.3 arising from the loss of the Boc group (Figure 2.10); no minor ions were evident. *Fmoc-Lys(Boc)* contains two amide bonds; considering the base peak arises from loss of the Boc group (-100 Da), the bond between Boc and lysine is being preferentially cleaved during (+)APCI-MS ionisation.

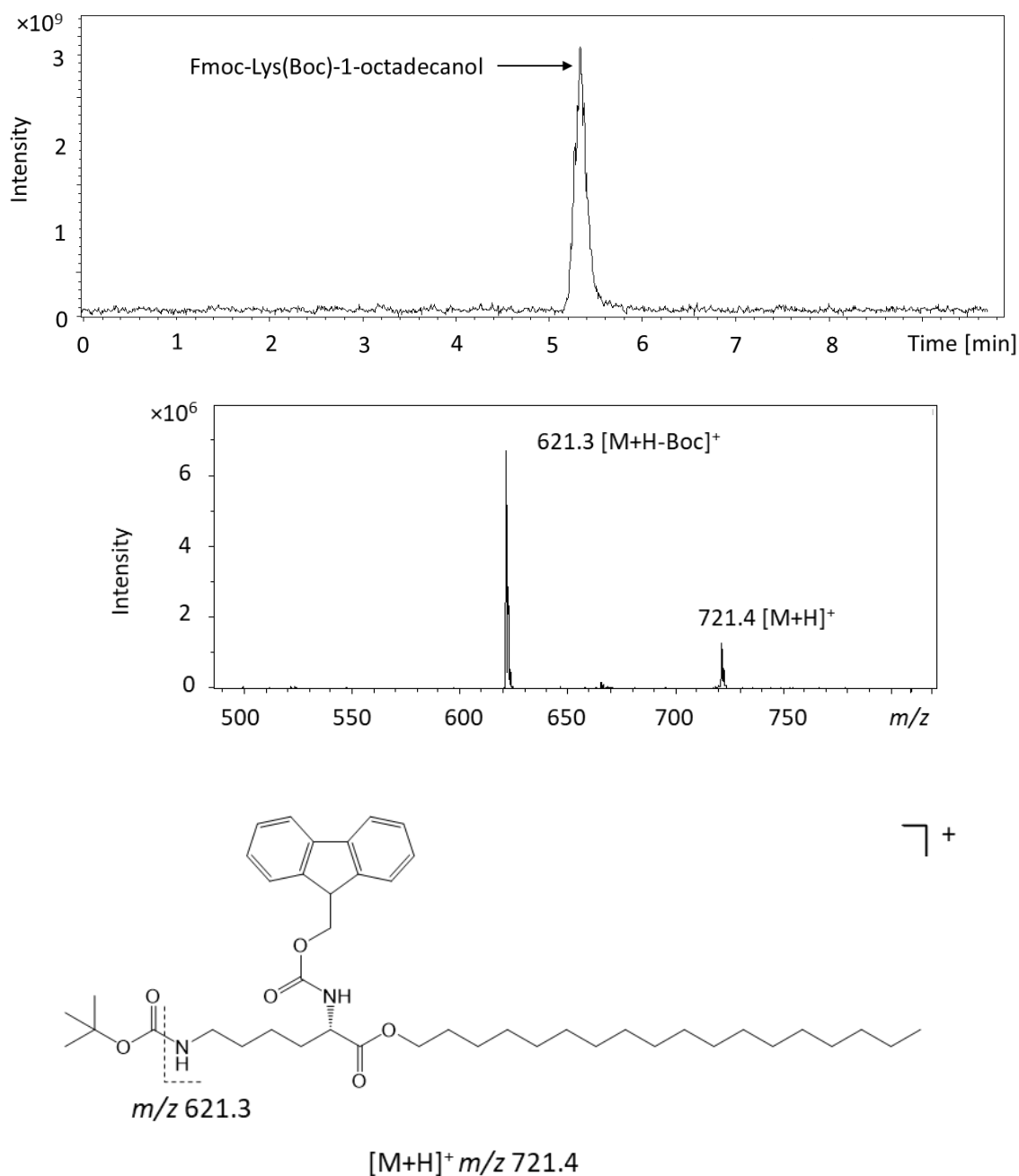


Figure 2.10. (Top) HPLC-MS BPC m/z 220-1000 of Fmoc-Lys(Boc)-1-octadecanol; (middle) (+)APCI-MS spectrum of Fmoc-Lys(Boc)-1-octadecanol and (bottom) structure of derivative showing the main fragment formed.

2.2.1.4. Esterification of 1,12-dodecanediol with Fmoc-Gly

To esterify the diester of 1,12-dodecanediol with Fmoc-Gly, the molar equivalents of the reagents were doubled to account for the two alcohol groups on the lipid standard (Section 7.3.1). Reversed-phase HPLC-MS analysis of the derivatised Fmoc-Gly-1,12-dodecanediol exhibited two peaks at 3.9 min and 5.5 min with signal intensity ratio of 1:3.5 (Figure 2.11). The spectrum of the earlier eluting

component contained an ion at m/z 482.2 corresponding to the protonated molecule of the monoester, and the base peak ion at m/z 260.0, arising from loss of the Fmoc group. Minor ions corresponding to loss of the fluorenyl (m/z 318.1) and fluorenylmethoxy groups (m/z 286.0) were observed (Figure 2.12). An ion at m/z 438.3, arising from the loss of 44 Da could be the result of a rearrangement, giving rise to the loss of CO_2 (Figure 2.12). Tandem MS of the monoester at m/z 482.2 shows fragment ions m/z 438.3 (loss of CO_2), m/z 286.0 (loss of fluorenylmethoxy) and m/z 260.0 (loss of Fmoc group; Figure 2.13). MS^2 of product ions at m/z 438.3 and 318.1 shows the formation of ion after loss of fluorenylmethyl carbamate (m/z 242.0) in addition to the fragment ions also evident in the MS spectrum after loss of fluorenylmethoxy (m/z 286.0) and Fmoc group (m/z 260.0; Figure 2.13). MS^2 of the ion at m/z 260.0 exhibits fragments at m/z 242.0 (loss of fluorenylmethyl carbamate) and the intact 1,12-dodecanediol (m/z 202.7), not evident in the MS^2 of the other product ions (Figure 2.13).

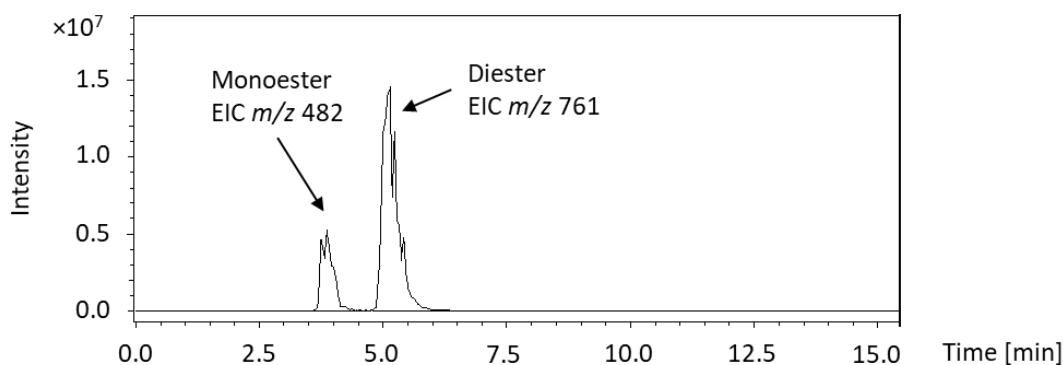


Figure 2.11. HPLC-MS BPC m/z 220-1000 of Fmoc-Gly-1,12-dodecanediol.

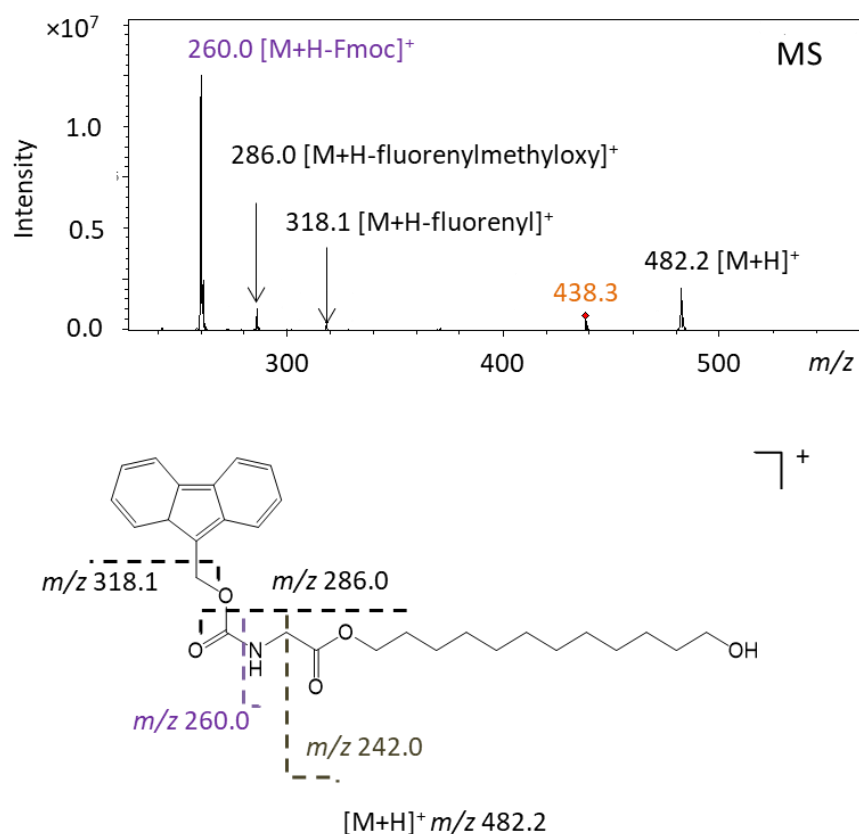


Figure 2.12. (Top) (+)APCI-MS spectrum of the monoester of the Fmoc-Gly-1,12-dodecanediol derivative and (bottom) structure of the derivative showing the main fragments formed.

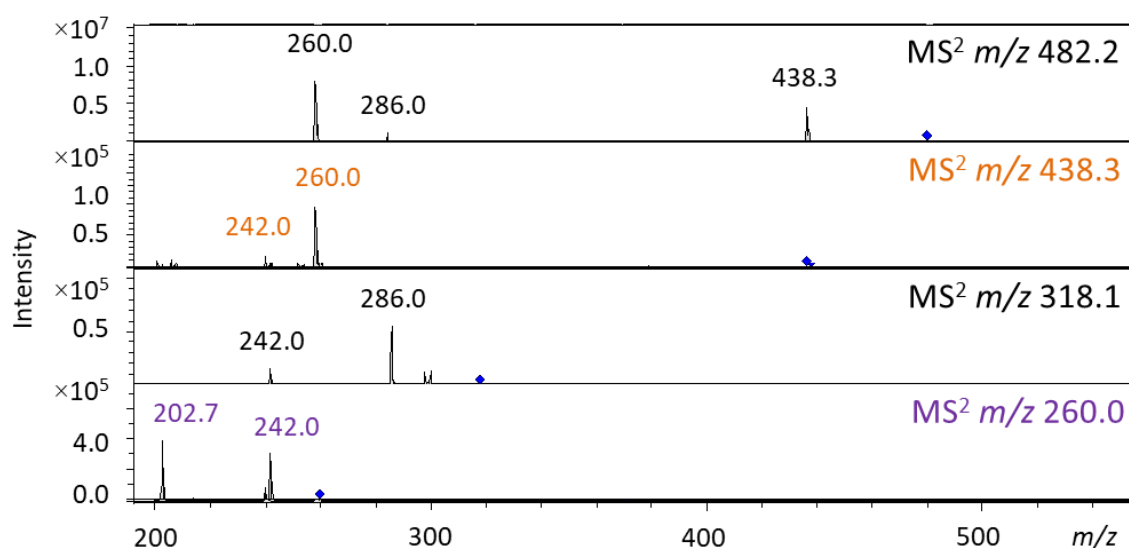


Figure 2.13. (+)APCI-MS² spectrum of the monoester of Fmoc-Gly-1,12-dodecanediol derivative.

The mass spectrum of the second peak (Figure 2.11) can be divided into three regions (Figure 2.14): the first region exhibits an ion at m/z 761.4, corresponding to the protonated molecule of the

diester; in the second region an ion at m/z 539.3 represents the loss of one Fmoc group from the diester. The third region of the spectrum shows a multitude of ions corresponding to fragment ions after loss of one fluorene and Fmoc groups (m/z 375.2), loss of one fluorene and part of the glycine (m/z 343.2) and loss of one fluorene and Fmoc-Gly (m/z 317.2). In addition, fragment ions at m/z 286.1, 260.1 and 242.0 were observed (Figure 2.14), as discussed previously in relation to the monoester (Figure 2.13). The MS² spectrum of the protonated molecule m/z 761.4 showed m/z 343.3 (loss of one fluorene and part of the glycine) and m/z 317.2 (loss of Fmoc-Gly) as main product ions (Figure 2.15). The tandem MS of m/z 539.3, 375.2, 343.2 and 317.2 all showed the product ions previously mentioned, confirming the formation of the diester (Figure 2.15).

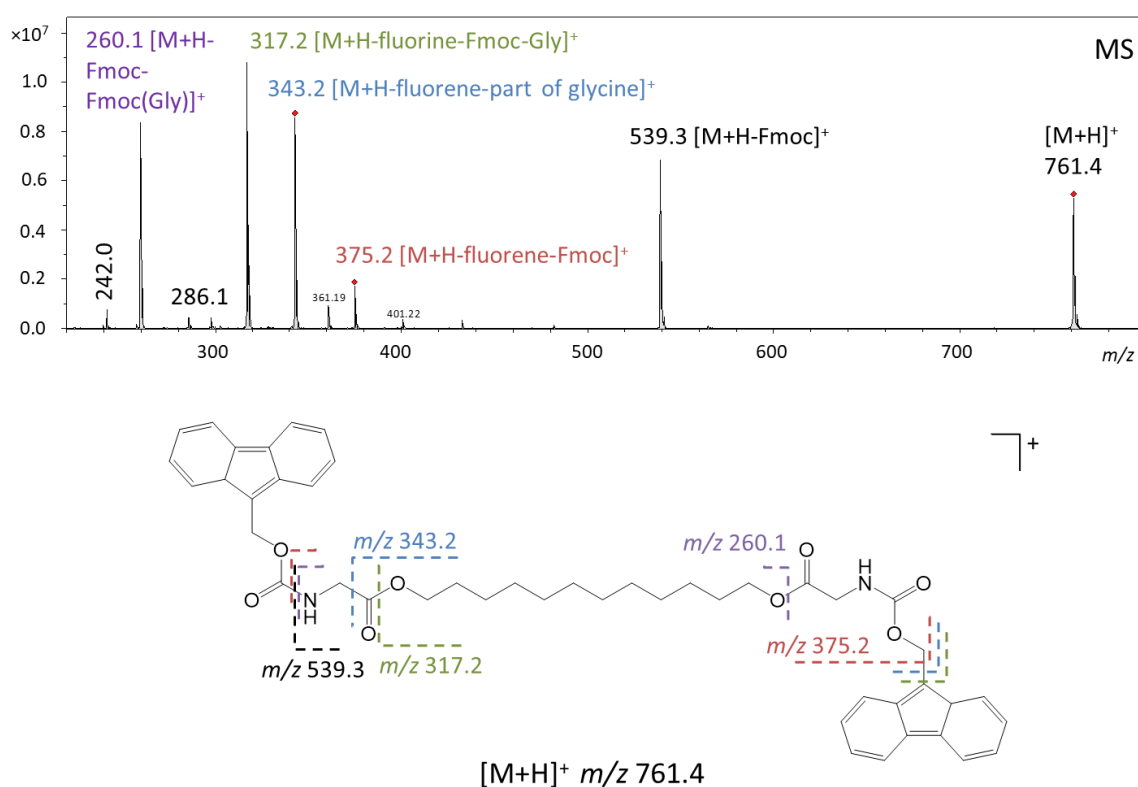


Figure 2.14. (Top) (+)APCI-MS spectrum of the diester of Fmoc-Gly-1,12-dodecanediol derivative and (bottom) structure of derivative showing the main fragments formed.

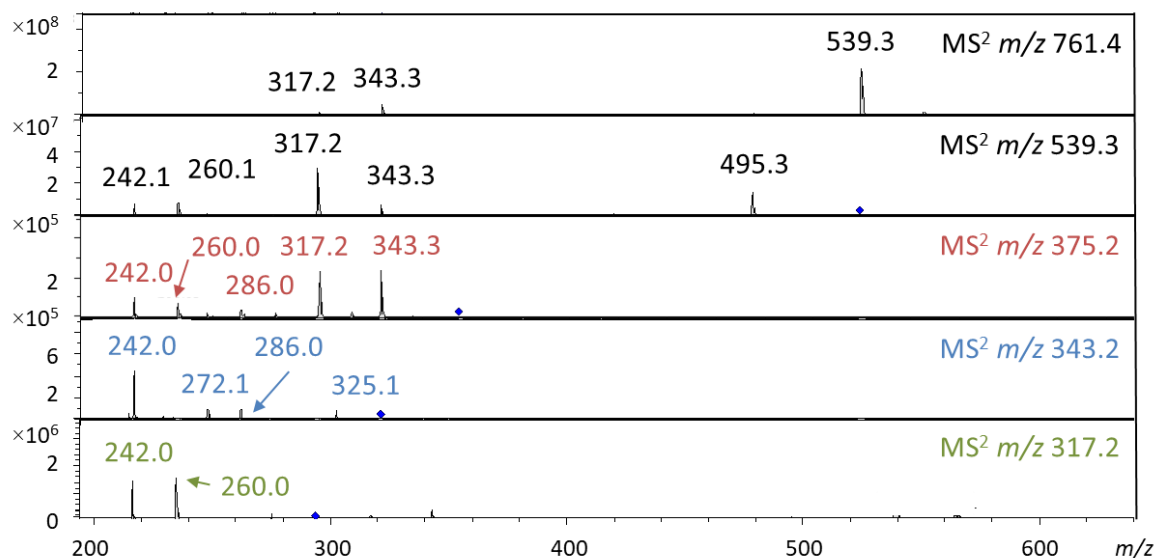


Figure 2.15. (+)APCI-MS² spectrum of the diester of Fmoc-Gly-1,12-dodecanediol derivative.

The predominance of the fragment ion arising from cleavage of the amide bond between the Fmoc group and the amino acid indicates that the fragment ion is more stable than the protonated molecule. The presence of both the monoester and the diester of Fmoc-Gly-1,12-dodecanediol indicates that sonication for 1 h was insufficient for complete formation of the diester. The reaction mixture was sonicated for 3 h and tested by thin-layer chromatography (TLC) after 1, 2, 2.5 and 3 h; in all cases, the monoester was still present in the TLC plate although in lower abundance in HPLC-MS than seen in Figure 2.11. The prolonged sonication of the diol revealed that extending the sonication time was not enough to form the diester, possibly suggesting that the reagent quantities should be altered. To this end, the molar equivalents were doubled to 2 eq. of DMAP, 4 eq. of Fmoc-Gly and 8 eq. of EDC for each alcohol group. The reaction was sonicated for 1, 2 and 3 h. In each case, the starting material was not observed by TLC and only the diester was formed. This was confirmed by HPLC-MS analysis of the products showing only one peak in the chromatogram with m/z 761.4, representing the protonated molecule of the diester.

In conclusion, the esterification of 1,12-dodecanediol produced monoester and diester with prolonged sonication requiring doubling the molar equivalents of reagents to preferentially form only the diester product Fmoc-Gly-1,12-dodecanediol.

It is evident that cleavage of the amide bond is the dominant fragmentation process for straight chain alcohols, as shown by 1-octadecanol and 1,12-dodecanediol, whereas Fmoc-Gly-cholesterol readily fragments to leave the cholesteryl cation, meaning that the stability of the cation makes the process more favourable. These tests have shown that mild ionisation by APCI only marginally

affects the fragmentation of the derivatives, especially in the case of straight chain alcohols, therefore allowing easy recognition of the protonated molecule. These features would be beneficial when more complex environmental samples are esterified and analysed by HPLC-MS.

2.2.2. HPLC-FLD and HPLC-UV quantification

Quantification of the product yields of the derivatisation reactions was carried out by extrapolation from the calibration curve of derivatised Fmoc-Lys(Boc)-1-octadecanol (FLB-o; 90% weighed yield). The calibration curve based on the HPLC-UV and -FLD (Section 7.4.5) peak areas for FLB-o over a range of concentrations showed excellent correlation (R^2 0.97 ($n=4$) and 0.98 ($n=5$), respectively) on a limited range of concentrations (0.3-6.7 pmol on column; Figure 2.16). The resulting limits of detection (LOD), assuming that $LOD > 3$ times the signal to noise (S/N) ratio, were 0.6 pmol on column for HPLC-UV and 0.3 pmol for HPLC-FLD. These results are comparable to the values calculated for the Fmoc-Gly, -Trp, -Pro, -Phe derivatives of 1-octadecanol synthesised by Poplawski (2017; 6.3-8.9 pmol for HPLC-UV and 0.2-2.2 pmol on column for HPLC-FLD). The limit of detection for the FLB-o standard by HPLC-MS was 0.3 pmol on column, similar to that for HPLC-FLD.

Above 33.6 pmol on column, the FLB-o response was non-linear. In UV-vis spectroscopy, the response of the molecule can deviate from the expected linear response of the Beer-Lambert Law due to a number of reasons: stray radiation, refractive index of the solvent, dissociation or reaction of analytes during the UV-vis measurements (Skoog *et al.*, 1996). The real limitation to the Beer-Lambert Law, however, is the lack of linearity at high concentrations due to the effect of charge distribution of UV-sensitive analytes when the average molecular distance is reduced. Electrostatic interactions can modify the ability of a molecule to absorb at the required wavelength reducing the absorbance (Skoog *et al.*, 1996; 1998). Similarly, in fluorescence linearity is lost at high concentrations due to self-quenching, i.e. the result of unexcited analyte molecules absorbing the fluorescence produced by other analyte molecules, thus decreasing the fluorescence power and HPLC-FLD area (MacDonald, 1990; Skoog *et al.*, 1996; 1998). Due to the non-linearity of the calibration curve at high concentrations, all samples were diluted in order to fall in the linear part of the calibration curve.

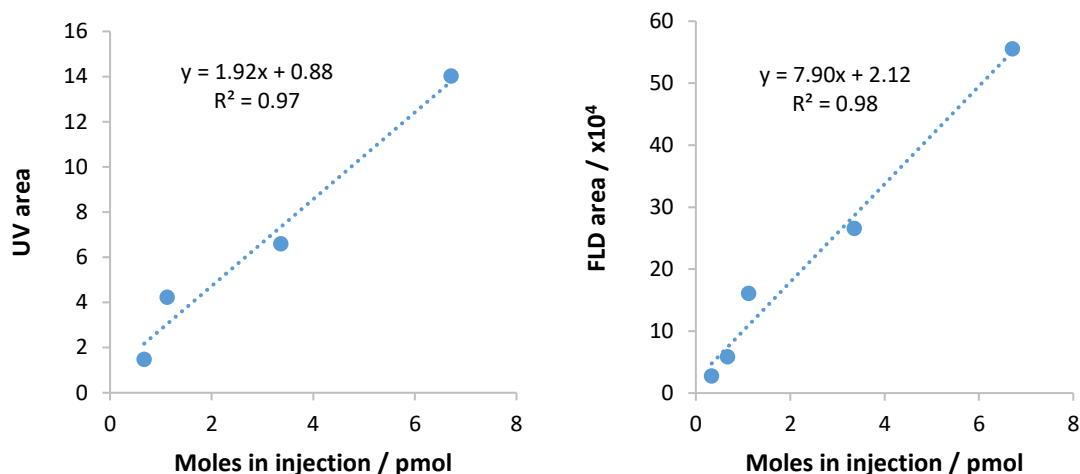


Figure 2.16. Calibration curve of Fmoc-Lys(Boc)-1-octadecanol (FLB-o): (left) concentration vs HPLC-UV area; (right) concentration vs HPLC-FLD area.

2.2.3. Derivatisation of 1-octadecanol with Fmoc-Lys(Boc) with microwave irradiation

After showing that esters of cholesterol, 1-octadecanol and 1,12-dodecanediol required 1 h for their formation, the many advantages of microwave irradiation – including shorter reaction times and higher yields – meant that there was considerable potential in applying microwave irradiation to derivatisation of 1-octadecanol with Fmoc-Lys(Boc) in order to speed up the protocol. As detailed in Section 7.3.2, the alcohol was mixed with the reagents in a specific vial just before being subjected to microwave irradiation; temperature, time and power of irradiation were varied to assess the best conditions for formation of high yields of Fmoc-Lys(Boc)-1-octadecanol (FLB-o). HPLC-UV and HPLC-FLD analysis was performed (Sections 7.4.5) and the yields of the reactions were calculated using the calibrations in Section 2.2.2.

In the first instance, the FLB-o sample was heated at constant power (850 W) for 30 s at temperatures ranging from 50°C to 120°C (Figure 2.17). The low yields determined by HPLC-UV and HPLC-FLD (5-12%) and the presence of 1-octadecanol starting material, as indicated by TLC, showed that these conditions give incomplete esterification (Figure 2.17). Furthermore, the formation of side products was indicated by the presence of at least three extra spots on TLC, and additional peaks on HPLC-FLD and HPLC-UV. The yields doubled between 60°C and 70°C (5.9% and 12%, respectively), remaining nearly constant until 110°C, where a sudden decrease was observed between 110°C and 120°C (11.7% and 6.1%, respectively), due to the high temperatures leading to the formation of *N*-acylisourea (Section 2.1.1.1; Figure 2.2; Slebioda *et al.*, 1990; Iwasawa *et al.*, 2007).

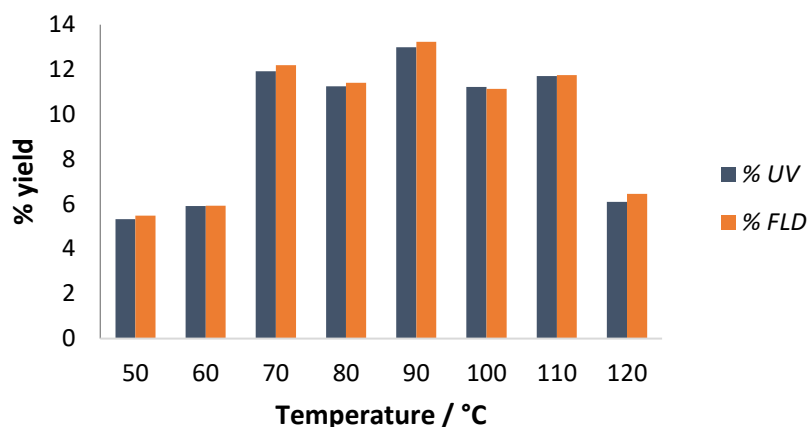


Figure 2.17. HPLC-FLD and HPLC-UV yields for the microwave synthesis of FLB-o heating for 30 s at increasing temperatures.

Analysis of the reaction mixture by TLC at the 30 s time point showed the presence of starting material, possibly as a consequence of short reaction times or limited availability of reagents due to side reactions. Further reactions were performed over longer time intervals and a range of temperatures between 60 and 100°C in an attempt to inhibit the formation of *N*-acylisourea and other side products. Six samples were esterified at 80°C with microwave irradiation for 30 s, 2, 5, 10, 20 and 30 min. The maximum FLD yield, 11.1%, was achieved after 30 s, after which time the yield decreased abruptly to 0.05% at the 2 min point. After 10 min, a slight increase in yield to 0.38% was observed, followed by values below the limit of detection after 20 and 30 min (Figure 2.18). Lower yields with increasing reaction times were also observed at 100, 90 and 60°C for 0.5, 1, 2 min (Figure 2.19): yields halved from 9.8% to 4.0% at 100°C after 30 s and 2 min, respectively; at 90°C yields were 11.6% after 30 s and 1.0% after 2 min. Reactions at 60°C gave a low yield (5.1%) after 30 s but the same reaction after 20 and 60 min showed no product detected by HPLC-UV and HPLC-FLD (Figure 2.19). The experiments confirm that high temperatures and exposure to heat for long periods of time are detrimental to the reaction with incomplete esterification and formation of side products.

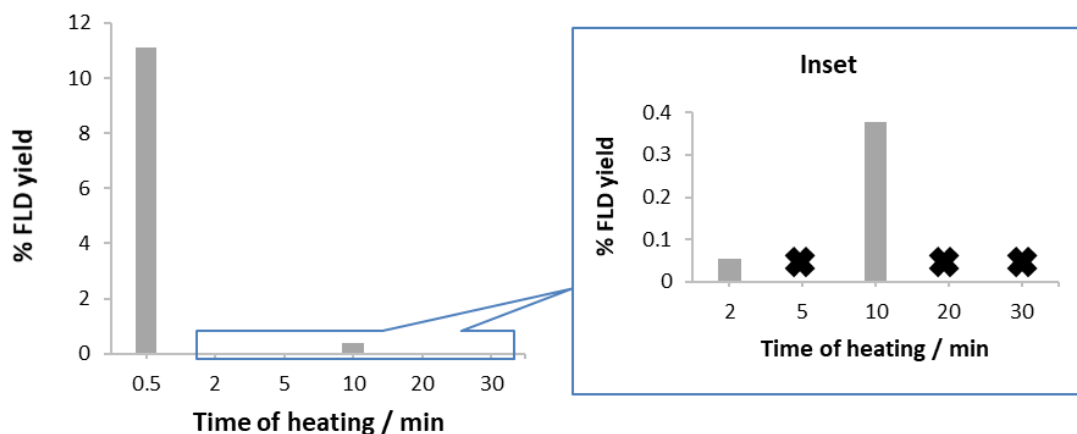


Figure 2.18. HPLC-FLD yields for the microwave synthesis of FLB-o heating at 80°C for an increasing amount of time. ✕ Indicates signal below limit of detection.

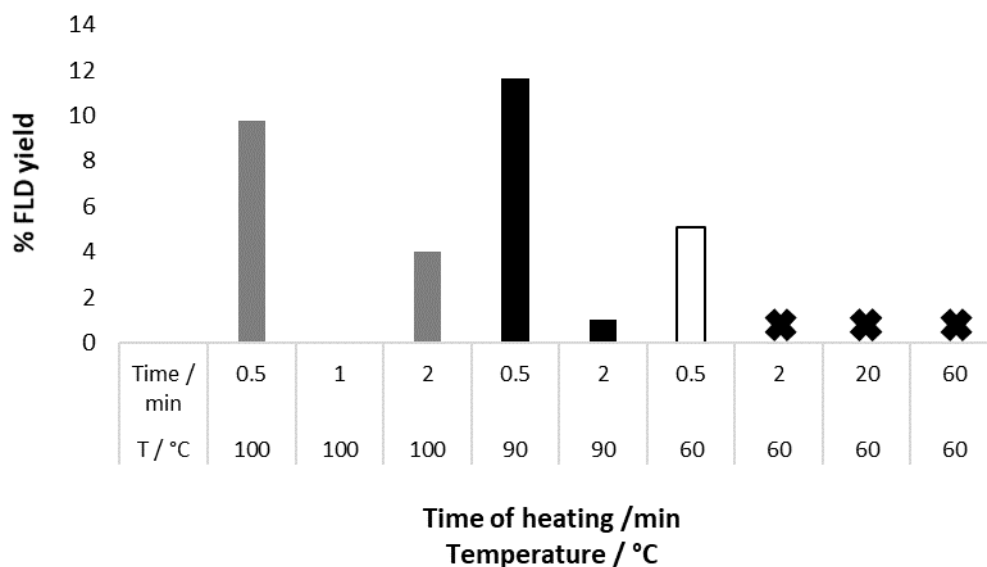


Figure 2.19. HPLC-FLD yields for the microwave synthesis of FLB-o heating at 100°C (in grey), 90°C (in black) and 60°C (in white) for an increasing amount of time. ✕ Indicates signal below limit of detection.

The initial experiments suggested that the highest power (850 W) produced temperatures greater than 30°C even with as little as 20 s of irradiation, resulting in low yields (0.3-6.9%) and poor repeatability. Accordingly, the microwave power was reduced to ensure as little heating as possible. Notably, however, irradiation times greater than 30 s at powers lower than 850 W still resulted in the sample being heated above 30°C. The longest reaction carried out at 5 W for 1800 s (30 min) produced a reaction temperature of 60°C and very low yields (UV 1.2%, FLD 1.5%). Side products were evident by TLC and HPLC-FLD, possibly indicating the formation of *N*-acylisourea

even at 60°C. The highest yield, UV 8.6%, FLD 9.0%, was at 1 W for 300 s (5 min) with reaction temperatures remaining below 40°C (Figure 2.20); though this seemed promising, attempts to increase the yield by extending the reaction time raised the temperature of the system, reducing yields of reaction.

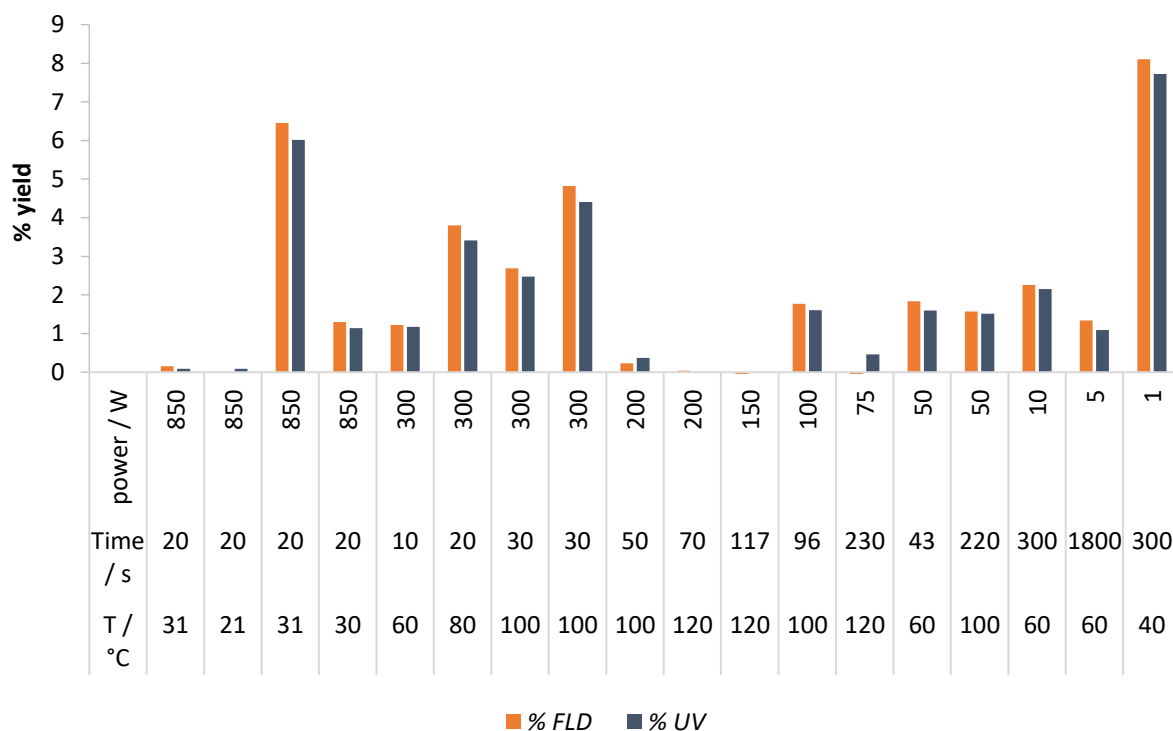


Figure 2.20. HPLC-FLD and HPLC-UV yields for the microwave synthesis of FLB-o heating at varying powers, time and temperatures.

In conclusion, although microwave-assisted reactions can be controlled by changing the temperature, power and time of the reaction, complete esterification was not observed under any of the conditions tested. The major limiting factor was high temperature, which reduced the yields through formation of side products, possibly including *N*-acylisourea, which stops the formation of the ester. Even at low power, microwave irradiation resulted in excessive heating, low yields and formation of side products.

Incomplete esterification and formation of side products were not observed in reactions by sonication even after 3 h, as described in Section 2.2.1.4 for Fmoc-Gly-1,12-dodecanediol. The microwave tests confirmed sonication to be a more efficient way of carrying out the Steglich esterification of the alcohols with the Fmoc-protected amino acids, and therefore sonication was used in the following tests.

2.2.4. Evaluation of Fmoc-Lys(Boc)-1-octadecanol (FLB-o) HPLC-UV and HPLC-FLD yields of multiple derivatives in a plastic rack and a beaker

Prior to the application of the esterification to large batches of GDGTs from sediments, studies on batches of Fmoc-Lys(Boc) derivatives of 1-octadecanol (FLB-o) were carried out to assess the variation in reaction yields in different positions in a plastic rack, and compare this to yields obtained when undertaken in a beaker (Poplawski, 2017). The positions chosen for the derivatisation of 10 FLB-o samples are shown in Figure 2.21. The sample vials, immersed in the rack, were sonicated for 1 h and separated by flash column chromatography (Section 7.3.1) prior to HPLC-UV and HPLC-FLD analysis (Section 7.4.5).

	1	2	3	4	5	6	7	8	9	10	11	12
E												
D												
C												
B												
A												

Figure 2.21. Grid representing the positions in the plastic rack for derivatisation of 10 samples (red cells).

The yields of FLB-o in a rack (Figure 2.22, Table 2.1) assessed by HPLC-UV and HPLC-FLD were in good agreement. Triplicate experiments showed all yields to lie within the error bars (1 standard deviation, s) with mean UV yields between 46.8% and 91.0% and FLD yields between 52.2% and 94.6%. The highest standard deviations were observed for positions E8 ($s=65.4$ UV, 60.1 FLD) and D2 ($s=33.6$ UV, 38.6 FLD), indicating low repeatability. Positions C4, B6, C8 and E12 showed the lowest standard deviations with values below 12 (C4 $s=4.55$ UV, 9.00 FLD; B6 $s=2.80$ UV, 8.84 FLD; C8 $s=8.03$ UV, 11.1 FLD; E12 $s=11.6$ UV, 6.04 FLD) for both UV and FLD yields. These positions within the sonic bath might be considered optimal to ensure good repeatability and high yields. In general, positions along rows B-D and columns 4-9 show low standard deviations, high yields and could potentially be considered in further derivatisation experiments.

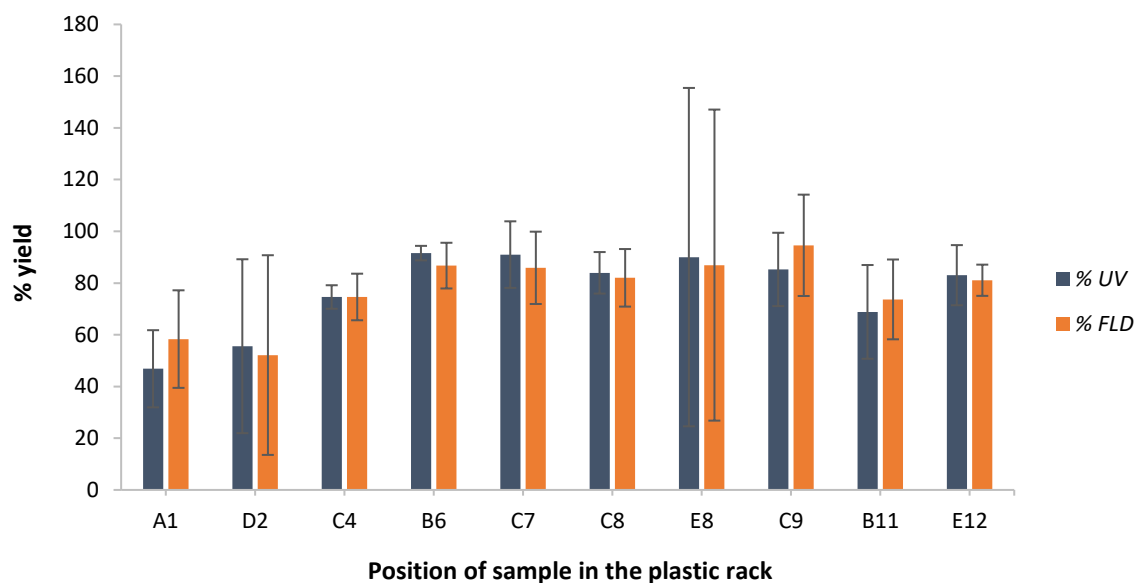


Figure 2.22. Mean HPLC-UV (in blue) and HPLC-FLD (in orange) percentage yields for the esterification product *Fmoc-Lys(Boc)-1-octadecanol*. The error bars represent one standard deviation, $n = 3$.

Table 2.1. Percentage, mean and 1 standard deviation of HPLC-UV and HPLC-FLD yields for the three replicates of *Fmoc-Lys(Boc)-1-octadecanol* derivatives.

Position	Yield by UV measurements / %		Yield by fluorescence / %	
	Replicate $n = 3$	Mean $\pm 1s$	Replicate $n = 3$	Mean $\pm 1s$
A1	60.0, 26.0, 54.6	46.8 \pm 14.9	81.1, 34.9, 59.0	58.3 \pm 18.9
D2	103.1, 31.1, 32.5	55.6 \pm 33.6	105.3, 36.4, 14.8	52.2 \pm 38.6
C4	79.9, 68.8, 75.1	74.6 \pm 4.55	84.6, 62.8, 76.4	74.6 \pm 9.00
B6	94.8, 91.9, 88.0	91.6 \pm 2.80	98.9, 83.2, 78.1	86.7 \pm 8.84
C7	82.1, 81.7, 109.2	91.0 \pm 12.9	80.5, 72.1, 105.0	85.9 \pm 14.0
C8	91.5, 72.8, 87.5	83.9 \pm 8.03	96.4, 69.3, 80.3	82.0 \pm 11.1
E8	111.2, 1.44, 157.5	90.0 \pm 65.4	92.8, 10.5, 157.5	86.9 \pm 60.1
C9	90.5, 65.9, 99.4	85.3 \pm 14.2	109.5, 66.9, 107.4	94.6 \pm 19.6
B11	94.4, 57.8, 54.3	68.8 \pm 18.1	95.1, 59.5, 66.4	73.7 \pm 15.4
E12	82.9, 68.8, 97.3	83.0 \pm 11.6	81.3, 73.6, 88.3	81.1 \pm 6.04

Although the results, in general, indicate good yields, they are slightly lower than the weighed yields (>90%) previously reported by Poplawski (2017) for the same reaction carried out in a beaker rather than in a plastic rack. The disparity in yields could be due to the different reliability of measurements by weight and by spectroscopic methods, especially in small scale experiments like

this one. It is also possible that deflection or dissipation of ultrasound waves from the higher number of vials immersed in the bath affects the efficiency of sonication (Luche, 1998; Nascentes *et al.*, 2001).

These results showed that the use of a plastic rack could be suitable for a reduced number of samples placed in the central positions (row B-D, columns 4-9) that showed the lowest standard deviation and highest yields. Another test was performed to compare the yields of five samples derivatised in a beaker with those derivatised in rack positions C4, B5, C7, B8 and D9. The yields were compared by weight, HPLC-UV and HPLC-FLD (Figure 2.23, Table 2.2). All yields lay within the error bars, indicating that similar yields were obtained by derivatisation in the rack (69.5-83.5%) and the beaker (63.2-83.5%). The products of derivatisation in the plastic rack, however, showed lower standard deviations by HPLC-UV, HPLC-FLD and weight than the products derivatised in the beaker (Figure 2.23; Table 2.2). It was noted that the yields by weight were c. 15% higher than the yields measured by HPLC-UV and HPLC-FLD for derivatisation in the rack and the beaker, whereas there was better consensus between the yields by HPLC-UV and -FLD with a difference <6.5% in a rack and in a beaker. The standard deviations obtained by derivatisation in a plastic rack were lower than derivatisation in a beaker (Figure 2.23; Table 2.2). Testing esterification of 10 samples and comparing yields of esterification of FLB-o in a rack and beaker showed that fewer than 10 samples, placed in the central positions of the rack (row B-D, columns 4-9), can be handled simultaneously. This approach could be applied for high throughput derivatisation of GDGTs from sediments.

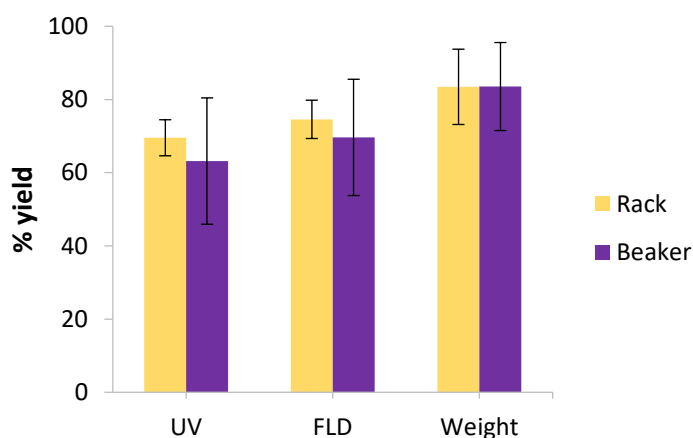


Figure 2.23. Yields by weight, HPLC-UV, HPLC-FLD for the esterification reaction of Fmoc-Lys(Boc) with 1-octadecanol in a plastic rack (in yellow) and in a beaker (in purple). The error bars represent one standard deviation, $n = 5$.

Table 2.2. Mean percentage of HPLC-UV, HPLC-FLD and weighed yields for synthesis of Fmoc-Lys(Boc)-1-octadecanol in a plastic rack and in a beaker.

Vessel for derivatisation	Mean yield by UV measurements / % $\pm 1s$	Mean yield by fluorescence / % $\pm 1s$	Mean yield by weight / % $\pm 1s$
Rack	69.5 \pm 4.92	74.6 \pm 5.23	83.5 \pm 10.3
Beaker	63.2 \pm 17.3	69.6 \pm 15.9	83.5 \pm 12.0

2.2.5. Derivatisation of GDGTs from sediments with Fmoc-Lys(Boc)

Following the analysis of the results obtained in different rack positions, it was considered feasible to esterify less than 10 samples in the central parts of the rack ensuring relatively high yields and low standard deviations. Prior to applying this method to large batches of GDGTs extracted from sediments, application of FLB derivatisation to a single sample of GDGTs from sediments was explored using the polar fraction of a sediment extract from the Loch of Stenness (Orkney, Scotland). The polar fraction (Sections 7.2.1, 7.2.3) was first examined for native GDGTs using reversed-phase HPLC-MS, following the method devised by Poplawski (2017; Figure 2.24; Sections 7.4.6, 7.4.10). The lipid cores identified were archaeal tetraethers caldarchaeol (**G1**), GDGT-1, -2, -3 (**G2-G4**) and crenarchaeol (**G5**) together with bacterial branched GDGTs Ia, Ib, Ic, IIa, IIb, IIIa and smaller amounts of IIc, IIb, IIc (**G6-G14**).

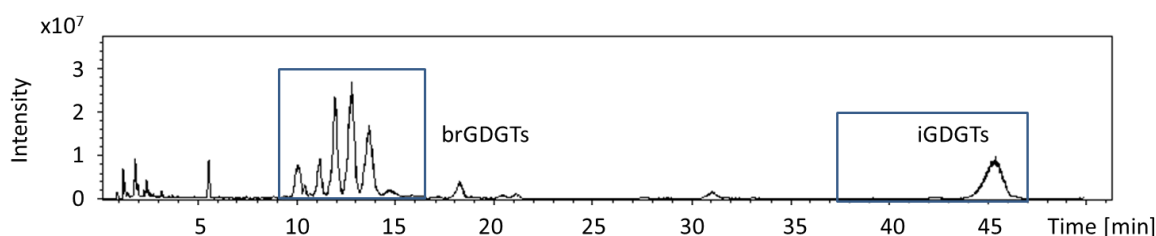


Figure 2.24. Reversed-phase HPLC-MS of the native GDGTs in the polar lipid fraction from a sample from Loch of Stenness: BPC m/z 1000-1350.

Previous work by Poplawski (2017) suggested that complex sediment samples should be sonicated for 2 h, therefore this protocol was followed in this case (Section 7.3.3). As previously shown for FLB-o, the mass range selected was for the base peak ion formed by loss of one Boc group (Figure 2.10). The base peak chromatogram (BPC) chosen to include derivatised branched and isoprenoid GDGTs (m/z 1810-2110, Figure 2.25a) did not show clear peaks. Thus, ion chromatograms were extracted (EIC); three peaks eluting over the range 22-27 min with masses corresponding to the derivatives of branched GDGT (brGDGT) Ia, IIa and IIIa (Figures 2.25c-e, 2.26) and a peak at 62 min

corresponding to FLB-caldarchaeol were identified (Figure 2.25b, 2.26). The comparable ions for the derivatives of crenarchaeol, GDGT-1, -2, -3, or the branched GDGTs Ib, Ic, IIb, IIc, IIIb and IIIc were not observed, due to their low relative abundance as native species.

A considerable difference in MS signal intensity was observed for the native lipids and their Fmoc-Lys(Boc) derivatives: the native species gave an intensity of c. 10^7 whereas the derivatives gave an intensity of c. 10^4 , indicating a drop in the signal of the derivatives of approx. three orders of magnitude. The low signal to noise ratio (S/N 3-5) for the derivatives indicates that the structures that were not detected are below the limit of detection of the MS instrument. Neither the HPLC-UV nor HPLC-FLD yielded peaks at the elution times for the GDGT derivatives, suggesting that the limit of detection of FLB-GDGTs in sediments was worse for HPLC-FLD and HPLC-UV than for HPLC-MS.

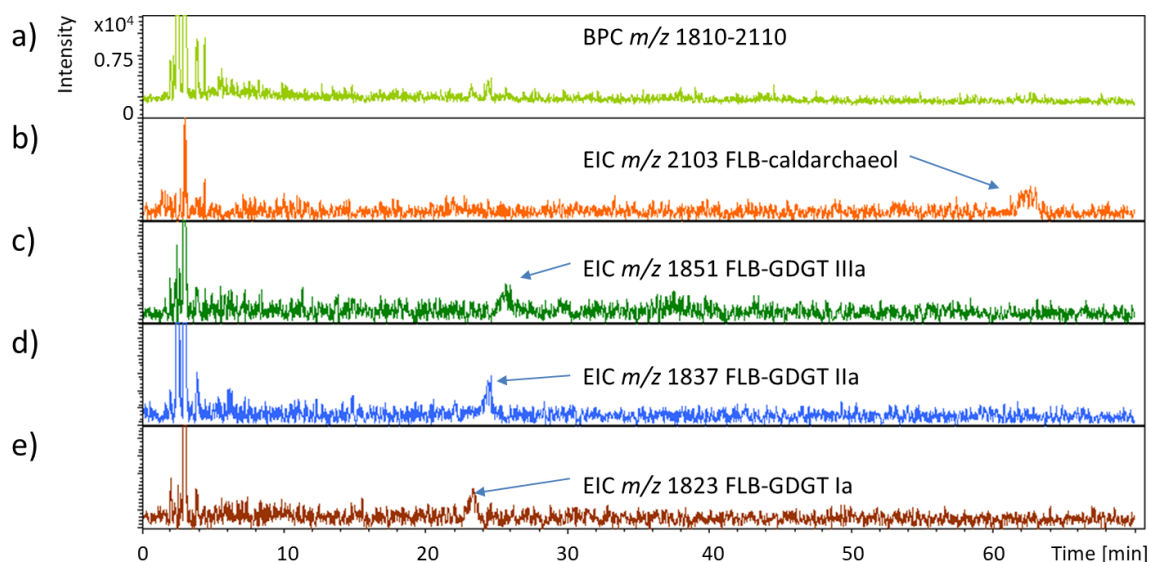


Figure 2.25. Reversed-phase HPLC-MS of the Fmoc-Lys(Boc) derivatives of GDGTs in the polar lipid fraction from a sample from Loch of Stenness: a) BPC m/z 1810-2110, b) extracted ion chromatogram (EIC) for FLB-caldarchaeol m/z 2103, c) EIC for FLB-GDGT IIIa m/z 1851, d) EIC for FLB-GDGT IIa m/z 1837, e) EIC for FLB-GDGT Ia m/z 1823. Note: the MS intensity scale is the same for all chromatograms.

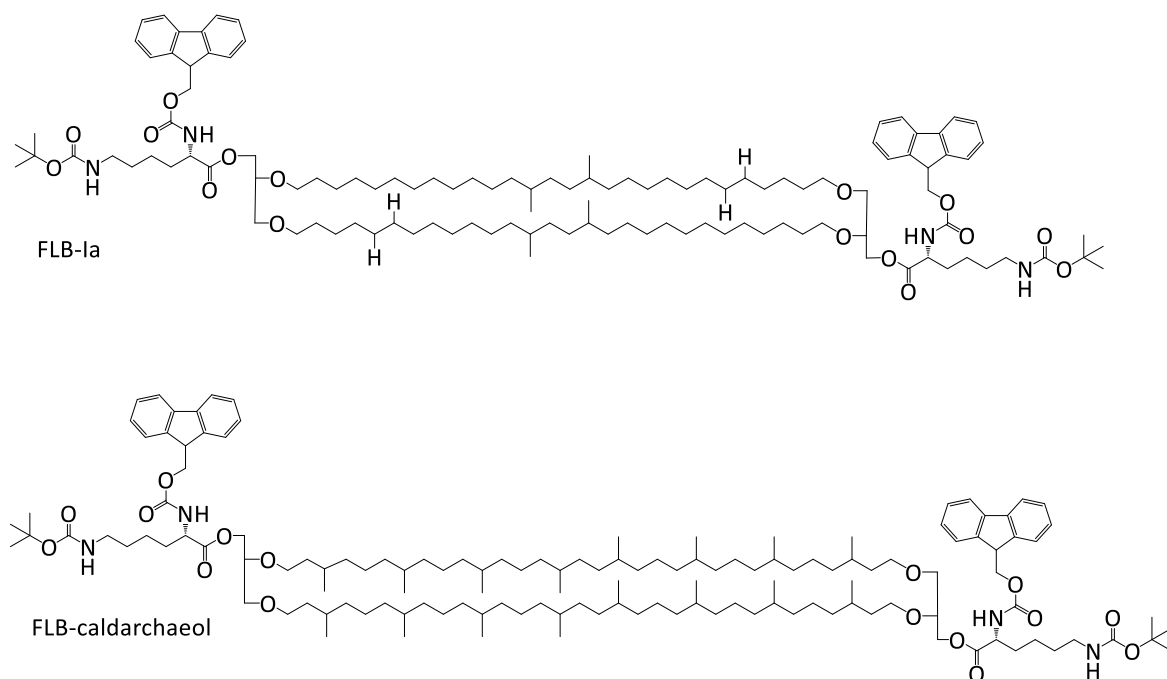


Figure 2.26. (Top) structure of FLB-1a and (bottom) structure of FLB-caldarchaeol.

To test the efficacy of this derivatisation approach on another sample, the polar fraction of the extract from a sediment from the Pliocene Willershausen basin, Germany, (Meischner, 2000; sample located 1.2 m above the fossil band) was also examined. The reversed-phase HPLC-MS of the underivatised polar fraction gave ions corresponding to caldarchaeol, GDGT-1, -2, -3, crenarchaeol and branched GDGTs 1a, 1b, 1c, 2a, 2b, 2c, 3a, 3b, 3c (Figure 2.27).

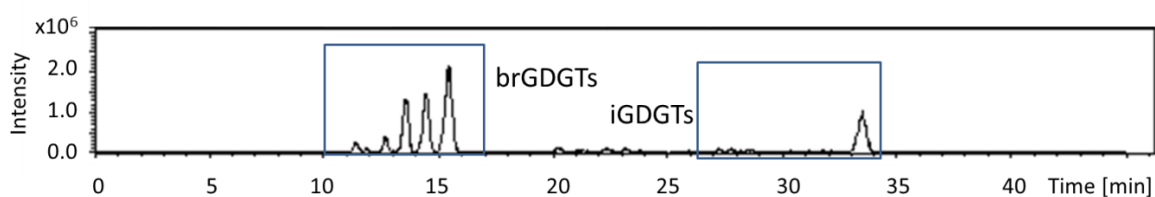


Figure 2.27. Reversed-phase HPLC-MS of the native GDGTs in the polar lipid fraction from Willershausen 1.2 m above the fossil band: BPC m/z 1000-1350.

The base peak chromatogram for the FLB derivatives showed peaks in the retention time ranges for branched and isoprenoid GDGTs (Figure 2.28a). Extracted ion chromatograms (EIC) corresponding to FLB-brGDGT ions gave peaks in the ranges 20-23 min (Figure 2.28d-h), enabling identification of FLB-brGDGTs 1a, 1b (m/z 1823, 1821), 2a, 2b, 2c (m/z 1837, 1835, 1833), 3a (m/z 1851). EIC corresponding to isoprenoid GDGT derivatives enabled identification of GDGTs eluting at 42 and 54 min as FLB-crenarchaeol m/z 2093 and FLB-caldarchaeol m/z 2103, respectively (Figure 2.28b-c).

The derivatives gave 1.5-2 orders of magnitude lower response than the native species. Derivatised branched GDGTs Ia, IIa, IIIa – the most abundant components – and caldarchaeol were also evident in HPLC-UV and HPLC-FLD analyses (Figure 2.29). The peaks appear very weak, hence MS would give better limits of detection and more reliable peak areas, meaning that APCI-MS would be a more viable detector for checking the formation of the derivatives in the first instance. Although Poplawski (2017) showed similar limits of detection (LOD) between UV, FLD and MS for derivatised lipid standards, the analysis of derivatised GDGTs from sediments showed higher signal from MS rather than FLD or UV.

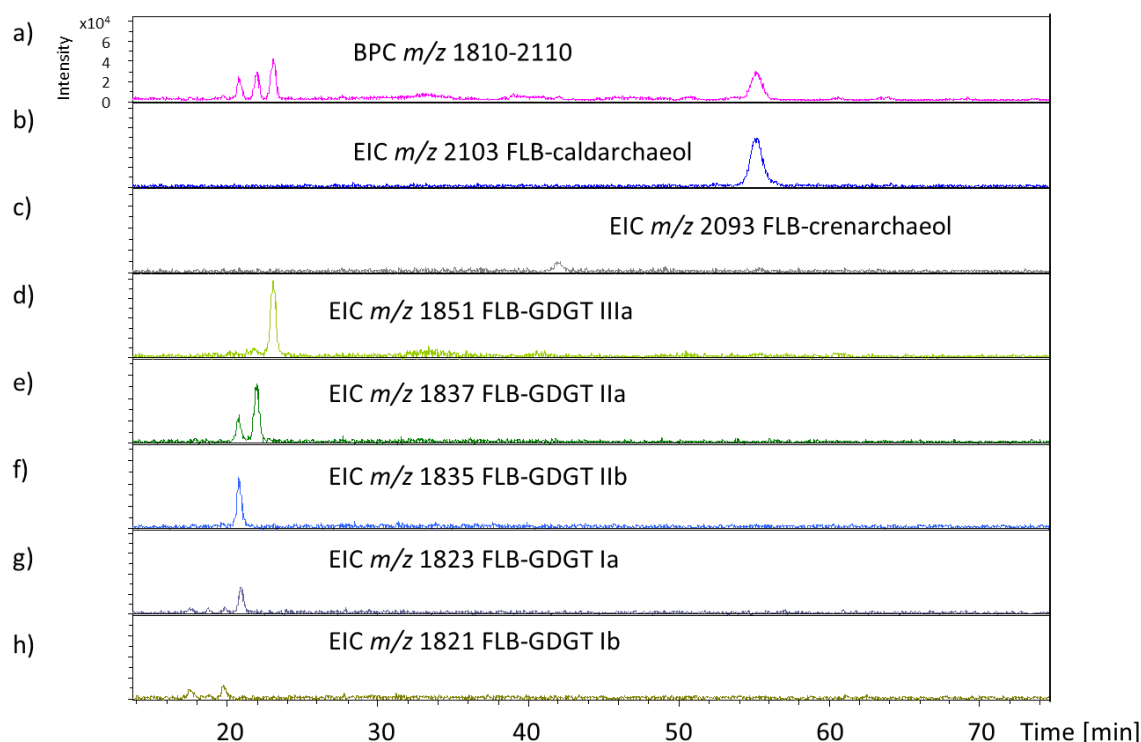


Figure 2.28. Reversed-phase HPLC-MS of the *Fmoc-Lys(Boc)* derivatives of GDGTs in the polar lipid fraction from Willershausen 1.2 m above the fossil band: a) BPC *m/z* 1810-2110; b) EIC for FLB-caldarchaeol *m/z* 2103, c) EIC for FLB-crenarchaeol *m/z* 2093; d) EIC for FLB-IIIa *m/z* 1851; e) EIC for FLB-IIa *m/z* 1837; f) EIC for FLB-IIb *m/z* 1835; g) EIC for FLB-Ia *m/z* 1823; h) EIC for FLB-Ib *m/z* 1821. Note: the MS intensity scale is the same for all chromatograms.

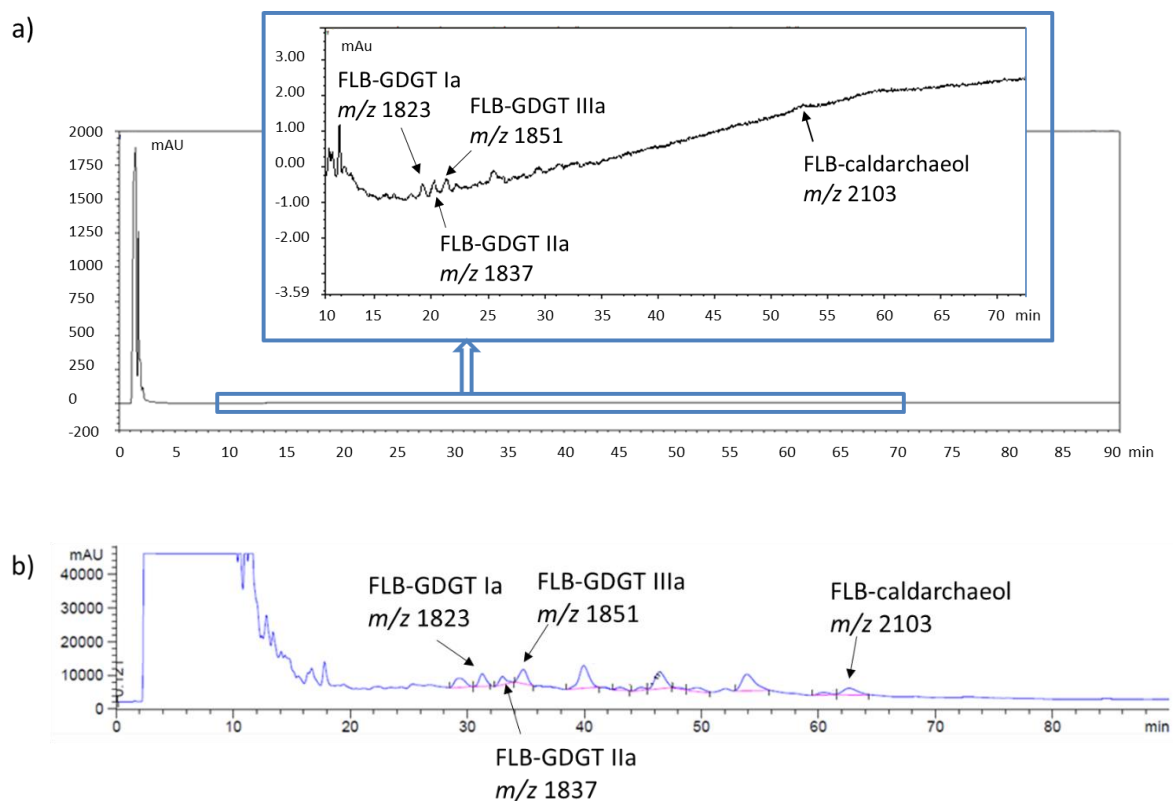


Figure 2.29. Reversed-phase HPLC analysis of the Fmoc-Lys(Boc) derivatives of GDGTs in the polar lipids from Willershausen 1.2 m above the fossil band: a) HPLC-UV analysis λ_{max} 263 nm and detail of FLB-GDGTs in the inset; b) HPLC-FLD analysis λ_{ex} 263 nm, λ_{em} 309 nm. Derivatives of branched and isoprenoid GDGTs are indicated.

Previous work, carried out by Poplawski (2017), reported an improvement in the MS signal by 1-2 orders of magnitude of the FLB derivatives of cholesterol and of 1,2-di-*O*-octadecyl-*rac*-glycerol (*r*-dOG) compared with the native alcohols, improving the limit of detection considerably (Figure 2.30a). A similar result was therefore expected for FLB-GDGTs in sediments. This was not observed when applied to either the Stenness or Willershausen samples, instead a decrease in the signal by 2-3 orders of magnitude was observed (Figure 2.30b-c).

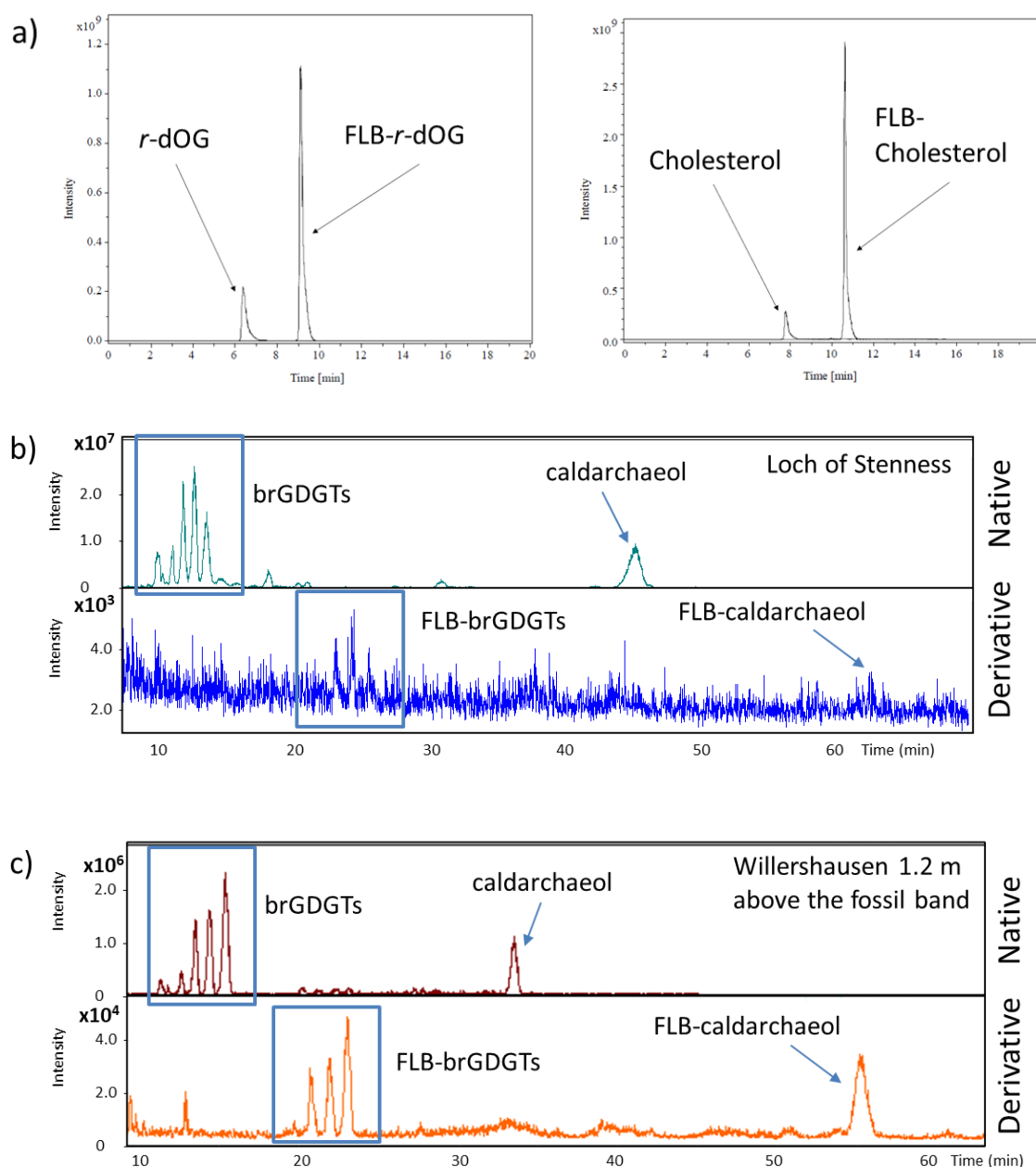


Figure 2.30. Comparison of HPLC-MS signal of native and FLB derivatives of: a) *r*-dOG and cholesterol (reproduced from Poplawski, 2017); b) GDGT lipids from Loch of Stenness sediments; c) GDGT lipids from Willershausen sediments 1.2 m above the fossil band.

The lower signal of the derivatives might indicate incomplete derivatisation of the GDGTs in sediments as opposed to standards. Increasing the equivalents of DMAP (20 eq.) and EDC (100 eq.) used to derivatise another polar fraction from Willershausen did not yield an improved signal for the derivatives, with a response 4 orders of magnitude lower than for the response obtained for the native species (not shown).

A further derivatised extract of Willershausen (sample 1.2 m above the fossil band) was divided into two samples. Sample A was columned to separate the FLB-GDGT derivatives from the reactants (1:1 hexane:ethyl acetate); sample B was separated into medium polar (4:1 hexane:ethyl acetate) and high polar fractions (1:1 DCM:MeOH) to check for the presence of underderivatised GDGTs. Sample A showed the same pattern and peaks as in the sample previously esterified (Figure 2.27). Native GDGTs were not observed in the medium or the high polar fraction from sample B, indicating that the low signal obtained for the esterified GDGTs does not result from incomplete esterification.

It was thought that the derivatised compounds might have adsorbed onto the silica and had therefore not been eluted from the column during the fractionation step; a derivatised sample injected onto HPLC-MS prior to flash column chromatography showed no improvement in the signal detected. This demonstrates that the lower MS signal of FLB-GDGTs compared to the native species is not due to loss of components in the column chromatography step.

The appearance of very intense peaks at the beginning of the run (0-10 min) for both the native and FLB-derivatised samples would be consistent with derivatisation of other alcohols present in the extract. These would include straight chain alkanols, sterols, hopanols and monoesters of GDGTs expected to elute earlier than diester GDGTs. No monoesters of GDGTs were detected with BPC m/z 1360-1405 for brGDGTs and m/z 1640-1655 for iGDGTs. The early eluting compounds have lower masses and are more polar than GDGTs, consistent with derivatives of alkanols, sterols and hopanols. Their HPLC-MS analysis within the early part of the run was complicated by coelution, precluding identification of individual components. Nevertheless, these early eluting components were always present with higher MS signal compared to the GDGTs, possibly meaning that their derivatisation is more facile than the GDGTs.

To determine if the complexity of the sample reduced the yields of derivatised GDGTs or impacted on their MS ionisation, on-line HPLC fractionation (Section 7.4.7) was performed to isolate branched (Figure 2.31a) and isoprenoid GDGTs (Figure 2.31b). After esterification, no derivatives were detected for either fraction. It is possible, however, that the derivatisation was indeed successful but the FLB-GDGTs were below the limit of detection of MS. The results indicate that the lower MS signal intensities obtained for the FLB derivatives of isolated GDGTs by fraction collection were not due to the presence of other alcohols that compete in the derivatisation reaction.

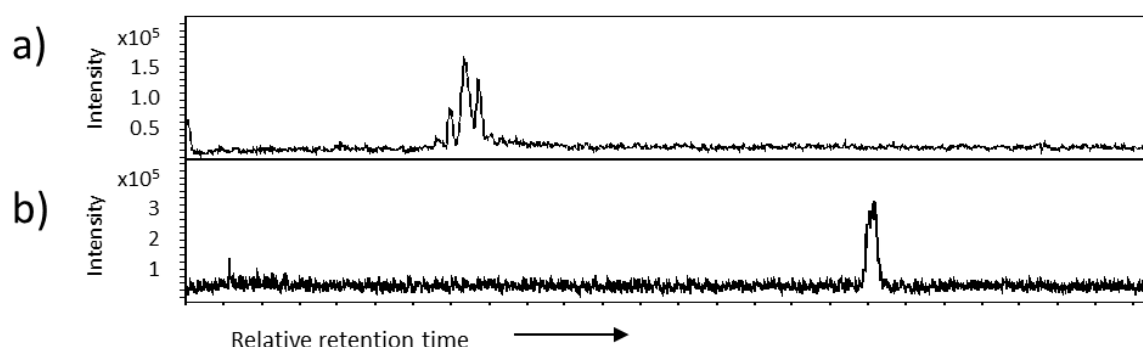


Figure 2.31. Reversed-phase HPLC-MS of native and Fmoc-Lys(Boc) derivatives of GDGTs in the polar lipids from Willershausen 1.2 m above the fossil band: a) native brGDGTs BPC m/z 1000-1060; b) native iGDGTs BPC m/z 1290-1305.

In conclusion, under the conditions tested some success has been shown in the esterification of polar fractions from sediments containing GDGTs, although the MS signal for the derivatives was 2-4 orders of magnitude lower than for the native species. The lower signal is not due to incomplete derivatisation or competition for the reactants from the presence of numerous other compounds present in the complex sediment samples.

The success in increasing MS signal for fluorescent derivatives in complex clinical and environmental samples, as reported in previous literature studies (You *et al.*, 2010; Nelson, 2011), and for lipid standards FLB-*r*-dOG and FLB-cholesterol (Poplawski, 2017) indicated the potential of applying FLB derivatisation to sedimentary lipids. The unsuccessful results shown here on GDGTs in sediments may suggest that further tests are necessary to adjust the method for widespread application. Ohtsubo and co-workers (1993) noticed that the fluorescence intensity of 9-anthroylnitrile derivatives of diester caldarchaeol was fivefold weaker than the monoester and similar data was shown by Bayliss *et al.* (1988), where diethylene glycol (DEG) 9-anthroyl diester had lower fluorescence intensity than the monoester by a factor of 9. The authors suggest that the lower FLD signal is due to the “partial formation of a non-fluorescing intramolecular excimer, favoured by the conformational freedom afforded to the DEG diester by the ethereal oxygen” (Bayliss *et al.*, 1988, pp. 397-398). This may explain the very low FLD and UV signals from the FLB-GDGTs, but fails to clarify the lower signal arising from MS ionisation. Plausible yet untested suggestions include the possibility of formation of crystalline material that evades analysis by HPLC-MS, and the formation of a special conformation of the derivative that inhibits efficient ionisation. The presence of two hydroxyl groups capped with FLB, a rather bulky compound, would favour a particular conformation, possibly dominated by intramolecular forces such as π - π stacking and van

der Waals forces. These interactions would be weaker in monoesters and may explain why the diesters of GDGTs behave differently than lipid standard monoesters analysed by Poplawski (2017).

2.3. Conclusions

In order to increase the limits of detection of GDGTs including low abundant isomers, the potential for derivatising alcohol groups in lipid standards and GDGTs with Fmoc-amino acids was examined. Derivatisation, aided by sonication, of 1-octadecanol and 1,12-dodecanediol standards with Fmoc-Gly and Fmoc-Lys(Boc) yielded the derivatised compounds. These gave rise to MS base peak ions by loss of Fmoc or Boc groups. Fmoc-Gly-cholesterol showed the cholesteryl cation as the base peak. The presence of two alcohol groups on 1,12-dodecanediol meant that an increase in the equivalents of DMAP (4 eq.), Fmoc-Gly (8 eq.) and EDC (16 eq.) was required to preferentially form the diester in 1 h with sonication.

Microwave irradiation, known to be able to reduce reaction times and increase yields, was tested on derivatisation of Fmoc-Lys(Boc)-1-octadecanol (FLB-o). Temperature, power and time of irradiation were altered in order to obtain the highest yields but the recorded HPLC-FLD and HPLC-UV yields were incredibly low under the tested conditions (from 0% to 11.9%). An increase in reaction temperature resulted in incomplete derivatisation and formation of side products, possibly including *N*-acylisourea. This side product, which forms preferentially at high temperatures and inhibits the esterification of alcohols, was not observed in derivatisation by sonication, thus sonication was deemed more efficient for esterification by FLB.

The potential application of Steglich esterification to GDGT lipids from sediment extracts requires a high throughput method. Yields by weight, HPLC-UV and HPLC-FLD were evaluated for multiple samples of 1-octadecanol derivatised with FLB. Derivatisation of 10 FLB-o samples suspended in a plastic rack in the ultrasonic bath indicated that the central positions gave the most reproducible results with lowest standard deviations ($s < 12$) and high yields ($> 75\%$). A comparison of derivatisation by sonication of five samples in a rack and a beaker determined that the former gave lower standard deviations. Finally, for the equipment used in the study, it was concluded that fewer than 10 GDGT samples should be derivatised simultaneously in the central positions of the rack.

Application of FLB esterification to GDGTs in sediment extracts showed that the MS signal for the derivatives was, unexpectedly, 2-4 orders of magnitude lower than for the native species. Under the conditions tested in this study, the difference was not due to incomplete derivatisation, loss of components during column fractionation or competition for the reactants from the presence of

numerous other compounds in the sediment extracts. It is evident that an unknown mechanism affects the formation, behaviour and / or detection of the GDGT derivatives in sediments, such as the formation of crystalline material or a molecular conformation that reduces MS ionisation efficiency. Further understanding of the mechanism, performance of further tests, identification of other synthetic routes and of the side products were limited by time constraints and were beyond the scope of this project.

It seems clear that at the present time, given the lower MS response for the Fmoc-Lys(Boc) derivatives than for the native GDGTs, analysis of the GDGTs as the native lipid cores should be employed in the evaluation of environmental proxies, until more tests and a more viable derivatisation strategy are devised. Therefore, the native GDGTs, in conjunction with other lipid markers and chlorophyll pigments, were analysed in order to study sea-level fluctuations in Quaternary cores from UK coastal locations (Chapters 3 and 4).

3. Molecular fossils as a tool for tracking Holocene sea-level change in the Loch of Stenness, Orkney

This chapter was submitted for publication to the Journal of Quaternary Science and is currently under review following revision. The format was adapted to the thesis but the content is similar to the submitted publication.

Authors: Conti, M.L.G., Bates, M.R., Preece, R.C., Penkman, K.E.H., Keely, B.J.

Collection of samples, molecular fossil analyses and interpretation was carried out by Conti. The manuscript was written by Conti with inputs from Bates, Preece, Penkman and Keely.

3.1. Introduction

Changes in sea level have been studied extensively to understand their causes and impacts on the environment and human populations (Rollins *et al.*, 1979; Jablonski, 1980; Gaffney *et al.*, 2009; Hodgson *et al.*, 2009; Bates *et al.*, 2016; Benjamin *et al.*, 2017; Shennan *et al.*, 2018; SROCC, 2019). Similarly, predictions of future sea-level change have been based on evidence from Quaternary glacial and interglacial cycles in order to decouple the contributions from the eustatic and isostatic components (Church *et al.*, 2008; Murray-Wallace and Woodroffe, 2014).

Transgressions and regressions can lead to changes in the dominance of terrestrial or marine sources of organic matter (OM) at a particular location. Localised fluctuations between terrestrial-dominated and marine-dominated conditions in coastal / near coastal regions can be inferred from seismic mapping, palaeontological analysis, changes in the nature and morphology of the sediments, and changes in the composition and nature of OM (Cattaneo and Steel, 2003; Shennan *et al.*, 2015). Environmental proxies for tracking transgressions based on soil and sediment analysis exploit shifts in the populations of plant macrofossils, insects, pollen and spores, foraminifera, diatoms, molluscs and ostracods (Kjemperud, 1981; Horton *et al.*, 1992; Bunting, 1994; Mazzini *et al.*, 1999; Gehrels *et al.*, 2001; Davis *et al.*, 2003; Farrell *et al.*, 2014; Bates *et al.*, 2016; Barlow *et al.*, 2017; Benjamin *et al.*, 2017). While a major challenge in using macro- and micro-fossil evidence is their extent of preservation and / or limited number of specimens, it is often possible to extract organic geochemical molecular fossils incorporated into the sediment matrix. Through their relation to the biological molecules from which they originate, the molecular fossils can reflect specific OM inputs (Figure 3.1) and thereby reveal characteristics of, and changes in, the environment inhabited by the source organisms (Poynter and Eglinton, 1990; Meyers and Ishiwatari, 1993; Meyers, 1997; Castañeda and Schouten, 2011).

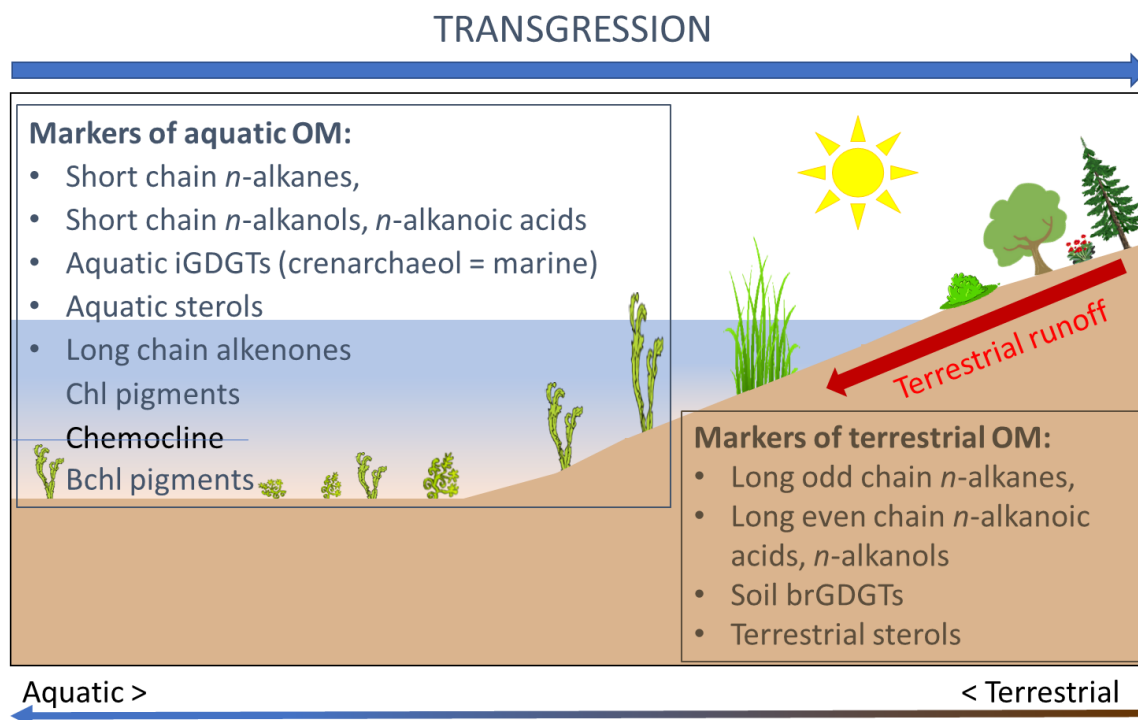


Figure 3.1. Summary of key biological markers employed in this study and their association with particular organic matter sources. Abbreviations: OM = organic matter; iGDGTs = isoprenoid glycerol dialkyl glycerol tetraethers; Chl = chlorophyll pigments; Bchl = bacteriochlorophyll pigments; brGDGTs = branched glycerol dialkyl glycerol tetraethers.

Molecular fossils can be analysed within milligram to gram quantities of sediment, a much smaller scale than the few grams needed for traditional macro and microfossil analyses (Shennan *et al.*, 2015). Hence, sampling resolution can be reduced, even to the millimetre scale where justifiable, enabling higher temporal resolution analyses (Airs and Keely, 2002). Robust lithological and morphological studies are key in identifying the areas of undisturbed sediments which are ideal for palaeoenvironmental and molecular fossil analyses, avoiding compromised areas (e.g. where bioturbation or burrowing has occurred).

3.1.1. Molecular fossils inferring sea-level changes

The widespread occurrence of molecular fossils in sediments and their derivation from both aquatic and terrestrial sources allows the recognition of allochthonous and autochthonous sources of OM in sediments (Eglinton and Hamilton, 1967; Cranwell, 1982; Killops and Killops, 1993; Keely, 2006; Castañeda and Schouten, 2011; Schouten *et al.*, 2013). Extensive research on the diagenetic transformation of various biomarkers enables reconstructions based on the principal molecular fossils of primary producers, such as chlorophyll pigments, *n*-alkanes, alcohols, fatty acids,

tetraether lipids (Eglinton and Hamilton, 1967; Harradine *et al.*, 1996; Volkman, 2005; Schouten *et al.*, 2013). Notably, however, the use of molecular fossils to identify and study sea-level fluctuations has been largely overlooked, with only a few studies reported in the literature (e.g. Ficken and Farrimond, 1995; Squier *et al.*, 2002; Bendle *et al.*, 2009; van Soelen *et al.*, 2010; Carr *et al.*, 2015; De Jonge *et al.*, 2016; Li *et al.*, 2017).

The combined use of several molecular fossils is key to identifying sea-level changes (Figure 3.1). Environmental changes affect the conditions and the balance of the OM input: a transgression increases water volume and alters nutrient availability, reworking, degradation, sedimentation rate and, most importantly, the primary production of OM (Cattaneo and Steel, 2003; Murray-Wallace and Woodroffe, 2014). Transgressions lead to increased reworking and may restrict sedimentation (Long *et al.*, 2015), affecting the nature and populations of the biota (Cattaneo and Steel, 2003; Murray-Wallace and Woodroffe, 2014). As a result of a transgression, it can be expected that molecular fossils exhibit a shift from mostly terrestrial OM (from either land runoff or *in situ* production) to a dominance of aquatic and / or marine OM input.

Terrestrial OM reflects the vegetation in the hinterland through the distributions of: sterols that occur widely in higher plants (Volkman, 1986), long odd chain *n*-alkanes (*n*-C₂₅ to *n*-C₃₅) and long even chain *n*-alkanols and *n*-alkanoic acids (*n*-C₂₂-C₃₀) prominent from higher plant waxes (Cranwell, 1973; 1982). Furthermore, branched glycerol dialkyl glycerol tetraether lipids (brGDGTs), structural cores of the polar membrane lipids of eubacteria, represent soil microbial communities (Figure 3.1; Schouten *et al.*, 2013). By contrast, aquatic conditions are represented by a different suite of markers, some of which are specific to marine conditions. Hence, among isoprenoid GDGTs (iGDGTs), derivatives of structural membrane lipids of Archaea common in aquatic conditions (Schouten *et al.*, 2013), crenarchaeol is a specific marker for marine Archaea (Damsté *et al.*, 2002). Although low level production of iGDGTs in soil and some brGDGTs in aquatic environments have been noted (DeLong, 1992; DeLong *et al.*, 1994; Hershberger *et al.*, 1996; Tierney and Russell, 2009; Fietz *et al.*, 2012; Li *et al.*, 2015), the general source distinction between the two groups is employed widely for tracing the origin and transport patterns of soil OM (Sun *et al.*, 2011; Doğrul Selver *et al.*, 2012). Other markers of aquatic conditions include short chain length *n*-alkanes (*n*-C₁₇ to *n*-C₂₄), common in bacteria and algae (Cranwell, 1973), and predominance of short even chain *n*-alkanols and *n*-alkanoic acids (*n*-C₁₆ and *n*-C₁₈), though these also occur in some plants (Meyers and Ishiwatari, 1993). Long chain unsaturated alkenones (*n*-C₃₇₋₃₉), especially C_{37:3} and C_{37:2}, are common markers of haptophyte algae in marine sediments (Marlowe *et al.*, 1984). In freshwater lake systems C_{37:4} occurs alongside C_{37:3} and C_{37:2} (Cranwell, 1985; Bendle *et al.*, 2009).

Changes in the availability of nutrients in aquatic environments can be reflected by fluctuations in the concentrations of particular chlorophyll pigments (broadly described as chlorins) produced by the photosynthetic organisms inhabiting the water column (Figure 3.1; Keely, 2006). The physicochemical conditions in the water column are reflected by particular pigment structures. Photoautotrophs that live in oxygen-rich waters, including aquatic plants, photosynthetic algae and cyanobacteria, produce chlorophyll pigments (chls; Scheer, 1991). In contrast, bacteriochlorophylls (bchls) are the photoreceptors in the purple and green bacteria that are restricted to anoxic waters (Figure 3.1; Pfennig, 1977). Covariance in organic carbon and chlorin accumulation provides evidence that pigment concentrations reflect changes in productivity during glacial / interglacial cycles (Harris *et al.*, 1996). Short term transgressions can be evident in changes in the nature and distribution of chlorophyll pigments (Squier *et al.*, 2002; Hodgson *et al.*, 2009).

Specific proxies, indicators of palaeoenvironmental conditions, have been suggested to distinguish inputs of plant OM (average chain length, ACL; Section 1.4.4.3; Poynter and Eglinton, 1990), terrestrial from marine OM based on brGDGTs and crenarchaeol (branched and isoprenoid tetraether index, BIT; Section 1.4.4.4; Hopmans *et al.*, 2004), and terrestrial from freshwater OM based on *n*-alkane carbon chain lengths (proxy of aquatic macrophytes, P_{aq} ; Section 1.4.4.2; Ficken *et al.*, 2000). In immature sediments, the carbon preference index (CPI; Section 1.4.4.1; Bray and Evans, 1961) can reflect predominance of either terrestrial or algal OM (Clark and Blumer, 1967; Ortiz *et al.*, 2004). The diol index (DI; Section 1.4.4.9; Versteegh *et al.*, 1997), based on C_{30} and C_{32} 1,15 diols, has been used to distinguish freshwater and marine OM (Versteegh *et al.*, 1997; van Soelen *et al.*, 2010). The tetraether index of 86 carbons (TEX₈₆; Section 1.4.4.5; Schouten *et al.*, 2002), based on iGDGTs, is a proxy for sea-surface water temperature (SST), and mean annual air temperature (MAAT) can be reconstructed from the methylation of branched tetraethers (MBT; Section 1.4.4.6; Weijers *et al.*, 2007). A proxy proposed to reconstruct soil pH is based on brGDGTs (cyclisation of branched tetraethers, CBT; Section 1.4.4.6; Weijers *et al.*, 2007). Other proxies for temperature estimations exist but are not applied in this work; for example, U_{37}^k is based on long chain alkenones (Section 1.4.4.7; Brassell *et al.*, 1986; Prahl and Wakeham, 1987), RAN₁₃, RAN₁₅ and RAN₁₇ on 3-OH fatty acids (Section 1.4.4.8; Wang *et al.*, 2016; Yang *et al.*, 2020) and HDI₂₆, HDI₂₈ and HTI₂₈ on heterocyst glycolipids (Section 1.4.4.10; Bauersachs *et al.*, 2015a). Correlations between molecular fossils and environmental conditions have enabled the development of various proxies that can be used to infer sea-level changes (Ficken and Farrimond, 1995; Bendle *et al.*, 2009; van Soelen *et al.*, 2010; Carr *et al.*, 2015; De Jonge *et al.*, 2016; Li *et al.*, 2017).

3.1.2. Aims

There is considerable potential for routinely using molecular fossils for sea-level studies. In the UK, Holocene transgressive sequences have been extensively studied in many of the larger estuaries and coastal environments in England (Devoy 1977; Long *et al.*, 2000; Sidell, 2003; Bates and Stafford, 2013) and Scotland (Long *et al.*, 2016; Palamakumbura, 2018). In most cases, however, the precise nature and duration of the flooding event remains difficult to determine. Sea-level index points from Scottish sites show sea-level fluctuations (12-3 ka) resulting from glacio-eustasy and isostasy, subsequently approaching present-day levels (3 ka-present; Shennan, 1989; Shennan and Horton, 2002; Selby and Smith, 2007). The timing of the fluctuations in the Mid-Late Holocene varies regionally; for example, Orkney sea-level approached present values approx. 5-4 ka BP (Shennan and Horton, 2002). Seismic and palaeoenvironmental analyses of a series of late-glacial to Holocene sediment cores from the Loch of Stenness, Orkney, demonstrated the impact of the transgression on the local geography and how it might have impacted human settlement (Bates *et al.*, 2016).

Building on the existing research on sea-level change at the Loch of Stenness, the overall aim of this study was to use this well-constrained transgression record to develop a complementary method to study sea-level change using molecular fossils, and assess their potential in sea-level studies.

Analysis of a combination of molecular fossils could provide a valuable record of marine and terrestrial OM inputs and changes associated with the transgression. This approach has the potential to provide more detailed and explicit environmental records of the impact of the transgression on sedimentary OM allowing better constraints on the timing of events.

Table 3.1. Proxies developed from biological markers of terrestrial, aquatic and marine organic matter (OM).

Proxy	What it represents	Markers	Values and inference (see Appendix 3, Table A3.2 for equations)	Reference
Carbon preference index (CPI)	Extent of input of fresh terrestrial and reworked OM	Long chain <i>n</i> -alkanes <i>n</i> -C ₂₃₋₃₃	>5: fresh terrestrial OM <5: algal, reworked OM	Bray and Evans, 1961
Proxy for aquatic macrophytes (P _{aq})	Ratio used to discriminate between higher plant and aquatic macrophyte OM	Long odd chain <i>n</i> -alkanes <i>n</i> -C ₂₃ , <i>n</i> -C ₂₅ , <i>n</i> -C ₂₉ , <i>n</i> -C ₃₁	<0.1: terrestrial plants 0.1-0.4: emergent macrophytes 0.4-1: submerged/floating macrophytes	Ficken <i>et al.</i> , 2000
Average chain length (ACL)	Average carbon number of terrestrial plants	<i>n</i> -alkanes <i>n</i> -C ₂₇ , <i>n</i> -C ₂₉ and <i>n</i> -C ₃₁	Predominance <i>n</i> -C ₂₇ : forest Predominance <i>n</i> -C ₃₁ : grasses	Cranwell, 1973; Poynter and Eglinton, 1990
Branched and isoprenoid tetraether (BIT)	Ratio that discriminates terrestrial runoff from marine OM	brGDGTs and crenarchaeol	0: marine OM 1: terrestrial OM	Hopmans <i>et al.</i> , 2004
Tetraether index of 86 carbon atoms (TEX ₈₆)	Reconstruction of sea-surface temperature	iGDGTs, including crenarchaeol stereoisomer	Sea-surface water temperature in °C	Schouten <i>et al.</i> , 2002
Lake temperature	Lake water temperature	brGDGTs	Lake-water temperature in °C	Pearson <i>et al.</i> , 2011

Cyclisation of branched tetraethers (CBT)	Reconstruction of soil pH	brGDGTs	pH values	Weijers <i>et al.</i> , 2007
---	---------------------------	---------	-----------	---------------------------------

3.2. Materials and methods

[Please note that the following section contains a shortened version of analytical methods that are reported in full in Chapter 7]

3.2.1. Site description

The Loch of Stenness is a ca 4 km long brackish lake situated in the main island of the Orkney archipelago, Scotland (Figure 3.2a), and connected to the sea at the Brig O'Waithe (Figure 3.2b). The area has been inhabited since at least 3500 BC; the extensive archaeological evidence forms part of the Heart of Neolithic Orkney World Heritage Site (Farrell *et al.*, 2014). Core 2014-1 (Bates *et al.*, 2016) was obtained in 2014, stored in Lampeter and was subsampled for this study in 2016 at 10 depths between 197 and 14 cm (Figure 3.3).

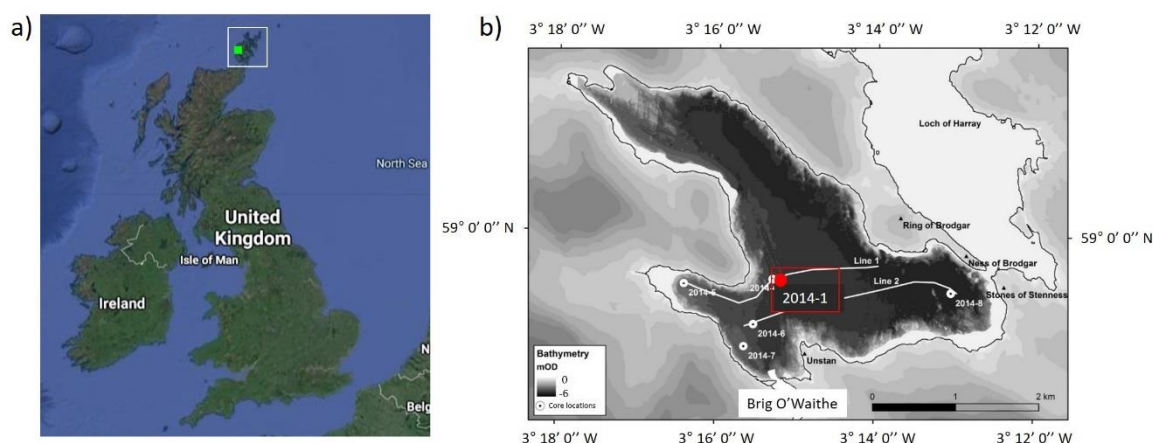


Figure 3.2. a) Map of the British Isles showing the Orkney archipelago (white square) and the Loch of Stenness (green square, adapted from Google Maps); b) map of the Loch of Stenness showing the location of core 2014-1 in the red rectangle. Bathymetry only shown for the Loch of Stenness (adapted from Bates *et al.*, 2016).

3.2.2. Previous studies of the Loch of Stenness core 2014-1 (Bates *et al.*, 2016)

The core lithology consists of a grey-brown organic silt with mollusc shells between 200 and 141 cm, overlaid by a pale grey silt with occasional shell fragments (141-81.5 cm). The uppermost sediments (81.5-0 cm) comprise soft dark grey silt with occasional shell fragments of brackish species. The loss-on-ignition profile (Figure 3.3) indicates that the organic component was >20% below 140 cm depth and between 10% and 17% above 140 cm depth; higher values are associated

with the coarsest sediments of the core. Carbonate-rich sediments below 85.5 cm (10-26%) are associated with slower sedimentation and controlled deposition in a freshwater environment.

Palaeoenvironmental reconstruction, inferred from foraminifera, mollusc and ostracod assemblages, suggests two main environmental settings: a freshwater coastal lake (200 and 104 cm core depth) and a brackish loch (102 and 0 cm core depth). The brackish environment was further subdivided on the basis of the molluscan fauna: 102-81 cm shows onset of tidal access under very low brackish conditions and 80-0 cm represents a brackish environment in which decalcification occurred and a restricted foraminiferal assemblage existed. Microscopy showed exclusively freshwater ostracods from 200 to 104 cm, brackish and freshwater ostracods in the 102-80 cm section, and brackish molluscs and foraminifera from 80 to 0 cm (Appendix 3, Table A3.1).

Radiocarbon dating of lymnaeid sp. shells at 92-94 cm and at 82-84 cm showed that the incursion began between ~5939 and 5753 cal a BP (5130±30 ¹⁴C age BP) and was fully established between ~5862 and 5612 cal a BP (4980±30 ¹⁴C age BP).

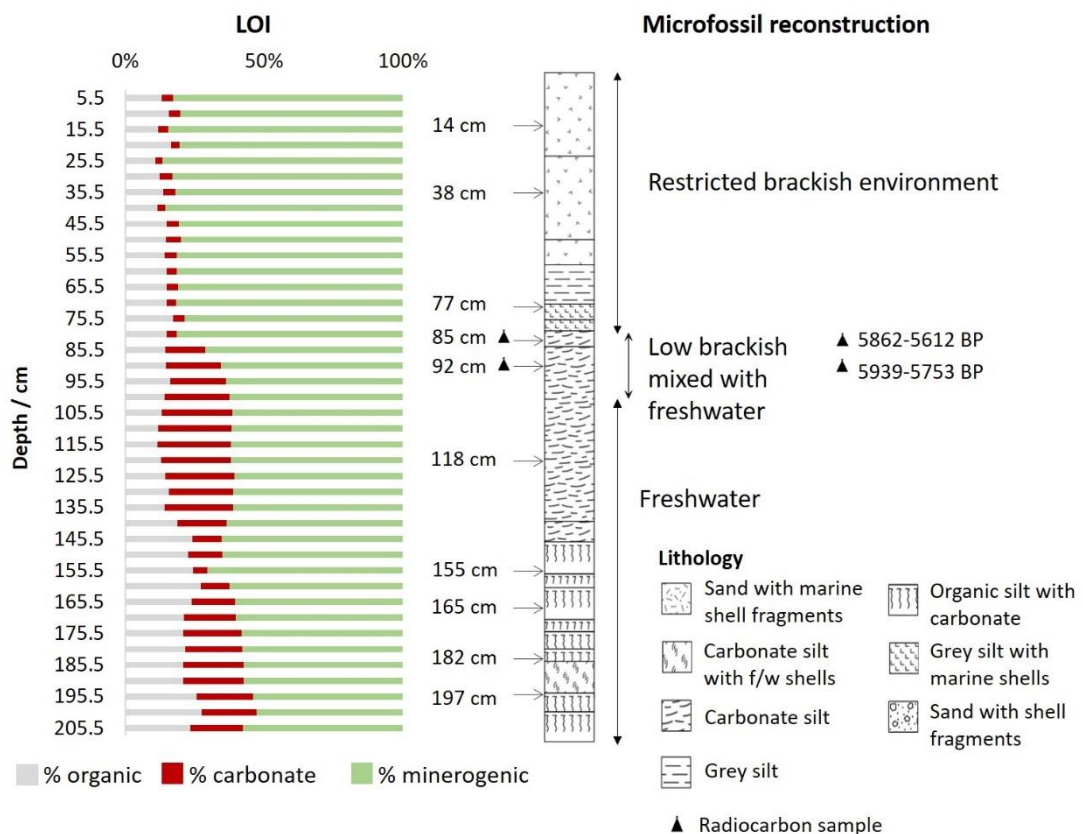


Figure 3.3. Stenness core 2014-1 showing the main lithological zones, the loss-on-ignition results (sampled every 5 cm) and the dates of the beginning and end of transgression according to Bates et al. (2016); sampling depths analysed in this study are marked with arrows.

3.2.3. Separation of mollusc shells

The freeze-dried sediment was inspected for intact gastropod shells before grinding and sieving. Any shells found were removed with a spatula and / or forceps and sonicated in deionised water to remove sediment residues. The species were identified after air-drying in a fumehood overnight.

3.2.4. Extraction and analysis of molecular fossils

For complete methods, see Chapter 7. The core was subsampled at 10 depths (Figure 3.3; Section 7.1.3). The freeze-dried sediment was homogenised and sieved (Section 7.1.4; Saesaengseerung, 2013). Extraction of OM from this fraction was carried out using accelerated solvent extraction (ASE; Section 7.2.1; Schouten *et al.*, 2007; Saesaengseerung, 2013). The lipids were separated into four distinct polarity fractions using flash column chromatography (Section 7.2.3; Green, 2013). These fractions were analysed by HPLC-MS (for the GDGT lipids; Sections 7.4.3, 7.4.11; Schouten *et al.*, 2007) and by GC-FID for other lipids (Sections 7.2.4, 7.4.1) and selected samples by GC-MS (Section 7.4.2; Green, 2013). Following extraction (Section 7.2.1) and derivatisation with diazomethane (Section 7.2.2), chlorophyll pigments were analysed by UHPLC-DAD (Section 7.4.4) and UHPLC-MS (Section 7.4.9; Saesaengseerung, 2013).

3.3. Results and discussion

Shells of the freshwater gastropods *Gyraulus crista*, *Gyraulus laevis* and *Radix balthica* were identified between 197 and 85 cm depth, supporting the findings of Bates *et al.* (2016) who identified predominantly freshwater ostracods with some brackish species between 200 and 82 cm (Section 3.2.2; Appendix 3, Table A3.1). The following sections build on interpretation of Bates *et al.* (2016), that the core sequence represents a freshwater lake (200-104 cm), the onset of marine conditions (102-81 cm) and the formation of a brackish loch (80-0 cm), reporting the molecular fossil data from these critical horizons (Table 3.2).

Table 3.2. Depth ranges of key environmental transitions identified by Bates et al. (2016) in the core from the Loch of Stenness, and the depths subsampled here for molecular fossil analysis.

Identified zone	Bates <i>et al.</i> , 2016	This study
	Depth / cm	
Brackish loch	80-0	77, 38, 14
Onset tidal access	102-81	92, 85
Freshwater coastal lake	200-104	197, 182, 165, 155, 118

3.3.1. The freshwater lake (200-104 cm)

The predominance of brGDGTs and the absence of marine marker crenarchaeol confirmed a freshwater lake environment in the lowest part of the core (Table 3.3; Figure 3.4), with a prevalence of terrestrial OM input from runoff. The input of fresh OM was revealed by the occurrence of long odd chain *n*-alkanes and high CPI values (Table 3.3; Appendix 3, Table A3.2). Prevalence of terrestrial OM was further indicated by dominance of soil-derived brGDGTs (Figure 3.4), long even chain *n*-alkanols and *n*-alkanoic acids (Figure 3.5b; Cranwell, 1982; Meyers and Ishiwatari, 1993), long odd chain *n*-alkanes (Figure 3.5a; Bray and Evans, 1961; Cranwell, 1973) together with stigmasterol and β -sitosterol, the major sterols of higher plants (the latter also an abundant component in emergent water plants; Meyers and Ishiwatari, 1993). Further evidence of terrestrial input comes from the presence of the sterol obtusifolol of *Sphagnum* moss and vascular plant origins (Figure 3.5c; Ronkainen *et al.*, 2013). Although brGDGTs can have terrestrial and minor contributions from aquatic sources, the dominance of other plant/terrestrial markers suggests input from soils.

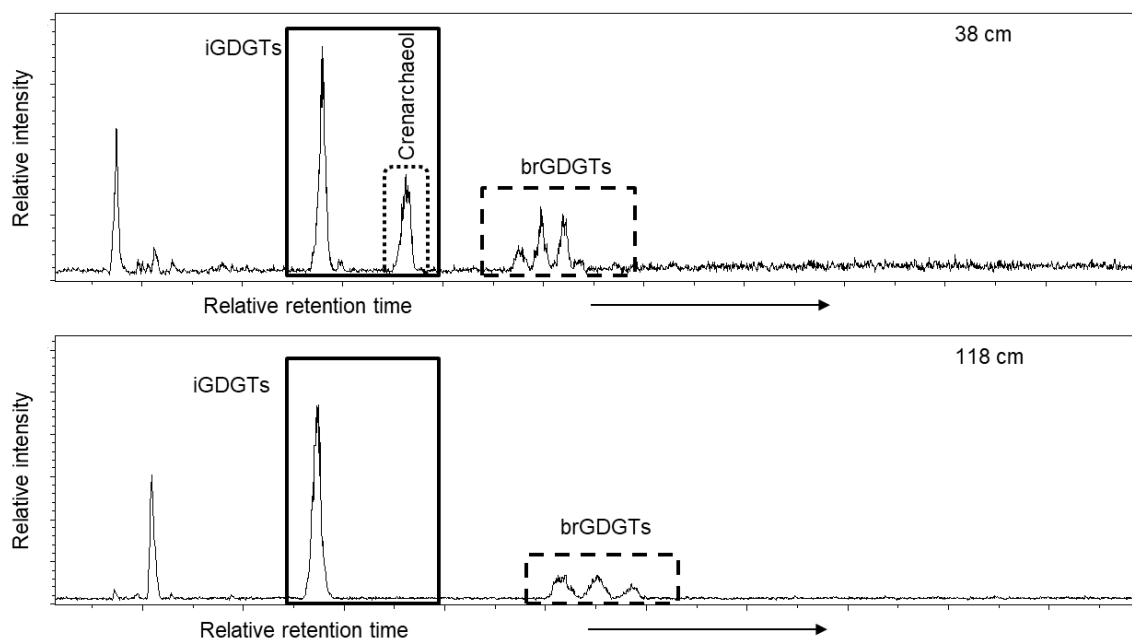


Figure 3.4. HPLC-MS chromatograms m/z 950-1500 of GDGTs from the Loch of Stenness from depths of 38 cm (top) and 118 cm (bottom). The boxes indicate iGDGTs (solid line), brGDGTs (dashed line) and crenarchaeol (dotted line). Note the presence of marine marker crenarchaeol at 38 cm.

Mixed terrestrial and emergent macrophyte origins for the n -alkanes, consistent with a permanent body of water during the freshwater stage, was evident by the occurrence of markers both for higher plant waxes and for aquatic macrophytes, reflected in the P_{aq} index values (Table 3.3; Figure 3.6; Ficken *et al.*, 2000). Evidence for an aquatic OM contribution from Archaea, algae and / or bacteria comes from small amounts of iGDGTs (Figure 3.4; Powers *et al.*, 2010; Bischoff *et al.*, 2016; De Jonge *et al.*, 2016) and from short chain n -alkanoic acids occurring above 182 cm (Figure 3.5b; Cranwell, 1982).

Notably, at 118 cm there is a change in the OM: algal markers became the dominant components, reflecting a relative reduction in terrestrial deposition and increase in algal OM production, possibly enhanced by increased preservation resulting from water column anoxia (Figure 3.5a, b, d). This observation probably indicates the disruption of the freshwater lake conditions associated with the early stages of the marine transgression identified from the microfossil assemblage at 102 cm (Bates *et al.*, 2016).

Detail on the water column conditions was provided by the chlorophyll and bacteriochlorophyll pigments. As is commonly observed, intact and early diagenetic transformation products (formed via enzymatic, herbivore grazing and oxidative processes) were incorporated into the sediment (Appendix 3, Figure A3.1; Shuman and Lorenzen, 1975; Hendry *et al.*, 1987; Harradine *et al.*, 1996;

Ma and Dolphin, 1996; Walker *et al.*, 2002; Keely 2006). The fluctuations in the summed concentrations of chl and bchl pigments implies short term changes in primary production (Figure 3.5d). At 197 cm the predominance of chlorophyll pigments indicates a fully oxidised water column. The presence of bacterioviridin *a* (bvir *a*), an oxidation product of bacteriochlorophyll *a* (Wilson *et al.*, 2004), suggests either a shallow-water environment or even desiccation occurred at this time. Depths between 182 and 118 cm record a mixed primary producer community with the dominant oxygenic population separated from a deeper anoxygenic population by a chemocline (Pfennig, 1977; Gervais, 1998). Chemoclines form in zones of oxygen depletion and reducing environments (Pfennig, 1977). The presence of a fully developed chemocline and absence of bvir *a* from 182 to 118 cm indicates that the OM was not affected by fluctuations in oxygenation, suggesting that the water column was deeper than at 197 cm.

3.3.2. The marine transgression (102-81 cm)

Signatures of *n*-alkanes were absent / below the detection limit at 92 cm core depth (94-92 cm ¹⁴C dated 5939-5753 BP; Bates *et al.*, 2016). Increasing dominance of aquatic OM (algal *n*-alkanols) at the expense of terrestrial OM (*n*-alkanoic acids and *n*-alkanols) at 92 cm depth reflects the continuation of the marine transgression (Figure 3.5a-c). A much-reduced population of anaerobic photosynthetic organisms most likely reflects disruption of the chemocline.

At 85 cm (84-82 cm ¹⁴C dated 5862-5612 BP; Bates *et al.*, 2016), a low CPI value of 4.39 (Table 3.3; Figure 3.6) was recorded. This can indicate a dilution in the terrestrial OM by algal *n*-alkanes, even though concentrations are low, as shown by the *n*-alkane profile (Figure 5; Clark and Blumer, 1967; Ortiz *et al.*, 2004). The presence of algal OM is also confirmed by short chain *n*-alkanoic acids and pigments. The low P_{aq} proxy indicates enhanced terrestrial OM input and a decrease in freshwater macrophytes compared with the samples in earlier horizons (Table 3.3; Figure 3.6; Ficken *et al.*, 2000).

While microfossil evidence enabled recognition of brackish conditions being established from 102 cm, the detection of crenarchaeol at 85 cm depth indicates the onset of production by a small population of marine Thaumarchaeota (Figures 3.4, 3.6; Table 3.3). The contrast with other lipid analyses that suggest that the freshwater lake was disrupted from as early as 118 cm core depth could reflect a lag in the production of Thaumarchaeota with them only becoming prominent once stable marine / brackish conditions became established towards the end of the transgression.

The absence of bchls at 85 cm reveals the disappearance of the chemocline with establishment of a fully oxic water column (Figure 3.5d). Such a shift in the primary producer community can be a

result of turbulent changes to the water column (Squier *et al.*, 2002). It is evident that the sample at 85 cm represents a switch between a turbulent environment (from the pigments) and a stable environment (from the GDGTs) representing the ongoing transgression event.

3.3.3. The established brackish loch (80-0 cm)

Established marine production with terrestrial OM input is indicated by the presence of crenarchaeol and soil brGDGTs (77, 38 and 14 cm core depth; Figure 3.4). The range of BIT values observed is comparable to open coastal environments (Table 3.3, Figure 3.4; Hopmans *et al.*, 2004; Doğrul Selver *et al.*, 2012; 2015). The *n*-alkanol and *n*-alkanoic acid distributions and concentrations indicate the dominance of terrestrial over aquatic OM (Figure 3.5b). The similarity of the lipid concentrations to those preserved in the freshwater lake environment (Section 3.3.1), is consistent with cessation of the disruption associated with the transgression (Figures 3.5, 3.6). The high CPI values throughout the brackish loch section confirm the predominance of fresh terrestrial OM (Table 3.3; Figure 3.6). The absence of chlorophyll pigments in this section of the core is consistent with a strongly oxidative environment leading to the total destruction of pigments (Figure 3.5d; Hendry *et al.*, 1987).

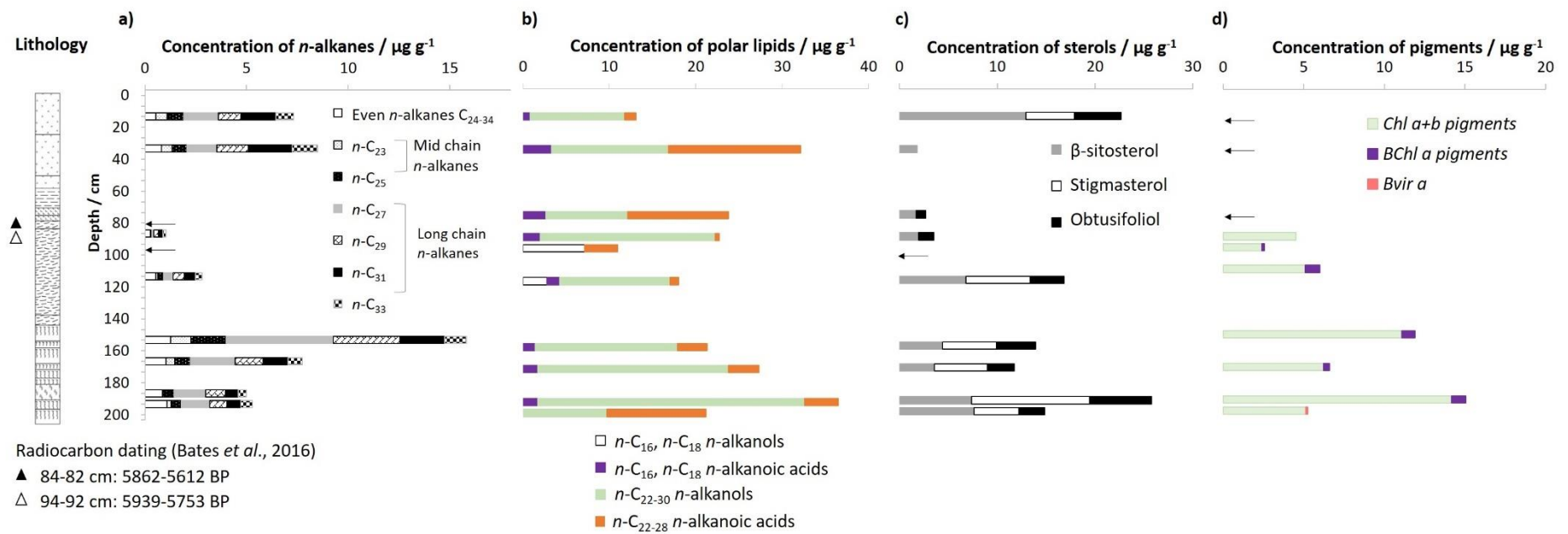


Figure 3.5. Lithology and radiocarbon dating from Bates et al. (2016), and a) Concentrations of *n*-alkanes *n*-C₂₃₋₃₅; b) concentrations of *n*-C₁₆, *n*-C₁₈ and *n*-C₂₂₋₃₀ *n*-alkanols, and *n*-C₁₆, *n*-C₁₈ and *n*-C₂₂₋₂₈ *n*-alkanoic acids; c) concentrations of sterols; d) concentrations of chlorophyll *a*+*b*, bacteriochlorophyll *a* pigments and bacterioviridin *a* in the Loch of Stenness sediments. The arrows indicate sample depths where lipids or pigments were not detected.

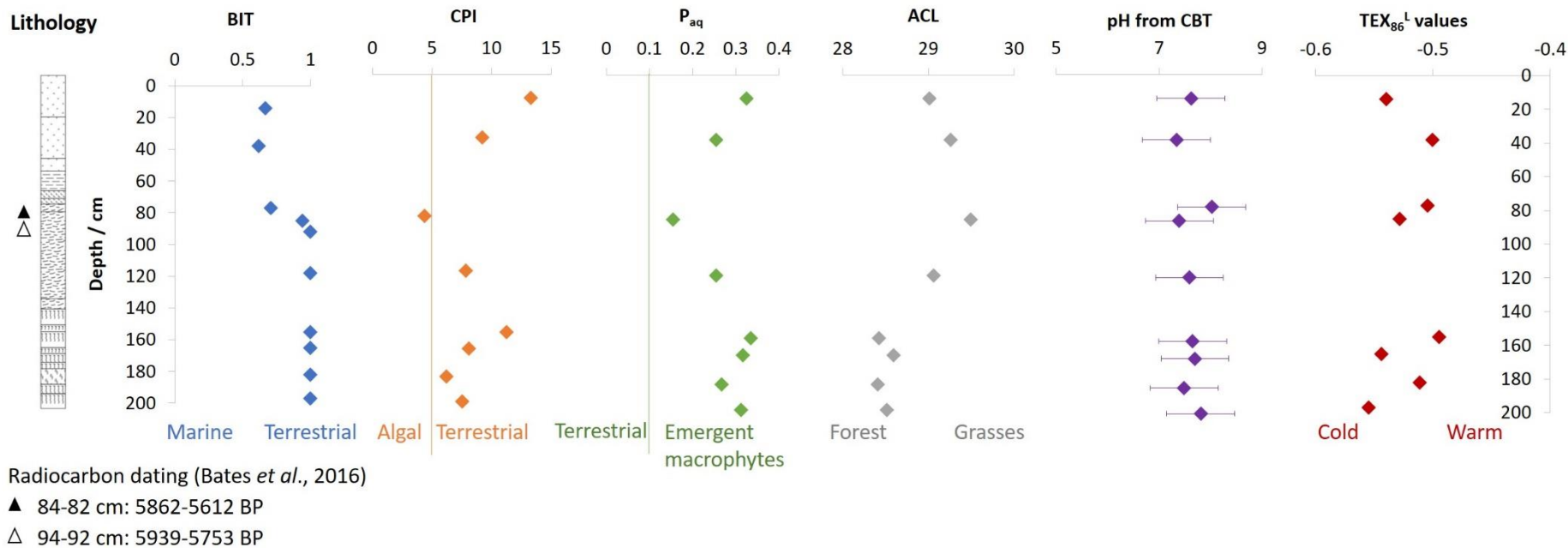




































Figure 3.6. (Left to right) Lithology and radiocarbon dating from Bates *et al.* (2016), and proxies applied to the Loch of Stenness sediments: BIT (branched and isoprenoid tetraether lipids), CPI (carbon preference index based on *n*-alkanes), P_{aq} (proxy of aquatic macrophytes based on *n*-alkanes), ACL (average chain length based on *n*-alkanes), pH calculated from CBT (cyclisation of branched tetraether lipids) and TEX_{86}^L values (tetraether index of 86 carbons – low) for sea-surface temperature calculations.

3.3.4. Signatures of terrestrial vegetation as markers of changing environment

The higher plant-derived *n*-alkanes show a shift in chain length with depth, the maximum increasing from *n*-C₂₇ between 197 and 155 cm to *n*-C₃₁ at 85 cm depth (Figure 3.5a), reflected in the lower ACL values between 197 and 155 cm and higher values above 85 cm (Figure 3.6; Table 3; Poynter and Eglinton, 1990). Such an increase has been suggested to reflect a change in the surrounding vegetation from mainly forest vegetation to mainly grasses (Cranwell, 1973; Chikaraishi *et al.*, 2004; Ortiz *et al.*, 2004; Wang and Liu, 2012; Fang *et al.*, 2014). This would imply that the Stenness catchment area experienced gradual deforestation from the freshwater period (prior to ~5939-5753 cal a BP) with grassland dominating after inundation (~5862-5612 cal a BP). This observation provides a tantalising view of the changing environment and should be a stimulus for further work that could involve identification of more specific grass / forest biomarkers, palynological studies and modelling to gain further insights into the palaeoclimatic conditions (Fisher *et al.*, 2003; Zech *et al.*, 2013; Li *et al.*, 2018).

Palynological analysis of a core from Crudale Meadow, located ~3 miles north-west of the Loch of Stenness, suggests a predominance of arboreal pollen (AP) mainly *Betula* and *Pinus sylvestris* with <15% herbs, between 8.1 and 5.7 ka BP (Bunting, 1994). A decline in AP to 40% and increase in herbs and Filicales (ferns) are apparent from 5.7-4.7 ka BP, and a predominance of herbaceous taxa (Cyperaceae and Poaceae >75%) between 4.7 ka BP and today (Bunting, 1994). Similar results were obtained from Blows Moss, approximately 25 miles south of the Loch of Stenness site (Farrell *et al.*, 2014). The vegetation change is thought to have resulted from a cooling climate and human activity in the surrounding area (Keatinge and Dickson, 1979; Bunting, 1994; Farrell *et al.*, 2014; Bates *et al.*, 2016). The decrease in AP at Crudale Meadow by 5.7-4.7 ka BP coincides with the end of the Loch of Stenness transgression and the observed shift towards longer chain *n*-alkanes indicative of grassland dominance (~5862-5612 cal a BP; Appendix 3, Figure A3.2). Thus, the combination of these two independent sources of evidence provides a compelling indication of a local change in vegetation from forest to grassland cover.

Table 3.3. CPI, P_{aq} , ACL and BIT indices, TEX_{86}^L values and sea surface temperatures (SST) calculated from TEX_{86}^L , and mean summer lake temperature for the Loch of Stenness sediments.

Depth / cm	CPI † terrestrial vs. reworking ^a	P_{aq} ‡ terrestrial vs. aquatic ^a	ACL * grass vs. forest ^a	BIT § terrestrial vs marine	TEX_{86}^L values ¶ ^b	SST from TEX_{86}^L ¶ / °C ±4.0 ^b	Lake water temperature ⋈ / °C ±2.1 ^b
14	13.3 	0.32 	29.0 	0.71 	-0.54	10.5	
38	9.20 	0.25 	29.3 	0.62 	-0.51	13.1	
77	n.a.	n.a.	n.d.	0.55 	-0.50	12.8	
85	4.39 	0.15 	29.5 	0.95 	-0.53		
92	n.a.	n.a.	n.d.	1 	n.d.		
118	7.85 	0.25 	29.1 	1 	n.d.		18.6
155	11.3 	0.33 	28.4 	1 	-0.49		21.0
165	8.09 	0.32 	28.6 	1 	-0.54		21.4
182	6.23 	0.27 	28.4 	1 	-0.51		20.5
197	7.56 	0.31 	28.5 	1 	-0.55	23.8	21.4

n.d.: not determined because below the detection limit.

^a Lack of n-alkanes precluded the calculation of CPI and P_{aq} .

^b Lack of key GDGTs precluded the calculation of SST from TEX_{86}^L and/or soil pH from CBT.



: terrestrial OM;



: aquatic OM;



: marine OM;



: mixed origin of OM;



: grass;



: forest.

Water temperature: warm water, cold water. Note: absolute values are probably not appropriate, but the general trend is likely to be indicative of palaeoenvironmental change.

† CPI: carbon preference index (Appendix 3, Table A3.2).

‡ P_{aq} : proxy for aquatic macrophytes (Appendix 3, Table A3.2).

* ACL: average chain length (Appendix 3, Table A3.2).

§ BIT: branched and isoprenoid tetraether index (Appendix 3, Table A3.2).

¶ TEX_{86}^L : tetraether index of 86 carbon atoms (low) (Appendix 3, Table A3.2).

⌈ Mean summer lake temperature (Appendix 3, Table A3.2).

3.3.5. Water temperature and pH from GDGT-based indices

The pollen data from Crudale Meadow suggested that climate cooling coinciding with the transgression was partly responsible for the shift from arboreal to grass vegetation (Keatinge and Dickson, 1979; Bunting, 1994). Sea-surface temperature (SST) estimates could not be inferred from the TEX₈₆ index (Equations 1.7-1.8; Schouten *et al.*, 2002) and lake temperature index (Powers *et al.*, 2010) due to lack of crenarchaeol stereoisomer, a component that is essential to the index (note: the former assignment as regioisomer was superseded; Sinninghe Damsté *et al.*, 2018). Lack of all components precluded the estimation of MAAT via the MBT index (Weijers *et al.*, 2007). The alternative TEX₈₆^L proxy for calculation of SST (Appendix 3, Table A3.2), does not include the crenarchaeol stereoisomer and performs best in subpolar marine settings (below 15°C, such as northern Scotland; Kim *et al.*, 2010). Therefore, the TEX₈₆^L calibration was applied to the brackish samples (77-14 cm) and showed low TEX₈₆^L values (Figure 3.6), indicating low SST ranging from 10.5 to 13.1°C ±4°C (Table 3.3). Notably in this setting, where the proxy should be most accurate, SSTs are remarkably similar to the present day average SST of Orkney, ranging from 7.1°C in March, the coldest month, to 13.2°C in August, the warmest month, giving an average yearly temperature of 10.1°C (Sea temperature_Orkney).

A proxy developed for freshwater lake sediments based on brGDGTs (Pearson *et al.*, 2011; Appendix 3, Table A3.2) was applied to the freshwater samples (from 197 to 118 cm). The results show a reconstructed summer lake temperature of 18.6-21.4°C. In recognition of the use of two GDGT palaeothermometers and that BIT >0.5 the calculated temperatures in the Loch of Stenness should not be considered as absolute values: a shift in the archaeal and bacterial populations and / or a possible contribution of archaeal GDGTs produced in sediments could also account for the observed temperature change. The general trends are, however, likely to reflect changing environmental conditions. The two temperature reconstructions imply a general cooling of the lake water during and after the seawater incursion. The decrease in temperature recorded by GDGT proxies over the period represented by the core is consistent with inundation by cool marine waters during a period of reduced summer insolation (Wanner *et al.*, 2008). A similar temperature decline was identified for this period in the North Atlantic (Wanner *et al.*, 2008) using the U₃₇^K proxy (based on long chain alkenones; Equation 1.20; Prahl and Wakeham, 1987; Müller *et al.*, 1998). In addition, mean summer air temperatures estimated from analysis of chironomids from Scotland were consistent with declining summer insolation during the Mid-Late Holocene (1.5-2°C; Dalton *et al.*, 2005).

Structural variations in brGDGTs have been correlated with soil pH, via the cyclisation of branched tetraether index (CBT; Weijers *et al.*, 2007). The applicability to lake sediments was established via a modification of the calibration (Tierney *et al.*, 2010; Appendix 3, Table A3.2). The CBT-calculated pH values show a narrow range of mildly alkaline sediments between 7.34 and 8.02 ± 0.66 (Figure 3.6), values consistent with the geology of the area (Kellock, 1969).

3.3.6. Contextualising the transgression

North eastern Scotland experienced a positive isostatic rebound of $+0.53 \text{ mm yr}^{-1}$ over the last 6000 years BP (Shennan, 1989) and Orkney experienced a rebound of $<0.0 \text{ mm yr}^{-1}$ over the last 4000 years BP (Shennan and Horton, 2002; de la Vega-Leinert *et al.*, 2007). The latter value shows that present sea levels were reached by approximately 4000 years ago, indicating that the inundation of the Loch of Stenness between ~ 5939 and 5612 cal a BP could not have been caused by isostatic depression.

The transgression at the Loch of Stenness cannot be attributed to melting of the Orkney island ice sheet which occurred much earlier, between 16.0 and 14.8 ka (Ballantyne, 2010). By contrast, modelling shows that the Antarctic Ice Sheet (AIS) continued thinning until at least 6 ka (Mauz *et al.*, 2015) and in some cases until 3 ka (Hein *et al.*, 2016; Small *et al.*, 2019), and has been invoked to explain the Mid-Late Holocene sea-level increase in sites across the globe (Mauz *et al.*, 2015). Notably, however, during the Mid-Late Holocene, sea-level fluctuations at Scottish sites have shown both transgressions and regressions indicating that regional factors, such as crustal movements and tidal dynamics (Smith *et al.*, 2017) cannot be excluded. Indeed, local factors such as the creation and destruction / modification of bay mouth barriers (lying -5 m OD in the Loch of Stenness) are likely to have played an important role in the timing and nature of transgressions in the Loch of Stenness (Bates *et al.*, 2016). Shennan and Horton (2002) suggested that Orkney sea levels reached present values 5-4 ka, in agreement with the radiocarbon dates for this core (Bates *et al.*, 2016) and the present study on the Loch of Stenness.

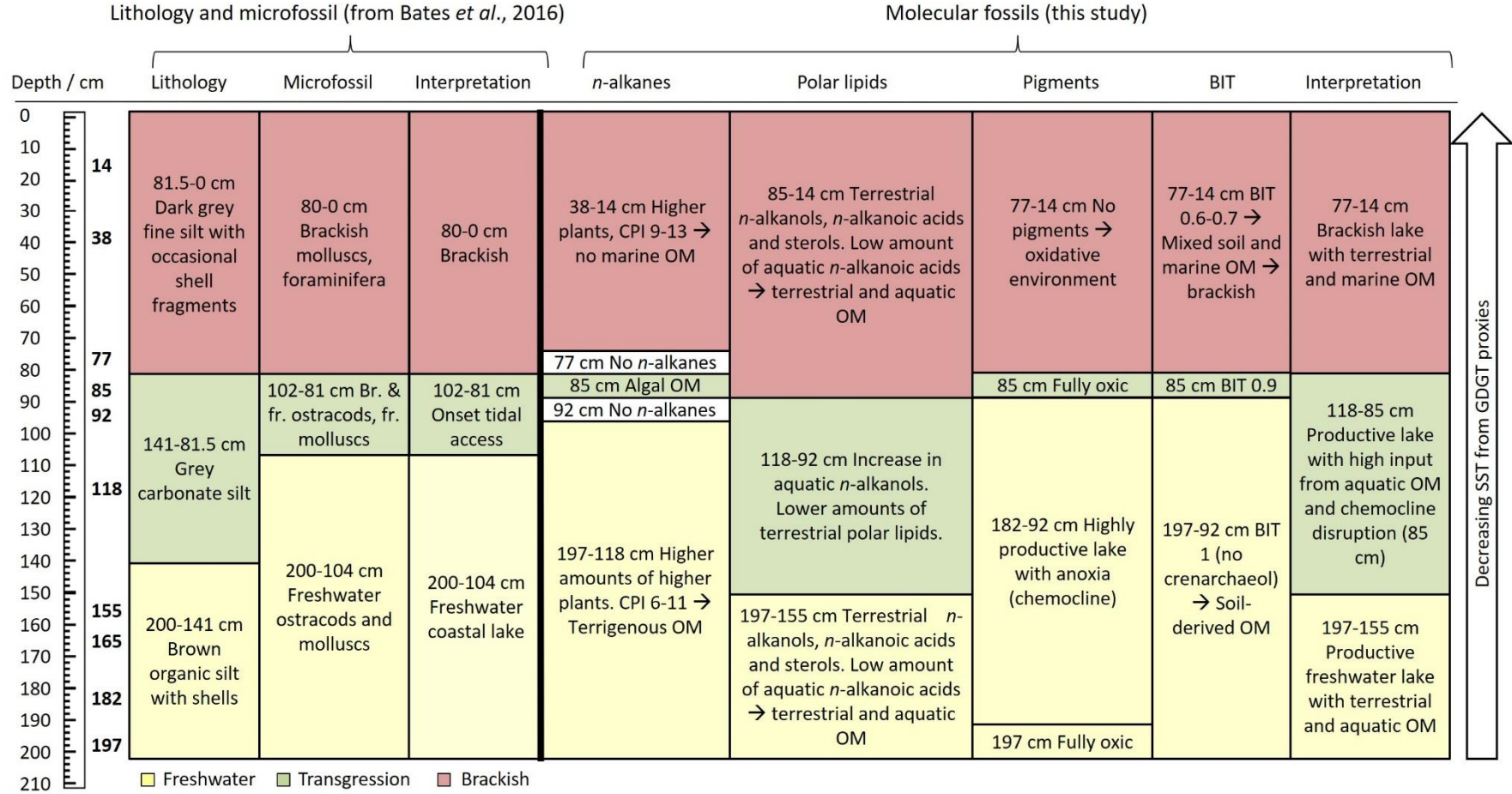


Figure 3.7. Scheme summarising the main findings from the core from the Loch of Stenness, Orkney: lithology, microscopy, *n*-alkanes, polar lipids, pigments and BIT index.

3.4. Conclusions

The analysis of microfossils from the Loch of Stenness (Orkney) core reveals initial freshwater conditions (200-104 cm depth), followed by a transgression (102-81 cm depth) leading to brackish conditions (80-0 cm depth). The molecular fossil record indicates greater complexity during the transgression than had been apparent from palaeoecological records alone. The initial freshwater lake was a productive environment with input both from in situ aquatic production and terrestrial runoff (197, 182, 165 and 155 cm). The first disruption of the OM balance was recorded at 118 cm, indicating an earlier initiation of the transgression than is evident from microfossil analysis (Bates *et al.*, 2016). An increase in aquatic OM production was observed at 92 cm with the marine marker crenarchaeol being detected above 85 cm, consistent with the establishment of stable marine conditions (Figure 3.7). In the brackish zone (77, 38 and 14 cm) marine OM was detected and the extent of terrestrial runoff was similar to that of the freshwater stage, indicating the end of the transgression.

The change in *n*-alkane chain lengths suggests a shift in vegetation from forest to grasses towards the top of the core, supported by pollen data (Bunting, 1994; Farrell *et al.*, 2014), most likely in response to cooling conditions associated with reduced summer insolation as well as human activity. The proxy-calculated SST indicates higher temperatures in the freshwater lake followed by cooling towards values close to present-day water temperatures at 77, 38 and 14 cm ($13.1\text{--}10.5^{\circ}\text{C}\pm 4^{\circ}\text{C}$). It cannot be excluded that the change in temperature is due to production of iGDGT in soil, high BIT values and / or a shift in archaeal and bacterial populations.

Piloted on a well-constrained Holocene transgression, this study has shown that molecular fossils can add valuable environmental evidence to the information garnered from more conventional estimates of palaeoclimate change from microfossil, palynological and lithological studies. The nature and specific origins of molecular fossils enables a more insightful and refined study of the impact of the transgression on the primary producers inhabiting the basin and the surrounding environment. The widespread nature, greater frequency of occurrence and excellent preservation potential of molecular fossils unlocks a far wider set of sediments that can be used to study sea-level change across the world, including during Pleistocene times and where macro- and micro-fossils are lacking.

4. Pleistocene transgression in East Anglia: the Nar Valley (Norfolk) and Woodston (Cambridgeshire)

4.1. Introduction

The application of organic geochemical markers in the study of the Holocene transgression of the Loch of Stenness (Scotland; Chapter 3) provided information that corroborated previous microfossil and lithological studies, as well as providing more extensive insights into the transgression. The success of the approach raised the possibility of applying the method to studying sea-level changes of Pleistocene (2.5 Ma to 11.8 ka) samples. Previous studies have shown evidence of Pleistocene sea-level changes along the south and east coasts of England (Bates *et al.*, 1997, 2003; Roe, 2001; Bridgland *et al.*, 2013), representing transgressions and regressions that occurred between MIS 13 and MIS 5 (500-80 ka; Appendix 2). Particular interest is centred on MIS 11 (425-375 ka; Railsback *et al.*, 2015), having analogous orbital configuration to present day and on MIS 11 and MIS 9 (325-280 ka) because global atmospheric CO₂ concentrations were similar to the pre-industrial Holocene levels (286-300 ppm; Past Interglacials working group of PAGES, 2016). To test the utility of molecular fossils for understanding past Pleistocene sea-level change, Nar Valley Pleistocene deposits (Figure 4.1a) attributable to MIS 11 and / or MIS 9 were targeted for molecular fossil analysis.

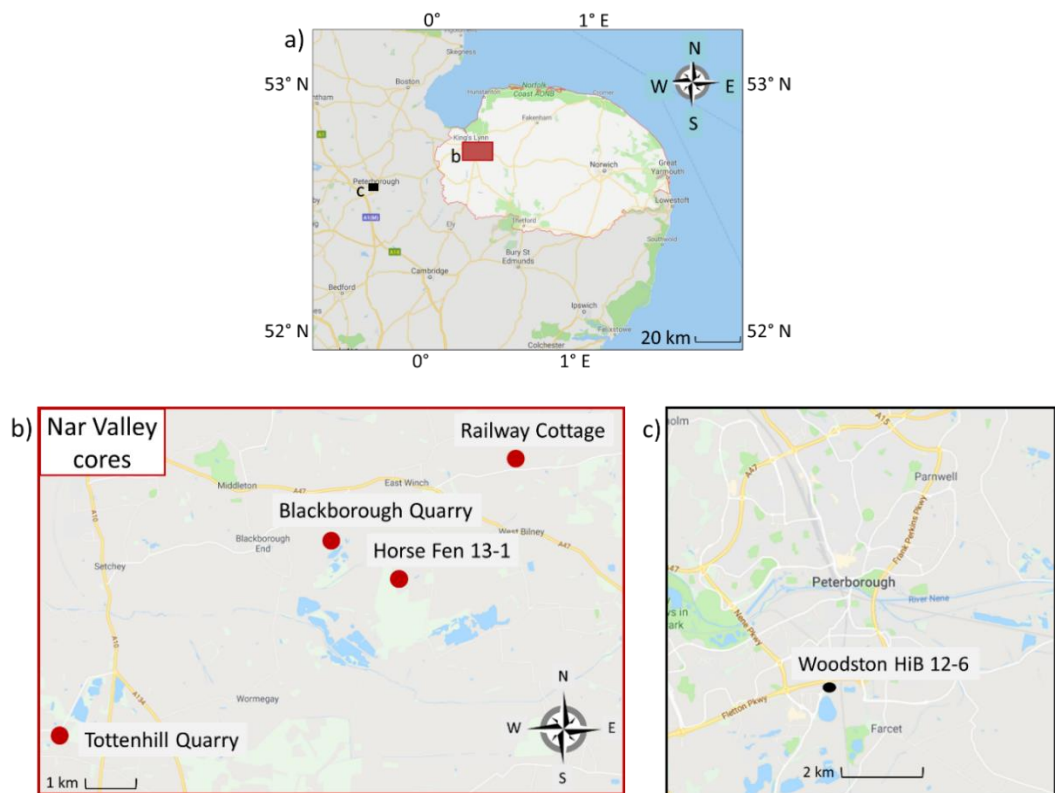


Figure 4.1. a) Map of south-east England showing Norfolk and the locations of the Nar Valley cores (red) and Woodston (black); b) map showing the location of the Nar Valley cores; c) map showing the location of Woodston HiB 12-6 core (maps adapted from Google Maps).

4.1.1. Geology of the Nar Valley Pleistocene deposits

The Quaternary deposits forming the Nar Valley Freshwater Beds include glacial diamicton overlain by proglacial lake laminated clays and peat (Stevens, 1959). These deposits are overlain by the Nar Valley Clay, fine clays with evidence of marine fauna (Stevens, 1959; Ventris, 1996), and therefore interpreted as a sea-level transgression. In many locations the Nar Valley Clay is covered by sands and gravels (Ventris, 1996; Figure 4.2). The Nar Valley Clays represent at least one Pleistocene interglacial marine transgression that was correlated originally on the basis of pollen with the British “Hoxnian” interglacial (Table 4.1; Stevens, 1959). However, more recent studies have shown that the “Hoxnian” pollen signature is evident in more than one UK interglacial (Schreve, 2001; Thomas, 2001; Preece *et al.*, 2007; Roe *et al.*, 2009; Bridgland *et al.*, 2013), which complicates the age interpretation of this suite of sites.

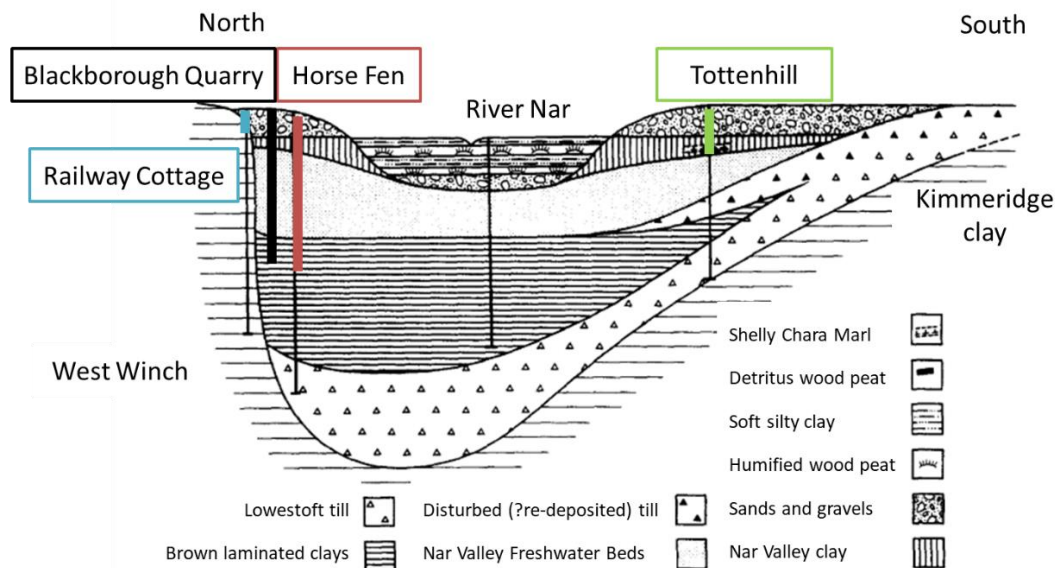


Figure 4.2. Cross section of the lower Nar Valley showing the sedimentation zones (adapted from Ventris, 1996; not to scale).

4.1.2. Uncertainty in age of the Nar Valley Pleistocene deposits

Early work showed that the pollen assemblage of the UK site of Hoxne could be differentiated from the pollen assemblage at sites dating from the Eemian (Last Interglacial, MIS 5e) and the Cromerian (originally termed “First Interglacial”, MIS 19-13) interglacials (West, 1956). Thus, West (1956) distinguished the Hoxne deposits as a separate interglacial, the “Hoxnian” Interglacial, and also correlated pollen assemblages from localities in north-west Europe to the Hoxnian (West, 1956). The pollen succession from Hoxne was divided into four sub-stages forming an interglacial period:

late-glacial, early-temperate, late-temperate and early-glacial. Subsequent amino acid racemisation (AAR) dating of the Hoxne deposits enabled correlation with MIS 11 (Penkman *et al.*, 2007; 2013; Ashton *et al.*, 2008). Notably, however, similarities between the pollen profiles of the Hoxne site and sediments from both MIS 11 and 9 were observed (Thomas, 2001), challenging the separation of these two stages based solely on pollen, and increasing evidence from mammalian and molluscan biostratigraphy as well as aminostratigraphy has shown that a “Hoxnian” pollen assemblage cannot be used to differentiate MIS 11 and MIS 9 (Schreve, 2001; Thomas, 2001; Preece *et al.*, 2007; Roe *et al.*, 2009; Bridgland *et al.*, 2013). The latest study on the Nar Valley included the cores shown in Figure 4.1b (Barlow *et al.*, 2017). Palynological analysis of the cores showed some similarity to the “Hoxnian” pollen description (Section 4.2.4) but AAR dating on two cores from the Nar Valley showed correlation with both MIS 11 and 9 (Section 4.2.5), thus uncertainty on the date of transgression in the Nar Valley remains (Barlow *et al.*, 2017).

4.1.3. Aims

The overall aim of this study was to test if organic geochemical markers reveal either differences or similarities among the horizons deposited during the transgressive phases recorded in the Nar Valley cores from four different sites (Blackborough Quarry, Horse Fen 13-1, Tottenhill Quarry and Railway Cottage (Figures 4.1b, 4.2, 4.3)) and to assess if they provide additional information on changes in the palaeoenvironment represented within the sequences. A fifth core from Woodston (Figure 4.1c), ~3 miles away from Peterborough, was also studied as the transgression in a previous core from this site is more securely dated to MIS 11 (Horton *et al.*, 1992). The specific objectives of the study were:

- To analyse organic geochemical biomarkers to the Nar Valley sediments to characterise the transgression;
- To observe any similarities and / or differences between the results from this study and the microfossil analysis from Barlow *et al.* (2017);
- To study the characteristics of the Woodston core, to test if the molecular fossils can reveal the presence or absence of a transgression, and yield any information to identify the environmental changes associated with the possible transgression;
- To assess if the five cores from East Anglia represent the same or two different sea-level inundation events.

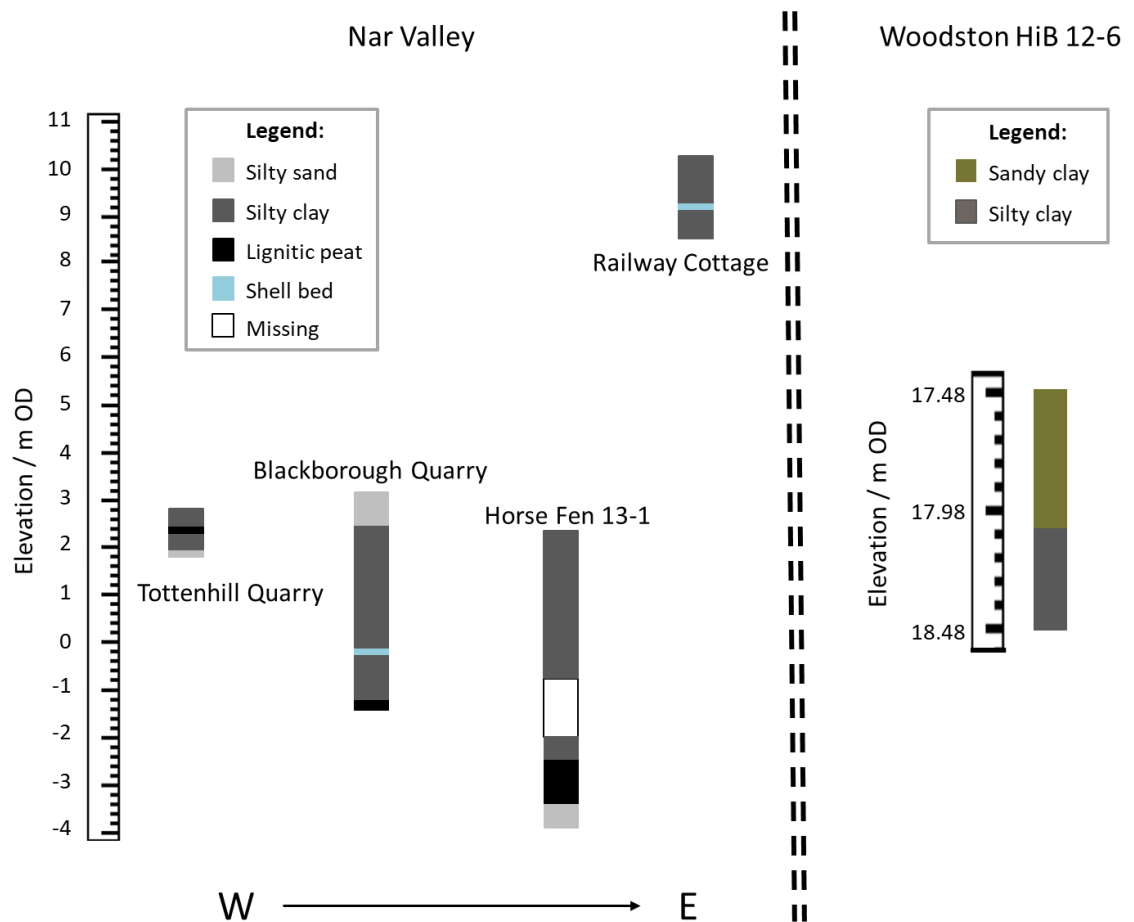


Figure 4.3. Borehole lithology of Nar Valley cores redrawn from Barlow *et al.*, 2017 and Woodston HiB 12-6.

4.2. Site description and previous work on the Nar Valley

The cores employed for molecular fossil analysis presented in this chapter were previously analysed by Barlow *et al.* (2017). The environmental analyses from their work on the Nar Valley cores are summarised here, collating the results based on lithological horizons (Section 4.2.1). It should not be assumed that similar lithological horizons are contemporaneous across the cores.

4.2.1. Lithology of Nar Valley cores

The four cores analysed for molecular fossils from the Nar Valley were Tottenham Quarry, Blackborough Quarry, Horse Fen 13-1 and Railway Cottage (Figure 4.3). Although at different elevation due to the underlying glacial till, the Tottenham Quarry and Horse Fen cores both exhibit a light grey silty sand overlain by dark grey silty clay (Figures 4.4, 4.5; Barlow *et al.*, 2017). A very dense black lignitic peat is present in the Tottenham Quarry, Blackborough Quarry and Horse Fen

cores (Figures 4.4-4.6), where it is succeeded by dark grey silty clay. This latter horizon extends through the entire core from Railway Cottage (Figures 4.7). A shell bed of marine mollusc *Ostrea edulis* was present in the cores from both Blackborough Quarry and Railway Cottage, forming a discrete horizon within the dark grey silty clay (Figures 4.6, 4.7). The Horse Fen 13-1 core was incomplete due to loss of material arising from water saturation during core recovery (from -2.19 m to -0.74 m ordnance datum (OD); Figure 4.5). In the core from Blackborough Quarry the dark grey silty clay was overlain by grey-brown silty sand (2.61-3.06 m OD; Figure 4.6).

4.2.2. Loss-on-ignition

The loss-on-ignition (LOI) data (Figure 4.4-4.7) show low organic carbon contents in the silty sand layer (<10%) increasing up to 40% in the dark grey silty clay (Barlow *et al.*, 2017). The organic carbon content gradually increased to c. 85% in the lignitic peat horizon, followed by a marked decrease in the silty clay section to <30% of organic carbon in the Horse Fen core (Figure 4.5). In the Blackborough Quarry and Tottenhill Quarry cores the organic carbon content decreased more gradually from 80-87% in the peat to c. 10-15% in the silty clay horizon (Figures 4.4, 4.6).

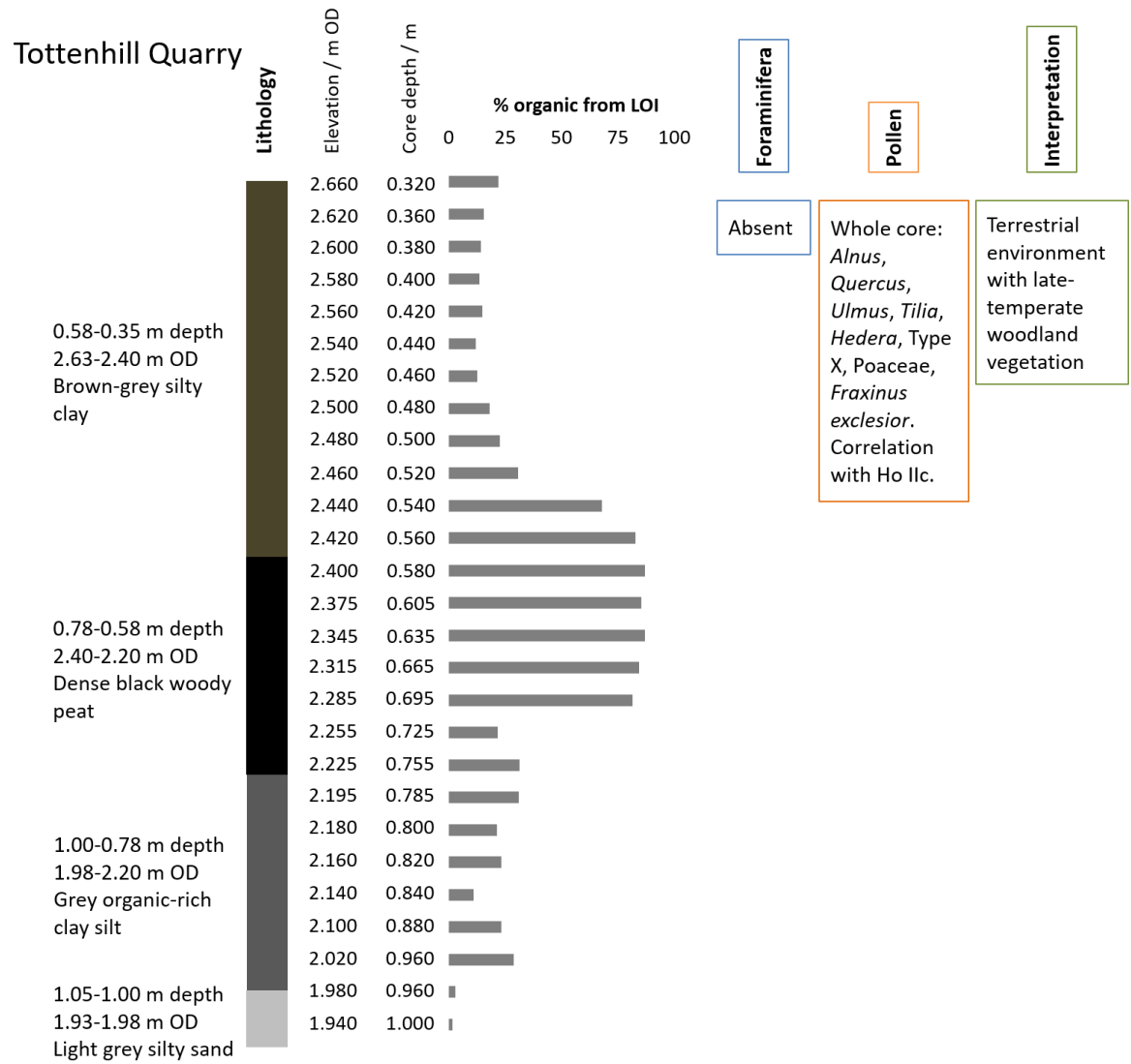


Figure 4.4. Scheme of lithology, loss-on-ignition (showing the percentage of organic carbon), foraminifera, pollen and interpretation of the palaeoenvironment of Tottenhill Quarry samples (redrawn from Barlow et al., 2017).

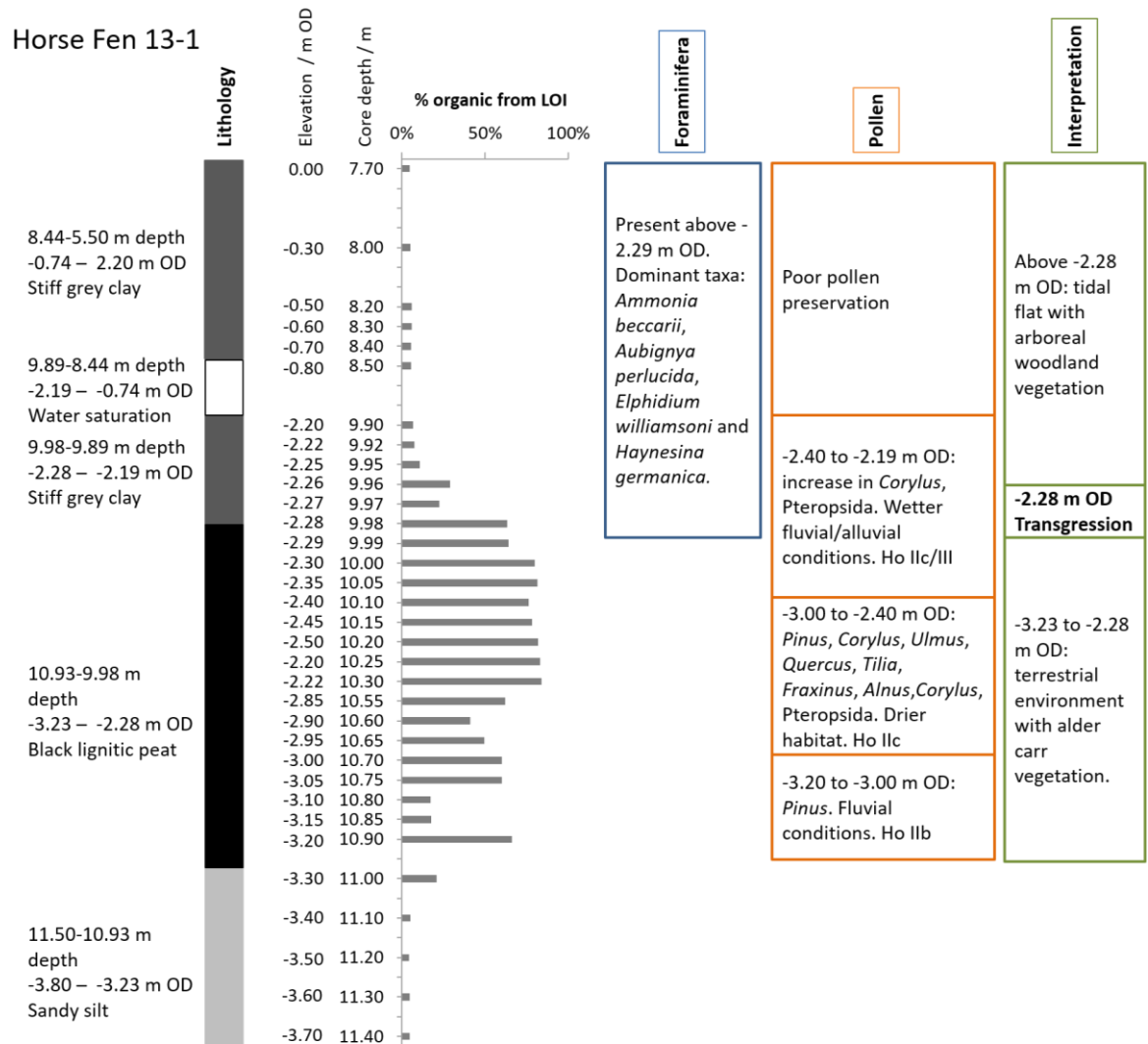


Figure 4.5. Scheme of lithology, loss-on-ignition (showing the percentage of organic carbon), foraminifera, pollen and interpretation of the palaeoenvironment of Horse Fen 13-1 samples (redrawn from Barlow et al., 2017).

Blackborough Quarry

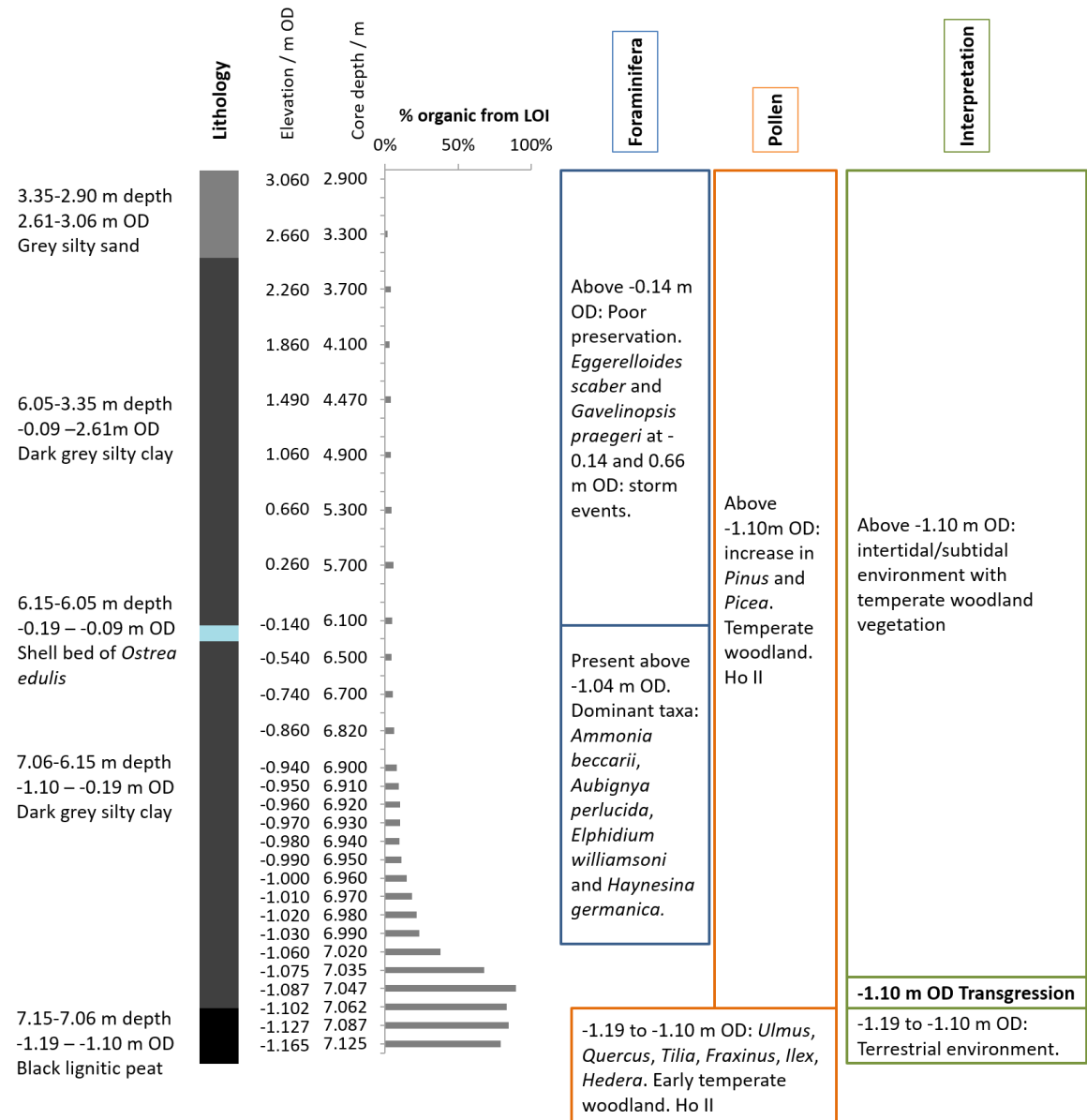


Figure 4.6. Scheme of lithology, loss-on-ignition (showing the percentage of organic carbon), foraminifera, pollen and interpretation of the palaeoenvironment of Blackborough Quarry samples (redrawn from Barlow et al., 2017).

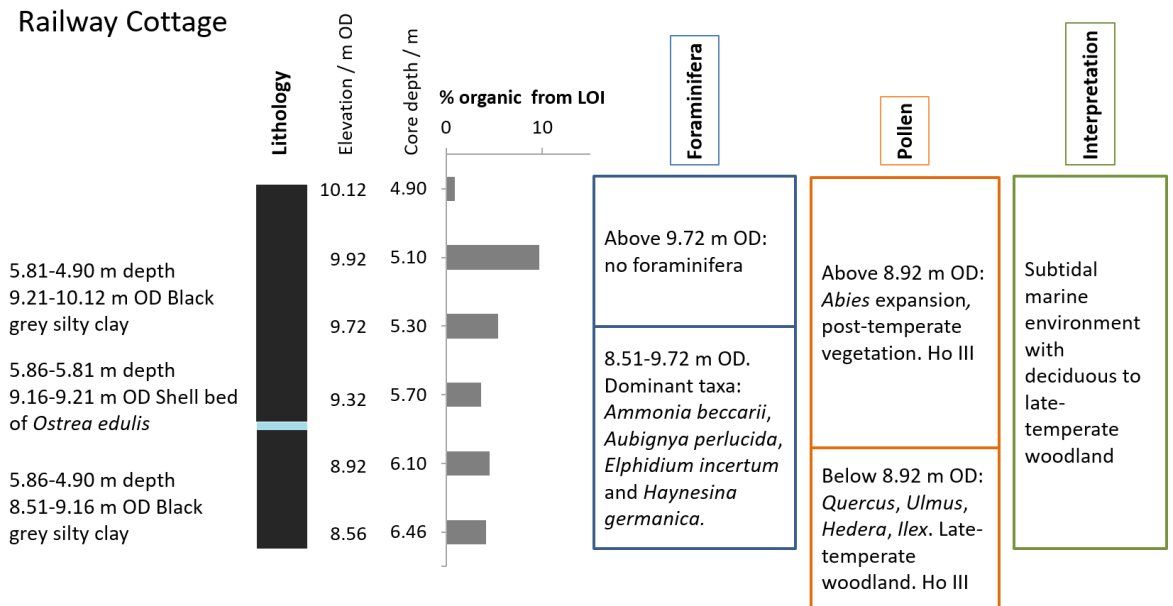


Figure 4.7. Scheme of lithology, loss-on-ignition (showing the percentage of organic carbon), foraminifera, pollen and interpretation of the palaeoenvironment of Railway Cottage samples (redrawn from Barlow *et al.*, 2017).

4.2.3. Foraminifera

Foraminifera, microfossils indicative of marine conditions, were absent in the Tottenhill Quarry core, likely an indication of a non-marine environment (Figure 4.4; Barlow *et al.*, 2017). At Horse Fen and Blackborough Quarry foraminifera occurred in the clay section (Horse Fen above -2.29 m OD; Figure 4.5; Blackborough Quarry above -1.04 m OD; Figure 4.6), and in the clay at Railway Cottage they were retrieved between 8.51 and 9.72 m OD (Figure 4.7). In these three cores the foraminifera assemblage was dominated by *Ammonia beccarii*, *Aubignya perlucida*, *Elphidium williamsoni* and *Haynesina germanica*, all intertidal species. At Horse Fen between 2.00 and 1.00 m OD high numbers of *E. gerti* and low numbers of *A. beccarii* were correlated with an increase in water depth indicating a fully marine environment. Preservation was poor at Blackborough Quarry (from -0.14 to 2.26 m OD) with some tests of *A. beccarii*, *Elphidium* spp. and *H. germanica* being observed. At -0.14 m OD and 0.66 m OD foraminifera species of *Eggerelloides scaber* and *Gavelinopsis praegeeri* were found; these are sub-tidal species possibly indicative of deeper waters arising from storm events (Figure 4.6; Murray, 2006; Barlow *et al.*, 2017). At Railway Cottage the foraminifera assemblage consisted of *A. beccarii*, *A. perlucida*, *H. germanica* and *E. incertum* from the base to 9.72 m OD. A slight change in species is observed at 9.23 m OD where *A. beccarii f. tepida* was substituted by *A. beccarii f. parkensoniana*, a possible indication of higher salinities. Above 9.72 m OD no tests occurred (Figure 4.7). The foraminifera indicate an intertidal / subtidal

environment at Blackborough Quarry, a tidal flat at Horse Fen and intertidal marine environment at Railway Cottage (Barlow *et al.*, 2017).

4.2.4. Pollen

Barlow *et al.* (2017) correlated the pollen from the Nar Valley cores with “Hoxnian” pollen stage (Ho I-IV; Table 4.1). In the Tottenhill Quarry core the pollen sequence, truncated due to quarry excavations above 2.63 m OD, showed dominance of deciduous taxa *Alnus*, *Quercus* and *Ulmus*. *Tilia*, *Hedera* and Type X were also observed. A rise and fall in *Corylus* and *Ulmus* pollen counts was observed between 2.28 and 2.58 m OD and between 2.28 and 2.48 m OD, respectively. *Pinus*, Poaceae and *Fraxinus excelsior* were present throughout the core. Overall, the pollen indicates an environment consistent with the later stages of early-temperate woodland, correlated with stage Ho IIc (Figure 4.4).

In the Horse Fen core pollen preservation was poor from above 2.88 m OD, nevertheless, certain trends were observed. *Pinus* grains were prevalent with lower amounts of *Betula*, Poaceae, Cyperaceae and reworked pre-Quaternary palynomorphs (from -3.20 to -3.00 m OD), an indication of deposition under fluvial conditions. In the lignified peat, evident until -2.40 m OD, *Pinus* continued to prevail but also *Ulmus*, *Quercus*, *Tilia*, *Fraxinus*, *Alnus* and *Corylus avellana* increased. The latter taxa increased above -2.40 m OD as well as high levels of Pteropsida (*Dryopteris* type), reflecting flora that develop on drier ground. The absence of sediments between -2.19 and -0.74 m OD precluded sampling of sediment for pollen and foraminifera analyses. The initial fluvial conditions (*Pinus* prevalence) were substituted by a drier habitat supporting the formation of the lignified wood peat (*Alnus*, *Quercus*, *Ulmus*, *Dryopteris* type). Following the peat, *Pinus*, *Dryopteris* type and *Corylus avellana* prevailed, indicating the establishment of arboreal woodland deposited under wetter, fluvial / alluvial conditions. The pollen assemblage can be correlated to Ho IIb (-3.20 to -3.00 m OD), Ho IIc (-3.00 to -2.40 m OD) and Ho IIc / III (-2.40 to -2.19 m OD; Figure 4.5).

The pollen assemblage in the Blackborough Quarry core represents an early-temperate woodland with thermophiles such as *Ulmus*, *Quercus*, *Tilia*, *Fraxinus*, *Ilex* and *Hedera* in the peat section. After the peat-clay transition these taxa decreased and conifers, *Pinus* and *Picea*, increased, representing a temperate woodland tentatively correlated with Ho IIa-c (Figure 4.6).

In the Railway Cottage core below 8.92 m OD, the pollen is dominated by deciduous woodland of *Quercus*, *Ulmus*, *Hedera* and *Ilex* representing a late-temperate pollen stage (Ho III). A rapid expansion of *Abies* pollen is observed above 8.92 m OD, suggesting climate changing into post-temperate conditions (Figure 4.7; Barlow *et al.*, 2017).

Table 4.1. Summary of the Hoxnian-type pollen assemblages and tentative assignments of Hoxnian stage to the Nar Valley cores (redrawn from Barlow et al., 2017).

Zone name	Pollen stage	Pollen assemblage	Nar Valley core
Post temperate / early glacial	Ho IV	Non-arboreal pollen increases. Early glacial, arctic conditions	
Late temperate	Ho III a&b	Gradual increase in <i>Pinus</i> , <i>Picea</i> , <i>Abies</i> , <i>Carpinus</i> . Decline of <i>Quercus</i> , <i>Ulmus</i>	Horse Fen, Railway Cottage
Early temperate	Ho II d	Mixed oak forest with expansion of <i>Ulmus</i>	Tottenham Quarry, Horse Fen
	Ho II c	Rapid expansion of <i>Alnus</i>	
	Ho II b	<i>Quercus</i> dominant	Blackborough Quarry
	Ho II a	<i>Betula</i> , <i>Pinus</i> colonising	
Pre-temperate / lateglacial	Ho I	Scrub, some <i>Betula</i>	

4.2.5. AAR dating

AAR dating of freshwater gastropod *Bithynia opercula* from two cores, Tottenham Quarry (9 samples) and Horse Fen 13-1 (1 sample; Figure 4.1b), correlated with MIS 11 but a MIS 9 age could not be excluded for Tottenham Quarry (Barlow et al., 2017). Thus, it is not yet established if the Nar Valley Clay represents a single interglacial period during which marine inundation occurred. However, the series of cores analysed in this study do represent sea-level changes during MIS 11 and / or MIS 9.

4.2.6. Change in sea level

From the lithology and the lack of foraminifera, Tottenham Quarry does not exhibit a transgression but rather a terrestrial environment throughout the core (Figure 4.4). Similarly, Railway Cottage exhibits stable subtidal marine conditions in the core (Figure 4.7). By contrast, Horse Fen and Blackborough Quarry cores exhibit a peat-clay transition that indicates a change from a terrestrial environment to a tidal flat and an intertidal / subtidal environment, respectively, consistent with a transgression (Figures 4.5, 4.6; Table 4.2; Barlow et al., 2017).

Table 4.2. Summary of lithology, foraminifera, pollen and palaeoenvironment of the Nar Valley cores after Barlow et al. (2017).

Site	Lithology	Foraminifera	Pollen	Interpretation of environment
Tottenhill Quarry	Silty clay and peat	Absent	Late early-temperate wooded environment	Terrestrial
Horse Fen	Sandy silt, silty clay, peat	Tidal flat	Alder carr to arboreal woodland	Transgression from terrestrial to tidal flat recorded at -2.28 m OD
Blackborough Quarry	Sandy silt, silty clay, peat	Intertidal to subtidal	Early-temperate to temperate woodland	Transgression from terrestrial to intertidal / subtidal recorded at -1.10 m OD
Railway Cottage	Silty clay	Subtidal	Deciduous woodland to late-temperate	Subtidal marine

4.3. Materials and methods

The four cores from the Nar Valley were subsampled at specific depths in 1 cm slices. The Woodston core was subsampled every 10 cm with samples 2-3 cm-wide (Section 7.1.3). After freeze-drying and homogenisation (Section 7.1.4), molecular fossil extraction was carried out with accelerated solvent extraction (ASE; Section 7.2.1). Flash column chromatography separated the lipids depending on polarity (Section 7.2.3) and derivatisation of pigments and lipids prior to analysis was carried out (Sections 7.2.2, 7.2.4). Analysis of lipids was carried out as described in Sections 7.4.1, 7.4.2, 7.4.3, 7.4.11. Chlorophyll pigment analysis was carried out as outlined in Sections 7.4.4, 7.4.9.

4.4. Results and discussion

The molecular fossil results from the four cores reveal differences and similarities in distribution between and within the main lithologically distinct horizons from the different sites (Figure 4.8). It was possible to determine 6 “types” of distinct molecular fossil distribution (A-F; Table 4.3); accordingly the results are presented and discussed here by these defined types, exploring their relationship to the distinct palaeoenvironments identified previously from the Nar Valley sites

(Section 4.2; Barlow *et al.*, 2017). Although each defined type of distribution from the different cores is treated together, it is important to recognise that this does not presume that the sediments are of the same age.

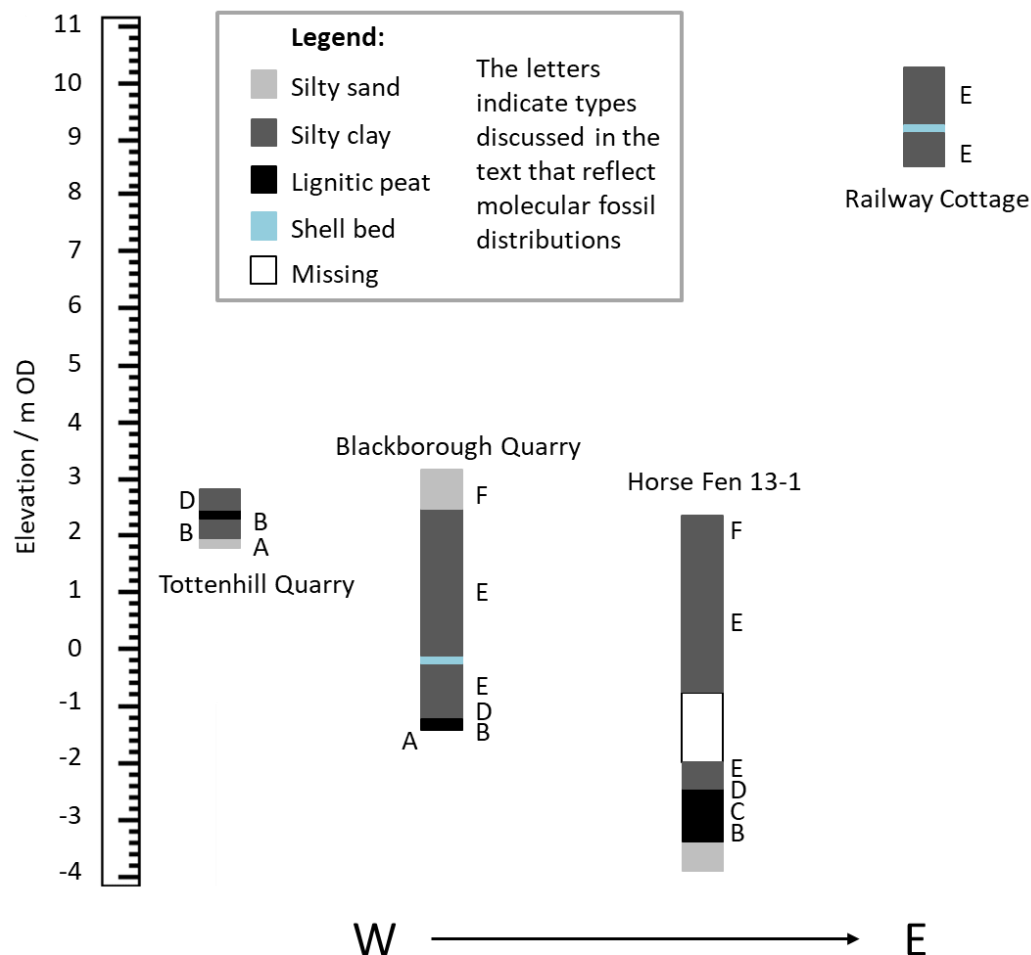


Figure 4.8. Nar Valley borehole lithology from Barlow *et al.*, 2017 and separation of the six types of sediment reflecting the molecular fossil distributions from this study.

Table 4.3. Summary of the main environmental information for each molecular fossil type defined in this study from the Nar Valley: terrestrial and aquatic lipids, alkenones, BIT, pigments and interpretation of results.

Type	Terrestrial lipids	Aquatic lipids	Alkenones	BIT	Pigments	Interpretation
A	Low concentration	Low concentration	Absent	>0.8	Oxygenic photoautotrophic communities in low concentration	Terrestrial-dominated environment, low OM concentration. Tottenham: marine conditions.
B	Dominant OM input. High concentration	Low concentration	Absent	>0.9	Oxygenic & anoxygenic photoautotrophic communities with a semi-permanent chemocline	Terrestrial lignitic peat environment with conifer trees. High OM concentration. Blackborough Quarry: beginning of transgression.
C	Dominant. High concentration	Low concentration	Traces	0.99	Bchl _s > chl _s : eutrophication	Eutrophication likely marking transgression in Horse Fen.
D	High concentration	Increasing concentration	Present	0.8-1	Oxygenic & anoxygenic photoautotrophic communities	Marine inundation of terrestrial environment.
E	Declining concentrations	Low concentration	Present	0.4-0.8	Oxygenic & anoxygenic photoautotrophic communities	Marine contribution increases. Blackborough Quarry: certain depths similar to Type B → erosion from storm events
F	Low concentration	Low concentration	Absent	0.5	Oxygenic photoautotrophic communities	Aquatic marine conditions, low OM concentration.

4.4.1. Molecular fossils common in all Nar Valley cores

Markers of terrestrial organic matter (OM), long odd carbon chain *n*-alkanes (**A1**) and *n*-alkanones (**A2**), and long even chain *n*-alkanals (**A3**), *n*-alkanoic acids (**A4**) and *n*-alkanols (**A5**) with chain lengths $>n\text{-C}_{18}$, were prevalent in all cores (Figures 4.10, 4.11, 4.13, 4.14, 4.16, 4.17, 4.21, 4.22; Eglinton and Hamilton, 1967). Further evidence of terrestrial runoff was represented by widespread occurrence of β -sitosterol (**T11**) and 5 α -stigmastanol (**T9**) in all of the cores (Figures 4.11, 4.14, 4.17, 4.22; Eglinton and Hamilton, 1967; Volkman 1986). 5 α -Stigmastanol has been reported in some plants and also in soil where it has been designated as a product of bacterial degradation of plant phytosterols (De Deckker *et al.*, 2014 and references therein). The conifer marker friedelan-3-one (**T4**; Otto *et al.*, 2005) was prominent in the lignified peat horizons in Blackborough Quarry, in the peat and clay horizons in Horse Fen and in the clay in the Railway Cottage core (Figures 4.13, 4.16, 4.21) where *Pinus* or *Abies* pollen were dominant (Barlow *et al.*, 2017). The proportions of terrestrial and aquatic macrophyte OM in the Nar Valley cores, assessed from P_{aq} values >0.1 (Section 1.4.3.2, Equation 1.5), indicate a mix of terrestrial and aquatic OM (Ficken *et al.*, 2000). Aquatic input was confirmed by the presence of the dinoflagellate marker dinosterol (**T10**; Volkman, 2003) in the clay horizons of the Tottenhill Quarry, Horse Fen and Railway Cottage cores, and *n*-C₁₆₋₁₈ *n*-alkanoic acids (**A4**; Cranwell, 1982) in the clays of the Blackborough Quarry and Railway Cottage cores (Figures 4.11, 4.14, 4.17, 4.22). Short chain *n*-C₁₆₋₁₈ *n*-alkanoic acids can represent both aquatic and terrestrial OM (Cranwell, 1982; Chikaraishi *et al.*, 2004; Wang and Liu, 2012; Fang *et al.*, 2014; Wang *et al.*, 2019). Their presence in aquatic sediments and lack of them in the terrestrial peat might indicate an aquatic OM origin in the Nar Valley cores.

Photosynthetic pigments, representing aquatic *in situ* production, were recorded in all cores with a dominance of chlorophyll *a*- and *b*-derived pigments indicative of oxygenated water conditions (Pfennig, 1977). Phaeophytin (phe; **C6-C7**), pyropheophytin (pphe; **C8-C9**), phaeophorbide (phorb; **C10**) and pyropheophorbide (pphorb; **C11**) were detected in all cores (Figures 4.12, 4.15, 4.18, 4.23) indicating early degradation of chlorophylls most likely resulting from enzymatic transformation in the water column (Keely, 2006). Following its laboratory synthesis under alkaline conditions (Ma and Dolphin, 1996), chlorophyllone (chlone; **C3-C4**) has been found in sediments and faecal pellets where it is suggested to originate from either algal enzymes or grazing (Talbot *et al.*, 1999; Airs *et al.*, 2001; Aydin *et al.*, 2003). Markers of herbivore grazing in marine and lacustrine water columns are pyropheophorbide steryl chlorin esters (pphorb SCE; **C12**), structures in which mixtures of sterols are esterified to the algal pigment pphorb (Harradine *et al.*, 1996; Talbot *et al.*, 1999). Such structures were evident in all cores, with differences in sterol carbon number

distributions (C_{27-30} identified by MS/MS) representing differences in the primary producer populations. Dominance of C_{27} sterols can be attributed to marine organisms, C_{28} and C_{29} to algae (Volkman, 1986; 2003; Meyers and Ishiwatari, 1993). Notably, however, the sterol profiles of the SCEs can only provide a broad indication of source. In selected subsamples of all cores, lower amounts of bacteriochlorophyll a -derived pigments (**B1**) indicate a stratified water column (development of a chemocline (Pfennig, 1977)), with anoxic conditions extending into the photic zone (Figures 4.12, 4.15, 4.18, 4.23). At certain elevations in the Tottenhill Quarry, Blackborough Quarry and Horse Fen cores, bacterioviridin a (bvir a ; **B4**) was identified from its retention time (12 min) and UV/vis absorption spectrum (λ_{\max} 385, 410, 680 nm; Figures 4.12, 4.15, 4.18). In addition, a family of bacterioviridin-like components (with UV-vis spectrum identical to bvir a but different retention times (Appendices 4.3, 4.4)) was observed in certain sediments from Blackborough and Tottenhill Quarry. Bacterioviridins are oxidation products of bacteriochlorophylls, their presence indicating either a suppression of the chemocline followed by oxidation, or a periodic oxygen ingress at the time of deposition (Wilson *et al.*, 2004). Thus, the occurrence of bvirs most likely indicates either desiccation or the presence of shallow waters (Wilson *et al.*, 2004).

An unidentified carotenoid (designated as P7), eluting at 3.6 min and absorbing at λ_{\max} 387, 405, 431 nm (Figure 4.9), was present in all samples and under all environmental conditions of the Nar Valley cores. The early elution under reversed-phase UHPLC indicates that the pigment is relatively polar, possibly a xanthophyll (Figure 1.9).

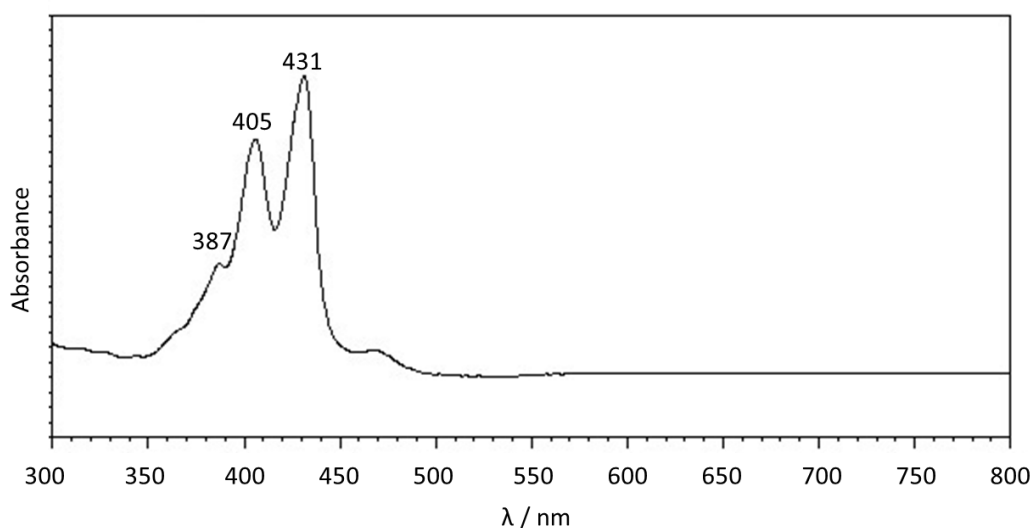


Figure 4.9. UV/vis spectrum of unidentified carotenoid peak 7 (P7).

4.4.2. Molecular distribution type A

The type A molecular distribution was identified in the silty sand of the Tottenhill Quarry (1.95 m OD) and the bottom of the peat of the Blackborough Quarry cores (-1.190 and -1.185 m OD). Type A samples show very low concentrations of lipids and chlorophylls. Terrestrial OM was prevalent (Figures 4.10, 4.11, 4.13, 4.14; Eglinton and Hamilton, 1967; Volkman 1986) confirmed by BIT values of 1 in the Blackborough Quarry samples (Table 4.4; Equation 1.7; Hopmans *et al.*, 2004). In the Tottenhill Quarry sample, BIT was 0.80 indicating a low contribution from marine crenarchaeol (**G5**; Table 4.4). The CPI (Equation 1.4) of 2.3 suggests a mix of terrestrial and aquatic OM (Table 4.4; Bray and Evans, 1961; Meyers and Ishiwatari, 1993; Ortiz *et al.*, 2004).

Pigments were absent in the Blackborough Quarry samples of type A, inferring either destruction by oxidation or lack of production (Figure 4.15; Appendix 4.4; Hendry *et al.*, 1987). The pigment profile in type A at Tottenhill Quarry consisted of chlorophyllone (chlone *a*; **C3**) and unidentified carotenoid P7 (Figure 4.12; Appendix 4.3). Considering the contribution of terrestrial, aquatic OM and possible contribution of marine OM at Tottenhill Quarry, a specific origin of the carotenoid cannot be established. The higher abundance of P7 and the paucity in chlorophyll pigments (chlorophyllone to carotenoid P7 ratio of 0.82) indicate low productivity and environmental conditions that did not favour preservation (Table 4.4; Hendry *et al.*, 1987). Low productivity is also evident in the low concentrations of lipids (Figures 4.10, 4.11) and low organic carbon contents from LOI analysis (<3%; Figure 4.4).

In conclusion, type A sediments, identified in Tottenhill Quarry and Blackborough Quarry samples (Table 4.4; Figures 4.10-4.15), suggest a terrestrially dominated environment with unfavourable conditions for the production and / or preservation of chlorophyll pigments and lipids. Marine organisms were minor contributors at Tottenhill Quarry, as evident from the BIT value.

Table 4.4. Elevation, BIT, CPI, P_{aq} and ratio of chlorophylls / carotenoids of samples with molecular distributions of type A.

Site	Elevation / m OD	BIT	CPI	P _{aq}	Ratio chls/cars
Tottenhill	1.950	0.80	2.13	0.23	0.82
Blackborough	-1.185	0.96 ^b	n.a. ^d	n.a. ^d	n.a. ^a
	-1.190	0.96 ^b	n.a. ^d	n.a. ^d	n.a. ^c

^a No chlorophylls or carotenoids

^c Not analysed due to low amounts of sediments

^b Some GDGTs below LOQ <10

^d No *n*-alkanes

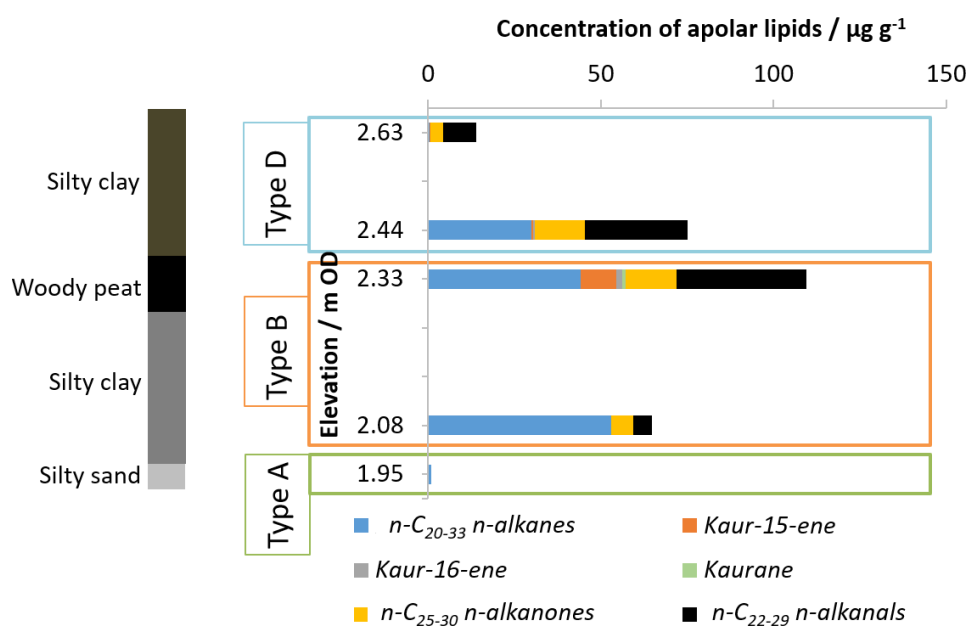


Figure 4.10. Concentrations of *n*-alkanes, kaur-15-ene, kaur-16-ene, and kaurane, *n*-alkanones and *n*-alkanals in the Tottenhill Quarry samples.

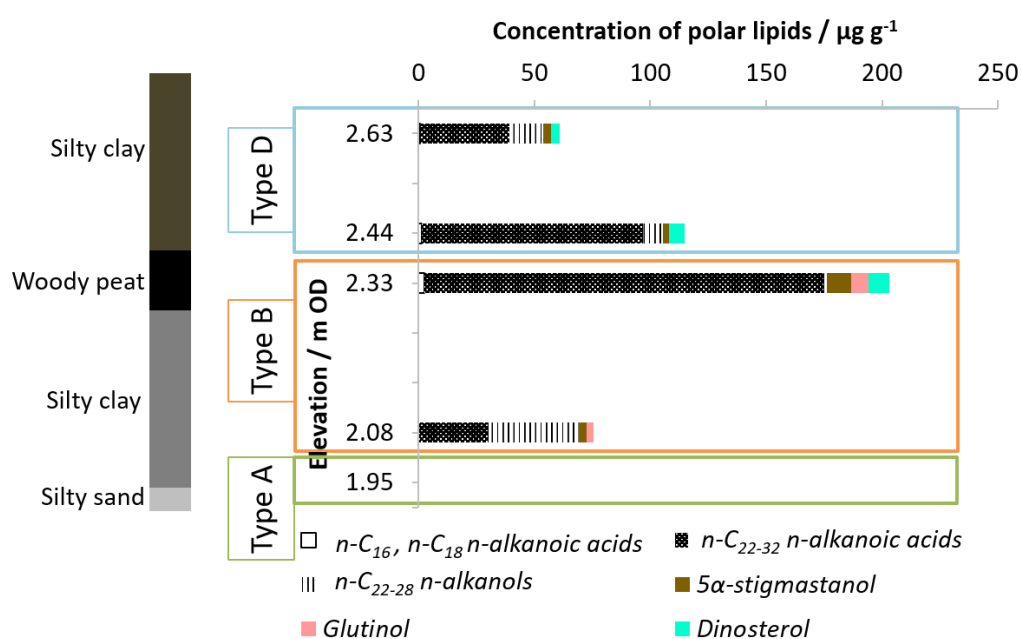


Figure 4.11. Concentrations of *n*-alkanoic acids, *n*-alkanols and terpenoids in the Tottenhill Quarry samples.

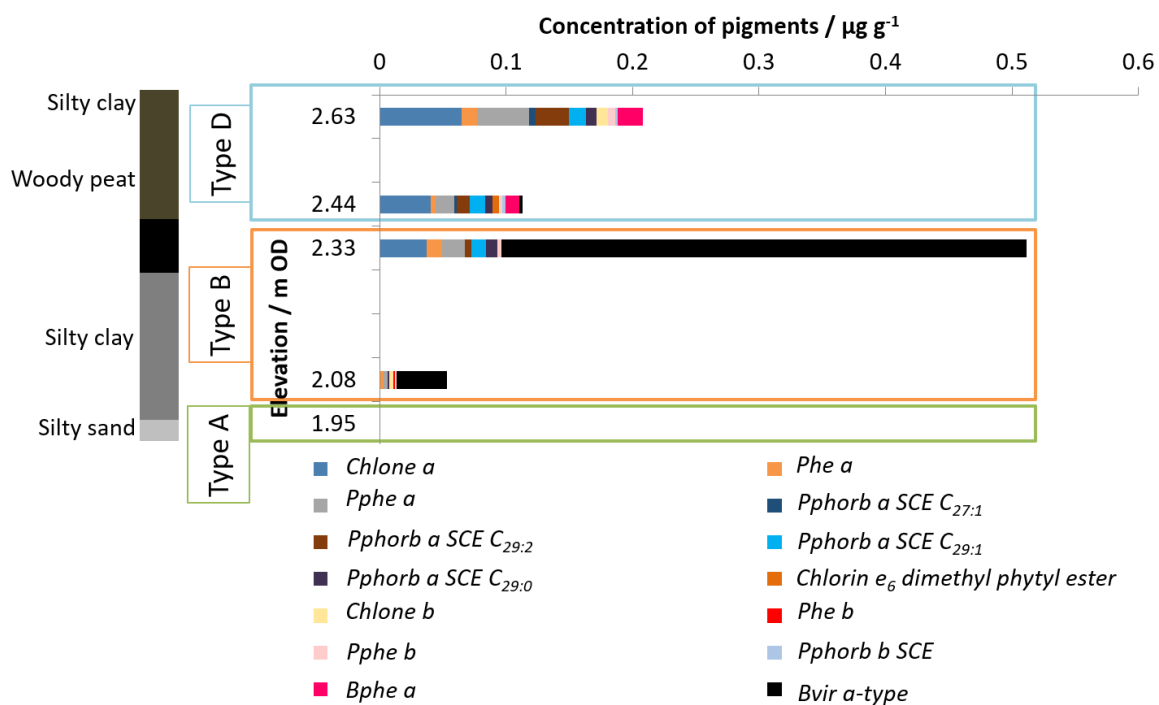


Figure 4.12. Concentrations of chlorophyll and bacteriochlorophyll pigments in the Tottenhill Quarry core.

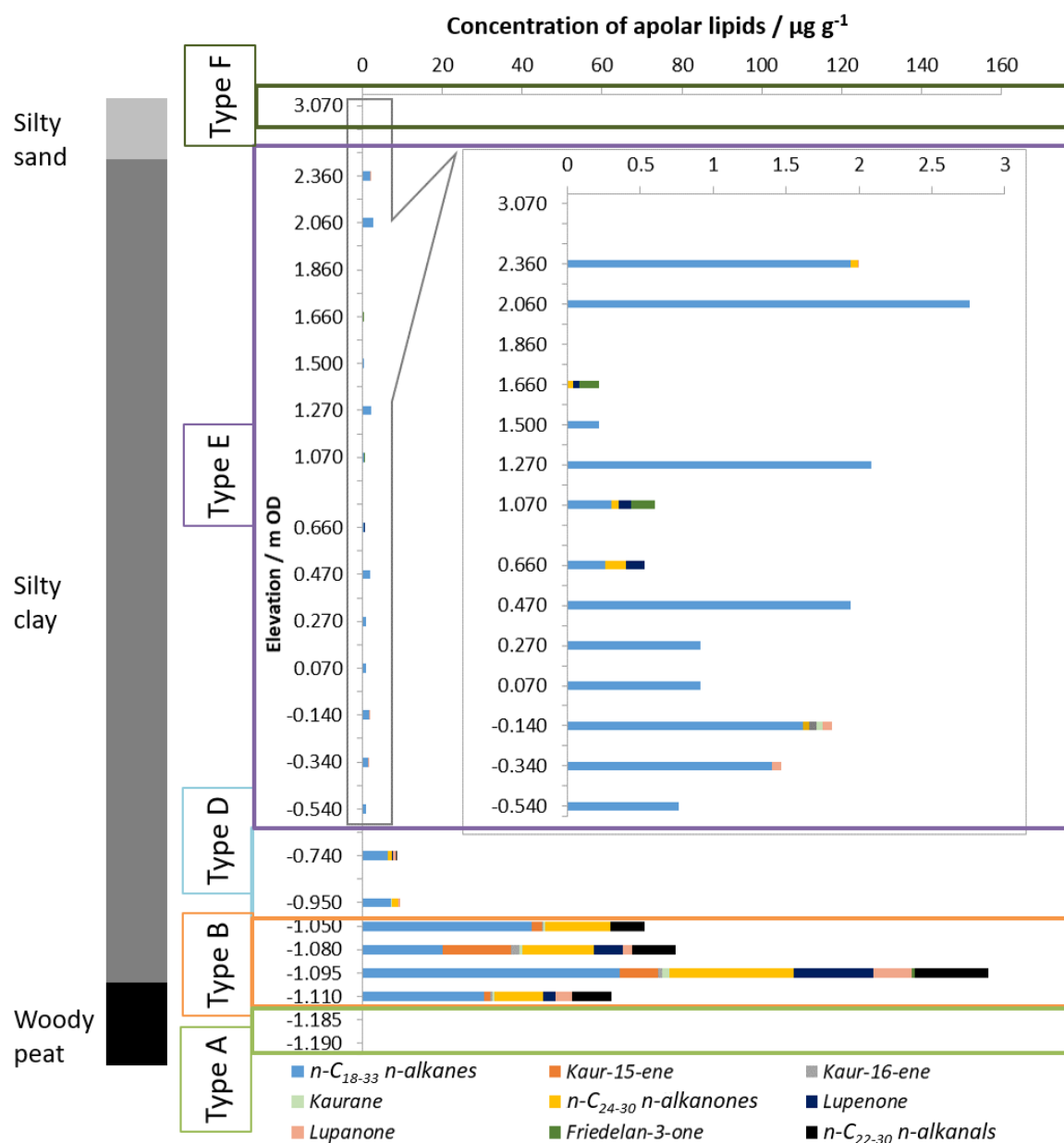


Figure 4.13. Concentrations of *n*-alkanes, kaur-15-ene, kaur-16-ene, and kaurane, *n*-alkanones, lupenone, lupanone, friedelan-3-one and *n*-alkanals in the Blackborough Quarry samples.

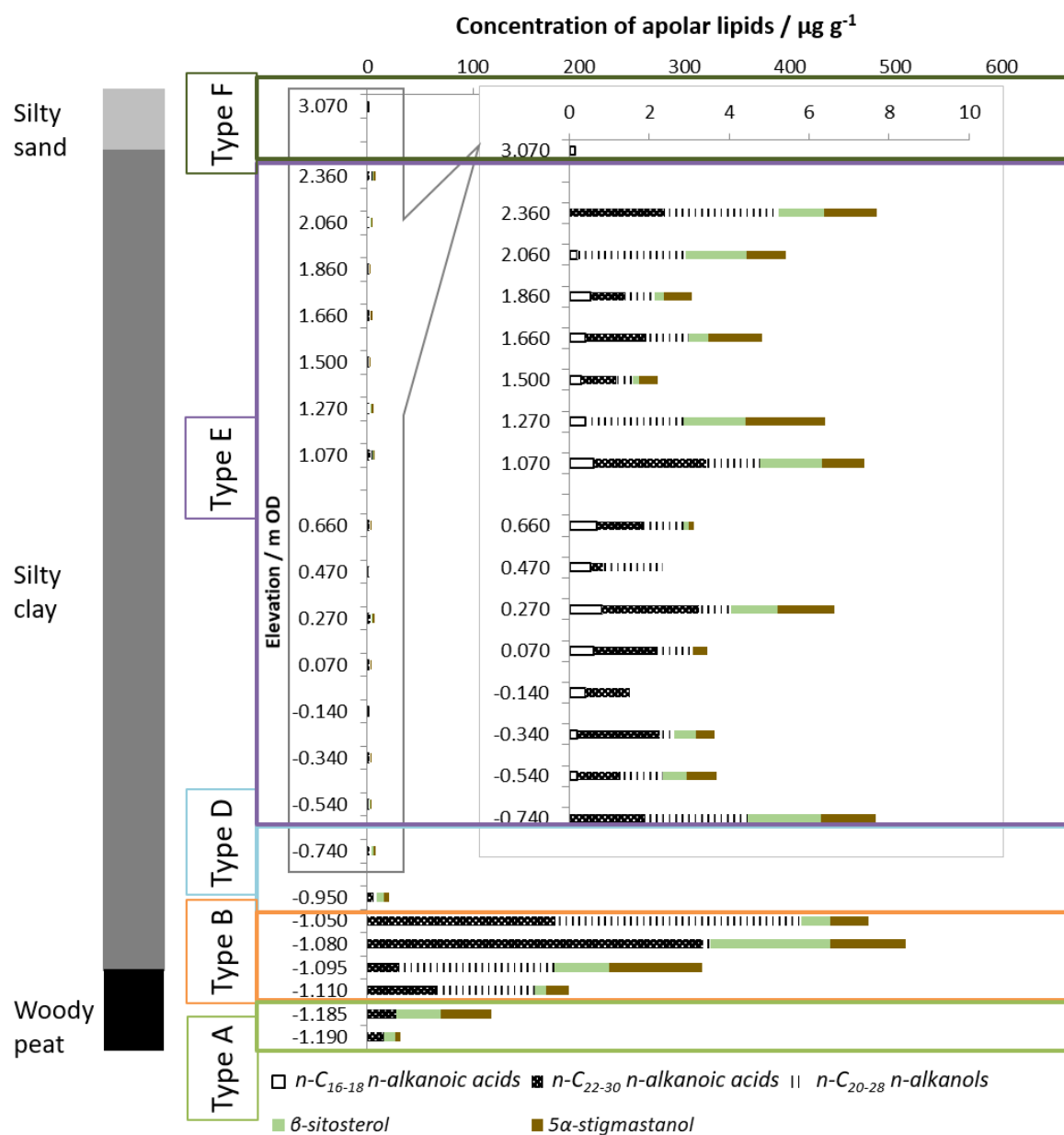


Figure 4.14. Concentrations of *n*-alkanoic acids, *n*-alkanols and terpenoids in the Blackborough Quarry samples.

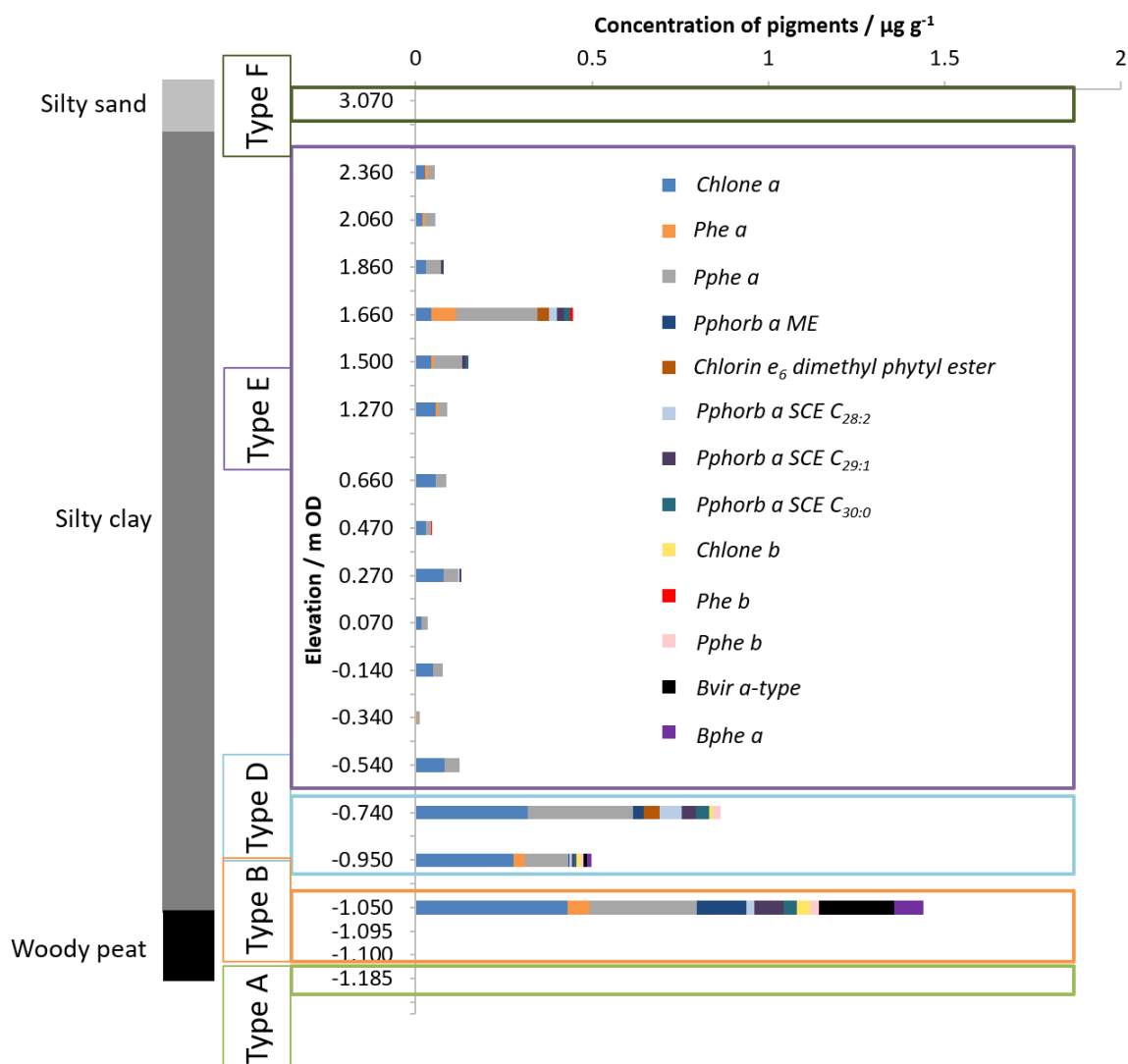


Figure 4.15. Concentrations of chlorophyll and bacteriochlorophyll pigments in the Blackborough Quarry core.

4.4.3. Molecular distribution type B

Type B molecular distributions were designated in the clay and peat horizons in Tottenhill Quarry (2.08, 2.33 m OD), in the peat in Horse Fen (-3.13, -3.03, -2.56, -2.48 m OD) and in the peat-clay transition in Blackborough Quarry (-1.10, -1.095, -1.080, -1.050 m OD; Table 4.5). The lipid profile shows abundant lipids of terrestrial origin in much higher concentrations than for type A, indicating a much more productive environment (Figures 4.10, 4.11, 4.13, 4.14, 4.16, 4.17), consistent with the high organic carbon contents from the LOI (Figures 4.4-4.6). The terrestrial OM origin is confirmed by the CPI (generally >5) and BIT values (0.92 to 1; Table 4.5). Markers of lignitic peat, kaur-15-ene (**T1**), kaur-16-ene (**T2**) and kaurane (**T3**) were identified in all samples (Figures 4.10, 4.13, 4.16; Cranwell, 1982; Philp and Lewis, 1987; Del Rio *et al.*, 1992), coinciding with the horizons

where woody peat was identified by lithological analysis (Figures 4.4-4.6). In the Tottenhill Quarry core Type B terrestrial and peat markers were dominant and the BIT values of 0.88 and 0.98 indicated decreasing amount of marine OM. Comparison of BIT values between type A (0.80) and type B (0.88-0.98) indicate an increase in BIT and thus decrease of marine contribution to Tottenhill Quarry that could indicate onset of a regression. This change in relative sea level was not identified in previous studies of the core, where foraminifera were absent throughout (Barlow *et al.*, 2017). The possible regression in the Tottenhill Quarry core (1.95-2.33 m OD) indicates that molecular fossils can refine palaeoenvironmental studies.

The sediments at Horse Fen contained the conifer marker γ -sitostenone (**T7**) in addition to friedelan-3-one (**T4**; Section 4.4.1; Otto *et al.*, 2005) and α -tocopherol (**T14**). The latter occurs in the leaves of the fen plant *M. trifoliata* and in the foliage of various herbs and trees (Figures 4.16, 4.17; van Bergen *et al.*, 1997; Ronkainen *et al.*, 2013). At Blackborough Quarry, the presence of lupenone (**T6**) and lupanone (**T7**), indicative of tree bark, confirms the dominance of terrestrial sources of OM (Figure 4.13; Schnell *et al.*, 2014). These ketone terpenoids are formed by oxidation of alcohol functional groups indicating early diagenetic alteration under oxic conditions (Hollerbach, 1978). The terpenoid glutinol (**T8**), which occurred in Tottenhill Quarry and Horse Fen, has been correlated with plant matter of peat and fen origin, consistent with the lithology of Type B (Figure 4.11, 4.17; Zocatelli *et al.*, 2014). High BIT values (Table 4.5), dinoflagellate marker dinosterol (**T10**) and low concentrations of *n*-C₁₆ and *n*-C₁₈ *n*-alkanoic acids (Figure 4.11; Volkman, 2003; Cranwell, 1982) confirm the presence of freshwater conditions at Tottenhill Quarry. The start of the transgression at Blackborough Quarry is marked by an increase in marine crenarchaeol (**G5**), reflected in a BIT of 0.90 at -1.050 m OD (Table 4.5). The lag in the detection of the transgression from BIT compared with foraminifera (-1.04 m OD) and the peat-clay contact at -1.100 m OD indicative of the transgression probably indicates that the Thaumarchaeota only became established after stabilisation of the water column following the transgression.

The pigment profiles of the three cores differ, suggesting that water column conditions developed differently. At Tottenhill Quarry the pigments include numerous bacterioviridin α -type pigments (Figure 4.12), thus most likely indicating the presence of waters subject to oxidation or shallow levels (Wilson *et al.*, 2004). This pigment distribution can be related to a decrease in the level of the water table and the increase in BIT values confirm the occurrence of a regressive event (type A \rightarrow type B). In addition to the highly abundant bvirs, the chlorophyll pigments were dominated by chl *a* with lower amounts of chl *b*-derived pigments, chlorophyllone (chlone; **C3-C4**), phaeophytin (phe; **C6-C7**), pyropheophytin (pphe; **C8-C9**) and three phaeophorbide α steryl chlorin esters

(pphorb α SCE; **C12**; Figure 4.12). One of the SCE sterols was identified as C_{29:0} (m/z 933, 535) by APCI-MS/MS (cf. Airs, 2001) and tentatively attributed to algal OM origin (Volkman, 2003; Appendix 4.3). Carotenoid P7 was in very low concentrations in the samples, giving a ratio of chlorophylls over carotenoid of 61.3 (Table 4.5), indicating that the water column conditions were favourable for higher production of pigments than for Type A horizons (Section 4.4.2).

Chlorophyll pigments were absent between -1.185 and -1.095 m OD at Blackborough Quarry, the only pigment present being carotenoid P7 (Figure 4.15). From -1.050 m OD the pigment profile showed abundant chlorophylls with bacterioviridin α (**B4**) and lower concentrations of bacteriochlorophylls (Figure 4.15; Appendix 4.4). The pigment profile suggests a dynamic water column with a semi-permanent or unstable chemocline, affected by onset of marine waters.

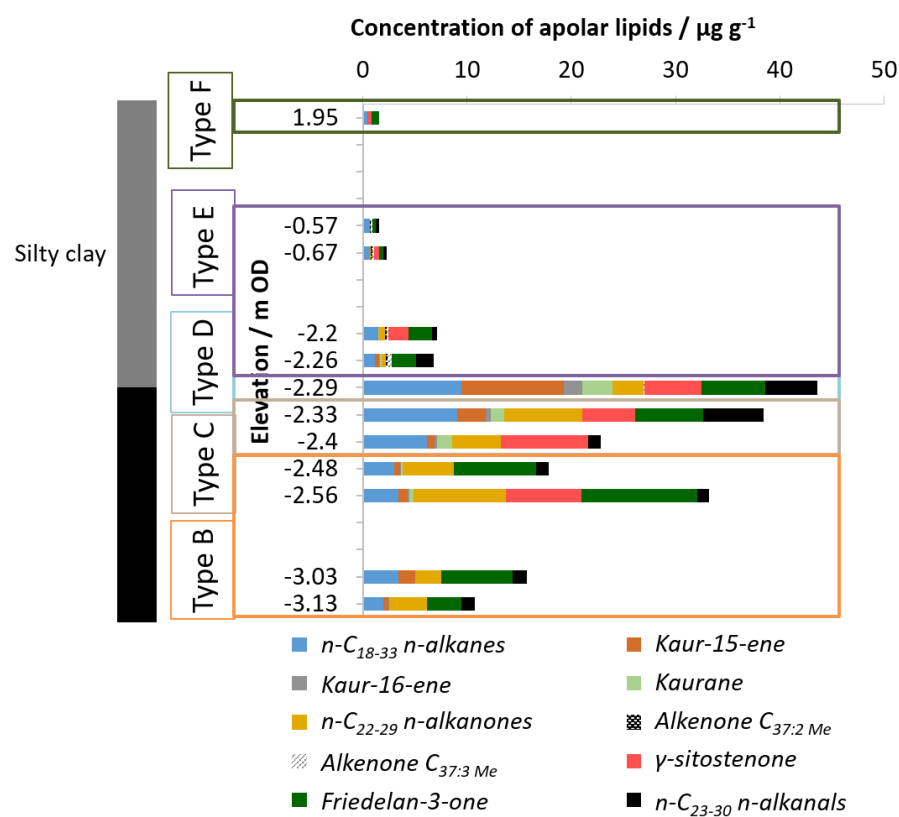
The presence of chlorophylls at Horse Fen -3.13 m OD suggests a fully oxic water column (Figure 4.18; Appendix 4.1). From -3.03 m OD a chemocline was formed as evident from the co-occurrence of chlorophylls a and b and bacteriochlorophyll a pigments, indicative of a very productive environment (Pfennig, 1977). Horizon -2.48 m OD was devoid of pigments, apart from carotenoid P7, possibly due to reduced production or unfavourable conditions for pigment preservation (Hendry *et al.*, 1987). Since the lipid profile and the P_{aq} values (Figures 4.16, 4.17, Table 4.5) suggest a mix of aquatic and terrestrial OM, it is likely that the absence of pigments at -2.48 m OD is due to destruction by oxidation.

Interestingly, in samples at Tottenhill Quarry 2.080 m OD, Horse Fen -3.030 m OD and Blackborough Quarry -1.050 m OD the chlorophylls are more abundant than carotenoids. The other samples in type B either contain only carotenoid P7 or chlorophylls in very low concentrations, which could be related to the relative stabilities of these different compound classes, or the changing water column conditions affecting pigment production and preservation.

The molecular fossil signatures of type B sediments represent a peat-clay environment surrounded by plants including conifers, consistent with the lithology, high organic carbon content from LOI and pollen data. Aquatic OM evident in all type B sediments indicates a productive environment with oxygenic and anoxygenic photoautotrophic communities with a semi-permanent chemocline. Noticeable changes in the BIT and pigment profiles of Tottenhill Quarry type A and B samples indicate a decrease in marine production and increase in terrestrial and peat OM, representing a regression. It is postulated that the sediment below the retrieved core represents a fully marine environment prior to the regression; however, a new core should be collected to confirm this hypothesis.

Table 4.5. Elevation, BIT, CPI, P_{aq} and ratio of chlorophylls / carotenoids of samples with molecular distributions of type B.

Site	Elevation / m OD	BIT	CPI	P_{aq}	Ratio chls/cars
Tottenhill	2.330	0.98	4.66	0.23	n.a. ^a
	2.080	0.88	8.75	0.12	61.3
Blackborough	-1.050	0.90	4.90	0.47	4.32
	-1.080	0.98	3.48	0.35	n.a. ^b
	-1.095	0.98	7.03	0.35	n.a. ^a
	-1.100	0.92	5.58	0.49	n.a. ^a
Horse Fen	-2.480	0.99	8.66	0.38	n.a. ^a
	-2.560	1.00	n.a. ^c	0.23	0.30
	-3.030	0.99	n.a. ^c	0.16	2.73
	-3.130	0.98	n.a. ^c	0.44	0.08

^a Only carotenoid P7 detected^c Missing some *n*-alkanes^b Not analysed due to low amounts of sedimentsFigure 4.16. Concentrations of *n*-alkanes, kaur-15-ene, kaur-16-ene, and kaurane, *n*-alkanones, alkenones $C_{37:2}$ and $C_{37:3}$, γ -sitostenone, friedelan-3-one and *n*-alkanals in the Horse Fen samples.

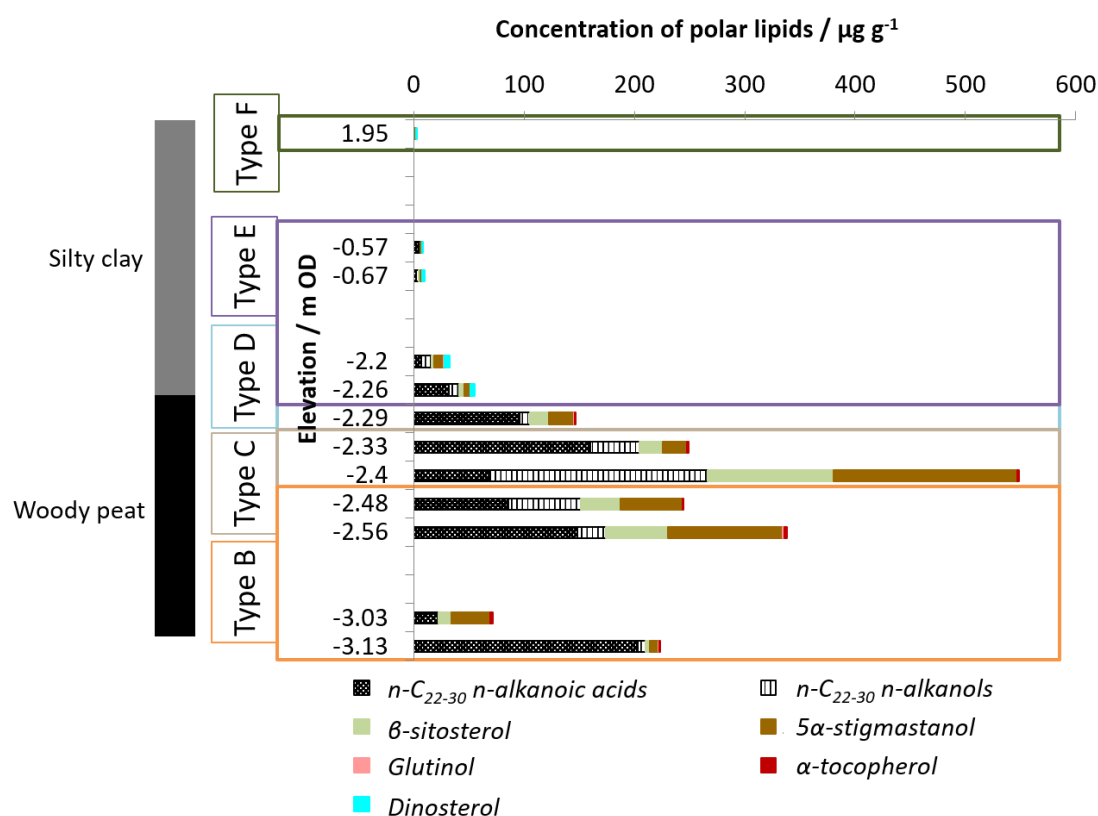


Figure 4.17. Concentrations of *n*-alkanoic acids, *n*-alkanols and terpenoids in the Horse Fen samples.

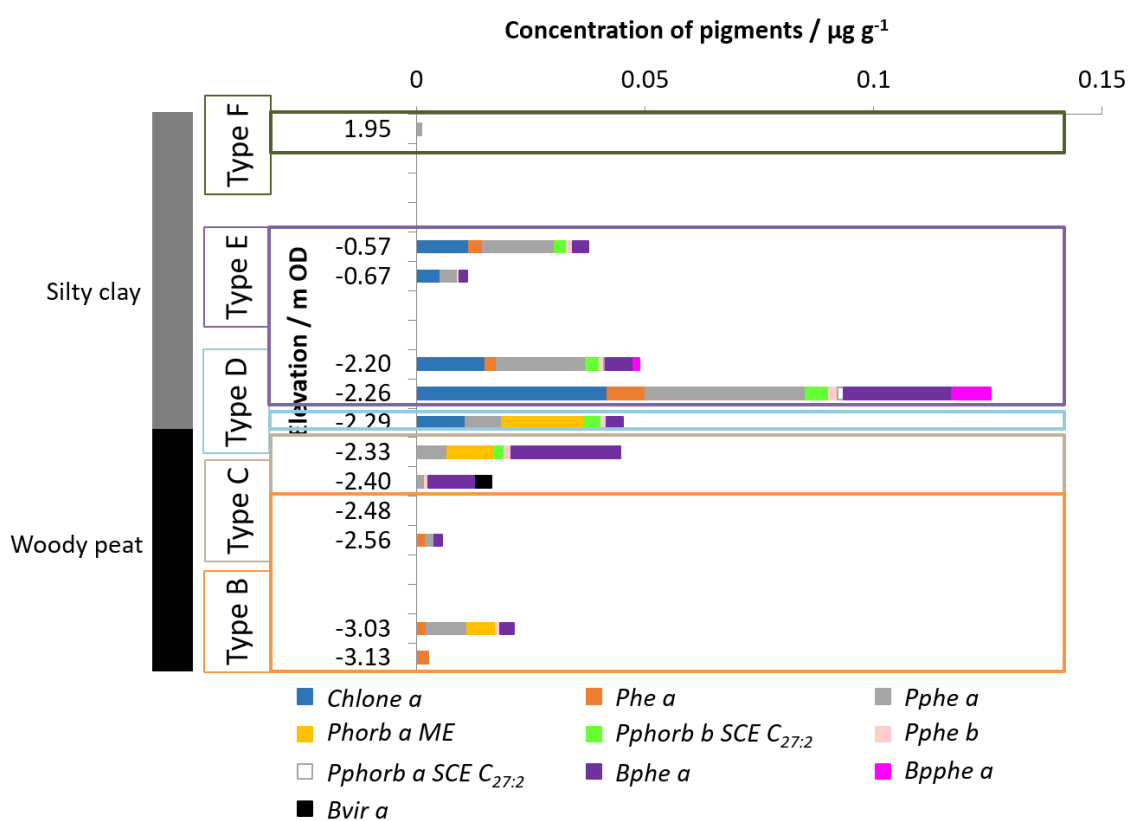


Figure 4.18. Concentrations of chlorophyll and bacteriochlorophyll pigments in the Horse Fen core.

4.4.4. Molecular distribution type C

Sediments containing molecular distribution type C were present only in the peat of the Horse Fen core at -2.40 and -2.33 m OD (Table 4.6). The lipid profile in type C is dominated by terrestrial OM from higher plants and indicators of lignitic peat, similarly to type B (Figures 4.16, 4.17). It differs from type B in containing low amounts of the haptophyte marker long chain alkenone $C_{37:3}Me$ (**A7**; Marlowe *et al.*, 1984). The alkenone was identified in trace amounts in the GC chromatogram of the aromatic hydrocarbon fraction, eluting after the long chain *n*-alkanones and *n*-alkanals (Appendix 4.6). Confirmation of the assignments was performed by GC-MS analysis and comparison with literature spectra (Rontani *et al.*, 2006; Longo *et al.*, 2013). The MS spectrum of $C_{37:3}Me$ alkenone shows the molecular ion at m/z 528 and the fragment ion formed by loss of the methyl group (m/z 513, -15 Da; Figure 4.19). The fragment at m/z 264 may arise from cleavage of the carbon chain; in the m/z range 30-100, the losses of 28 Da indicate the presence of alkyl and alkenyl chains.

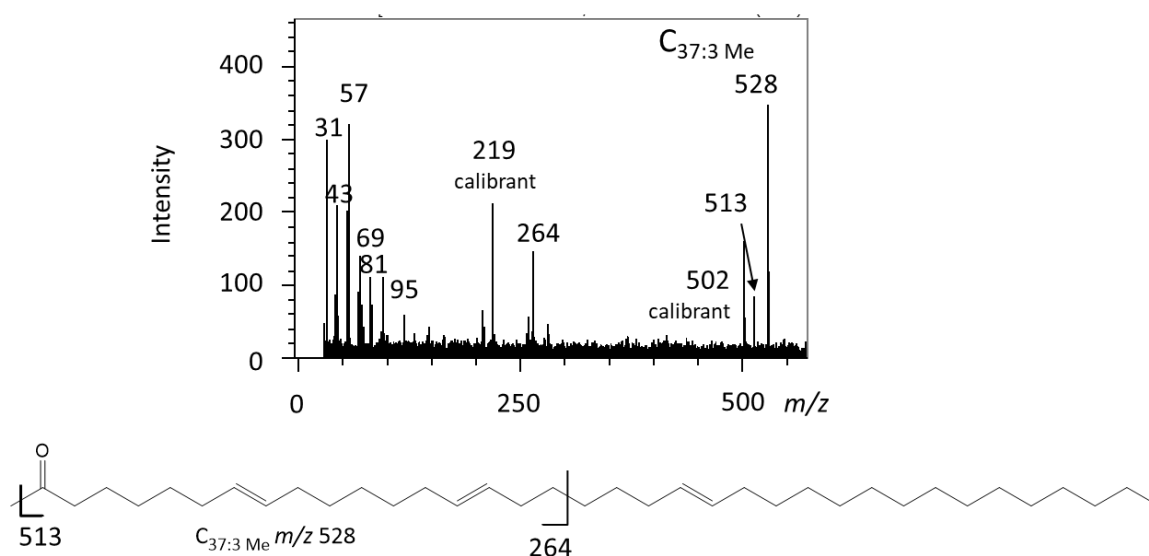


Figure 4.19. GC-El-MS spectrum and structure of the alkenone $C_{37:3}Me$ showing the most prominent fragments.

Although the lipid distribution is similar to type B, the pigment profile in type C samples is markedly different (Figure 4.18; Appendix 4.1). At -2.40 m OD small amounts of pphe *a* (**C6**) and higher concentrations of bphe *a* (**B2**) and bpphe *a* (**B3**) were detected, together with low concentrations of bvir *a* (**B4**). The high concentrations of bchls reflect a water column dominated by anoxic conditions and the low concentrations of the oxidation product bvir *a* (Wilson *et al.*, 2004) suggest a shallow environment. Squier *et al.* (2002) observed very high concentrations of bchls *c* and *d* (**B5**-

B6) with low concentrations of chls and SCEs in Antarctic lake sediments; this distribution was explained as coinciding with marine incursion, in which nutrient availability increases, thus OM increases leading to eutrophication and the marked development of an anoxygenic photoautotrophic community. In the Horse Fen sediments of type C bphe *a* concentrations are higher than those of chls indicating eutrophication from increased input of nutrients potentially related to transgression. Thus, the response of the photoautotrophic community apparent at -2.40 and -2.33 m OD and the presence of long chain alkenone C_{37:3Me} likely marks the onset of the transgression before the signal from foraminifera (at -2.28 m OD; Barlow *et al.*, 2017). At -2.33 several SCEs (**C12**) were detected (Figure 4.18), an indication of herbivore grazing (Harradine *et al.*, 1996; Talbot *et al.*, 1999). One of these SCEs was identified as pphorb *a* with sterol C_{27:1} (Airs, 2001), suggesting a marine algal contribution (Volkman, 1986).

Table 4.6. Elevation, BIT, CPI, P_{aq} and ratio of chlorophylls / carotenoids of samples with molecular distributions of type C.

Site	Elevation / m OD	BIT	CPI	P _{aq}	Ratio chls/cars
Horse Fen	-2.330	0.98	n.a. ^a	0.19	2.24
	-2.400	0.99	n.a. ^a	0.23	0.64

^a Missing some *n*-alkanes

4.4.5. Molecular distribution type D

The type D sediments were identified in three of the cores: Tottenhill Quarry (2.40 and 2.63 m OD), Horse Fen (-2.29 m OD) and Blackborough Quarry (-0.95 and -0.74 m OD; Table 4.7). Type D is characterised by a mix of terrestrial and marine OM, evident from BIT values lower than in types A-C (Table 4.7). Low concentrations of alkenone C_{37:3 Me} (**A7**) in Horse Fen confirms the onset of marine production following a transgression (Figure 4.16). The aquatic environment is represented by the presence of short chain *n*-C₁₆ and *n*-C₁₈ *n*-alkanoic acids (**A4**) and dinosterol (**T10**) at Tottenhill Quarry (Figure 4.11; Cranwell, 1982; Volkman 1986). Following the beginning of the transgression at Blackborough Quarry, identified at -1.050 m OD in type B sediments, an increase in algal *n*-alkanes was recorded (CPI values <5; Table 4.7; Meyers and Ishiwatari, 1993; Ortiz *et al.*, 2004). CPI values <5 were previously observed in Loch of Stenness (Chapter 3) during the transgressive event (85 cm), indicating a dilution of terrestrial OM with algal OM thus supporting the identification of a transgressive event at Blackborough Quarry. The Tottenhill Quarry core represents a terrestrial environment from microfossil analysis (Barlow *et al.*, 2017). The increase in P_{aq} values reveals a higher aquatic OM contribution to the samples in type D, compared to type B sample. The BIT from

the samples from Tottenhill Quarry (2.44, 2.63 m OD) suggest an increase in marine contribution consistent with the initial stages of a transgression. Decreasing BIT values between 1.95 and 2.33 m OD likely indicate the cessation of a regression (type A→type B). These features were not evident from microfossil analysis.

The pigments at Tottenhill Quarry, Horse Fen and Blackborough Quarry at -0.95 m OD indicate a stratified water column populated by oxygenic and anoxygenic photoautotrophs (Figures 4.12, 4.15, 4.18). In the Blackborough Quarry core from -0.74 m OD the molecular fossils indicate a fully oxidised environment (Figure 4.15; Appendix 4.4). In all three cores SCEs (**C12**) showed variability in sterol carbon numbers, representative of different primary producers and / or herbivore populations. At Blackborough Quarry, the SCEs identified were $C_{28:2}$ (m/z 915, 535), $C_{29:0}$ and $C_{30:0}$ (m/z 948, 535; Appendix 4.4); at Horse Fen $C_{27:1}$ (m/z 903, 535; Appendix 4.1) and at Tottenhill Quarry $C_{27:1}$, $C_{29:2}$ (m/z 929, 535), $C_{29:1}$ (m/z 931, 535) and $C_{29:0}$ were identified (Appendix 4.3). The SCEs in the Horse Fen and Tottenhill Quarry samples show marine algal OM (prevalence C_{27} sterol carbon number), while at Blackborough Quarry freshwater algal sources dominate (C_{28-30} ; Volkman, 1986; Meyers and Ishiwatari, 1993).

The sediments in type D reflect an environment surrounded by higher plants and inundated by marine waters with the development of oxygenic and anoxygenic photosynthetic organisms. Marine incursion resulted in an increase in algal production, as shown by the long chain alkenones, dinosterol, short chain alkanols and crenarchaeol contributions.

Table 4.7. Elevation, BIT, CPI, P_{aq} and ratio of chlorophylls / carotenoids of samples with molecular distributions of type D.

Site	Elevation / m OD	BIT	CPI	P_{aq}	Ratio chls/cars
Tottenhill	2.630	0.81	6.53 ^b	0.44	10.0
	2.440	0.93	5.19	0.52	n.a. ^a
Horse Fen	-2.290	0.97	n.a. ^d	n.a. ^d	7.90
Blackborough	-0.740	n.a. ^c	3.14	0.25	1.37
	-0.950	0.85	2.46	0.31	0.99

^a No chlorophylls or carotenoids

^c No brGDGTs detected

^b Missing n -C₃₂ n -alkane

^d Missing some n -alkanes

4.4.6. Molecular distribution type E

Type E samples are represented by the clays in Blackborough Quarry (from -0.54 to 2.36 m OD), Railway Cottage (8.74, 9.46, 9.93, 10.07 m OD) and Horse Fen cores (-2.26, -2.20, -0.67, -0.57 m OD). The terrestrial higher plant input was constant throughout type E sediments with concentrations being lower than in type D, reflecting the lower percentage of organic carbon from LOI (Figures 4.10, 4.11, 4.13, 4.14, 4.16, 4.17, 4.21, 4.22). Kaur-15-ene (**T1**), kaur-16-ene (**T2**) and kaurane (**T3**) were present in lower amounts than in type B-D at Horse Fen at -2.26 and -2.20 m OD (Figure 4.16) coinciding with the transition from lignitic peat to clay (Figure 4.5). In the sediments from Railway Cottage and the ones deposited after the transgression from Blackborough Quarry, the CPI values indicate a mix of algal and terrestrial OM (Table 4.8). By contrast, the samples at Horse Fen show CPI values >5, although aquatic input in all three cores was evident from the presence of short chain *n*-C₁₆ and *n*-C₁₈ *n*-alkanoic acids (**A4**) and dinoflagellate marker dinosterol (**T10**; Figures 4.14, 4.17, 4.22).

A marine gastropod shell, *Tritia* sp. (WoRMS *Tritia*), was identified at Railway Cottage at 8.74 m OD, and two specimens of the freshwater / brackish gastropod *Ecrobia ventrosa* (WoRMS *Ecrobia ventrosa*) at Horse Fen -2.26 m OD. These molluscs confirm the marine OM input in type E sediments. The BIT values, <0.8 at Railway Cottage and 0.4-0.6 at Blackborough and Horse Fen (Table 4.8), reflect marine influence in all these sites. This is supported at Horse Fen and Railway Cottage by the presence of C_{37:2}Me and C_{37:3}Me long chain alkenones at both sites, accompanied by the C_{38:2}Et (**A8**) homologue in the latter site (Figures 4.16, 4.21; Marlowe *et al.*, 1984). Similarly to the GC-MS spectrum of C_{37:3}Me, the spectra of C_{37:2}Me and C_{38:2}Et show the molecular ions, *m/z* 530 and 544, respectively (Figure 4.20); the fragment ion at *m/z* 264 is analogous to Figure 4.19 and fragments in the *m/z* range 40-140 suggest losses consistent with alkyl and alkenyl chains (28 Da; Figure 4.20).

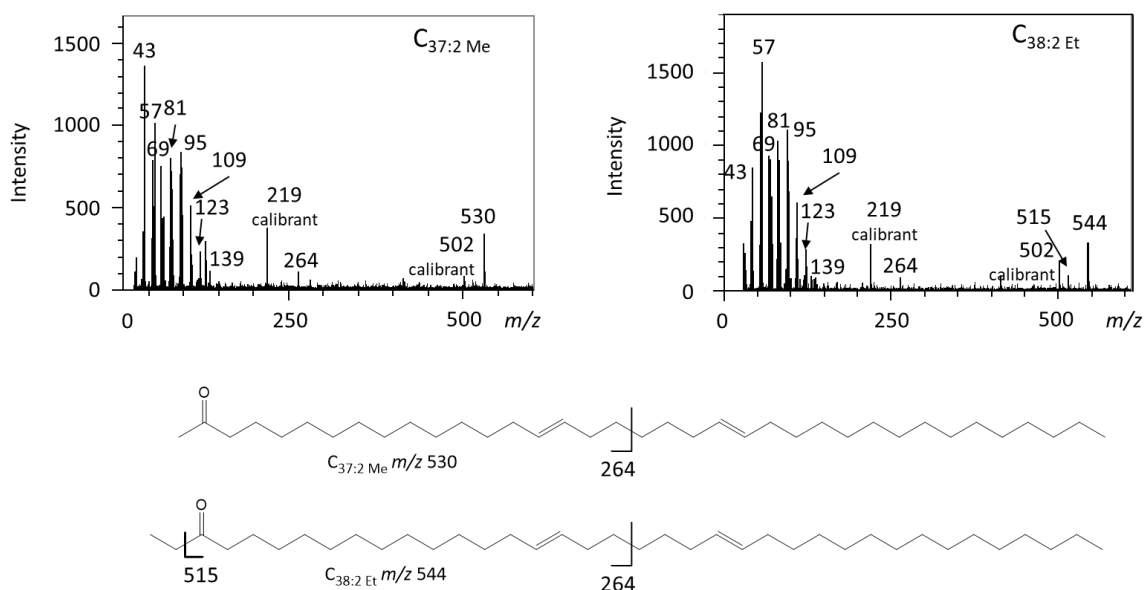


Figure 4.20. GC-El-MS spectra of long chain alkenones: $C_{37:2}$ Me and $C_{38:2}$ Et and structures showing the most prominent fragments.

The pigment profile at Blackborough Quarry exhibited only chlorophylls in decreasing concentrations, indicative of a fully oxidised and increasingly less productive environment (Figure 4.15; Appendix 4.4). Heterotrophic activity, demonstrated by the presence of a series of pphorb *a* SCE (**C12**; Harradine *et al.*, 1996; Talbot *et al.*, 1999), is evident at 0.27, 1.50, 1.66, 1.86 m OD which corresponds to horizons where chlorophyll productivity was highest in type E (Figure 4.15). The sterols were identified as $C_{28:2}$ (m/z 915, 535), $C_{29:1}$ and $C_{30:0}$ (Airs, 2001) and correlated to algal OM (Volkman, 1986). In type E samples from Blackborough Quarry, carotenoids, including P7, were more abundant than chlorophylls, resulting in ratios <1 (Table 4.8). This trend, previously observed in Tottenhill Quarry (1.95 m OD) and Horse Fen (-3.13, -2.56, from -2.26 to 1.95 m OD; Tables 4.4, 4.6), could suggest an unfavourable environment for chlorophyll preservation where only carotenoids were preserved (Hendry *et al.*, 1987).

Samples at -0.14, 0.27, 0.66, 1.07 and 1.66 m OD from the Blackborough Quarry core showed slight differences in the lipid and pigment profiles compared to the rest of type E sediments. These samples show an input of kaur-15-ene (**T1**), kaur-16-ene (**T2**), kaurane (**T3**), long chain *n*-alkanones (**A2**), lupenone (**T6**) and friedelan-3-one (**T4**) that represented the lignitic peat in type B before the transgression (Figure 4.13). The pigment profile indicates a productive environment with a rich community of producers and grazers (especially at 1.66 m OD; Figure 4.15) and higher ratios of chlorophylls over carotenoids (Table 4.8). The presence of molecular fossils from the peat, in addition to aquatic and marine markers, indicate mixed signatures from erosion or a turbulent

environment. Indeed, the foraminifera found at -0.14 and 0.66 m OD by Barlow *et al.* (2017) indicate the possibility of storm events being represented in these sediments.

Horse Fen and Railway Cottage pigments are dominated by chlorophylls with low concentrations of bacteriochlorophyll *a* pigments, suggesting a productive environment with bottom water anoxia (Figures 4.18, 4.23). Similarly to type D, pphorb *a* and *b* SCEs were identified with sterol carbon numbers C_{27:1} (pphorb *b* SCE *m/z* 917, 549) at Horse Fen (Figure 4.18; Appendix 4.1) and at Railway Cottage C_{27:1}, C_{29:2}, C_{29:1}, C_{29:0}, C_{30:1} (*m/z* 946, 535) and C_{30:0} (*m/z* 948, 535; Figure 4.23; Appendix 4.2; Airs, 2001), denoting marine organisms (C₂₇) and algal (C₂₈₋₃₀) origin of the sterol moieties (Volkman, 2003).

The lithological change from lignitic peat (types B-C) to grey clay (types D-E) in Horse Fen, Blackborough Quarry and Tottenhill Quarry indicates a transgression; this coincides with a decline in concentration of terrestrial biomarkers and an increase in aquatic and marine OM (Figures 4.10, 4.11, 4.13, 4.14, 4.16, 4.17). The terrestrial-dominated environment in the three cores was inundated by marine water and showed higher plant contributions from the hinterland. The establishment of a marine environment is evident in the higher concentrations of marine algal markers compared to terrestrial OM (long chain unsaturated alkenones, BIT). The Railway Cottage core was marine throughout, with an input of terrestrial OM from the hinterland (Figures 4.21, 4.22).

Table 4.8. Elevation, BIT, CPI, P_{aq} and ratio of chlorophylls / carotenoids of samples with molecular distributions of type E.

Site	Elevation / m OD	BIT	CPI	P _{aq}	Ratio chls/cars
Blackborough	2.360	n.a. ^d	2.91	0.27	0.07
	2.060	0.61 ^a	2.83	0.21	0.17
	1.860	0.49	n.a. ^b	n.a. ^b	0.15
	1.660	0.63	n.a. ^b	n.a. ^b	0.78
	1.500	0.56 ^a	n.a. ^b	n.a. ^b	0.47
	1.270	n.a. ^d	1.99	0.30	0.72
	1.070	0.51 ^a	n.a. ^b	n.a. ^b	n.a. ^c
	0.660	0.49	n.a. ^b	n.a. ^b	0.32
	0.470	n.a. ^d	2.80	0.09	0.32
	0.270	n.a. ^d	1.37	0.30	0.75
	0.070	0.46	1.88	0.26	1.11
	-0.140	0.38	1.61	0.37	0.64
	-0.340	n.a. ^d	2.31	0.26	0.57
	-0.540	0.43	2.50	0.21	0.42
Horse Fen	-0.570	0.40	7.55	0.30	0.29
	-0.670	0.66	9.31	0.30	0.25
	-2.200	0.62	8.73	0.34	0.35
	-2.260	0.67	8.00	0.47	0.62
Railway	10.07	0.80	3.17	0.35	4.97
	9.930	0.75	3.27	0.19	9.55
	9.460	0.66	2.84	0.20	1.26
	8.740	0.54	3.42	n.a. ^b	2.55

^a Some GDGTs below LOQ <10^c Not analysed due to low amounts of sediments^b No *n*-alkanes^d Some GDGTs missing

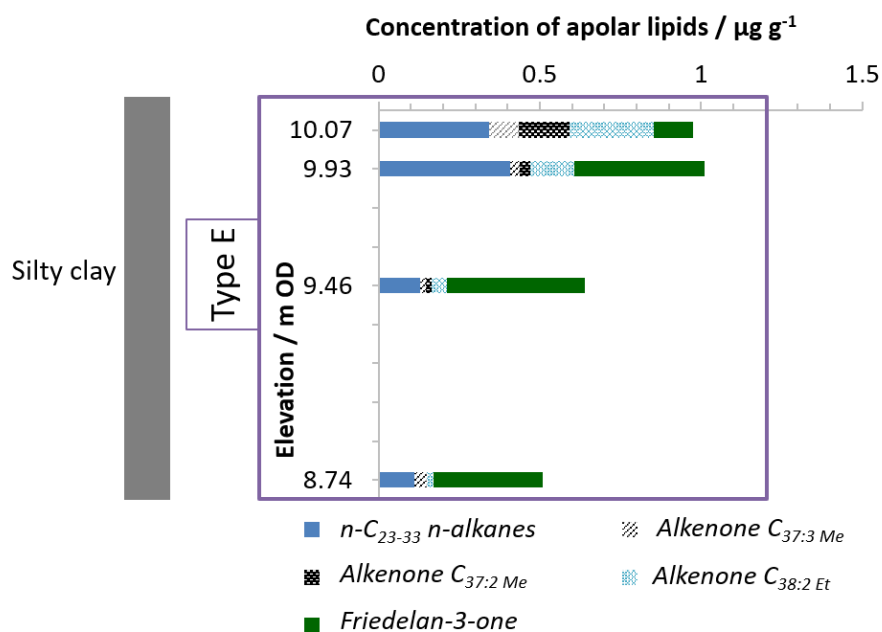


Figure 4.21. Concentrations of n -alkanes, alkenones $C_{37:2}$, $C_{37:3}$ and $C_{38:2}$ and friedelan-3-one in the Railway Cottage samples.

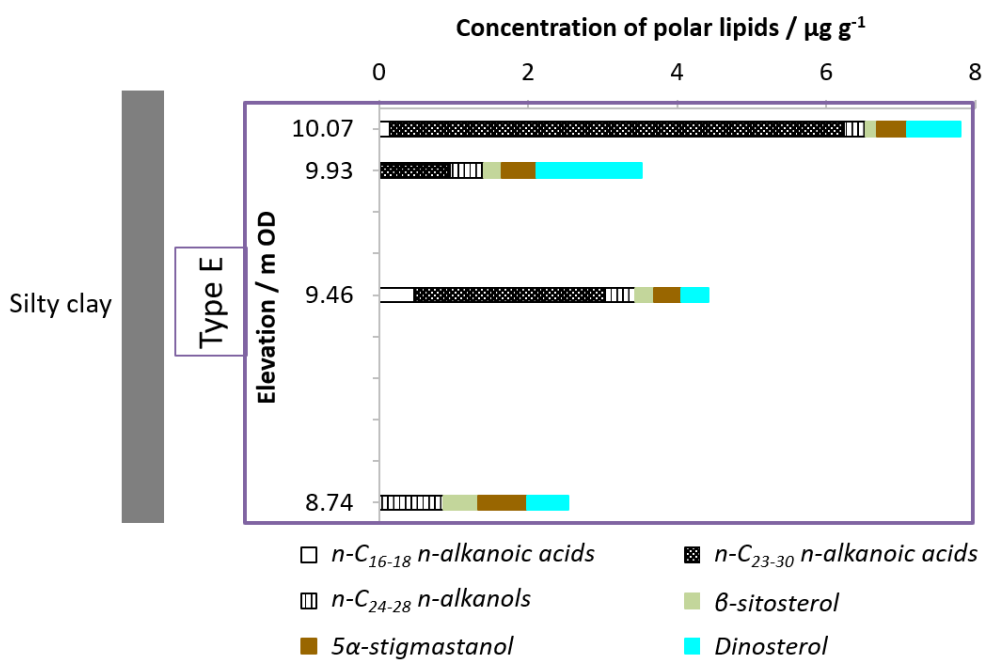


Figure 4.22. Concentrations of n -alkanoic acids, n -alkanols and terpenoids in the Railway Cottage samples.

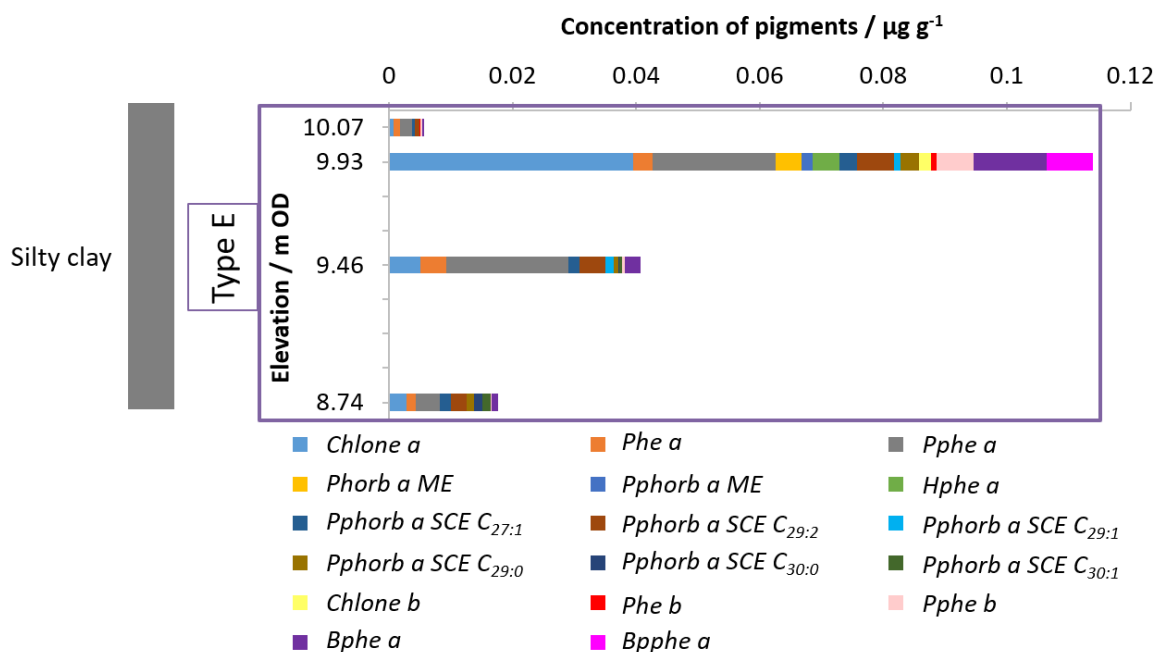


Figure 4.23. Concentrations of chlorophyll and bacteriochlorophyll pigments in the Railway Cottage core.

4.4.7. Molecular distribution type F

Type F sediments were collected from Blackborough Quarry at 3.07 m OD and Horse Fen at 1.95 m OD. The lipids, generally indicating terrestrial and marine OM, had low concentrations (Figures 4.13, 4.14, 4.16, 4.17; Table 4.9). Aquatic conditions are confirmed by the presence of short chain *n*-alkanoic acids (**A4**) in the Blackborough Quarry sample (Figure 4.14) and dinosterol (**T10**) in the Horse Fen sample (Figure 4.17). The low concentration of the pigments chlorophyllone (**C3**) at Blackborough Quarry and pyropheophytin *a* (**C8**) at Horse Fen indicate a low productivity oxic environment (Appendices 4.1, 4.4). Similarly to type A (Table 4.4), the ratio of chlorophylls to carotenoids was low, with carotenoid P7 as the dominant structure (Table 4.9). Type F samples represent a marine environment with low production and / or preservation.

Table 4.9. Elevation, BIT, CPI, P_{aq} and ratio of chlorophylls / carotenoids of samples with molecular distributions of type F.

Site	Elevation / m OD	BIT	CPI	P_{aq}	Ratio chls/cars
Blackborough	3.070	n.a. ^a	n.a. ^b	n.a. ^b	1.16
Horse Fen	1.950	0.55	4.18	0.32	0.11

^a No chlorophylls or carotenoids

^b Some GDGTs below LOQ <10

4.4.8. Reconstructed soil pH and sea-surface temperatures

The pH of the sediments was assessed by calculating the CBT index (Equation 1.12) and applying the calibration developed by Weijers *et al* (2007), resulting in slightly alkaline pH (ranging from 7.3 to 8.5) in all sediments, without variation before and after transgression. Application of the peat-specific pH calibration (Equations 1.15, 1.16; Naafs *et al.*, 2017) to peat sediments from Horse Fen, Blackborough Quarry and Tottenhill Quarry was not possible due to the lack of chromatographic separation of the 5Me (IIa, IIb, IIIa) and 6Me brGDGTs (IIa', IIb', IIIa'; **G6, G9, G10**).

Sea-surface temperatures (SST) were reconstructed in marine sediments using the GDGT-based proxies TEX_{86} (Equations 1.8, 1.9; Schouten *et al.*, 2002) and, where the crenarchaeol stereoisomer was absent, $\text{TEX}_{86}^{\text{L}}$ was used (Equation 1.10; Kim *et al.*, 2010). In the marine sediments at Horse Fen and Railway Cottage where long chain alkenones were identified (Figures 4.16, 4.21), the SST was calculated using the U^{K}_{37} proxy (Equation 1.20; Prahl and Wakeham, 1987; Müller *et al.*, 1998; Conte *et al.*, 2006). The alkenone $\text{C}_{37:4}$ was below the detection limit therefore confirming that the environment had marine influence (Bendle *et al.*, 2009). The mean annual air temperature of the peat samples at Tottenhill Quarry and Horse Fen (types A and B) could not be calculated using the MBT_{peat} index (Equations 1.17, 1.18; Naafs *et al.*, 2017) due to the lack of key brGDGT structures.

During the transgression at Horse Fen (-2.33 m OD) the SST value calculated with $\text{TEX}_{86}^{\text{L}}$ is 21.9 °C (Table 4.10). In type D the reconstructed temperature in Tottenhill Quarry was 30.3°C: such a high temperature is not likely to be realistic. Although marine markers (long chain alkenones) were detected in trace amounts (types C-D), biases from contributions of isoprenoid GDGTs from soil cannot be excluded due to the high BIT (>0.8; Powers *et al.*, 2010). Thus, care should be taken when considering the credibility of the magnitude of these temperate-warm values especially when possible production of iGDGTs in soil can result in overestimated temperature values. After the transgression (types E-F) at Blackborough Quarry and Horse Fen the temperatures from the GDGT-based proxies TEX_{86} and $\text{TEX}_{86}^{\text{L}}$ are temperate-warm, ranging from 13.6 to 19.0 °C, and those from the U^{K}_{37} proxy are much lower (8.4-13.4 °C; Table 4.10). This discrepancy between the two SST proxies has been observed previously and attributed to subsurface production of GDGTs and the differences in the growth seasons of Crenarchaeota and haptophytes (Huguet *et al.*, 2006; Castañeda *et al.*, 2010; Richey and Tierney, 2016).

Abnormally low SST estimates were obtained at 8.74 m OD in the marine horizon of the Railway Cottage core: -2.76 °C from $\text{TEX}_{86}^{\text{L}}$ and -0.47 °C from TEX_{86} . The low values may reflect an early period of coolness, for example the end of the glacial, but microfossil evidence suggests a

temperate woodland environment. While the proxies represent sea-surface temperature, the pollen reflects the air temperature range that a species can tolerate, resulting in a different response and resolution of the two markers. Nevertheless, the very low sea-surface temperatures would reflect a polar or tundra environment, similar to current conditions in Greenland in winter (Sea temperature_Nuuk), that is not reflected in the pollen assemblage of the relevant horizons. Environmental cooling was evident from the pollen assemblage from 9.02 m OD, but the specimens present do not match sub-polar temperature conditions. The very low reconstructed SST values are not biased by low signal from GDGTs, which lies well above the limit of detection. Factors either related to low production, or different sources of GDGTs, may explain the sub-zero SST values. Due to the lack of comparative evidence from the microfossils, it is concluded that the TEX_{86} and $\text{TEX}_{86}^{\text{L}}$ values from Railway Cottage at 8.74 m OD are not likely to be realistic. This study therefore shows that in similar sediment types, these calculated values should not be used indiscriminately.

Literature studies suggest that air temperature in south east England during MIS 11-9 was warmer than present, reaching 15-19°C in summer (Ashton *et al.*, 2008; Candy *et al.*, 2010). Warm conditions were also evident from summer sea-surface temperatures reconstructed from $\delta^{18}\text{O}$ of foraminifera from the north eastern Atlantic Ocean with SST reaching 13-16°C between MIS 11 and 5e (McManus *et al.*, 1999; Kandiano and Bauch, 2003). Thus, the TEX_{86} and $\text{TEX}_{86}^{\text{L}}$ -reconstructed SST in the Nar Valley, except at Railway Cottage, match literature values, especially when BIT values are <0.5. The abnormally low and high TEX_{86} and $\text{TEX}_{86}^{\text{L}}$ SST from Railway Cottage may arise from production of iGDGTs in soil (BIT >0.5) and / or possible shifts in archaeal populations. The agreement between reconstructed temperatures and summer SST from literature may confirm that Crenarchaeotal blooms occur in summer (Castañeda *et al.*, 2010; Richey and Tierney, 2016). U^{K}_{37} temperatures were lower than TEX_{86} and $\text{TEX}_{86}^{\text{L}}$ temperatures in the Nar Valley cores; this could be explained by the peak of the haptophyte bloom occurring in winter / early spring, thus at lower temperatures (Castañeda *et al.*, 2010; Richey and Tierney, 2016).

Table 4.10. Reconstructed sea-surface temperatures from TEX_{86} , TEX_{86}^L and $U^{K'}_{37}$ (calibration from Prah and Wakeham, 1987) proxies and BIT values in the Nar Valley cores. BQ = Blackborough Quarry, TQ = Tottenhill Quarry, HF = Horse Fen, RC = Railway Cottage. Blank spaces indicate that key components were absent or were below the LOQ >10. Colours indicate: transgression, marine environment.

Type	Site	Elevation / m OD	BIT	SST from TEX_{86} / °C ± 2.0 °C	SST from TEX_{86}^L / °C ± 4.0 °C	SST from $U^{K'}_{37}$ / °C ± 1.5 °C
C	HF	-2.330	0.98		21.9	
D	TQ	2.630	0.81		30.3	
E	BQ	1.860	0.49			
		1.660	0.63			
		0.660	0.49	16.0	13.6	
		0.070	0.46		17.9	
		-0.140	0.38	18.3	15.9	
		-0.540	0.43	15.8	17.8	
	HF	-0.570	0.40	15.5	16.7	10.4
		-0.670	0.66	17.2	18.4	13.4
		-2.200	0.62		19.0	8.4
		-2.260	0.67			11.4
	RC	10.07	0.80		26.8	17.7
		9.930	0.75		25.3	14.6
		9.460	0.66		21.6	13.0
		8.740	0.54	-0.49	-2.76	
F	HF	1.950	0.55		29.7	

4.4.9. Summary of the Nar Valley palaeoenvironment

The molecular fossil analysis of the samples from the peat and clay horizons in the Tottenhill Quarry (Figure 4.24), Blackborough Quarry (Figure 4.25) and Horse Fen (Figure 4.26) cores indicate a terrestrial environment with higher plants including conifers. The freshwater conditions of the basin allowed oxygenic and anoxygenic photoautotrophs to become established. At Tottenhill Quarry, the disappearance of the marine marker crenarchaeol in the bottom of the core may represent a regression; the top sample in the core exhibited a return of marine crenarchaeol that may infer the beginning of a transgression. This represents the first account of sea-level changes from this core: such fluctuations were not recognisable through microfossil analysis (Figure 4.24).

In the Horse Fen and Blackborough Quarry cores marine inundation was identified by detection of marine crenarchaeol and marine alkenone haptophyte algal markers. Similar marine influence was evident from the Railway Cottage core (Figure 4.27). The type E horizons from Blackborough Quarry represent marine conditions, where sporadic occurrence of peat markers at certain depths is suggested to represent erosion of the peat during storm events. In the Blackborough Quarry, Railway Cottage and Horse Fen cores, the SST reconstructed from TEX_{86} , $\text{TEX}_{86}^{\text{L}}$ and U_{37}^{K} were temperate-warm after the transgression, while soil pH from CBT was mildly alkaline throughout.

Assessing the timing and duration of the transgression can be problematic due to the high compression of the peat and the limited sampling resolution. However, the biomarkers can hint at initial changes in the environmental conditions and the cessation of the transgression. At Blackborough Quarry changes in BIT suggested the start of the transgression at -1.050 m OD, whereas a declining CPI with an increasing input of algal material, that could indicate a change in the influx of water, was evident from -1.080 m OD (Figure 4.25). Marine conditions with BIT values 0.4-0.6 and long chain alkenones were established from -0.54 m OD. At Horse Fen the increase in eutrophication evident from high concentrations of bacteriochlorophyll pigments at -2.40 m OD can be related to the initial onset of marine water, confirmed by the presence of long chain alkenones. The environment was marine by -2.26 m OD as confirmed by alkenones and BIT values (Figure 4.26). Due to the compression of the peat, a few centimetres can cover a longer time period, thus the 0.51 m and 0.14 m that separates the beginning to the end of the transgression in the Blackborough Quarry and Horse Fen cores, respectively, may indicate a slow inundation (a few hundreds to a thousand years). A higher resolution sampling (to millimetre scale) combined with high-resolution dating could aid our understanding of the timescale of the transgression.

The four cores show similar distributions of molecular fossils throughout the 6 defined types: although small differences are present, the fingerprint of the three peats (Tottenhill Quarry, Horse Fen, and Blackborough Quarry) is comparable (Figure 4.28). Although the transgression at Blackborough Quarry and Horse Fen shows differences in the photosynthetic populations, the marine clays of the cores, including Railway Cottage, present similar lipid distributions. Therefore, the similarities in the molecular fossil distributions and concentrations among the four cores for each type horizons (Figure 4.28), may indicate that the Nar Valley cores were deposited under similar environmental conditions. Pollen evidence from Tottenhill Quarry and Horse Fen suggested a correlation with the “Hoxnian” type pollen (Ho II-III), but, as discussed, assignment of such distribution to MIS 11 and / or MIS 9 is challenging. AAR dating from Horse Fen pointed towards a MIS 11 age, but age resolution was low as the results were based on only one specimen. Opercula

from Tottenhill may date to late MIS 11 or early MIS 9, but conclusive evidence cannot be established, thus two separate MIS could be represented in the Nar Valley Clay (Barlow *et al.*, 2017). More refined dating and a better understanding of the geology of the Nar Valley may solve the challenging assignment of the Nar Valley Clay to MIS 11, MIS 9 or both stages.

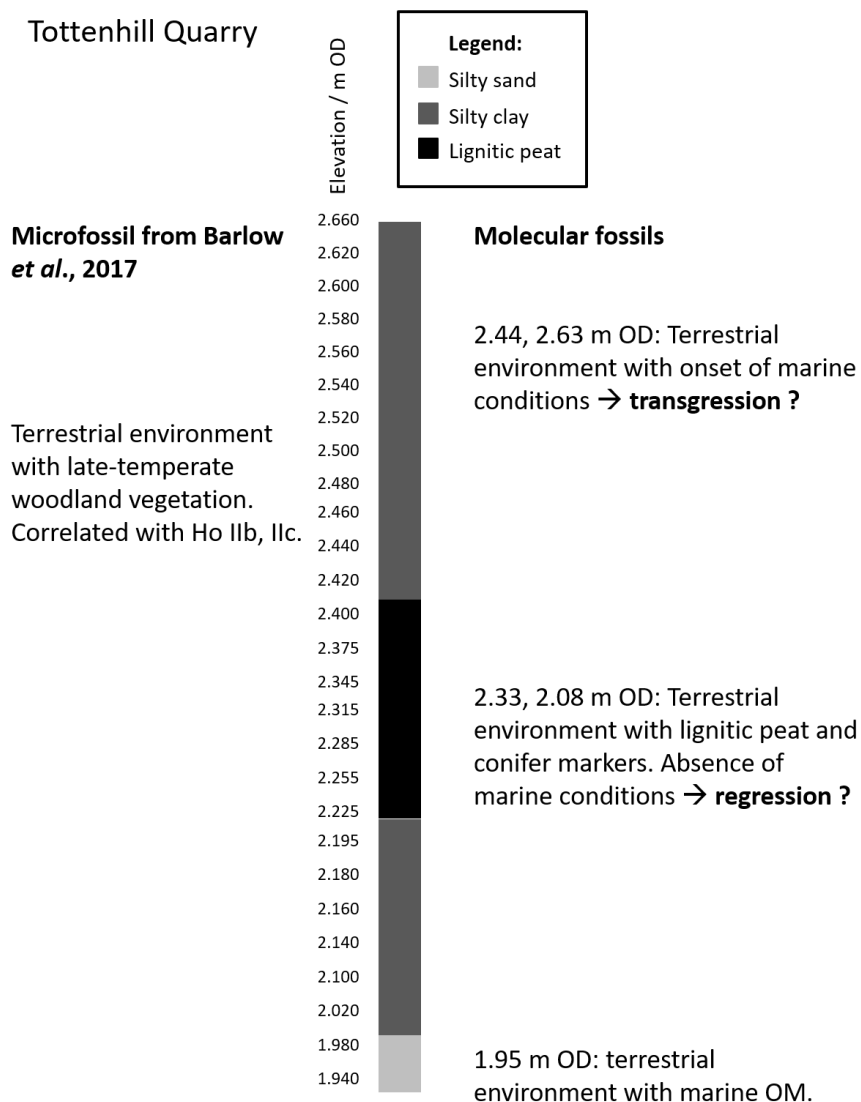


Figure 4.24. Summary of the key environmental conditions in the Tottenhill Quarry core; on the left of each core is the evidence from the lithology & microfossils (Barlow *et al.*, 2017); on the right is the evidence from the molecular fossils from this study.

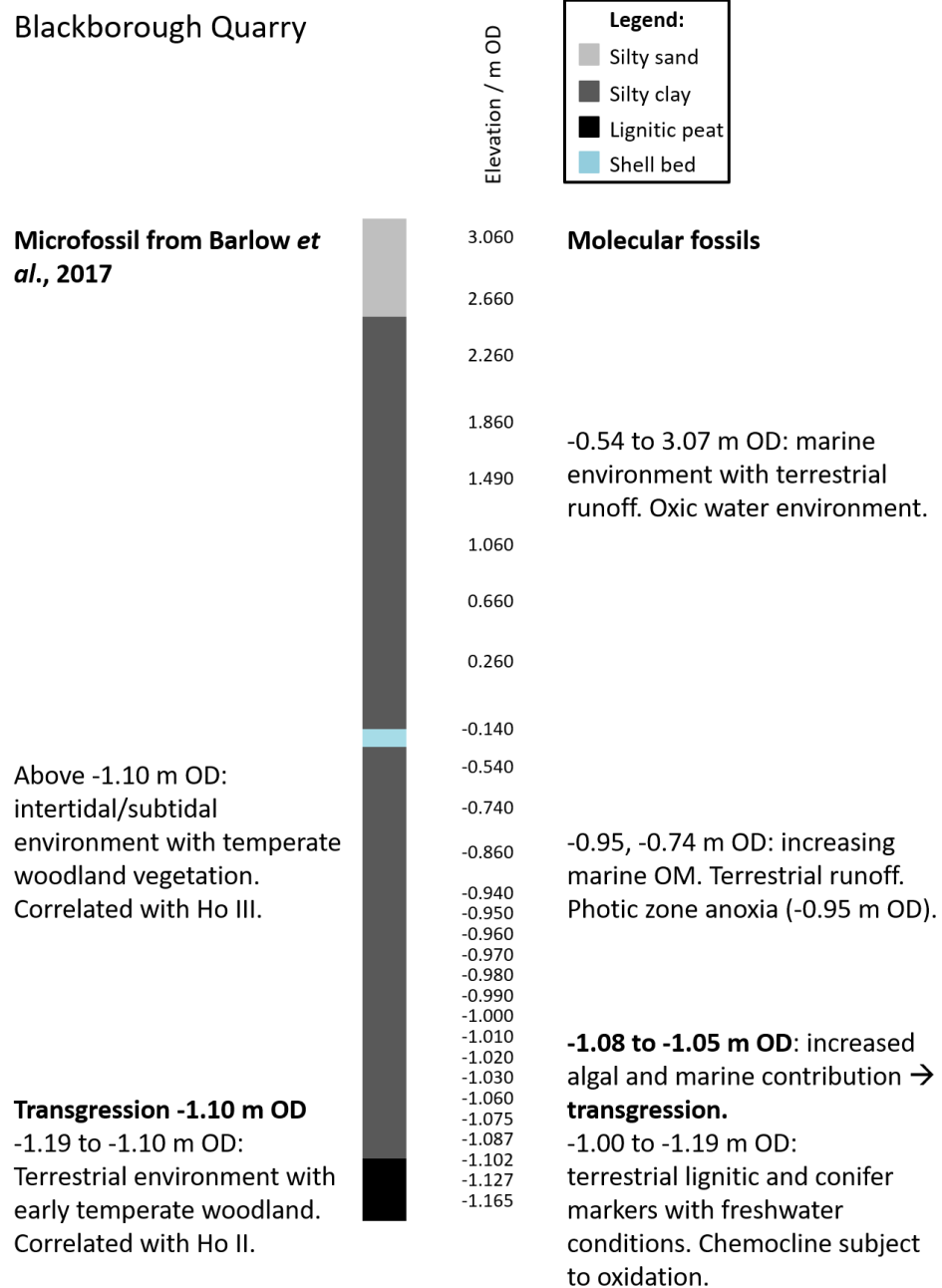


Figure 4.25. Summary of the key environmental conditions in the Blackborough Quarry core; on the left of each core is the evidence from the lithology & microfossils (Barlow *et al.*, 2017); on the right is the evidence from the molecular fossils from this study.

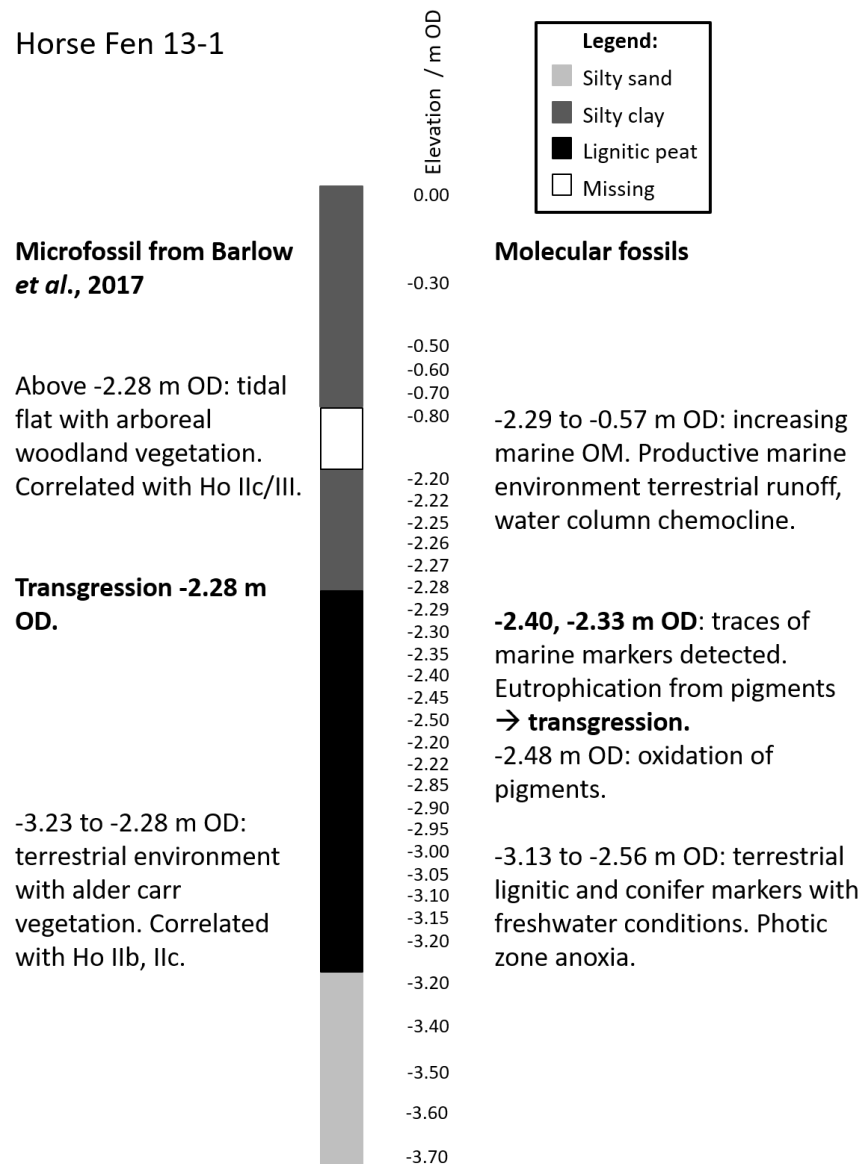


Figure 4.26. Summary of the key environmental conditions in the Horse Fen core; on the left of each core is the evidence from the lithology & microfossils (Barlow et al., 2017); on the right is the evidence from the molecular fossils from this study.

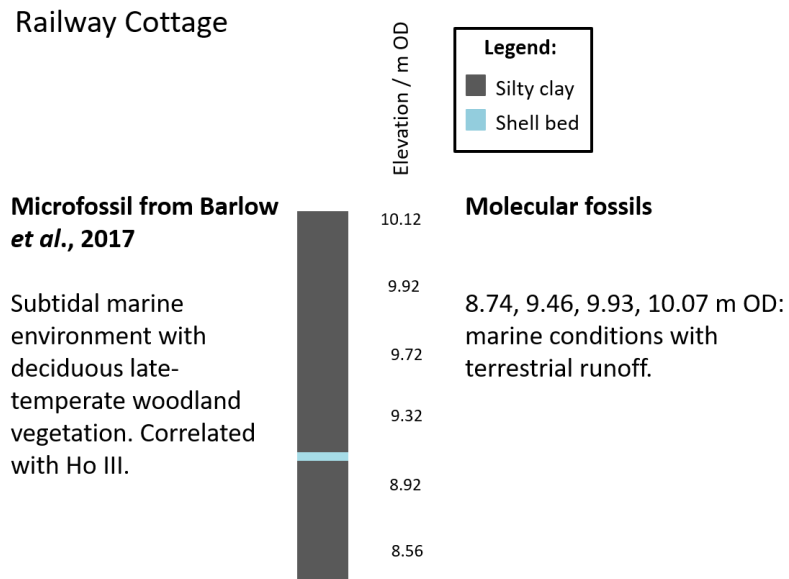


Figure 4.27. Summary of the key environmental conditions in the Railway Cottage core; on the left of each core is the evidence from the lithology & microfossils (Barlow *et al.*, 2017); on the right is the evidence from the molecular fossils from this study.

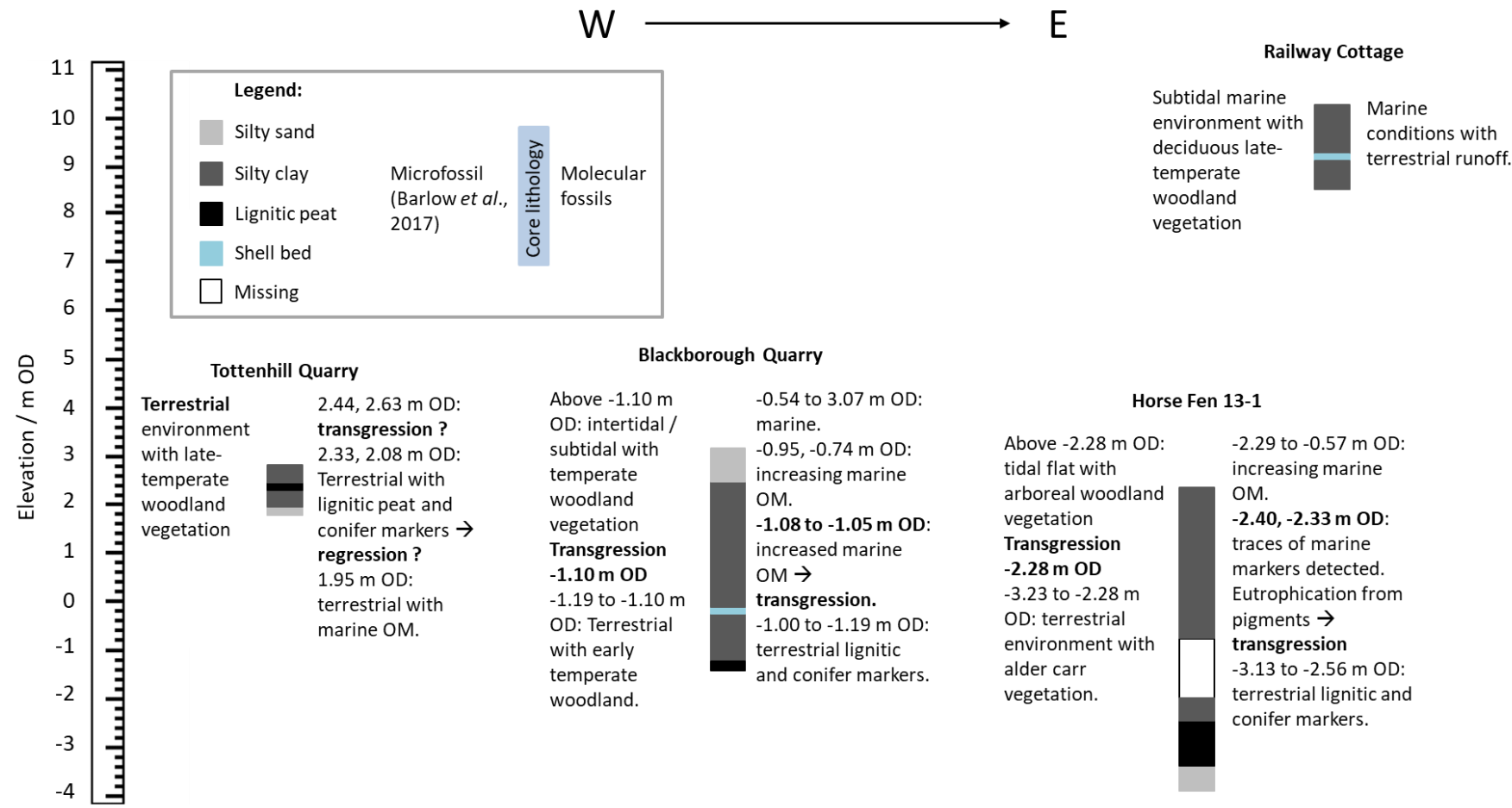


Figure 4.28. Summary of the key environmental conditions in the Nar Valley cores; on the left of each core is the evidence from the lithology & microfossils (Barlow *et al.*, 2017); on the right is the evidence from the molecular fossils from this study.

4.4.10. Transgression at Woodston

The core from Woodston (called HiB 12-6 from near Peterborough; Figure 4.1c), retrieved by Dr. N. Barlow in 2015, was collected to match the sequence covered by a set of cores collected by Horton *et al.* (1992). In the original study Horton *et al.* (1992) identified a transgression occurring during the Hoxnian interglacial based on pollen data (Table 4.1). AAR dating of molluscs correlated with MIS 11 (Horton *et al.*, 1992; Ashton *et al.*, 2005; Penkman *et al.*, 2011; 2013), supporting the evidence from mammalian fauna associated with MIS 11 (Schreve, 2001). As a more securely dated site and correlated through other evidence with the Nar Valley Clays (Gibbard *et al.*, 2018), the molecular fossil distribution of the Woodston core provides an opportunity for comparison with the Nar Valley cores, and to help establish whether the two regions represent the same transgression.

4.4.10.1. Previous work on Woodston core HiB 12-6

The lithology of the core comprised a grey-brown sandy clay between -18.42 and -18.10 m OD succeeded by a yellow-grey sandy clay with small shell fragments up to -17.48 m OD (Figure 4.29). Foraminifera, *Elphidium* spp., were recognised throughout the core at: -18.28, -18.18, -18.08, -17.98, -17.88, -17.68, -17.48 m OD. The poor preservation and low numbers of microfossils precluded reliable identification of the transgression, if present, or a change in the palaeoenvironment. Magnetic susceptibility, performed by Barlow (pers. comm.), indicates very low values from -18.48 to -18.38 m OD due to the damaged core upon collection. High magnetic susceptibility from -18.38 m OD is followed by decreasing values and a marked decrease from -18.03 m OD, that can be interpreted as increasing grain size of the sediments and decreasing OM content, among other factors (Figure 4.29; Singer and Fine, 1989; Sun and Liu, 2000).

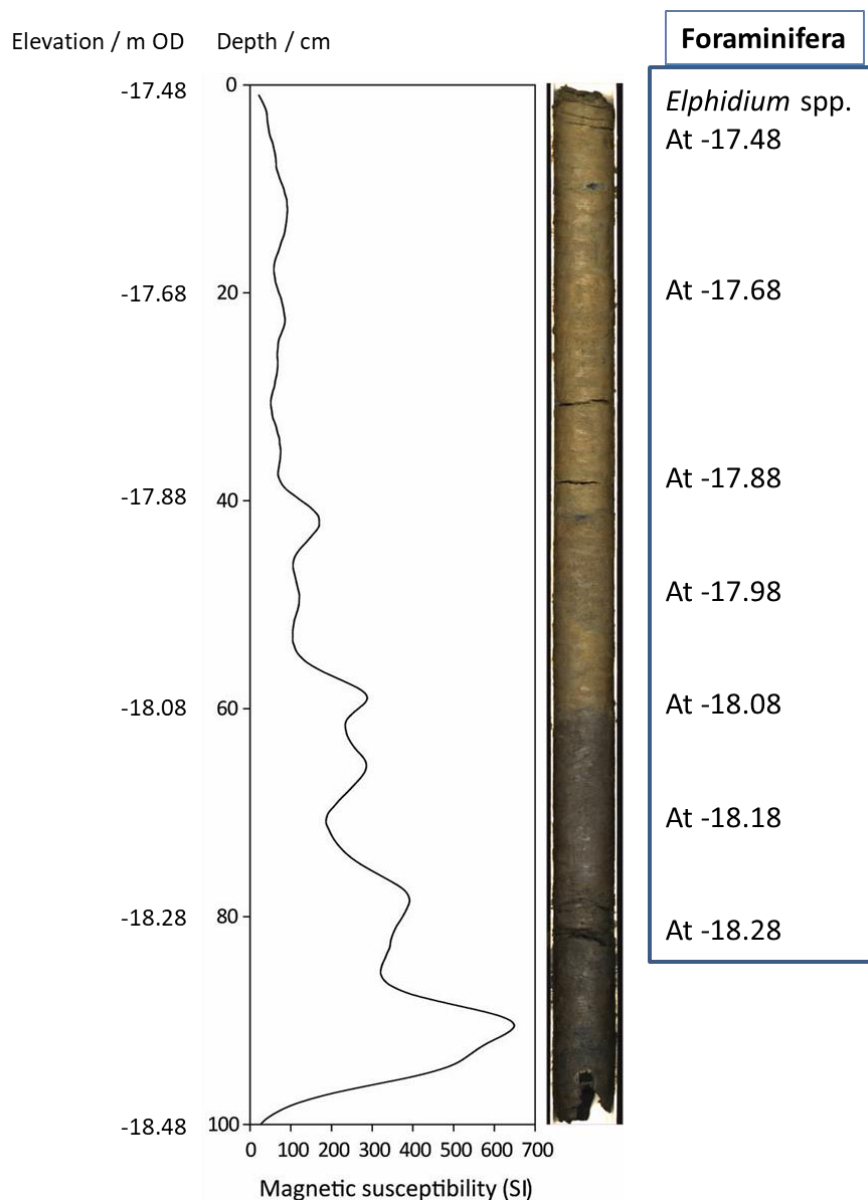


Figure 4.29. Lithology and magnetic susceptibility data from the core at Woodston (redrawn from Barlow, pers. comm.).

4.4.10.2. Molecular fossils at Woodston

Samples for molecular fossil analysis were collected every 10 cm to match the depths where the foraminifera were previously collected. The lipid concentrations were high from -18.42 to -18.12 m OD after which they gradually decreased (Figures 4.30, 4.31). Terrestrial OM was predominant throughout the core (Cranwell, 1982; De Deckker *et al.*, 2014), also confirmed by P_{aq} values of approx. 0.1 (Ficken *et al.*, 2000). Des-A-lupane (**T16**) and taraxerone (**T17**), markers of terrestrial plants (Trendel *et al.*, 1989; Volkman *et al.*, 2000), were detected from -18.42 to -18.02 m OD and from -18.32 to -17.92 m OD, respectively. The vegetation surrounding the basin comprised conifer

and fen vegetation, from the presence of friedelan-3-one (**T4**), β -sitosterol (**T11**) and glutinol (**T8**; Volkman 1986; Otto *et al.*, 2005; Zocatelli *et al.*, 2014).

Short chain *n*-alkanoic acids (**A4**) may indicate an aquatic and / or terrestrial OM contribution (Cranwell, 1982; Chikaraishi *et al.*, 2004; Wang and Liu, 2012; Fang *et al.*, 2014; Wang *et al.*, 2019). Hopanoid diploptene (**T18**), present throughout the core, has been detected in bacteria, cyanobacteria and ferns but also vascular plants suggesting terrestrial and / or aquatic OM (Figure 4.30, 4.31; Ishiwatari *et al.*, 1994). Marine OM input is indicated from BIT values between 0.81 and 0.92, with a slight decrease in BIT values above -17.92 m OD (Table 4.11). Therefore, the environment was marine throughout the core, although conclusive evidence of a transgression is lacking. The Woodston palaeoenvironment is similar to type D from the Nar Valley (Table 4.7), with high contribution of terrestrial OM and low concentrations of aquatic and marine markers.

The pigment profile (Figure 4.32) shows a productive environment with predominance of chl *a* and *b* pigments and occasional anoxia, represented by bpphe *a* (**B3**; Pfennig, 1977) at -18.32 and -18.12 m OD. Between -18.42 and -18.12 m OD low concentrations of pphorb *a* SCEs were detected, indicating herbivore grazing (Appendix 4.5); unfortunately due to the low abundance, identification of the sterol moieties was not possible. At -18.02 m OD, photosynthetic pigments exhibited a drastic drop in concentrations, indicating a change in environmental conditions. From -17.92 m OD chlorophyll pigments were not detected but carotenoids including P7 (Figure 4.9) were dominant, suggesting a change in the physicochemical properties of the water column affecting the primary producers (Figure 4.32; Hendry *et al.*, 1987).

The soil pH reconstructed from the CBT (Equation 1.11; Weijers *et al.*, 2007) identified slightly alkaline soils (Table 4.11), similar to the pH determined from the Nar Valley cores (Table 4.10). The sea-surface temperature was calculated with TEX_{86} (Equations 1.7, 1.8) and $\text{TEX}_{86}^{\text{L}}$ (Equation 1.9; Schouten *et al.*, 2002; Kim *et al.*, 2010) and shows generally temperate-warm values (Table 4.11). The high BIT values >0.5 may suggest partial production of iGDGT from soil, contributing to a high reconstructed SST. While TEX_{86} -reconstructed SSTs show a slight warming from 18.00 m OD, the $\text{TEX}_{86}^{\text{L}}$ temperatures indicate a slight cooling. Although the trend is discordant, the data suggests that palaeoenvironmental changes or a change in the archaeal population are recorded between 18.20 and 18.00 m OD, as previously identified in the lipid and pigment profiles.

The palaeoenvironment at Woodston is interpreted to represent an aquatic marine basin with adjacent terrestrial vegetation comprising conifers and fen plants. An increase in marine OM input is suggested from -17.92 m OD from the slight decrease in BIT values. These features coincide with

a decrease in the concentrations of chlorophyll pigments at -18.02 m OD followed by disappearance of chlorophylls and presence of only carotenoids from -17.92 m OD. A similar trend in the chlorophyll pigments was evident in the Loch of Stenness where, following transgression, the brackish sediments were devoid of pigments (Section 3.3.3). Although a transgression is not identified in this Woodston core, contrary to the cores examined by Horton *et al.* (1992), the environment is indicated to have been coastal / estuarine from the high terrestrial OM input and presence of marine OM (Wu *et al.*, 2014; De Jonge *et al.*, 2015). A change in the water chemistry caused unfavourable conditions for photoautotrophic production, explaining the lack of pigments above -17.92 m OD (Figure 4.32). By contrast, this event caused a gradual decrease in lipid concentrations (Figures 4.30, 4.31), suggesting that the environmental change that affected the water chemistry, evident from -18.02 m OD, did not affect the hinterland dramatically. Therefore, the absence of pigments (similar to the profile observed in the brackish sediments in the Loch of Stenness), the slight decrease in BIT values and the largely unaffected lipid distribution may suggest that an increase in salinity occurred at Woodston above -18.02 m OD, although conclusive evidence of a transgression is not evident. The similarities in the molecular fossil distribution between the Woodston core and the Nar Valley type D suggest that the sediments are likely to have been deposited under similar conditions, but association with the same MIS and interglacial cannot be established.

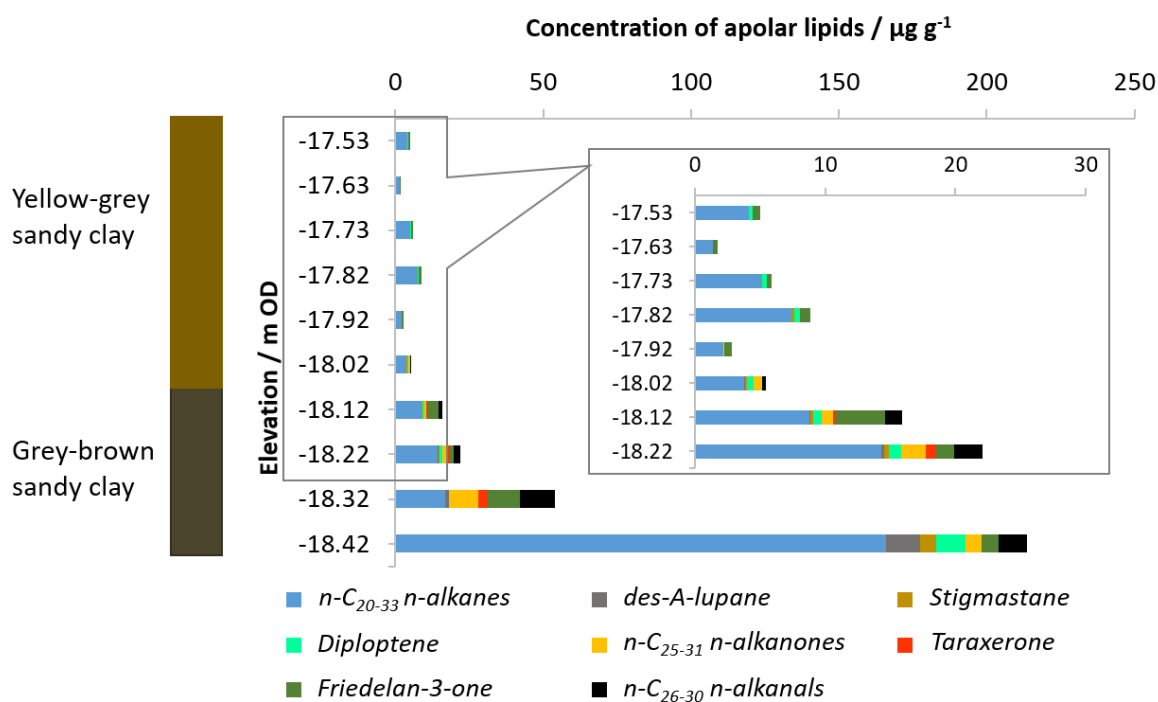


Figure 4.30. Concentrations of *n*-alkanes, *n*-alkanones, *n*-alkanals and terpenoids in the Woodston samples with inset from -18.22 to -17.53 m OD.

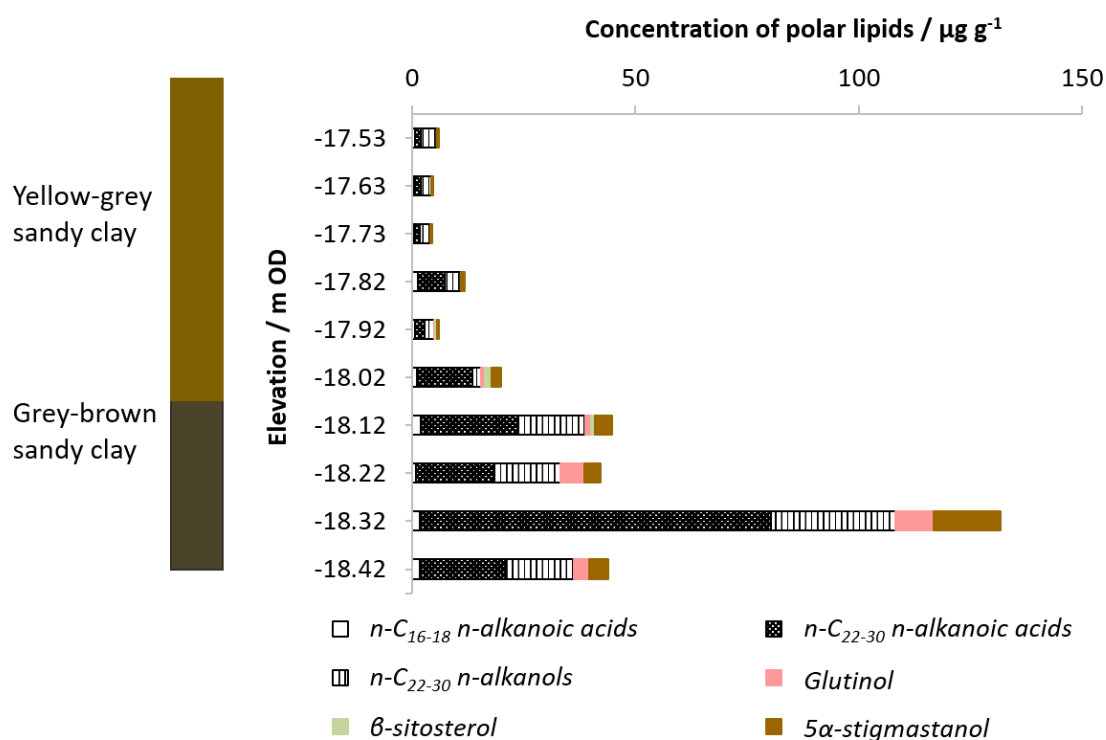


Figure 4.31. Concentrations of *n*-alkanoic acids, *n*-alkanols and terpenoids in the Woodston samples.

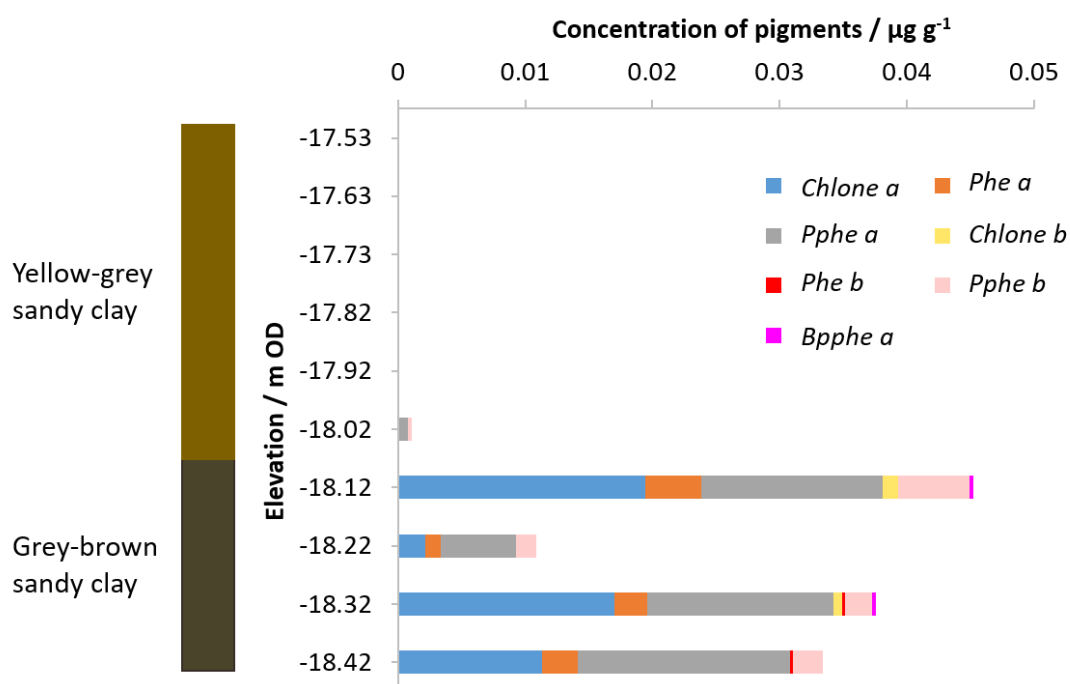


Figure 4.32. Concentrations of chlorophyll and bacteriochlorophyll pigments in the Woodston core.

Table 4.11. Elevation, CPI, P_{aq} , BIT, ratio of chlorophylls and carotenoids, soil pH from CBT and SST from TEX_{86} and TEX_{86}^L for the Woodston core.

Elevation / m OD	CPI	P_{aq}	BIT	Ratio chls/cars	SST from TEX_{86} / °C ± 2.0 °C	SST from TEX_{86}^L / °C±4.0	Soil pH from CBT / ± 0.7
-17.53	4.74	0.13	0.86	0	n.a. ^a	n.a. ^a	8.5
-17.63	n.a. ^b	0.10	0.85	0	22.8	20.3	8.4
-17.73	4.71	0.14	0.81	0	23.4	19.9	8.5
-17.82	5.63	0.10	0.83	0	24.0	20.1	8.5
-17.92	n.a. ^b	0.15	0.83	0	n.a. ^a	n.a. ^a	8.6
-18.02	n.a. ^b	0.10	0.88	0.26	20.5	24.1	8.4
-18.12	7.18	0.10	0.87	2.24	14.0	18.4	8.0
-18.22	8.63	0.10	0.84	0.29	18.0	22.3	8.2
-18.32	n.a. ^b	n.a. ^b	0.92	0.42	n.a. ^a	22.8	7.6
-18.42	7.75	0.07	0.90	0.46	16.7	19.9	7.9

^a Some GDGTs below LOQ <10

^b Missing *n*-alkanes

4.5. Conclusions

The microfossil and pollen data from the Nar Valley enabled the identification of a transgression at Blackborough Quarry and Horse Fen, while Railway Cottage was interpreted as an intertidal environment and Tottenhill Quarry as a terrestrial environment (Barlow *et al.*, 2017). The molecular fossils from these cores allowed the novel recognition of six types of distribution among the four cores. While types A and B are dominated by terrestrial OM, types C and D represent the beginning of the transgression at Horse Fen and at Blackborough Quarry, followed by types E and F where aquatic and marine OM increases, indicating marine conditions after transgression (Table 4.3). Within type F, five samples at Blackborough Quarry exhibit markers from type B, possibly indicating reworking or erosion from storm events. Reconstructed sea-surface temperatures (SST) with TEX_{86} , $\text{TEX}_{86}^{\text{L}}$ and U^{K}_{37} show a temperate-warm environment after the transgression, with values close to literature values of SST during MIS 11-9, although changes in archaeal and haptophyte populations or production of iGDGTs in soil (where BIT >0.5) cannot be excluded. The disparity in SST values between TEX_{86} , $\text{TEX}_{86}^{\text{L}}$ and U^{K}_{37} may be due to seasonal shifts in archaeal and haptophyte populations (Table 4.10). The classification of sediment horizons into types based on molecular fossil evidence complements the microfossil and pollen analyses of Barlow *et al.* (2017) and highlights palaeoenvironmental features that were not previously evident (Figure 4.28). The results demonstrate the value of molecular fossils in the study of sea-level and palaeoenvironmental change.

The core at Woodston showed a contribution of terrestrial and aquatic OM, with marine inputs throughout the core. The lipid profiles in the core are uniform, with a decrease in the total concentration above -18.02 and -17.92 m OD, denoting a changing environment. The pigments show the most marked change: the water column was productive and occasionally stratified between -18.42 and -18.12 m OD, followed by very low production at -18.02 m OD and disappearance of pigments above -17.92 m OD (Figure 4.32). Foraminifera were observed throughout the core, indicating marine conditions; BIT values slightly decreased from -17.92 m OD suggesting an increase in marine OM, although a transgressive event is not observed (Table 4.11). The high degree of similarity between the four Nar Valley cores type D and the Woodston core could indicate that the sequences relate to similar palaeoenvironmental conditions, though without conclusive dating across the five cores, correlation of the East Anglian cores to the same MIS remains uncertain.

5. Unknown glycerolipid structures found in sediments

5.1. Introduction

Glycerol dialkyl glycerol tetraether (GDGT) lipids form the membrane lipids of Archaea and some bacteria (Schouten *et al.*, 2013). The main distinction between archaeal and bacterial lipids lies in the nature of the dialkyl chain: isoprenoidal chains for Archaea and methyl branched chains in bacteria (**G1**, **G6**; Sturt *et al.*, 2004). Alongside GDGTs, several other glycerolipid structures with differences in dialkyl chains have been found both in archaeal cultures and in sediments. The simplest ether lipid cores are glycerol dialkyl diethers (GDD), such as archaeol (Figure 5.1a), containing two phytanyl chains bound to a glycerol moiety (Koga *et al.*, 1993). Archaeol has been detected in methanogenic bacteria (Koga *et al.*, 1993) and was proposed as a marker of methanogenic biomass (Lim *et al.*, 2012). The high abundance of archaeol compared to crenarchaeol (**G5**) in hypersaline environments has the potential to distinguish between different levels of salinity in palaeoenvironments (Turich and Freeman, 2011). Glycerol monoalkyl glycerol tetraether (GMGT) lipids have a covalent bond connecting the two biphytanyl alkyl chains giving rise to an “H-shaped” alkyl chain (Figure 5.1b; Morii *et al.*, 1998). Glycerol trialkyl glycerol tetraether (GTGT) lipids consists of one biphytane chain attached to two ether groups and two phytane chains attached to the other two ether groups (Figure 5.1c). Whereas both GMGTs and GTGTs have been isolated from hyperthermophilic Archaea and sediments (Morii *et al.*, 1998; Schouten *et al.*, 2008), GTGTs have been detected also in mesophilic archaeal cultures, indicating a more widespread occurrence including non-hydrothermal environments (Schouten *et al.*, 2008; Knappy *et al.*, 2014; Bauersachs *et al.*, 2015b). OH-GDGTs are GDGT structures with up to 2 extra hydroxyl groups on the biphytanyl chains and with 0-2 cyclopentane rings (Figure 5.1d). These compounds have been found in marine sediments and in cultures of Crenarchaeota and Euryarchaeota (Liu *et al.*, 2012a; 2012b). Monoglycerol structures equivalent to GMGTs, GMDs (glycerol monoalkanediol diethers; Figure 5.1e), have been detected in small amounts in hyperthermophilic Archaea (Knappy *et al.*, 2011; Bauersachs and Schwark, 2016). It is also possible that the monoglycerol lipids are diagenetic products of lipids with two glycerol groups (Knappy, 2010; Bauersachs and Schwark, 2016). Isoprenoidal-, branched- and OH-GDDs have been detected in marine sediments with similar methylation and cyclisation patterns to their GDGT counterparts, thus suggesting that the producers of GDGTs and GDDs are related (Liu *et al.*, 2012a).

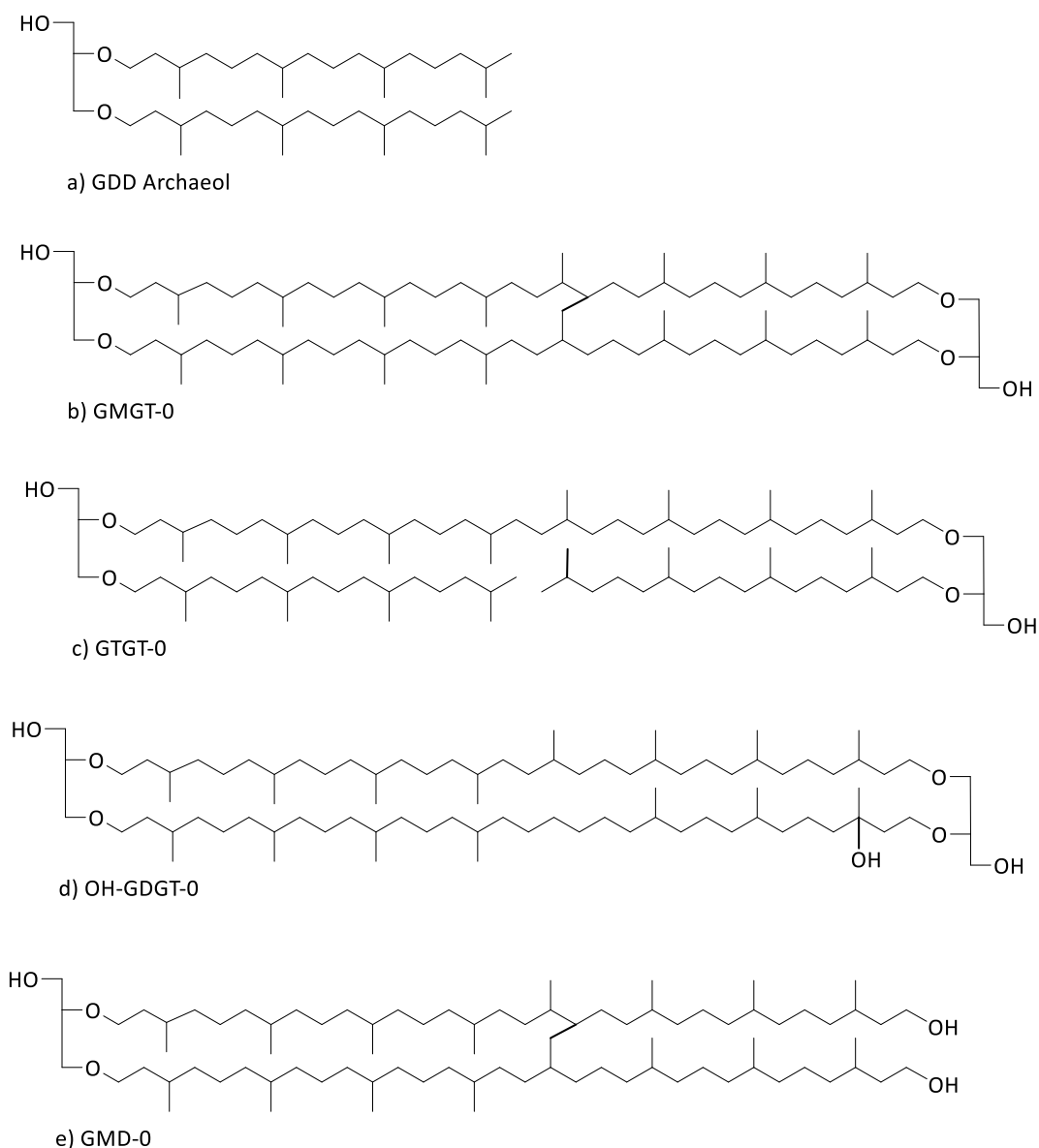


Figure 5.1. Structures of a) GDD archaeol, b) GMGD-0, c) GTGT-0, d) OH-GDGT-0 and e) GMD-0 (note that the position of the covalent bond between the isoprenoid chains is tentative and based on the position in GMGT-0).

5.1.1. Aims

The wide variety of glycerolipid structures found in cell culture and in sediments suggests multiple sources and as yet unknown transformation mechanisms. Culture studies have focused mainly on hyperthermophilic Archaea, hence the lipid profiles of the majority of Archaea have not been established. The structural diversity described above may also be applicable to branched GDGTs, though fewer studies have examined in detail the sources of such lipids (Knappy, 2010). The aim of this study was to elucidate the structures of unknown glycerolipids observed in the samples

reported in Chapters 3 and 4, to consider possible origins for these structures and their potential as novel biomarkers.

5.2. Materials and methods

Lipids were extracted from sediments by ASE from the Loch of Stenness, the Nar Valley and the Woodston cores (Section 7.2.1). The total lipid extract was separated by flash column chromatography into lipids of different polarity (Section 7.2.3). The polar fractions (Section 7.2.3), containing alcohols and acids, also included glycerolipids and were analysed by normal phase HPLC-MS/MS to separate them (Sections 7.4.3, 7.4.11, 7.4.12).

5.3. Results and discussion

5.3.1. Elucidation of structures by HPLC-MS and HPLC-MS/MS

The HPLC-MS chromatogram of the GDGT fraction of most of the sediments discussed in Chapters 3 and 4 exhibited peaks eluting approx. 20 minutes after the brGDGTs. These components were not previously recognised in sediments. The late elution time in normal phase HPLC suggests the components to have greater polarity than iGDGTs and brGDGTs. The three peaks had prominent ions at m/z 1048.3, 1034.3 and 1020.3, likely to represent protonated molecules (Figure 5.2). The difference of 14 m/z units between the three glycerolipids most likely suggests differing numbers of methyl branches. The position and exact number of the methyl branches is unknown, therefore, in this chapter the glycerolipid m/z 1020.3 presents no methyl branches, m/z 1034.3 has one methyl branch at carbon position 5 of the dialkyl chain and m/z 1048.3 shows two methyl branches, matching the position of the methyl branches in brGDGTs.

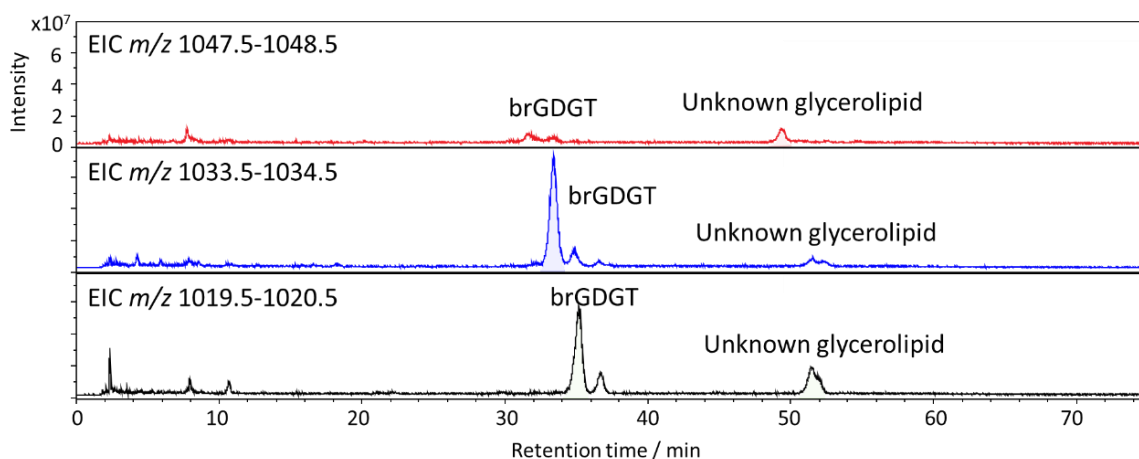


Figure 5.2. (+)APCI-MS extracted ion chromatograms (EIC) m/z 1047.5-1048.5, 1033.5-1034.5 and 1019.5-1020.5 of the polar fraction from sediments showing the brGDGTs and the peaks for the unknown glycerolipids. Note that the intensity scale is the same for the three EICs.

The MS² spectra (Section 7.4.12) of all three glycerolipids show losses of 18, 36 and 54 Da, suggesting three successive losses of water (Figures 5.3-5.5). Additional product ions showed the loss of CH₂+H₂O (-32 Da), C₃H₄O+H₂O (-74 Da), and glycerol (C₃H₄O+2H₂O; -92 Da; Figures 5.3-5.5). Other fragments included the losses of three molecules of water and C₃H₄O (-110 Da) and loss of the glycerol and two molecules of water (-128 Da). The lack of product ions in the m/z region 200-800 suggests that the two alkyl chains are bound together (“H-shaped”) to form a monoalkyl chain (Figures 5.3-5.5; Knappy, 2010).

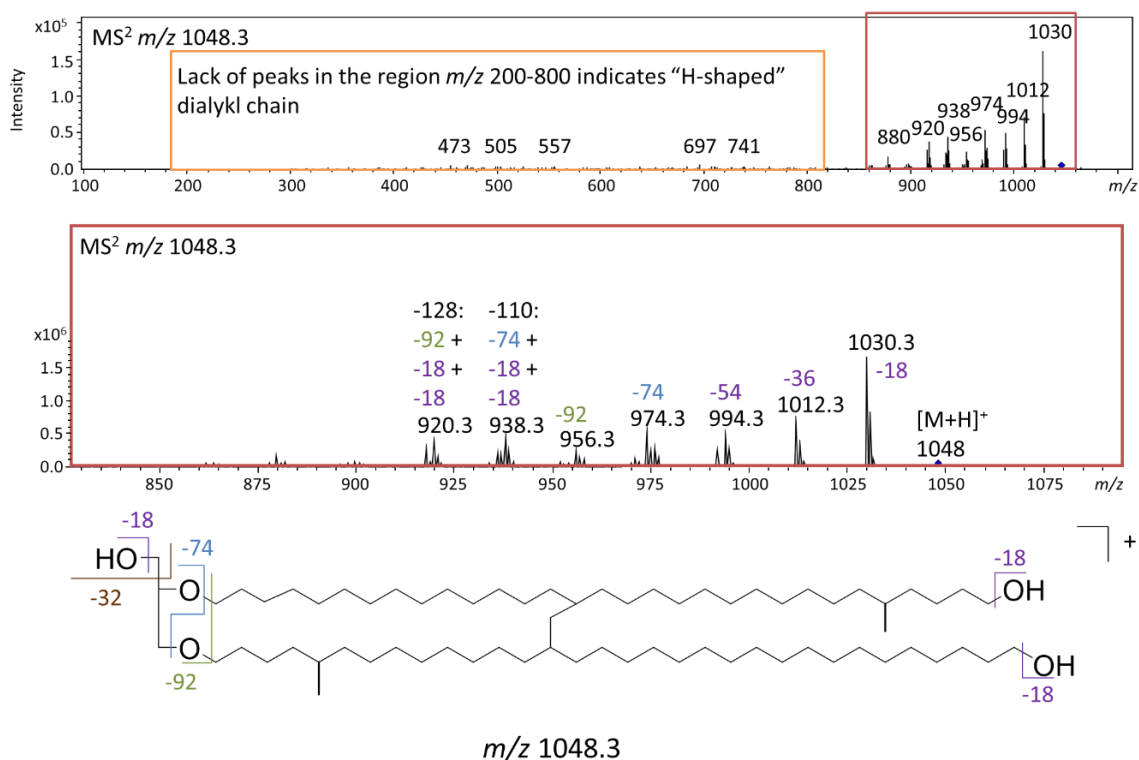


Figure 5.3. (Top) (+)APCI-MS² spectrum of glycerolipid m/z 1048.3, (middle) inset of the MS² m/z range 825-1100 and (bottom) suggested structure of glycerolipid m/z 1048.3 showing the most prominent losses. Note that the order of loss of each OH group, the position of the covalent bond between the alkyl chains and of the methyl branches are only suggested.

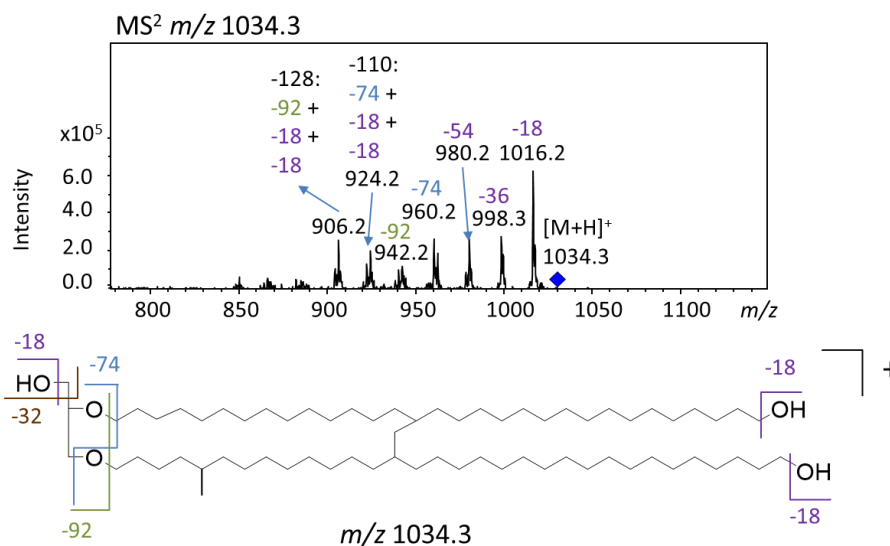


Figure 5.4. (Top) (+)APCI-MS² spectrum of glycerolipid m/z 1034.3 and (bottom) suggested structure of glycerolipid m/z 1034.3 showing the most prominent losses. Note that the order of loss of each OH group, the position of the covalent bond between the alkyl chains and of the methyl branch are only suggested.

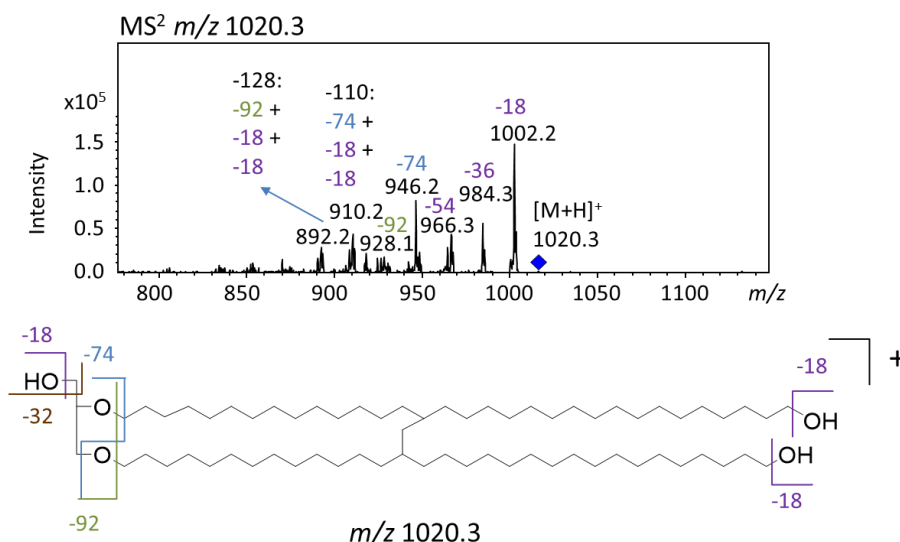


Figure 5.5. (Top) (+)APCI-MS² spectrum of glycerolipid m/z 1020.3 and (bottom) suggested structure of glycerolipid m/z 1020.3 showing the most prominent fragment ions. Note that the order of loss of each OH group and the position of the covalent bond between the alkyl chains are only suggested.

Following acetylation of the polar fraction (Sections 7.2.5, 7.2.6), the resulting acetate derivatives were examined by MS² to elucidate the number of alcohol groups and structures of the lipids (Sections 7.4.8, 7.4.11, 7.4.12). It was envisaged that the three alcohol groups would be acetylated to give triacetate glycerolipids and an increase in mass by three acetates (126 Da). Extracted ion chromatograms (EIC) of the tri-, di- and mono-acetates of m/z 1034 did not yield peaks representing the acetates, likely due to the lower concentrations of this glycerolipid in sediments (Figure 5.7). The MS and MS² spectra of the acetate derivatives of m/z 1020.3 and 1048.3 did not exhibit peaks corresponding to the triacetates, but masses corresponding to the diacetates were observed. This is due to the lack of complete derivatisation of the native glycerolipids to form triacetate derivatives. The MS² of the diacetate of m/z 1020.3 showed the protonated molecule at m/z 1104.1 (Figure 5.6). The most prominent fragment ions resulted from loss of one water molecule (-18 Da, m/z 1086.1), one acetic acid group (-60 Da, m/z 1044.1) and the acetylated C₃H₄O (-116 Da, m/z 988.1; Knappy, 2010). Other less prominent ions included the loss of one acetic acid group and water molecule (-78 Da, m/z 1026.1), loss of two acetic acid groups and one water molecule (-138 Da, m/z 966.1) and loss of one acetic acid group, one water molecule and one acetylated C₃H₄O (-194 Da, m/z 910.1). Although triacetates were not observed, the fragments product ions at m/z 966.1 and 910.1 confirm that the unknown glycerolipids are triols. The MS² spectrum of the acetate derivative of m/z 1048.3 exhibited the protonated molecule of the diacetate at m/z 1132 and the

same fragment ions as m/z 1104.1, thus confirming that the glycerolipid at m/z 1048 contains three hydroxyl groups.

The late retention time, MS^2 of the underivatised molecules and the diacetate derivatives suggest that the three lipids observed contain three alcohol groups and an “H-shaped” alkyl chain. Such glycerolipids are glycerol monoalkanol triols (GMT) according to the designation given by Knappy (2010) or glycerol monoalkanediol diethers (GMD) according to Bauersachs and Schwark (2016); in this work, the term GMD is used.

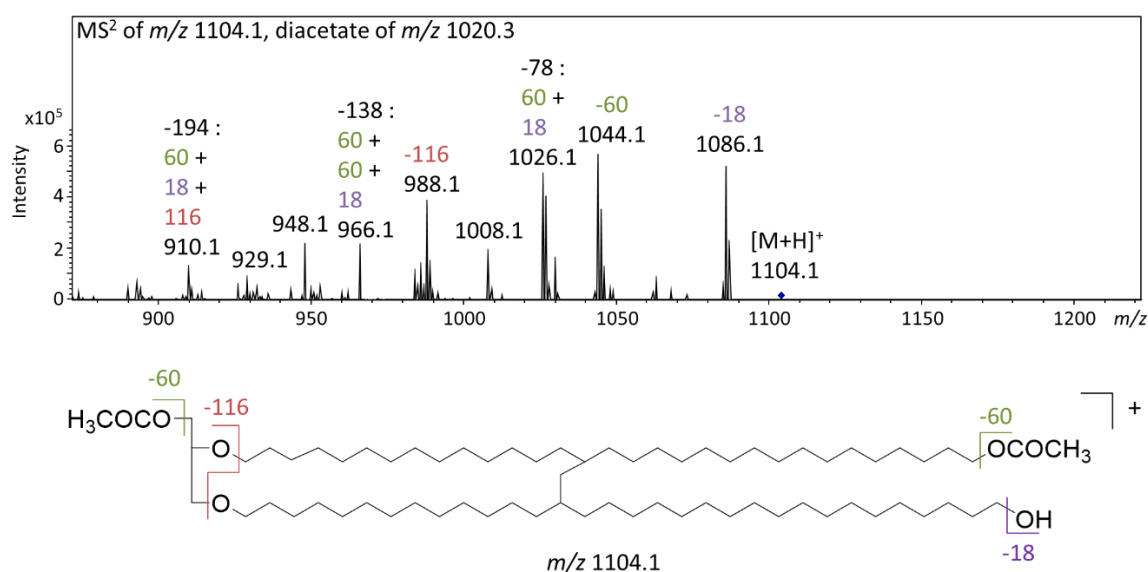


Figure 5.6. (Top) (+)APCI- MS^2 spectrum of the diacetate glycerolipid m/z 1104.0 and suggested structure of the acetate derivative showing the main losses. Note that the positions of the covalent bond between the alkyl chains and of the acetylated alcohol groups are only suggested.

Archaeal components eluting between 46 and 48 min, approx. 20 min after GDGT, GMGT and GDD, were identified in sediments deposited under hydrothermal conditions (Bauersachs and Schwark, 2016). These lipids exhibited m/z 1244, 1242 and 1240. The MS^2 profile suggested that these components are isoprenoidal GMDs. The m/z difference of 2 between the three structures was attributed to increasing number of pentacyclic rings, similarly to GDGTs (Bauersachs and Schwark, 2016). GMDs with lower molecular masses were observed by Knappy (2010) in the Vena del Gesso evaporitic sediments and in the Oxford Clay lake sediments. These glycerolipids eluted after isoprenoid and non-isoprenoid GMGTs and had alkyl chain lengths comprising C_{66-68} (m/z 1047.5-1048.5, 1061.5-1062.5, and 1075.5-1076.5) or C_{60} (m/z 965.5-964.5). The low molecular masses of the C_{66-68} GMDs suggest that these components have non-isoprenoid alkyl chains (Knappy, 2010). The glycerolipid at m/z 1048 discussed in this work shows the same MS^2 pattern as the GMDs

reported by Knappy (2010), supporting the assignment of the unknown glycerolipids as GMDs and their suggested structures. Therefore, the combination of the late retention time, MS² analysis and comparison with literature research (Knappy, 2010; Bauersachs and Schwark, 2016) confirms the assignment of these novel glycerolipids as GMD lipids with straight alkyl chains and increasing number of methyl branches on the alkyl chain.

The presence of rings is not evident from MS² and cannot be excluded, the collision-induced dissociation (CID) being insufficiently energetic to fragment the alkyl chain. Elucidation of the chain structures, including the positions of the methyl branches, would require ether cleavage followed by GC-MS analysis (Schouten *et al.*, 1998; Zhu *et al.*, 2014). The position of and exact nature of the covalent bond bridging the chain cannot be confirmed by HPLC-APCI-MS/MS and is located in the structures by analogy with GMGT-0 (Morii *et al.*, 1998). Due to the time-constraints of the project, isolation of the GMDs, cleavage of glycerol groups and analysis by GC-MS was not performed.

5.3.2. Distribution of GMD lipids in sediments

The GMDs were detected in all sediment types from the Nar Valley and in the Stenness and Woodston sediments, with *m/z* 1020 as the most abundant lipid, followed by *m/z* 1048 (Figure 5.7). In all sediments *m/z* 1034 was either absent or in very low amounts (Figure 5.7). Peak areas were the highest in the sediments with highest concentrations of molecular fossils (types B and D; Figures 4.10-4.22) and BIT values >0.8 (Figure 5.7). GMDs, where present, represented 0.7-8.3% of the total glycerolipid content (brGDGTs, iGDGTs, GMDs). At Horse Fen the highest percentage of GMDs (15%) was recorded in the sample at -2.26 m OD, representing the end of the transgression (Section 4.4.6), compared with 0.7-5.1% in the other samples. A similar level of difference in abundance (5.9-5.2% vs 2.2%) was evident at Blackborough Quarry between -1.05, -0.95 m OD (representing the beginning of the transgression; Sections 4.4.3, 4.4.5), and -0.54 m OD (representing the marine environment; Section 4.4.6). Also in the Tottenhill Quarry core, the percentage of GMDs was highest at 1.95 m OD (6.5% representing a possible regression; Section 4.4.2) and at 2.44 m OD (8.3% representing the beginning of the transgression; Section 4.4.6) compared to 2.0-3.7% in terrestrial sediments (Section 4.4.3). The increase of GMDs in core horizons representing transgressive conditions may indicate that their producers live under marine conditions with high terrestrial input and transitional phases between terrestrial and marine environments but not under fully marine or terrestrial conditions. This trend could also indicate that such conditions are unfavourable for the growth of the producers of iGDGTs and brGDGTs, resulting in a comparatively high percentage of GMDs being produced.

The origins and formation of GMDs is unclear; it cannot be ruled out that these compounds might be transformation products of tetraether lipids (GMGT) formed by enzymatic modification or grazing (Knappy, 2010; Bauersachs *et al.* 2015b). If that were the case, GMGTs would most likely also be present in the sediments, though base peak chromatograms did not contain peaks consistent with GMGT structures (m/z 1060-1100). Due to the absence both of GMGTs and of glycerol dialkyl diethers (GDD), the monoglycerol counterparts of the GMDs, it is unlikely that the GMDs are degradation products of GMGTs. Isoprenoid GMDs have, to date, been reported in archaeal cell cultures, ancient sediments (ca. 160 Ma and ca. 6 Ma), soil samples (Holocene to present; Knappy, 2010), in hydrothermal environments (Bauersachs and Schwark, 2016) and in hydrothermal vent methanogens (Baumann *et al.*, 2018). Since isoprenoidal GMD lipids have been found in extracts from archaeal cellular material (Knappy, 2010), the GMDs discussed in this work may be a direct input from the source organisms rather than a product of GMGT degradation. The low molecular mass is matched in GDGT from bacteria. The mass difference of m/z 14 between the three GMDs suggest an increasing number of methyl branches that is mostly common in bacterial brGDGTs. Methyl branches were observed also for iGDGTs and iGMGTs from cultures of *Pyrobaculum*, *Methanothermobacter thermautotrophicus* (MTH(Δ H)) and *Sulfolobus acidocaldarius* and from terrestrial soils and ancient sediments, though further studies are required to elucidate the origin and distribution of these isoprenoid lipids with extra branches (Knappy, 2010; Liu *et al.*, 2012a).

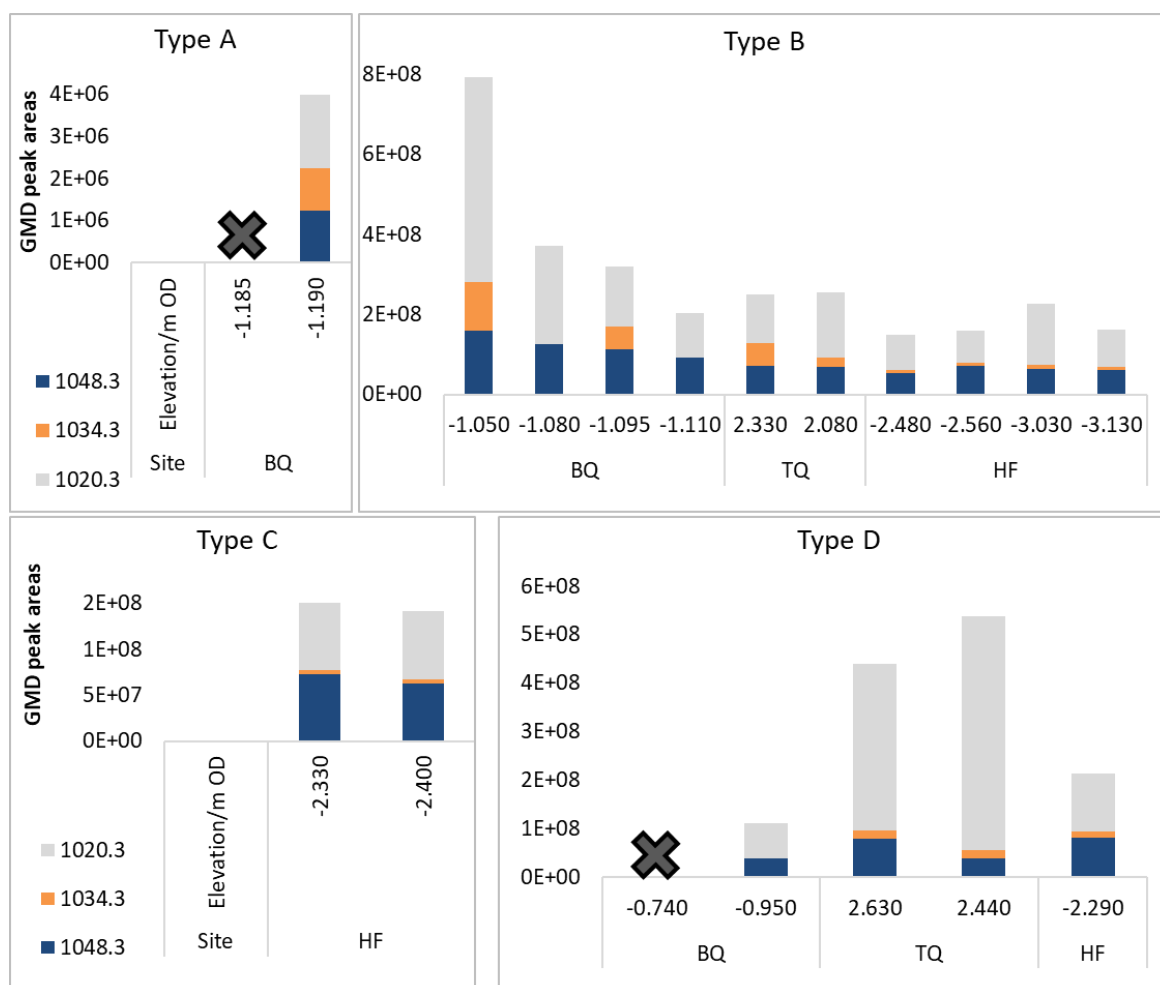


Figure 5.7. Peak areas of GMD lipids m/z 1048.3, 1034.3 and 1020.3 in the type sediments from the Nar Valley, in the Woodston and Loch of Stenness sediments. Abbreviations: BQ = Blackborough Quarry, TQ = Tottenhill Quarry, HF = Horse Fen, RC = Railway Cottage. The cross indicates absence of GMDs (continued over).

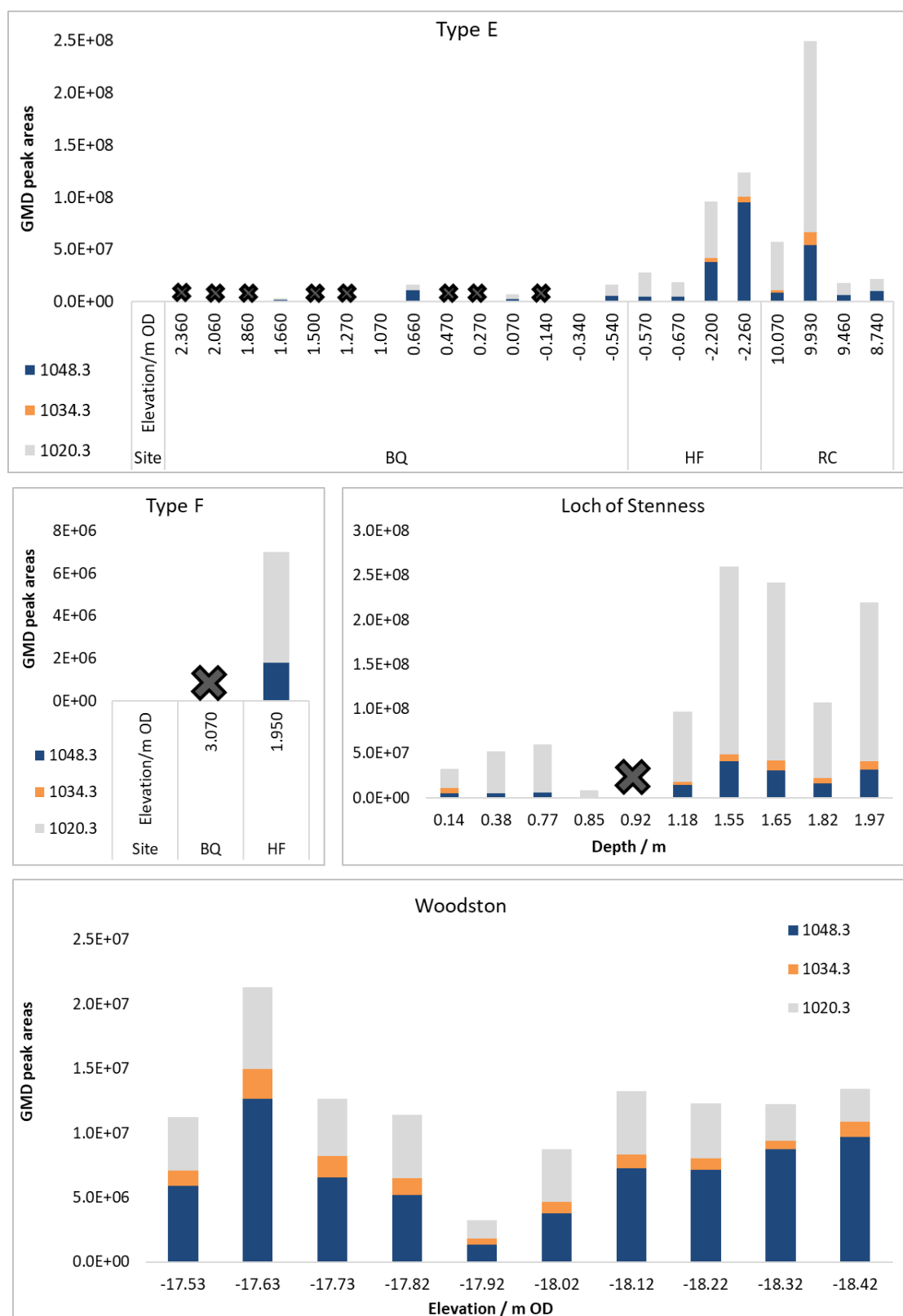


Figure 5.7. (continued) Peak areas of GMD lipids m/z 1048.3, 1034.3 and 1020.3 in the type sediments from the Nar Valley, in the Woodston and Loch of Stenness sediments. Abbreviations: BQ = Blackborough Quarry, TQ = Tottenhill Quarry, HF = Horse Fen, RC = Railway Cottage. The cross indicates absence of GMDs.

Correlation of the peak areas of GMDs with brGDGTs and iGDGTs shows linearity at Loch of Stenness, Blackborough Quarry and Railway Cottage ($R^2 > 0.60$; Figure 5.8, Table 5.1). At Tottenhill Quarry, the correlation was lower (R^2 0.47-0.48) and at Horse Fen higher correlation was observed between GMDs and iGDGTs (R^2 0.56). Thus, GMD areas covary with those of brGDGTs and iGDGTs; however, at the other sites, correlation was poor ($R^2 < 0.3$). Interestingly, separation of the sediments depending on terrestrial / freshwater and marine / brackish conditions showed improved correlation (R^2 0.50-0.95), possibly suggesting different sources of GMDs and GDGTs according to environmental conditions (Figure 5.8; Table 5.1). At Woodston, where peak areas of the GMDs and GDGTs were uncorrelated over the whole core (R^2 0.01, 0.04), separation of the sediments between marine sediments (from -18.42 to -18.02 m OD) and marine sediments after disruption of the water column (from -17.92 to -17.53 m OD) gave correlations above R^2 0.73. This may suggest that GMDs are not affected only by terrestrial, marine or freshwater sources but also by water column conditions, pointing towards aquatic producers of GMDs. Overall, a marginally better correlation was observed between GMDs and iGDGTs for both the whole core and within particular environmental types. The m/z increments of 14 Da, indicative of methyl branches, are common in bacterial brGDGTs but also in archaeal iGDGTs and iMGs. The similarities in mass to brGDGTs may indicate a bacterial origin of GMDs in sediments. This is supported by the higher concentration of GMDs in sediments with high input of terrestrial OM and high BIT values. It is evident that a specific origin of GMDs m/z 1048.3, 1034.3 and 1020.3 cannot be reliably established due to the widespread presence of GMDs in all sediments, the linearity of peak areas of GMDs with peak areas of both iGDGTs and brGDGTs, and the possibility of mixed sources of brGDGTs and iGDGTs as well as GMDs.

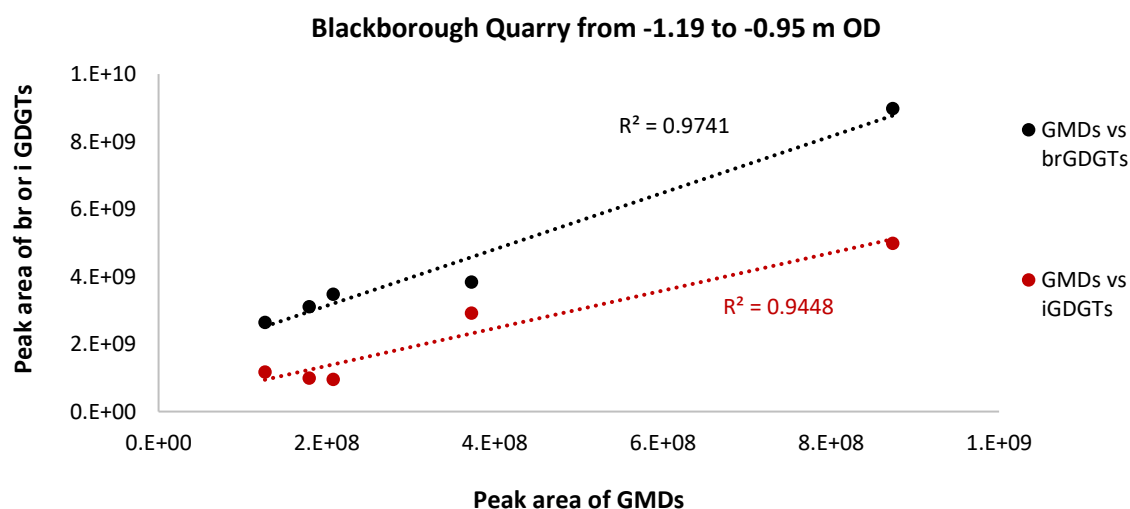


Figure 5.8. Example of correlation between peak areas of GMDs vs brGDGTs (in blue) and GMDs vs iGDGTs (in red) in Blackborough Quarry from -1.19 to -0.95 m OD.

Table 5.1. Correlations between GMDs vs brGDGTs and GMDs vs iGDGTs in all the cores analysed in this work for all the samples in the core and after separation of samples depending on terrestrial / aquatic or marine / brackish environment.

Site	Depth / cm	Environment	R ² correlation	
			GMDs vs. brGDGTs	GMDs vs. iGDGTs
Loch of Stenness	Whole core		0.60 (n=9)	0.66 (n=9)
	197-118	Freshwater	0.57 (n=5)	0.61 (n=5)
	85-14	Brackish	0.70 (n=4)	0.07 (n=4)
Site	Elevation / m OD	Environment	R ² correlation	
			GMDs vs. brGDGTs	GMDs vs. iGDGTs
Blackborough Quarry	Whole core		0.95 (n=11)	0.88 (n=11)
	From -1.19 to -0.95	Terrestrial	0.97 (n=5)	0.95 (n=5)
	From -0.74 to 3.07	Marine	0.96 (n=6)	0.95 (n=6)
Horse Fen	Whole core		0.02 (n=12)	0.56 (n=12)
	From -3.13 to -2.29	Terrestrial	0.18 (n=7)	0.56 (n=7)
	From -2.26 to 1.95	Marine	0.07 (n=5)	0.12 (n=5)
Tottenhill Quarry	Whole core	Terrestrial	0.47 (n=5)	0.48 (n=5)
Railway Cottage	Whole core	Marine	0.99 (n=4)	0.81 (n=4)
Woodston	Whole core		0.04 (n=10)	0.01 (n=10)
	From -18.42 to -18.02	Marine	0.77 (n=5)	0.73 (n=5)
	From -17.92 to -17.53	Marine, disrupted water column	0.80 (n=5)	0.97 (n=5)
Improved with palaeoenvironmental separation		Not improved with palaeoenvironmental separation		

5.4. Conclusions

A suite of novel glycerolipid structures was present in all of the cores from East Anglia (Chapter 4), as well as in the Loch of Stenness sediments (Chapter 3). These lipids had masses of m/z 1048.3, 1034.3 and 1020.3, the difference of m/z 14 attributed to increasing number of methyl branches. The late elution time of the glycerolipids approx. 20 minutes after brGDGTs (normal phase conditions) suggested higher polarity than brGDGTs. MS and MS² analysis of the native and diacetylated lipids identified three alcohol moieties. MS² spectra of the native structures gave evidence for the presence of three alcohol groups, one glycerol moiety and an “H-shaped” alkyl chain. Comparison with the literature led to the conclusion that the novel glycerolipids are glycerol monoalkanediol diethers (GMD) with increasing number of methyl branches and straight alkyl chains.

The origin of these lipids is unclear. Correlation between the peak areas of GMDs and brGDGTs or of GMDs and iGDGTs gave generally low correlations for all sediments in a core. Separation of samples according to marine / brackish or terrestrial / freshwater conditions gave higher covariance (Table 5.1). Notably, however, the similar covariance between GMD peak areas with both iGDGTs and brGDGTs, the GMD masses similar to brGDGTs (m/z 1048.3, 1034.3, 1020.3) and m/z increment of 14 Da, indicative of methyl branches, creates uncertainty regarding the origin of these glycerolipids in sediments. The widespread occurrence of these GMD lipids is interesting but further work is needed to establish the origin of these components in sediments before considering them potential biomarkers.

6. Conclusions and future work

6.1. Overall summary and conclusions

The primary aim of the work presented in this thesis was to study Quaternary transgressions using molecular fossils, exploiting distributional variations that result from palaeoenvironmental changes. The application of the approach to Holocene and Middle Pleistocene transgressions produced very useful data able to refine the onset and cessation of the inundations, as well as describing previously unrecognised and significant features of the palaeoenvironment. Molecular fossils have been shown to provide useful additional data on Quaternary sea-level change, and it is recommended that they become an integral part of sea-level studies.

In this work, key areas of research were:

1. Optimisation of detection of glycerol dialkyl glycerol tetraether (GDGT) by derivatisation of alcohol groups with fluorescent tags (Chapter 2).
2. Analysis of molecular fossils to study a well-constrained Holocene transgression in the Loch of Stenness (Chapter 3) and testing the applicability of molecular fossils to study marine transgressions from the Nar Valley (Norfolk) and Woodston (Cambridgeshire) dating back to the Middle Pleistocene (Chapter 4).
3. Elucidation of the structure of unknown glycerolipids found in all samples, suggestion of a possible origin of these compounds and evaluation of their biomarker potential (Chapter 5).

6.1.1. Optimisation of detection of glycerol dialkyl glycerol tetraether

Organic matter in sediment, although well-preserved, may be present in trace amounts, pushing the detection limits of analytical methods. Esterification of lipidic alcohol groups with protected amino acids, acting as fluorescent tags (Steglich esterification; Neises and Steglich, 1978; Poplawski, 2017), was applied to lipid standards and GDGT lipids from sediment samples (Chapter 2). Microwave irradiation, considered a quick and efficient alternative to classical synthetic methods, was applied to lipid standard 1-octadecanol and Fmoc-Lys(Boc). The experiments did not yield complete esterification and resulted in formation of side products, possibly caused by high reaction temperatures (> room temperature). Therefore, sonication was preferred. High yields were recorded for derivatisation by sonication of multiple lipid standard samples but, surprisingly, derivatisation of single GDGT samples from sediments indicated lower MS response than for the native lipids. Incomplete derivatisation, competition for the reagents and loss of product from flash column chromatography were ruled out as possible causes of the low MS response of the derivatives. Therefore, although derivatisation may be successful for lipid standards, the method

is not beneficial for increasing the limits of detection and resolution of GDGTs in sediments, under the tested derivatisation conditions. Following this unsuccessful application of the Steglich esterification to GDGTs in sediments, native species were analysed to study the sea-level transgressions in the Loch of Stenness and in cores from East Anglia (Chapters 3 and 4).

6.1.2. Molecular fossils to study Quaternary transgressions

Sea-level research is dominated by macro and microfossil studies, but these can occur in low amounts or be absent. The sediment matrix contains molecular structures that can be linked to OM produced by organisms (biomarkers). In Chapters 3 and 4, Quaternary transgressions and the associated palaeoenvironment were studied using molecular fossils.

The Holocene transgression from the Loch of Stenness was previously studied by Bates *et al.* (2016) using pollen and microfossil evidence. The core (200 cm-long) exhibited a freshwater period (between 200 and 104 cm), followed by a mix of brackish and freshwater microfossils (between 102 and 81 cm) and brackish conditions (between 80 and 0 cm core depth). The molecular fossils refined the depth of the transgression between 118 and 85 cm and provided additional information about the environment of the lake, the redox conditions of the water column and the estimated SST (Chapter 3). This study showed that molecular fossils, while commonly used for other palaeoenvironmental reconstructions, are also valuable in the study of sea-level transgressions. The success of this study and the extra information provided on the palaeoenvironment before, during and after the Holocene transgression in the Loch of Stenness provided the basis for studying Pleistocene sediments.

The Pleistocene sediments from East Anglia comprised four cores from the Nar Valley (Norfolk) and one core from Woodston (Cambridgeshire; Chapter 4). Pollen analysis identified the Nar Valley cores as “Hoxnian”-type but dating of these deposits is disputed, likely to correspond to MIS 11 and / or MIS 9 (Barlow *et al.*, 2017). Molecular fossils from the Nar Valley showed similar distributions among the four cores, allowing their separation by common and differing features defining six types of distributions, described for the first time in this thesis. The molecular fossil analysis identified the transgression at Blackborough Quarry and Horse Fen at different core elevations compared to the previous microfossil analysis (Barlow *et al.*, 2017). Interestingly, the Tottenhill Quarry core, which was characterised as a fully terrestrial environment without marine production by Barlow *et al.* (2017), potentially showed evidence of a regression at the bottom of the core (types A→B) and the beginning of marine production at the top of the core (types B→D).

Molecular fossil analysis of a fifth core from Woodston provided the opportunity for comparison of a Pleistocene transgression outside the immediate region with the Nar Valley cores. The Woodston core aimed to reproduce a series of cores showing a “Hoxnian”-type transgression analysed by Horton *et al.* (1992) and related to MIS 11 (Horton *et al.*, 1992; Ashton *et al.*, 2005; Penkman *et al.*, 2011; 2013). The molecular fossils showed marine input throughout the core, with a slight increase in BIT values from -17.92 m OD. Changes in the physicochemical properties of the water column, possibly salinity, affected pigment production from -18.02 m OD, and more markedly from -17.92 m OD, where only carotenoids were detected. The molecular fossil distribution in Woodston was similar to type D in the Nar Valley, suggesting that the five cores may have been deposited under similar palaeoenvironmental conditions.

The two studies of Holocene and Pleistocene cores exhibiting transgressions have shown that molecular fossils can provide useful additional data on sea-level change. The multiple molecular fossil approach can be used to support evidence from conventional microfossil analyses, as well as a distinct approach to studying sea-level change. Therefore, it is recommended that molecular fossils become an integral part of sea-level studies.

6.1.3. Structure and occurrence of unknown glycerolipids in sediments

In the HPLC-MS chromatograms alongside GDGTs, peaks eluting after brGDGTs were present. Further elucidation of their structures and occurrence in sediments was carried out to explore their potential as biomarkers. MS/MS of these glycerolipids enabled their identification as glycerol monoalkanediol diethers (GMD). The structures differed by m/z 14 (m/z 1020.3, 1034.3, 1048.3), likely an indication of increasing number of methyl branches. The GMDs were observed in all the sediment samples reported in this work. The lipids with m/z 1020.3 and m/z 1048.3 were the most abundant throughout the Loch of Stenness, Nar Valley and Woodston cores. High correlation between the peak areas of GMDs with both brGDGTs and iGDGTs and the presence of GMDs in samples from terrestrial, freshwater and marine conditions was inconclusive in suggesting an origin of GMD lipids. Thus, further work is needed before GMDs can be considered biomarkers.

6.2. Future work

The work presented in this thesis developed and successfully tested a molecular fossil-based approach to determine the palaeoenvironment and to refine the study of sea-level change as a supplement to conventional microfossil and sediment analyses.

The research described in this work highlights a number of areas that merit additional research work.

- The value of the Steglich esterification method as applied to GDGTs needs further work to assess why the MS, UV and FLD signal is very low for derivatives (Section 2.2.5). Further experimentation may include changing the ratios of reagents and / or fluorescent tags.
- The reasons behind the lower MS signal of GDGT derivatives compared to native lipids are unclear (Section 2.2.5). If the derivatised GDGTs are forming a special conformation, size-exclusion chromatography combined with UV, FLD or MS detectors may monitor changes in the GDGT structure and size (Righetti and Verzola, 2001).
- The high yields recorded from standard lipids with one protected hydroxyl group (Poplawski, 2017) indicates that it may be possible to apply the Steglich esterification method to complex sediment samples containing molecules with one alcohol group, such as sterols.
- The identification of the full structures of GMDs and carotenoid P7 and the analysis of further sediment samples from different environmental conditions may determine the origin of these compounds and their potential use as biomarkers.
- In this work, marine conditions were recognised based on presence of unsaturated long chain alkenones and crenarchaeol. Expanding the analysis to $\delta^{13}\text{C}$ isotopes may inform on the terrestrial or marine origin of OM.
- The cores presented in this work were studied before (to different extents) and / or visually showed peat-clay transitions, indicative of a transgression. Application of the molecular fossil approach to sediments where visual demarcation of the transgression is not evident and where microfossil preservation is problematic can corroborate the value of molecular fossils for studying sea-level changes.
- Accurate dating of Nar Valley cores would establish chronology to confirm if the cores date to the same transgression and if Woodston and the Nar Valley cores correlate to the same MIS. Although gastropod shells were not found in the cores from East Anglia, development of AAR dating on foraminifera (abundant in the marine sediments) would be a valuable tool

to confirm the date of the deposits (Hearty *et al.*, 2004; Kaufman, 2006; Kaufman *et al.*, 2008).

- Molecular fossil analysis can reveal glacial / interglacial cycles because of their effect on the environment and OM production. These cycles can be recognised by the levels of primary production from molecular fossils and by reconstructing water and soil temperature from GDGT and alkenones proxies in appropriate sediment samples (Brassell *et al.*, 1986; Schouten *et al.*, 2002; Weijers *et al.*, 2007).
- Ancient sediments contain molecular fossils that may have undergone transformations but that can be related to terrestrial, aquatic or marine OM (Killops and Killops, 1993), thus they can be used to identify transgressions beyond the Quaternary. Moreover, the widespread nature of molecular fossils suggests their application to study regressive events (Squier *et al.*, 2002).
- The molecular fossil approach can potentially enable correlation between sites by reconstructing their palaeoenvironmental changes, for example in areas that experienced the same environmental conditions, or that are present at different elevations due to the underlying geology of the area. It is postulated that this approach could be used to correlate sites that have undergone recent tectonic movements, and areas that have been inundated due to tectonic movements (Wilson *et al.*, 2007).

7. Experimental and analytical procedures

7.1. General procedures

7.1.1. Solvents and reagents

All solvents used were of analytical grade or higher and purchased from Fisher (Loughborough, UK), except methyl tert-butyl ether (MTBE, 99.8%) purchased from Scientific Laboratory Supplies (Nottingham, UK). The alcohol standards and derivatisation reagents, all of certified purity, were obtained from Sigma-Aldrich (Gillingham, UK): 1-octadecanol (99%), 1,12-dodecanediol (99%), Fmoc-Gly (98%), Fmoc-Lys(Boc) (98%), BSTFA (*N,O*-Bis(trimethylsilyl)trifluoroacetamide (99%) with trimethylchlorosilane (1%). DMAP (4-(Dimethylamino)pyridine (99%)) was obtained from Fluka Analytical (Münich, Germany). Cholesterol (biochemical grade) was obtained from BHD Chemicals Ltd. (Poole, UK). EDC (*N*-(3-Dimethylaminopropyl)-*N'*-ethylcarbodiimide hydrochloride) (>98%) was obtained from TCI (Tokyo Chemical Industry UK Ltd., Oxford, UK). Pyridine (99+%) and (trimethylsilyl)diazomethane (2.0 M in hexanes) were obtained from Acros Organics (Loughborough, UK). The reagents were stored according to the manufacturer's recommendations.

7.1.2. Glassware

To reduce the risk of contamination, all glassware used to carry out chemical reactions was soaked in a 1% solution of Decon-90 (Decon, Hove, UK) overnight, prior to thorough rinsing with deionised water and acetone. To remove organic contaminants, dried glassware was cleaned by heating to 400°C for at least 4.5 h in an oven (Barnstead Thermolyne Pyroclean® Trace). The same treatment was applied to HPLC mobile phase bottles, glass Pasteur pipettes, glass columns and HPLC vials.

7.1.3. Sample collection

Core 2014-1 from the Loch of Stenness, Orkney, UK was collected by Dr. Martin R. Bates (University of Wales Trinity Saint David, Lampeter, UK); its exact location is shown in Table 7.1 from Bates *et al.* (2016). The Stenness core was stored at +4°C at the University of Wales Trinity Saint David (Lampeter, UK), and later was subsampled for this study. Sampling was carried out by cutting 1 cm slices of sediments with a scalpel.

Nar Valley and Woodston (Norfolk, UK) cores were collected as part of the NERC iGlass project by Dr. Natasha L.M. Barlow and Prof. Anthony J. Long, between 2012 and 2014, and stored at +4°C at Durham University (Durham, UK). The coordinates of cores retrieved from Blackborough Quarry, Horse Fen 13-1, Railway Cottage and Tottenhill Quarry are reported in Table 7.1 from Barlow *et al.* (2017). Slices of 1 cm of sediment were collected from the Nar Valley cores. The Woodston HiB

12-6 core location (Table 7.1) is as reported in Horton *et al.* (1992). The Woodston core, which had been previously sliced in 1 cm samples, was subsampled collecting 2-3 cm slices of sediment.

Table 7.1. Coordinates of cores discussed in the thesis.

Site	Core name	Latitude	Longitude	Reference
Loch of Stenness, Orkney, Scotland	St-1	58.99585	-3.25280	Bates <i>et al.</i> , 2016
Blackborough End Quarry, Norfolk	BQ	52.70565	0.48763	Barlow <i>et al.</i> , 2017
Horse Fen, Norfolk	HF 13-1	52.70038	0.50385	Barlow <i>et al.</i> , 2017
Railway Cottage, Norfolk	RC	52.71964	0.54043	Barlow <i>et al.</i> , 2017
Tottenhill Quarry, Norfolk	TQ	52.66985	0.40428	Barlow <i>et al.</i> , 2017
Woodston, Norfolk	HiB 12-6	52.54632	-0.25031	Horton <i>et al.</i> , 1992

7.1.4. Sample storage and handling

Sediment core samples were subsampled and preserved in foil to avoid plastic contamination and were stored in the dark at -20°C. Prior to chemical extraction, samples were freeze-dried overnight (-56°C, ~1 hPa, HETO PowerDry PL3000; Thermo Scientific™). The dried sediments were ground with a pestle and mortar and sieved through 1 mm, 400 µm and 200 µm sieves, retaining the <200 µm fraction for extraction and analysis; shells, if present, was separated from the fractions >200 µm (Section 7.1.5). The homogenised sediment was kept at -20°C prior to extraction.

7.1.5. Separation of shells

The freeze-dried sediment was inspected for intact gastropod shells before grinding and sieving. Any shells found were removed with a spatula and / or forceps and sonicated in deionised water to remove soil residues. After air-drying in a fumehood overnight, species identification was performed by Dr. Richard C. Preece (University Museum of Zoology Cambridge, Cambridge, UK).

7.2. Extraction and isolation of organic compounds from sediments

7.2.1. Extraction of sediment

Extraction of the sediment (0.34-6.25 g per sample) was carried out using accelerated solvent extraction (Thermo Scientific™ Dionex™ ASE™ 350): 3 cycles of 5 min at ~1500 psi (Saesaengseerung, 2013). Solvent compositions were dichloromethane:methanol (DCM:MeOH, analytical grade) 9:1, v:v, 100°C for lipids, and acetone (HPLC grade) at 70°C for chlorophyll

pigments. The total extracts were dried using a rotary vacuum concentrator (CHRIST, RVC 2-25, 1310 rpm) and were weighed. A blank extraction was also performed every time to demonstrate the absence of contamination (Schouten *et al.*, 2007a; Saesaengseerung, 2013).

7.2.2. Preparation of diazomethane to methylate pigments

Following the methods of Airs *et al.* (2001), prior to chromatographic analysis, pigment extracts were methylated with freshly prepared diazomethane reacted in a special distillation apparatus (Aldrich® diazomethane-generator with system 45™ compatible connection) by dissolving potassium hydroxide (KOH) in water (6.6 M, 1.5 mL) and adding it dropwise to diazald (*N*-methyl-*N*-nitroso-*p*-toluenesulfonamide, 0.3 g, prepared by Dr. Phil Helliwell) dissolved in ethanol:diethyl ether (1:1, v/v, 2 mL). The distilled diazomethane was trapped in ice-cold diethyl ether (2-4 mL) and used after approx. 1 h. After use, excess diazomethane was destroyed with a few drops of acetic acid (Airs *et al.*, 2001).

7.2.3. Fractionation of the lipid extracts

Following the methods of Green (2013), the total lipid extract (Section 7.2.1) was loaded onto a fritted glass column (10 cm length, 1.5 cm i.d.) prepared by adding to the frit a small plug of DCM-washed cotton wool and approx. 1.5 cm of silica. The column was conditioned by washing with DCM:MeOH (1:1, v/v, 6 mL), hexane:ethyl acetate (4:1, v/v, 3 mL) and hexane (6 mL). The extract was dissolved in DCM (200 µL) and added to a few milligrams of pre-washed silica which was subsequently dried using the rotary vacuum concentrator (Section 7.2.1). The dried impregnated silica was loaded onto the top of the packed column. Fractionation was carried out by elution with 4.5 mL of: I) hexane, II) hexane:toluene (1:1, v/v), III) hexane:ethyl acetate (4:1, v/v) and IV) DCM:MeOH (1:1, v/v) to yield: I) aliphatic hydrocarbons, II) aromatic hydrocarbons, III) alcohols, and IV) carboxylic acids, respectively. Fractions were reduced to dryness using the rotary vacuum concentrator (Section 7.2.1; Green, 2013).

7.2.4. Methylation and silylation of polar fractions

Half of each of the polar fractions (III and IV) was reconstituted in DCM:MeOH (2:1, v/v, 300 µL) and reacted with (trimethylsilyl)diazomethane (2.0 M in hexanes) (20 µL) for 30 min, before drying under a gentle stream of N₂. Immediately prior to GC, the methylated polar fractions were treated with *N,O*-bis(trimethylsilyl)trifluoroacetamide (BSTFA; 100 µL, containing 1%

trimethylchlorosilane), 5 drops of pyridine and were heated for 1.5 h at 60°C, before drying under a gentle stream of N₂ gas (Green, 2013).

7.2.5. Fractionation of GDGTs prior to acetylation

Following the method from Knappy (2010) prior to acetylation of GDGTs, the total lipid extract was loaded onto a Pasteur pipette prepared by adding a small plug of DCM-washed cotton wool and alumina (50 mm length, 5 mm i.d.). The alumina was activated with hexane:DCM (9:1, v/v, 3 mL). The sample was loaded in the minimum amount of DCM. The unwanted apolar fraction was eluted with hexane:DCM (9:1, v/v, 3 mL) and the polar fraction containing the GDGTs was eluted with DCM:MeOH (1:1, v/v, 3 mL). The fractions were dried under a gentle stream of N₂.

7.2.6. Acetylation of glycerolipids

The GDGT fraction isolated in Section 7.2.5, was acetylated following the methods of Talbot *et al.* (2003). The fraction was dissolved in 1 mL of pyridine:acetic anhydride (1:1, v/v, 4 mL), heated at 50°C for 1 h and left at room temperature overnight. The next day, the derivatised fraction was dried under a gentle stream of N₂.

7.3. Steglich esterification of lipids

7.3.1. Derivatisation and fractionation of alcohol standards 1,12-dodecanediol, 1-octadecanol and cholesterol with Fmoc-Gly and Fmoc-Lys(Boc)

The alcohol standards 1,12-dodecanediol, 1-octadecanol and cholesterol were reacted with DMAP (1 eq.), Fmoc-amino acid (2 eq.) and EDC (4 eq.), the molar equivalents being calculated for each hydroxyl group. Reagents were dissolved in DCM (2 mL) and sonicated (Decon FS100b, frequency 35-45 kHz) for 1-3 h, after which thin-layer chromatography (TLC) was run to check the completion of the reaction (developed in 1:1 hexane:ethyl acetate, observed under a UV lamp, dipped in potassium permanganate (KMnO₄) dye and dried with a hot air blower; Neises and Steglich, 1978; Poplawski, 2017). Sonication of individual samples was carried out in a beaker immersed 0.5 cm below the water level in the sonic bath. A plastic rack, suspended by clamps into the sonic bath (2.1 cm from the metal walls on the long sides and 2.6 cm on the short sides, 1 cm immersed in the water) was used for testing the derivatisation of multiple samples positioned at various points in the rack (Figure 2.21). All products were isolated by flash column chromatography in glass Pasteur pipettes (230 mm length, 7 mm i.d.) on silica gel 60 (5 cm) primed with DCM (3 column volumes

(cv)). After loading the sample, the more apolar compounds were eluted and discarded with DCM (2 cv) and the esterified product eluted with 1:1 hexane:ethyl acetate (2 cv). The esterified product was dried under a gentle stream of N₂.

7.3.2. Derivatisation of 1-octadecanol with Fmoc-Lys(Boc) by microwave

The esterification of 1-octadecanol (1 eq.) was carried out using DMAP (1 eq.), Fmoc-Lys(Boc) (1.5 eq.) and EDC (2 eq.) in DCM (2 mL; Poplawski, 2017). The reaction mixtures were reacted in a microwave instrument designed for carrying out chemical reactions (Anton Paar GmbH - Monowave 300, Microwave synthesis reactor). The temperature of the sealed sample during reaction was monitored by infrared radiation. Homogenous microwave irradiation conditions were achieved using a small stirrer bar placed inside the microwave vessel (600 rpm). Formation of the desired product was firstly assessed by running TLC (Section 7.3.1) prior to instrumental analysis (Section 7.4.5).

7.3.3. Steglich esterification of GDGTs

Derivatisation of GDGTs in sediment extracts was performed by combining chromatographic fractions III and IV (Section 7.2.3), dissolving them in 2 mL of DCM, adding Fmoc-Lys(Boc) (50 eq.), DMAP (10 eq.), EDC (75 eq.), assuming that the target lipid caldarchaeol comprised the entire extract. The reagents were sonicated in a beaker (Section 7.3.1) for 2 h (Poplawski, 2017). The products were purified by silica flash column chromatography as in Section 7.3.1, prior to instrumental analysis (Section 7.4.6).

7.4. Analysis

7.4.1. Gas chromatography flame ionisation detection (GC-FID) of lipid fractions

The apolar and derivatised polar lipid fractions (Sections 7.2.3-7.2.4) of the Loch of Stenness sediments (Chapter 3) were analysed using a Thermo™ Trace GC Ultra gas chromatograph equipped with a Triplus autosampler, a fused silica capillary column (Agilent™ HP-5, 60 m × 0.32 mm i.d., 0.25 µm film thickness) and a flame ionization detector (FID). Samples were reconstituted in 20 µL of DCM and 1 µL injected onto the column in a split mode (280°C, split flow 5:1, split time 0.8 min).

The apolar and derivatised polar lipid fractions of the East Anglian sediments (Chapter 4) were analysed using a Thermo™ Trace 1300 GC gas chromatograph equipped with a AS 1310

autosampler, a fused silica capillary column (Thermo Scientific™ TG-SQC, 30 m × 0.25 mm i.d., 0.25 µm film thickness) and a FID. Following the methods of Green (2013), samples were reconstituted in 20 or 100 µL of DCM and 1 µL injected onto the column in a splitless mode. The hydrogen carrier gas flow rate was 2 mL min⁻¹; the FID was held at 320°C. The oven temperature was ramped from 70°C to 130°C at a rate of 20°C min⁻¹, then to 320°C at a rate of 4°C min⁻¹ and held constant for 40 minutes.

7.4.2. Gas chromatography-mass spectrometry (GC-MS) of lipid fractions

GC-MS analysis of the Loch of Stenness samples (Chapter 3) was carried out on selected fractions using a 7890A gas chromatograph (Agilent™) equipped with a 7683B Series autosampler coupled to a GCT Premier MS time-of-flight mass spectrometer (Waters). Separation was achieved on a fused silica capillary column (Zebron, ZB-1, 30 m × 0.25 mm i.d. 0.25 µm film thickness). The Nar Valley samples (Chapter 4) were analysed by GC-MS using a 7890B gas chromatograph (Agilent™) coupled to a Jeol T200 AccuTOF GCx plus reflectron time-of-flight mass spectrometer (Jeol™). Separation was achieved on a fused silica capillary column (Zebron, DB-5MS, 30 m × 0.32 mm i.d. 0.25 µm film thickness). The oven was programmed as in Section 7.4.1 using splitless injection. Mass spectra were acquired over the range *m/z* 50-750 using an electron ionisation energy of 70 eV (Green, 2013). Data analysis was carried out as described in Appendix 5.

7.4.3. Normal phase (NP) high-performance liquid chromatography (HPLC) of native GDGT lipid cores

Half of each of the polar fractions (III and IV; Section 7.2.3) were combined for analysis of the native glycerol dialkyl glycerol tetraether (GDGT) lipids, following the methods of Schouten and co-workers (2007a). The method used an Agilent™ 1200 system coupled with a Bruker HCTultra ETD II™ quadrupole ion trap mass spectrometer via an atmospheric pressure chemical ionization (APCI) source. Chromatographic separation was achieved using a Phenomenex® Luna CN column (150 × 2.0 mm i.d., 3 µm particle size) set at 30°C and eluted with linear gradient of hexane (A) and propan-2-ol (B) from 99:1 A:B (5 min) to 98:2 A:B over 45 min; re-equilibrating with the starting composition (15 min). The flow rate was 0.2 mL min⁻¹ and injection volume was 1 µL. Samples were dissolved in 100 µL of freshly prepared mobile phase 99:1 A:B. Mass spectrometry (MS) analysis was carried out as in Section 7.4.11. Data analysis was carried out as described in Appendix 7.

7.4.4. Ultra-high performance liquid chromatography-diode array detector (UHPLC-DAD) of chlorophyll pigments

Methylated chlorophyll pigments (Section 7.2.2) were analysed using a Dionex™ Ultimate 3000 ultra-high performance liquid chromatograph (UHPLC) equipped with a diode array detector (DAD) scanning wavelengths between 300 and 800 nm. Separation was achieved with a Waters Acquity UPLC BEH® C₁₈ column (150 mm × 3 mm i.d., 1.7 µm particle size). The column was heated at 45°C and the flow rate was 0.6 mL min⁻¹. Samples were reconstituted in 100 µL of acetone and the injection volume was 1 µL. The gradient elution is given in Table 7.2 (Saesaengseerung, 2013). Mass spectrometry (MS) analysis was carried out as in Section 7.4.9. Data analysis was carried out as described in Appendix 6.

Table 7.2. UHPLC-DAD solvent gradient for elution of pigments (Saesaengseerung, 2013).

Time / min	%A / Methanol	%B / Ethyl acetate	%C / 0.01 M Ammonium acetate	%D / Acetonitrile
0.00	80	0	10	10
0.50	80	0	10	10
7.00	64	21	5	10
16.0	50	40	0	10
18.0	31	63	0	6
18.5	19	80	0	1
19.5	19	80	0	1
20.0	80	0	10	10
23.0	80	0	10	10

7.4.5. Reversed-phase (RP) high-performance liquid chromatography with ultraviolet detector (HPLC-UV) and HPLC with fluorescence detector (FLD) method for scanning of derivatised standard lipids

The isolated derivatised standard lipids were analysed using an Agilent™ 1100 HPLC equipped with an ultraviolet detector (UV; set to λ_{max} 263 nm) and a fluorescence detector (FLD, Jasco FP-920: excitation wavelength λ_{ex} 263 nm and emission wavelength λ_{em} 309 nm). Samples were eluted through a Waters XBridge™ RP18 column (4.6 × 100 mm i.d., 3.5 µm particle size). In method A (for derivatised 1,12-dodecanediol and cholesterol) samples were eluted in methanol (A), ethyl acetate (B) and water (C) according to the gradient in Table 7.3. The flow rate was 0.4 mL min⁻¹,

the column temperature was held at 35°C and the injection volume was 1 μL (Poplawski, 2017). For Fmoc-Lys(Boc) derivatives of 1-octadecanol, the method was adapted to an isocratic elution with methanol, ethyl acetate and water (55:35:10) for 10 min. The flow rate was 0.4 mL min^{-1} , the column temperature was held at 30°C and the injection volume was 1 μL . MS analysis was carried out as in Section 7.4.10. Data analysis was carried out as described in Appendix 8.

Table 7.3. HPLC method A, used for separation of cholesterol and 1,12-dodecanediol derivatives.

Time / min	%A / Methanol	%B / Ethyl acetate	%C / Water
0	80	10	10
1.5	80	10	10
10	55	35	10
15	55	35	10
17	80	10	10
25	80	10	10

7.4.6. RP-HPLC-UV and HPLC-FLD analysis of native and derivatised GDGT lipids

Reversed-phase HPLC-UV of the native lipid cores employed the method of Poplawski (2017) using a DionexTM Ultimate 3000 UHPLC. The column was a Phenomenex[®] PFP (150 \times 4.6 mm i.d., 2.6 μm particle size). The isocratic method used 40:40:20 methanol:methyl tert-butyl ether (MTBE): 0.1% 6 M formic acid in water for 50 min. The flow rate was 1 mL min^{-1} and column temperature 45°C. The same method was used for the Fmoc-Lys(Boc) derivatives though with an increased elution time (75 min) and scanning with UV at λ_{max} 263 nm. For HPLC-FLD, the same method was used on AgilentTM 1100 HPLC equipped with a fluorescence detector (FLD, Jasco FP-920: excitation wavelength λ_{ex} 263 nm and emission wavelength λ_{em} 309 nm). Samples were reconstituted in 100 μL of MeOH and 1 μL injected on column. MS analysis was carried out as in Section 7.4.10. Data analysis was carried out as described in Appendices 7 and 8.

7.4.7. Fraction collection of native GDGT lipids

The branched (br) and isoprenoid (i) GDGTs from sediments were separated by HPLC fraction collection. The collector used was a Gilson FC 201. Using the method reported in Section 7.4.6, the first fraction contained brGDGTs (12.4-18.4 min) and the second fraction iGDGTs (29.4-44 min). Injection and fraction collection were performed three times. The fractions were dried using a

rotary vacuum concentrator (CHRIST, RVC 2-25, 1310 rpm) and were weighed prior to derivatisation (Section 7.3.3).

7.4.8. RP-HPLC of acetylated glycerolipids

Following acetylation of glycerolipids (Section 7.2.6), the fractions were analysed according to the method from Knappy (2010). The analysis employed DionexTM Ultimate 3000 UHPLC. Separation was achieved on a Waters XTerra C₁₈ column (100 × 4.6 mm i.d., 3.5 µm particle size). The isocratic method used 90:5:5 methanol:DCM:acetonitrile for 60 min. The column temperature was left at room temperature, the flow rate was 1 mL min⁻¹ and the injection volume was 1 µL. MS analysis was carried out as in Section 7.4.11. Data analysis was carried out as described in Appendix 8.

7.4.9. Atmospheric pressure chemical ionisation mass spectrometry (APCI-MS) detection of chlorophyll pigments

Chlorophyll pigments were analysed using DionexTM Ultimate 3000 (Section 7.4.4) coupled to a Thermo ScientificTM Orbitrap FusionTM TribridTM or Bruker HCT ultra ETD IITM quadrupole ion trap mass spectrometer configured with APCI source for analysis of chlorophyll pigments. The positive ion APCI-MS was operated under the following conditions: nebulizer pressure 60 psi, vaporizer temperature 300°C, drying gas (N₂) flow 6 L min⁻¹, drying gas temperature of 200°C, capillary voltage -4000 to -1500 V, corona discharge current 3µA, mass scan range *m/z* 400-1000 (Saesaengseerung, 2013). To enhance ionisation efficiency of metallated pigments, online demetallation was performed by introducing post-column formic acid by a syringe pump at 7 µL min⁻¹ (Airs and Keely, 2002). Data analysis was carried out as described in Appendix 6.

7.4.10 APCI-MS detection of derivatised lipid standards and derivatised GDGT lipids

Lipids were analysed using an AgilentTM 1100 HPLC (Sections 7.4.3 and 7.4.5) and DionexTM Ultimate 3000 (Section 7.4.6) coupled to a Bruker HCT ultra ETD IITM quadrupole ion trap mass spectrometer with an APCI source. Positive ion APCI-MS was performed under the following conditions: nebulizer pressure 40 psi, vaporizer temperature 400°C, drying gas (N₂) flow 4 L min⁻¹, drying gas temperature of 300°C, capillary voltage -4500 to -1500 V, corona discharge current 4 µA. The scan range was *m/z* 220-1000 for the derivatised lipid standards and *m/z* 1810-2110 for the GDGT derivatives. Data analysis was carried out as described in Appendix 8.

7.4.11. APCI-MS detection of native and acetylated GDGT lipids

Lipids were analysed using an Agilent™ 1100 HPLC (Sections 7.4.3 and 7.4.8) and Dionex™ Ultimate 3000 (Section 7.4.8) coupled to a Bruker HCT ultra ETD II™ quadrupole ion trap mass spectrometer with an APCI source. Positive ion APCI-MS was operated under the following conditions: nebulizer pressure 60 psi, vaporizer temperature 400°C, drying gas (N₂) flow 6 L min⁻¹, drying gas temperature of 250°C, capillary voltage -4000 to -1500 V, corona discharge current 3μA, mass scan range m/z 1000-1500 (Schouten *et al.*, 2007a). Data analysis was carried out as described in Appendix 8.

7.4.12. Tandem MS of native and derivatised lipids

MS/MS spectra were recorded using the HCT ultra ion trap mass spectrometer during LC-MS analysis. The Auto MSⁿ feature, which automatically selects the base peak ion in the mass spectra scan for collision induced dissociation (CID), was used. Isolation width was set to a m/z value of 1, maximum accumulation time set to 150 ms and fragmentation amplitude fixed at 1.7 V. Data analysis was carried out as described in Appendices 7 and 8.

7.5. Standard preparation and calculations

7.5.1. Standard pigments

A mixture of chlorophyll *a*, phaeophorbide *a* and phaeophytin *a* standards (prepared by Dr. Matthew D. Pickering) was used for generating the calibration curves. The starting molar amounts of each pigment were: chlorophyll *a* 1.87×10^{-7} mol, phaeophorbide *a* 3.66×10^{-7} mol and phaeophytin *a* 3.66×10^{-7} mol. Dilutions of these samples resulted in a max. 6-point calibration curve of the following percentages of the starting concentrations: 100%, 75%, 50%, 25%, 12.5% and 6.25% (Figure 7.1).

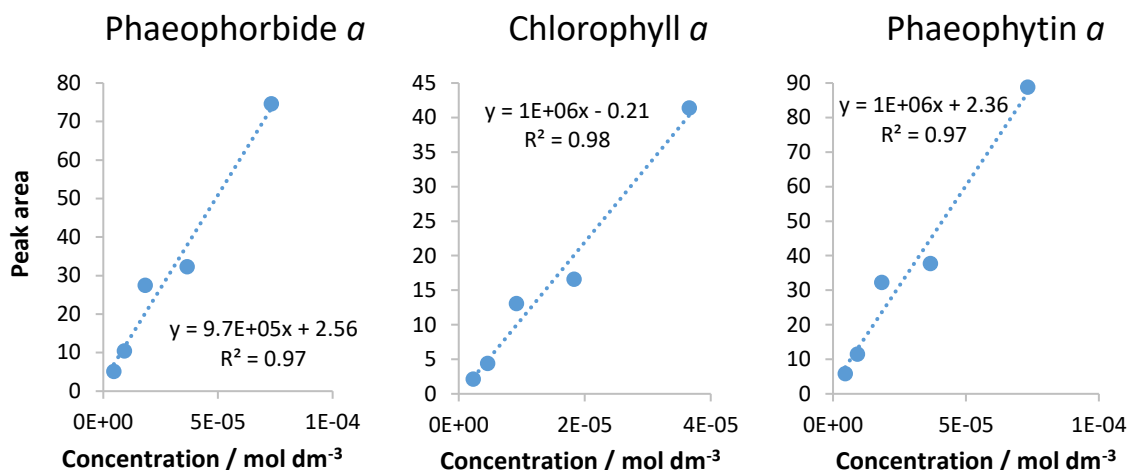


Figure 7.1. Calibration curves used for calculating chlorophyll pigment amount. From left to right: phaeophorbide *a*, chlorophyll *a* and phaeophytin *a*.

Yields of chlorophyll *a*, phaeophytin *a* and phaeophorbide *a* were calculated from calibration curves for the pure standards. The yields of pyropheophytin *a*, hydroxyphaeophytin *a* and pyropheophorbide *a* steryl chlorin esters (SCEs) were calculated via the molar response from the calibration curve for phaeophytin *a*. Pyropheophorbide *a* and the diastereomeric chlorophyllones were estimated via the molar response from the calibration curve for phaeophorbide *a*. The yields of chlorophyll *b* and bacteriochlorophyll *a* were calculated by correcting the standard chlorophyll *a* calibration curve using published absorption coefficients for the red absorption bands of chlorophyll *b* ($\epsilon = 4.76 \times 10^4 \text{ L mol}^{-1} \text{ cm}^{-1}$; Watanabe *et al.*, 1984), bacteriochlorophyll *a* ($\epsilon = 6.93 \times 10^4 \text{ L mol}^{-1} \text{ cm}^{-1}$; Permentier *et al.*, 2000) to compute correction factors for the Soret band absorption coefficients. Phaeophytin *b*, pyropheophytin *b*, bacteriophaeophytin *a* and pyrobacteriophaeophytin *a* were similarly quantified by correcting the calibration curve for phaeophytin *a* using the molar absorption coefficients phaeophytin *b* ($\epsilon = 2.93 \times 10^4 \text{ L mol}^{-1} \text{ cm}^{-1}$; Watanabe *et al.*, 1984) and bacteriophaeophytin *a* ($\epsilon = 4.75 \times 10^4 \text{ L mol}^{-1} \text{ cm}^{-1}$; Straley *et al.*, 1973). Pigment yield was calculated with the equation below (Equation 7.1):

$$\text{Amount of pigment} = \frac{\frac{\text{peak area}}{\text{gradient}} \times \text{sample volume} \times \text{MW of pigment}}{\text{mass of sediment extracted}}$$

Equation 7.1

7.5.2. Standard *n*-alkanes

A mixture of *n*-alkanes *n*-C₂₄, *n*-C₂₈, *n*-C₃₆, *n*-C₃₂ or *n*-C₃₈, and *n*-C₃₄ or *n*-C₃₈ was prepared with each hydrocarbon having a concentration of 0.5 or 1 mg mL⁻¹. The starting concentration was diluted to obtain the following dilutions: 80%, 60%, 40%, 20% of the starting composition (Figure 7.2).

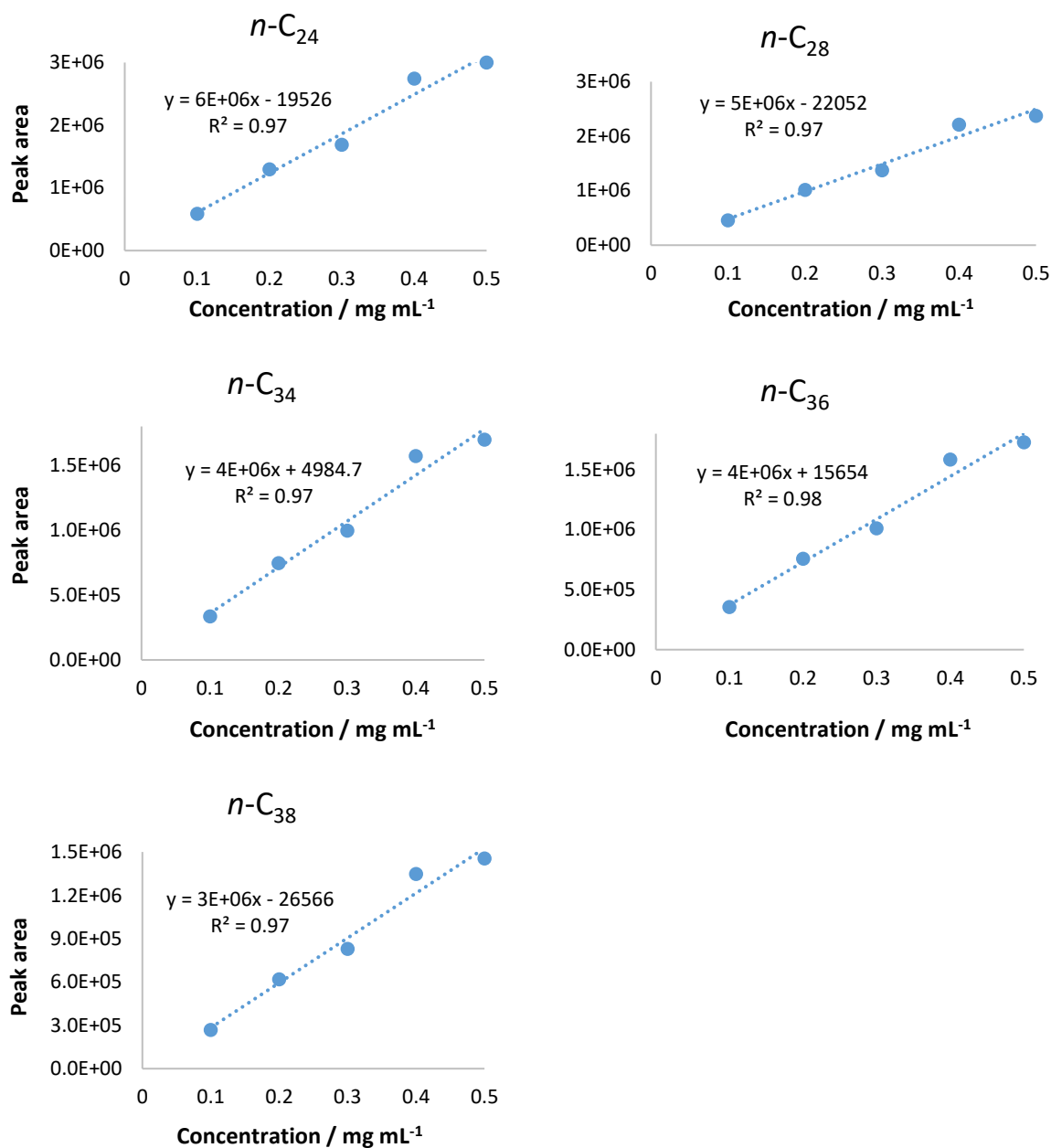


Figure 7.2. Calibration curve for calculating the concentration of lipids: *n*-C₂₄, *n*-C₂₈, *n*-C₃₄, *n*-C₃₆, *n*-C₃₈.

The resulting 5 point calibration curves were applied to polar and apolar lipids analysed by GC-FID. Depending on the retention time of the lipids, the most appropriate *n*-alkane calibration was applied. Lipid yield was calculated using Equation 7.2:

$$\text{Amount of lipids} = \frac{\frac{\text{peak area}}{\text{gradient}} \times \text{sample volume}}{\text{mass of sediment extracted}}$$

Equation 7.2

Appendices

Appendix 1. Definitions of terms and additional information relevant to their application in this work

This appendix aims to give definitions and brief information on specialist terms that may not be familiar to chemists and non-chemists. The terms in this appendix are underlined in the main body of text and only the first time that each term is used.

A

Aerobic: relating to, involving or requiring the presence of oxygen O₂.

Algae: a non-flowering typically aquatic plant.

Allochthonous: formed at a distance from the current position.

Amino acid racemisation (AAR) dating: dating technique based on the ratio of racemising amino acids from carbonate shells, tooth enamel, coral, ostrich eggshell, foraminifera (Kaufman, 2006; Kaufman *et al.*, 2008; Penkman *et al.*, 2008; 2013; Crisp *et al.*, 2013; Tomiak *et al.*, 2013; Dickinson *et al.*, 2019). Upon death of the organism, the amino acids in the L-configuration convert (racemise) over long periods of time (thousands to millions of years) to the D-configuration, ultimately reaching a D/L of 1 (Penkman, 2010). Ratios D/L correspond to age when compared to sites with independent dating (Penkman, 2010; Penkman *et al.*, 2011).

Anaerobic: environment without oxygen in the form of O₂ but various oxidised inorganic compounds are present (NO₃⁻, SO₄²⁻).

Anoxic: absence of oxygen.

Anoxygenic: see Photosynthesis.

Archaea: organisms with prokaryotic cells (Figure A1.1; Woese *et al.*, 1990). Archaea include Euryarchaeota from which Crenarchaeota, Korarchaeota and Thaumarchaeota are rooted (Raymann *et al.*, 2015). Their membrane contains isoprenoid glycerol diether and diglycerol tetraether lipids (Schouten *et al.*, 2013).

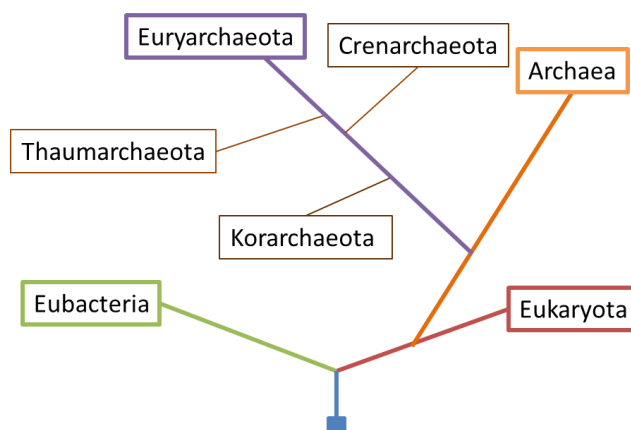


Figure A1.1. Phylogenetic tree of living organisms: the three main domains, Eubacteria, Eukaryota and Archaea; the separation of the Archaea into the major phyla, Korarchaeota, Euryarchaeota and Crenarchaeota showing the Thaumarchaeota strain (adapted from Raymann *et al.*, 2015).

Atmospheric pressure chemical ionisation (APCI): the heated vaporiser tube nebulises the liquid sample. Following a complex chain of reactions, the sample is ionised by electrons, emitted from a corona pin (<10 eV; Figure A1.2). Ionisation is carried out at atmospheric pressure to increase the collisions between the carrier gas (N₂) and the sample to form ions. The ionised sample is transported to the mass spectrometer for detection (Murray *et al.*, 2013). APCI can be interfaced with HPLC.

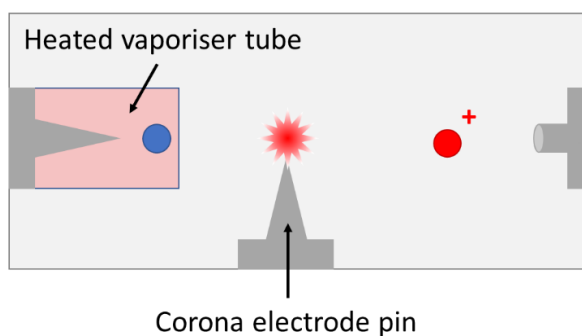


Figure A1.2. Ionisation of the sample in APCI (redrawn from Chromacademy_APCI).

Autochthonous: formed in its current position.

B

Bacteria: also called eubacteria, are microscopic prokaryotic unicellular organisms that live in almost every environment on Earth (Figure A1.1).

Base peak: in mass spectrometry, the peak that has the greatest intensity (Murray *et al.*, 2013).

Biomarker: molecule that can be unambiguously linked to biological precursors.

Bølling-Allerød: an interstadial warming event that occurred in Europe approx. 14,500 years ago and lasted until approx. 12,700 years ago (Lowe and Walker, 2015).

Brown algae: marine algae that perform oxygenic photosynthesis with major chlorophylls *a* and *c*.

Brown sulfur bacteria (strands of *Chlorobiaceae*): bacteria performing anoxygenic photosynthesis in anaerobic conditions (H₂S, CO₂). The brown species synthesise bacteriochlorophyll *e* (Pfennig, 1977).

C

Chemocline: in a body of water, it represents the boundary between surface and deeper waters that have very different water chemistries. A chemocline can separate surface oxic waters from deeper anoxic waters.

***Chlorobiaceae*:** anaerobic bacteria performing anoxygenic photosynthesis.

Chrysophyta: also called golden algae that live in freshwater environments. Most species are photosynthetic producing chlorophyll *c* as their main pigment.

Coccolithophores: unicellular haptophyte algae that secrete calcite platelets called coccoliths. The majority of coccolithophores live in marine water, but few species have been found in freshwater and brackish environments. Coccolithophore distribution is governed by salinity, light and temperature (Lowe and Walker, 2015).

Crenarchaeota: Archaea living in marine environments, hot springs and deep sea hydrothermal vents (Figure A1.1).

Croll-Milankovitch Hypothesis: the hypothesis suggests that Earth's orbital forcing (eccentricity, axial tilt and precession; Figure A1.3) affects the amount of solar intensity that reaches the Earth's surface thus driving Quaternary glacial-interglacial cycles (Lowe and Walker, 2015).

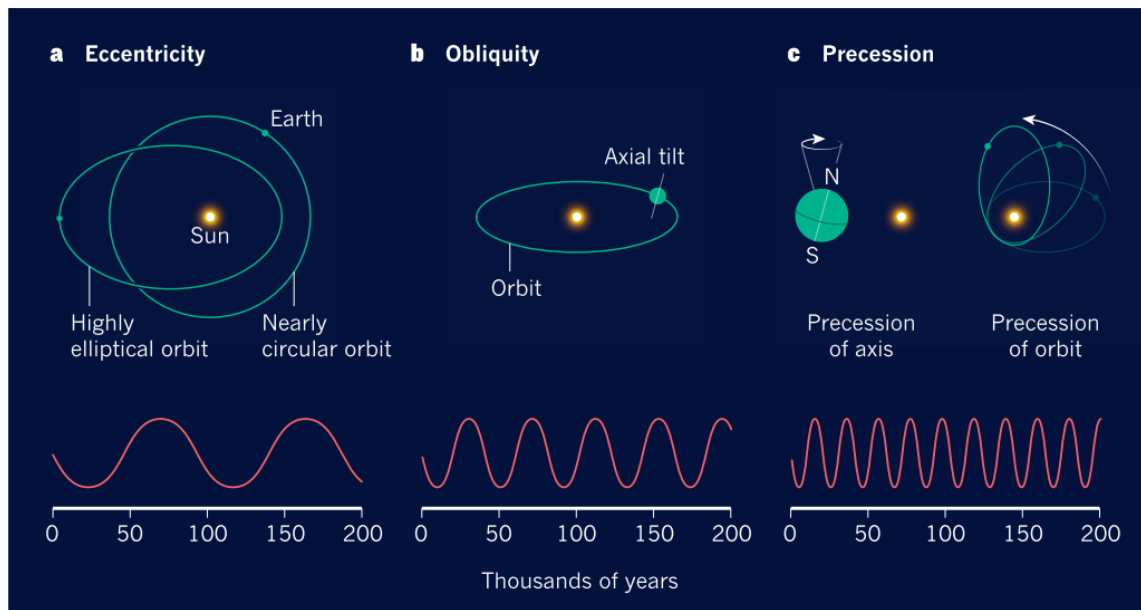


Figure A1.3. Depiction of the three factors that control Quaternary glacial-interglacial cycles according to the Croll-Milankovitch Hypothesis: a) eccentricity; b) obliquity; c) precession (from Maslin, 2016).

Cryptophytes: group of algae common in freshwater but also marine and brackish environments. They perform oxygenic photosynthesis with the aid of chlorophylls *a* and *c* pigments (Scheer, 1991).

Cyanobacteria: prokaryotes performing oxygenic photosynthesis with the aid of chlorophyll *a* (Pfennig, 1977; Scheer, 1991). They can live in almost every terrestrial and aquatic environment.

D

Diatom: unicellular microalgae living in aquatic environments. Diatoms have cell walls made of silica and most diatoms perform oxygenic photosynthesis (Shennan *et al.*, 2015).

Dinoflagellate: unicellular organism classified as plankton with two flagella. Most dinoflagellates live in marine environments but are also common in freshwater lakes, rivers and bogs. They perform oxygenic photosynthesis with chlorophylls *a* and *c* as the dominant pigments (Killops and Killops, 1993).

Diode array detector (DAD): diode array detection can provide detection at a range or single wavelength in the ultraviolet (UV) and visible (vis) light spectrum (UV-vis). For signal response, the sample needs to absorb in the UV-vis region (190-850 nm). The radiation from the UV and vis lamps is guided into the detector flow cell where the sample absorbs it. The transmitted light is dispensed by the diffraction grating and the light intensity is estimated and converted into a signal (Figure

A1.4; Chromacademy_HPLC detectors). When coupled to HPLC, the output is a chromatogram of all the molecules that have been separated by HPLC and absorb in the UV-vis spectrum (Figure A1.5).

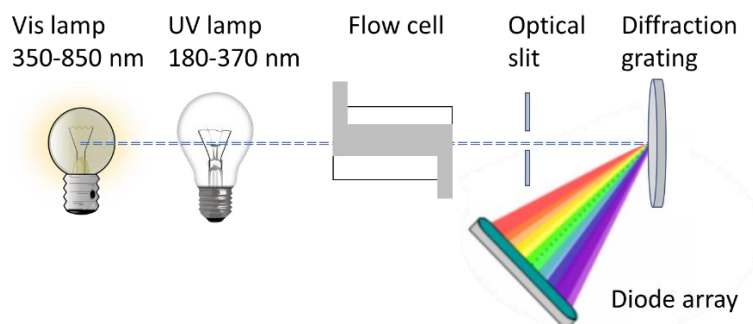


Figure A1.4. Schematic diagram of a diode array detector (redrawn from Chromacademy_HPLC detectors).

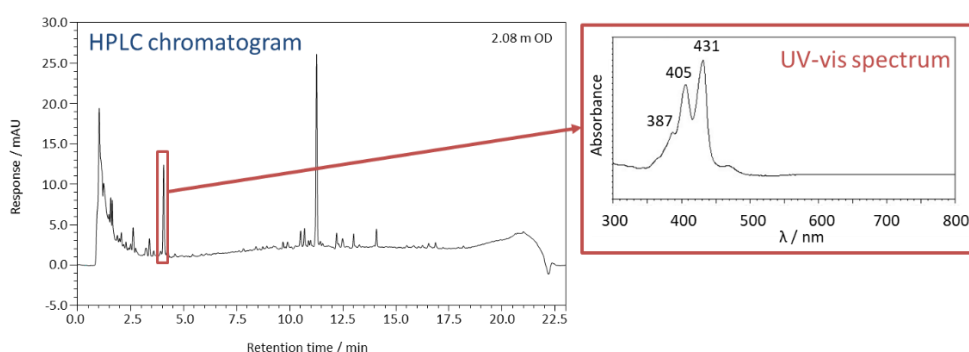


Figure A1.5. HPLC-DAD chromatogram of a sample containing compounds that absorb in the UV-vis range. Each peak has a specific UV-vis spectrum (right).

E

Electron ionisation (EI): in EI, one or more electrons are removed from an atom or molecule through interactions with high-energy accelerated electrons (10-150 eV; Murray *et al.*, 2013). The results of EI are molecular ions that are analysed by mass spectrometry.

Electrospray ionisation (ESI): a low voltage (<10 eV) is applied to the electrospray needle resulting in anion or cation formation (depending on the negative or positive ionisation mode; Murray *et al.*, 2013). The charged particles are transferred to the mass spectrometer for analysis (Figure A1.6). ESI is usually interfaced with HPLC.

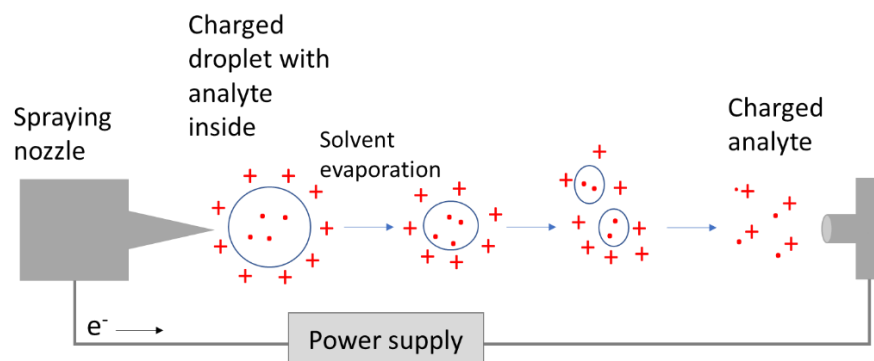


Figure A1.6. Schematic representation of the electrospray ionisation process (redrawn from Banerjee and Muzumdar, 2012).

***Emiliana huxleyi*:** haptophyte coccolithophore common in marine environments.

Euryarchaeota: Archaea, many of which are extremophiles, that inhabit salty aquatic environments and hot springs.

Eustigmatophyceae: group of freshwater and marine algae that are the producers of diols and ketols (Versteegh *et al.*, 1997; Volkman *et al.*, 1998; 1999).

F

Flame ionisation detector (FID): usually combined with gas chromatography (GC), the samples separated by GC are directed into an air / hydrogen flame. The flame ionises most organic compounds and the current produced by collecting these charge carriers is converted into the signal detected (Figure A1.7; Skoog *et al.*, 2004).

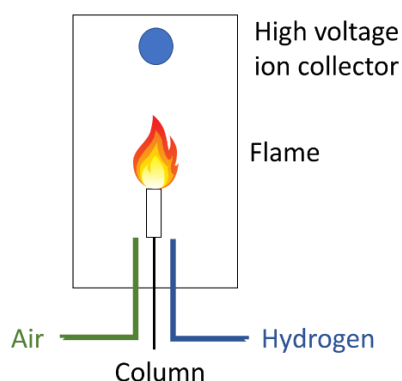


Figure A1.7. Schematic of the flame ionisation detection process .

Fluorescence: absorption of photon energy results in the molecule going into its excited state. Upon returning to the ground state, the photon energy is released as fluorescence. Because of the fluorescence mechanism, the absorption energy is of higher intensity than the emission, meaning that the absorption wavelength is always lower (higher energy) than the emission wavelength. A molecule that emits fluorescent radiation upon relaxation contains aromatic rings; few aliphatic carbonyl and conjugated double bond structures fluoresce (Skoog *et al.*, 2004). Fluorescence is measured with a fluorescent detector.

Fluorescent detector (FLD): it takes advantage of the fluorophore on molecules. A xenon lamp emits light (200-900 nm). The monochromator, set to a specific excitation wavelength, selects that wavelength to excite the sample into the flow cell. The emission monochromator reflects the emitted light. The detector records the absorption signal of the sample at the emission wavelength resulting in a fluorescent spectrum (Figure A1.8; Chromacademy_HPLC detectors).

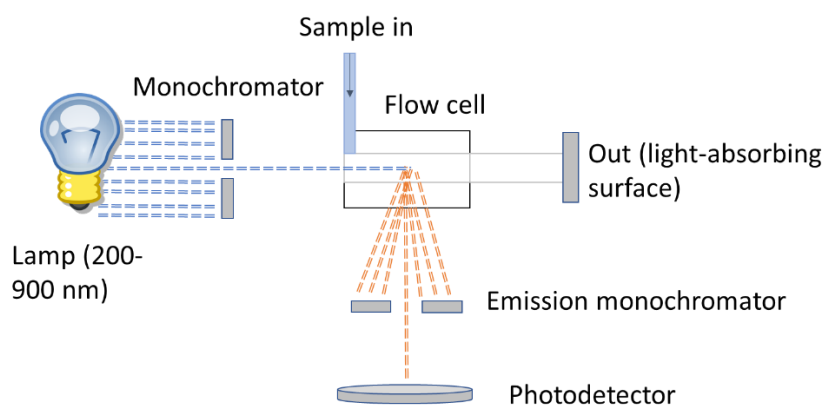


Figure A1.8. Scheme of the general principles of fluorescent detector.

Foraminifera: marine protozoa that secrete a calcareous shell. They can be benthic, inhabiting deep sea waters and seafloor sediments, or planktonic, found at various depths of the sea water column.

Fragment ion: in MS, it is the product ion from dissociation of a precursor ion or protonated molecule (Murray *et al.*, 2013).

G

Gas chromatography (GC): type of chromatography to separate volatile and thermally stable compounds that can be vaporised at high temperatures. The stationary phase of GC is a long column (5-60 m long) of bonded functional groups that vary in polarity according to the analytes

that need to be separated. The mobile phase is a gas, usually hydrogen or helium. After injection at high temperatures, the sample is vaporised and introduced into the column stored in an oven. The temperature of the oven, the partition between the stationary phase and the sample and the sample's boiling point dictates the retention time (Figure A1.9; Chromacademy_Theory and instrumentation of GC Introduction). The separated compounds are transferred to a detector; the most commonly used are flame ionisation detection and mass spectrometry.

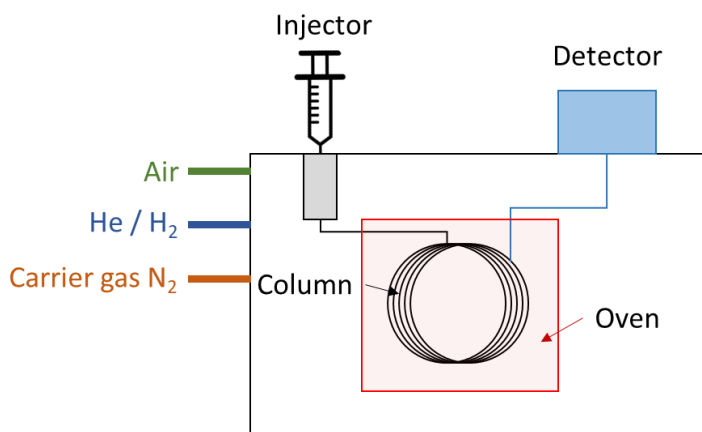


Figure A1.9. Schematic representation of gas chromatograph.

Gastropod: class of organisms of the mollusc phylum. They include snails and slugs from marine, freshwater and terrestrial environment. A calcitic operculum seals the aperture of the shell.

Glacial: relating to ice age.

Glacio-eustasy: ice-cap melting / development resulting in sea-level rise / fall.

Green algae: aquatic algae performing oxygenic photosynthesis through chlorophyll *a* and *b*, the latter in lower amounts.

Green sulfur bacteria (strand of *Chlorobiaceae*): bacteria performing anoxygenic photosynthesis under anaerobic conditions (H_2S , CO_2). They synthesise bacteriochlorophyll *c* or *d* (Pfennig, 1977).

H

Haptophyte (algae): photosynthetic algae, primarily unicellular. The majority of haptophyte algae live in oceans. Coccolithophores are haptophytes.

Herbivores: animals that get energy from eating plants.

Heterotrophs: organisms that consume organic matter produced by primary producers to gain energy. Heterotrophs span from herbivores, the first link in the grazing food chain, to carnivores, occupying the top of the food chain (Killops and Killops, 1993).

High-performance liquid chromatography (HPLC): chromatography technique that separates compounds in the liquid phase. HPLC is applicable to thermally unstable compounds and with varying polarity and volatility. The stationary phase is a packed column with small sized particles that interact with the sample dictating the elution order. The mobile phase is made of organic and / or aqueous solvents that are delivered by a pump at adjustable flow rates and percentage of each solvent; in HPLC the pressure delivered to the column reaches a maximum of 400-600 bar, depending on instruments (Figure A1.10). The interaction between the sample, the mobile phase and the stationary phase dictates the separation of compounds (Skoog *et al.*, 2004). The separated compounds are detected by UV-vis, diode array detector, fluorescence detector or mass spectrometry, among others.

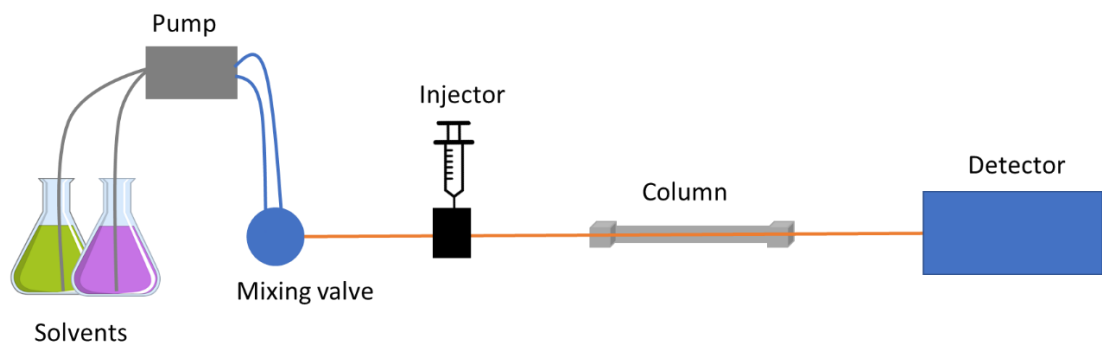


Figure A1.10. Schematic diagram of high-performance liquid chromatography.

Higher plants: vascular land plants with vascular tissue.

Holocene: part of the Quaternary period, the Holocene is the current epoch that started 11,700 years ago (IUGS, 2020).

I

***In situ*:** in the original place.

***In vitro*:** taking place in a culture dish or test tube, outside the living organism

***In vivo*:** in the living place.

Interglacial: a period of mild and warmer climate compared to glacial periods.

***Isochrysis* (sp.):** genus of haptophytes.

Isostasy: fluctuations in sea level due to the uplift and depression of land masses after melting and accumulation of ice caps, respectively (Lowe and Walker, 2015).

L

Last glacial maximum (LGM): or MIS 2, it is the glacial period spanning from 26,000 to 20,000 years ago in which sea levels were lowest and maximum extent of ice sheets was reached worldwide (Murray-Wallace and Woodroffe, 2014). The LGM is part of the last glacial period (120,000 to 11,700 years ago) and is followed by the Holocene interglacial.

M

Macrofossil: a fossil large enough that can be identified without the use of a microscope.

Macrophyte: aquatic plants living in marine and freshwater environments. Emergent macrophytes grow in water but emerge above the water level for more efficient photosynthesis (e.g. reeds). Floating macrophytes are rooted in the sediment beneath water with the leaves exposed to air (e.g. water lily). Submerged macrophytes grow completely underwater (e.g. hornwort).

Magnetic susceptibility: defined as “magnetisability”, it measures the degree to which a material can be magnetised. Magnetic susceptibility reflects production or concentration of magnetic minerals (Lowe and Walker, 2015).

Mass spectrometer: instrument that measures the m/z values and abundances of ions formed in the gas-phase (Murray *et al.*, 2013).

Mass spectrometry (MS): study of molecules through the formation of gas-phase ions. Their mass, charge, structure and / or physicochemical properties are studied using a mass spectrometer (Murray *et al.*, 2013).

***Methanothermobacter thermoautotrophicus* (MTH)ΔH:** thermophilic methanogenic Archaea.

Microbe: microscopic organisms that are too small to be visible to the naked eye and require a microscope to be observed.

Microbial mat: horizontal stratification of different microbial organisms, mainly bacteria and Archaea (Stal, 2001).

Microfossil: fossil of small size that is visible only under a microscope.

Molecular fossil: organic compound in sediment that can be related to its precursors in present sources. Molecular fossils that can trace particular organisms or processes because they undergo little transformations prior to sedimentation are called biomarkers (Philp and Lewis, 1987; Castañeda and Schouten, 2011).

Molecular ion: in mass spectrometry, ion formed by the removal of one or more electrons from a molecule (Murray *et al.*, 2013). Molecular ions are formed in hard ionisation techniques such as EI-MS.

Mollusc: invertebrates that possess a hard calcitic shell or exoskeleton (Lowe and Walker, 2015).

***m/z*:** formerly mass-to-charge ratio, it represents the ratio of the mass of an ion over its charge number in mass spectrometry (Murray *et al.*, 2013).

N

Normal phase (in chromatography): it indicates a type of chromatography in which the stationary phase is polar (CN, NH₃) and the mobile phase consists of apolar solvents (hexane, propanol). In normal phase, more polar analytes are retained longer than less polar analytes, thus the former elute first (Skoog *et al.*, 2004).

O

Operculum: a lid that closes the aperture of many gastropod shells. This is a feature common in marine gastropods, less common in freshwater gastropods and rare in terrestrial gastropods (Beedham, 1972).

Ostracod: organism of the Crustacea class that secretes a bivalve carbonate exoskeleton. Ostracods inhabit most aquatic environments with a wide range of salinities and temperatures (Lowe and Walker, 2015).

Oxic: oxygen-rich.

Oxygenic: see Photosynthesis.

P

Photic zone: also called euphotic zone, it is the surface of the water where photosynthesis readily occurs (Didyk *et al.*, 1978).

Photoautotrophs: organisms that produce their own organic matter from inorganic species to gain energy by performing photosynthesis.

Photosynthesis: it is the process that reduces CO₂ and water to carbohydrates and oxygen. Photosynthesis occurs in the chloroplasts that contain chlorophylls. Most plants, algae and some bacteria carry out photosynthesis.

Oxygenic photosynthesis: it is performed by higher plants, photosynthetic algae and cyanobacteria (Scheer, 1991). The organisms oxidise water to produce oxygen and carbohydrates (Equation A1.1).



(Equation A1.1)

Anoxygenic photosynthesis: performed by green, brown and purple bacteria, these organisms do not use water as electron donor, but reduced sulfur compounds, molecular hydrogen or organic compounds with lower redox potential than water (Equation A1.2). The organisms depend on anaerobic conditions that allow the presence of these substances (Pfennig, 1977).



(Equation A1.2)

Phytoplankton: microorganisms, usually unicellular, able to carry out photosynthesis. Phytoplankton includes unicellular algae, cyanobacteria, dinoflagellates and photosynthetic bacteria (Killops and Killops, 1993).

Pliocene: epoch in the Quaternary period spanning from 5.33 to 2.58 million years ago (IUGS, 2020).

Pleistocene: epoch in the Quaternary period spanning from 2.58 million years ago to 11,700 years ago (IUGS, 2020).

Precursor ion: in MS, it represents an ion that reacts to form fragment ions (or product ions) or undergoes neutral losses (Murray *et al.*, 2013).

Prochlorophytes: prokaryotic algae that perform oxygenic photosynthesis with the aid of both chlorophyll *a* and chlorophyll *b* (Lewin, 1976).

Product ion: ion formed as a product of fragmentation of the precursor ion (Murray *et al.*, 2013).

Protonated molecule: in mass spectrometry, ion formed by the interaction of a molecule with a proton, represented by [M+H]⁺ (Murray *et al.*, 2013). A protonated molecule is formed in soft ionisation techniques such as APCI and ESI-MS.

Proxy: measures of palaeoenvironmental conditions based on biomarkers.

Purple bacteria: bacteria performing anoxygenic photosynthesis. They synthesise bacteriochlorophyll *a* as their main pigment (Pfennig, 1977).

***Pyrobaculum*:** hyperthermophilic aerobic crenarchaeota.

Q

Quaternary (period): period spanning the last 2.58 million years and also colloquially known as the Ice Age period (Gibbard and Head, 2009).

R

Regression (sea level): decrease in sea level.

Relative (sea-level change): indicates a rise or fall in sea level where the cause cannot be appointed to a change in land or sea or both (Murray-Wallace and Woodroffe, 2014).

Reversed-phase (in chromatography): it indicates a type of chromatography in which the stationary phase is apolar (C_8 , C_{18}) and the mobile phase consists of polar solvents (water, methanol, acetonitrile). In reversed-phase, apolar analytes are retained longer than more polar analytes, thus the former elute first (Skoog *et al.*, 2004).

Reworking (of sediment): change in the properties and structures of the sediment due to animal and / or sedimenturbation. Bioturbation: reworking of sediment by organisms such as grazing. Sedimenturbation: old material mixed into newer sediment.

S

***Sulfolobus acidocaldarius*:** hyperthermophilic aerobic crenarchaeota.

Stratification (of water column): the surface of the water column is called the epipelagic or photic zone, where light penetrates, and photosynthesis occurs. Below this, is the mesopelagic or disphotic zone, with only dim light and no photosynthesis occurring. The bottom water is called aphotic zone where there is complete absence of light, no plant production but only herbivore feeders (Didyk *et al.*, 1978).

Suboxic: transitional zone between oxic and anoxic waters where oxygen concentrations are very low.

T

Taxonomic rank: classification of living and extinct organisms. The classification occurs with a succession of groups forming an inverted pyramid (Figure A1.11).

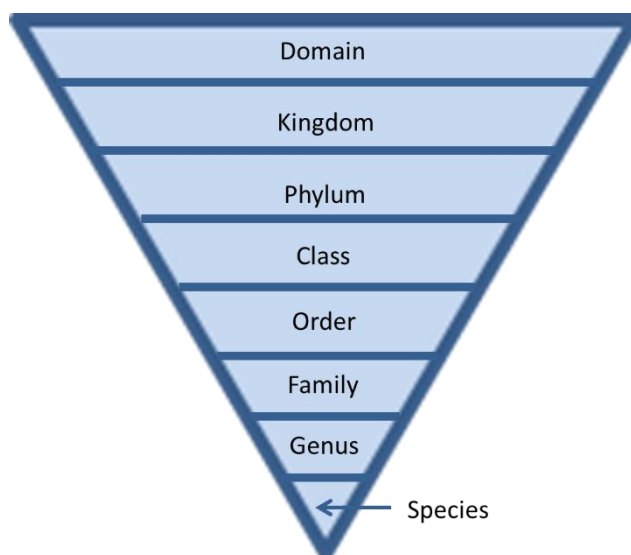


Figure A1.11. Diagram of the taxonomic rank for organisms.

Thaumarchaeota: formerly Group 1 crenarchaeota, it is a phylum of the Archaea domain that includes ammonia-oxidising organisms (Figure A1.1). Thaumarchaeota inhabit marine waters, soils and freshwater sediments (Stieglmeier *et al.*, 2014).

Thin-layer chromatography (TLC): planar chromatography consisting of a thin layer of a polar or apolar stationary phase mounted on a metal surface. The mobile phase (polar or apolar) moves through the stationary phase by capillary action. TLC separates analytes based on their affinity for the stationary and mobile phases (Figure A1.12). The technique is mostly used for monitoring reactions, checking purity and to develop optimal chromatographic conditions for separation by column chromatography and HPLC (Skoog *et al.*, 2004).

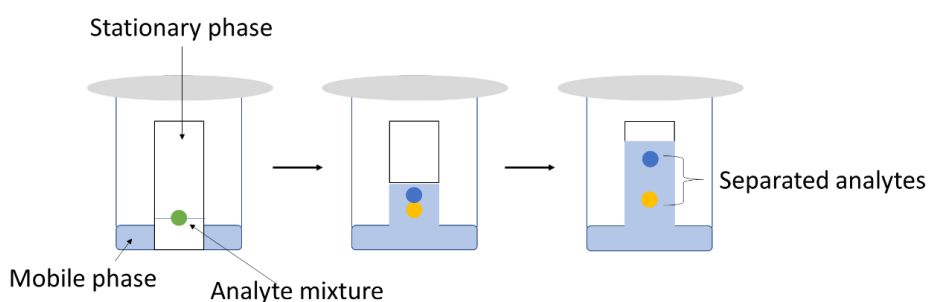


Figure A1.12. Diagram of TLC sequence to separate multiple analytes.

Transgression (sea level): increase in sea level.

U

Ultra-high performance liquid chromatography (UHPLC): similar to HPLC but it uses smaller particles in the stationary phase increasing the pressure of the system, narrowing the peak width and reducing the time of analysis.

UV-vis: UV-vis can provide detection at a single wavelength in the ultraviolet (UV) and visible (vis) light spectrum (UV-vis). For signal response, the sample needs to absorb in the UV-vis region (190-850 nm). The detector comprises UV and vis lamps that emit radiation in the UV-vis spectrum. A monochromator selects a specific wavelength of light to transmit through the sample which absorbs it. The radiation that passes through the sample is detected and the light intensity is converted into a signal (Figure A1.13 Chromacademy_UV-vis). When coupled with HPLC, the output is a chromatogram of all the samples that have been separated by HPLC and absorb the selected UV-vis wavelength.

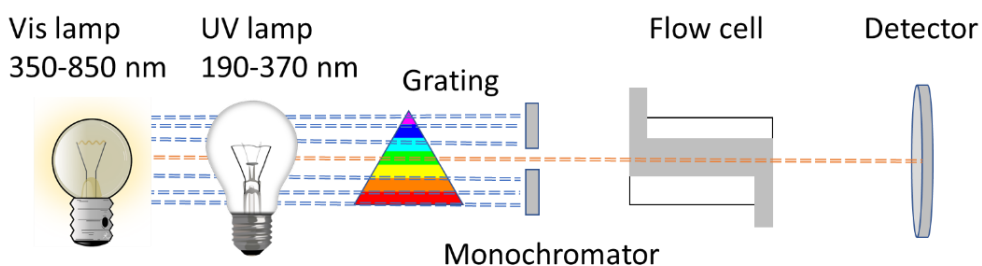


Figure A1.13. Schematic diagram of a UV-vis detector.

W

Waxes (of plants): organic compounds that are secreted by plant cuticles to control evaporation and hydration.

Y

Younger Dryas: cold episode that occurred in northwest Europe during the Pleistocene approximately between 12,800 and 11,500 years ago (Lowe and Walker, 2015).

Z

Zooplankton: plankton living in both fresh and seawater. They are heterotrophs and graze on microscopic suspended particulate matter. Zooplankton includes foraminifera, dinoflagellates, crustaceans, molluscs, among others (Harradine *et al.*, 1996).

Appendix 2. Marine isotope stages and substages of the last 1.05 million years

The following figure is taken from Railsback *et al.* (2015) and represents the marine isotope stages and substages of the last 1.05 Ma based on the $\delta^{18}\text{O}$ record from Lisiecki and Raymo (2005). Odd numbers indicate interglacial and even number are glacial stages; the letters are substages. The roman numerals indicate terminations, i.e. transitions from glacial to interglacial stages.

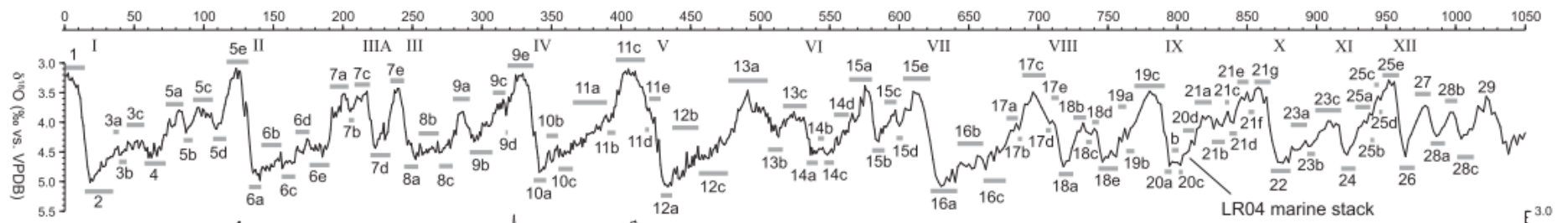


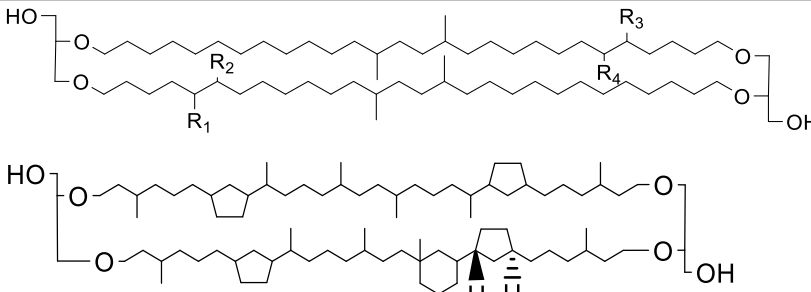
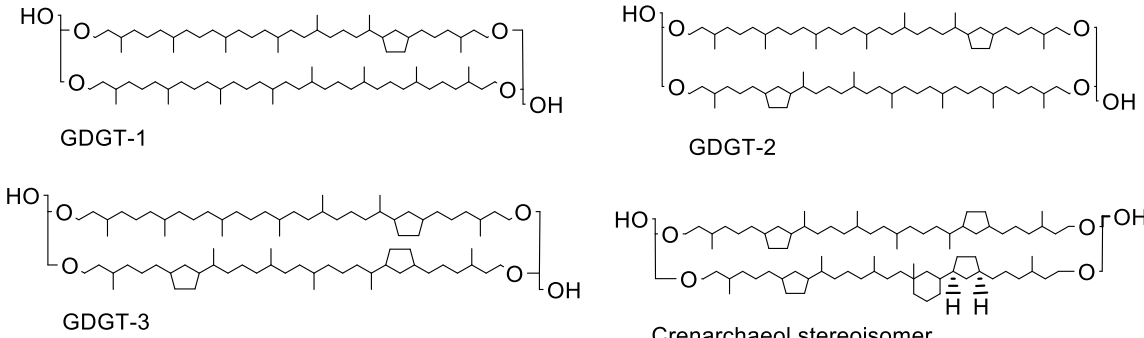
Figure A2.1. Marine isotope stages and substages for the last 1.05 Ma (from Railsback *et al.*, 2015).

Appendix 3. Appendices to Chapter 3

Table A3.1. Lithological and microfossil analysis from Loch of Stenness (Orkney, Scotland) core 2014-1.

Study	Bates <i>et al.</i> , 2016			This study
Depth / cm	Lithology	Ostracods	Foraminifera	Gastropods
0-80	Dark great soft silt. Brackish sedimentary environment with decalcification		Brackish: <i>Miliammina fusca</i> <i>Elphidium williamsoni</i> <i>Haynesina germanica</i>	
81-102	Pale grey silt. Loch with onset tidal access, initially very low brackish	Brackish: <i>Cyprideis torosa</i> Freshwater: <i>Cyclocypris ovum</i> <i>Candona candida</i> <i>Cyclocypris laevis</i> <i>Pseudocandona rostrata</i> <i>Limnocythere inopinata</i> <i>Sarscypridopsis aculeata</i>		Freshwater: <i>Radix balthica</i> <i>Gyraulus crista</i> <i>Gyraulus laevis</i>
104-200	Grey-brown silt. Coastal freshwater loch	Freshwater: <i>Cyclocypris ovum</i> <i>Candona candida</i> <i>Cyclocypris laevis</i> <i>Pseudocandona rostrata</i> <i>Limnocythere inopinata</i>		Freshwater: <i>Radix balthica</i>

Table A3.2. Equations for *n*-alkane-based proxies CPI , P_{aq} and ACL , and GDGT-based proxies BIT , TEX_{86} , TEX_{86}^L , mean summer lake temperature and CBT . Structures of GDGTs discussed in the table are included.

Equation	Reference
$CPI = \frac{1}{2} \left(\frac{C_{25} + C_{27} + C_{29} + C_{31} + C_{33}}{C_{24} + C_{26} + C_{28} + C_{30} + C_{32}} + \frac{C_{25} + C_{27} + C_{29} + C_{31} + C_{33}}{C_{26} + C_{28} + C_{30} + C_{32} + C_{34}} \right)$	Bray and Evans, 1961
$P_{aq} = \frac{(C_{23} + C_{25})}{(C_{23} + C_{25} + C_{29} + C_{31})}$	Ficken <i>et al.</i> , 2000
$ACL = \frac{(27 \times [C_{27}]) + (29 \times [C_{29}]) + (31 \times [C_{31}])}{[C_{27}] + [C_{29}] + [C_{31}]}$	Poynter and Eglinton, 1990
$BIT = \frac{Ia + IIa + IIIa}{Ia + IIa + IIIa + \text{crenarchaeol}}$	Hopmans <i>et al.</i> , 2004
 <p>a br GDGT Ia R1, R2, R3, R4 = H IIa R1= Me; R2, R3, R4 = H IIIa R1, R3= Me; R2, R4 = H</p> <p>Crenarchaeol</p>	
$TEX_{86} = \frac{2 + 3 + \text{crenarchaeol stereoisomer}}{1 + 2 + 3 + \text{crenarchaeol stereoisomer}}$ $\text{Sea surface temperature (SST)} = \left(\frac{TEX_{86}}{0.015} \right) - 0.28$	Schouten <i>et al.</i> , 2002
 <p>GDGT-1</p> <p>GDGT-2</p> <p>GDGT-3</p> <p>Crenarchaeol stereoisomer</p>	
$TEX_{86}^L = \log \frac{2}{1 + 2 + 3}$ $SST = (67.5 \times TEX_{86}^L) + 46.9$	Kim <i>et al.</i> , 2010
$\text{Summer lake T} = 20.9 + (98.1 \times \text{GDGT Ib}) - (12.0 \times \text{GDGT IIa}) - (20.5 \times \text{GDGT IIIa})$	Pearson <i>et al.</i> , 2011
$CBT = -\log \frac{Ib + IIb}{Ia + IIa}$ $pH = 10.32 - (CBT \times 3.03)$	Tierney <i>et al.</i> , 2010

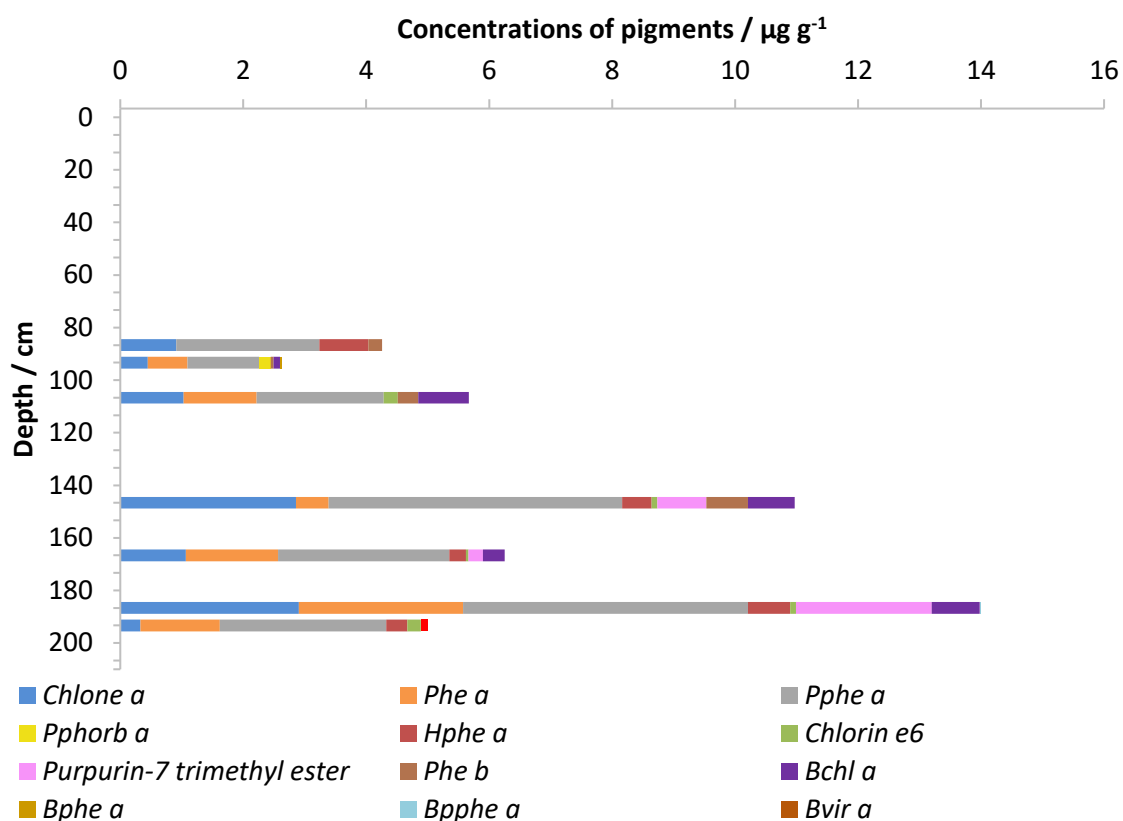
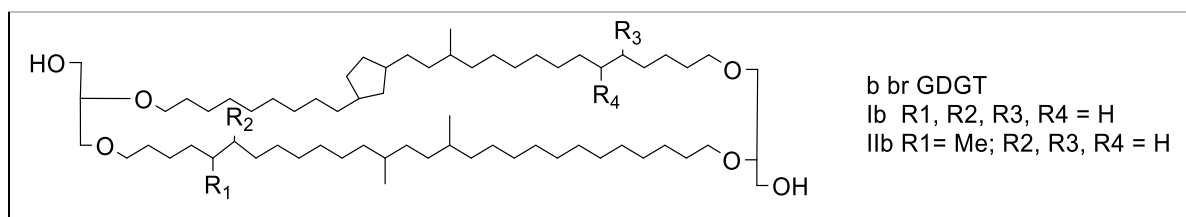


Figure A3.1. Concentrations of chlorophyll pigments in the Loch of Stenness core 2014-1: chlorophyllone (chlone), phaeophytin a (phe a), pyropheophytin a (pphe a), pyropheophorbide a (pphorb a), hydroxyphaeophytin a (hphe a), purpurin-7 trimethyl ester, chlorin e6, phaeophytin b (phe b), bacteriochlorophyll a (bchl a), bacteriopheophytin a (bphe a), pyrobacteriopheophytin a (bpphe a), and bacterioviridin a (bvir a)..

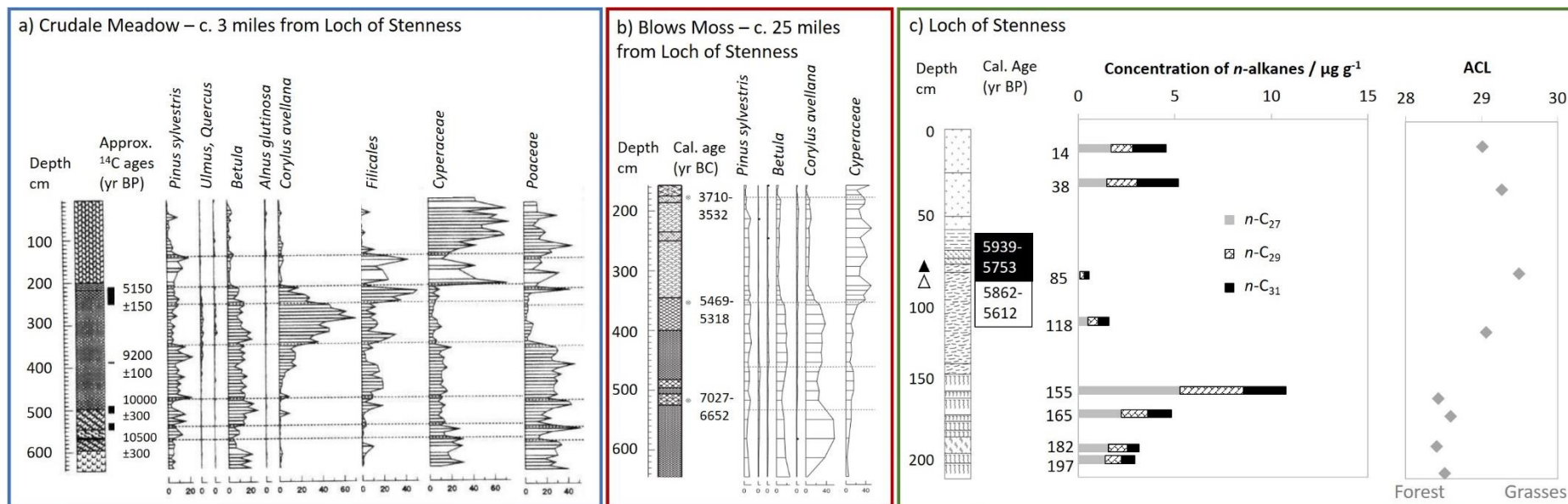


Figure A3.2. Comparison of vegetation changes in three cores from Orkney: a) Crudale Meadow (Bunting, 1994); b) Blows Moss (Farrell et al., 2014); c) Loch of Stenness (this study).

Appendix 4. Appendices to Chapter 4

Appendix 4.1. Chromatogram and table of peaks of chlorophyll pigments from Horse Fen 13-1

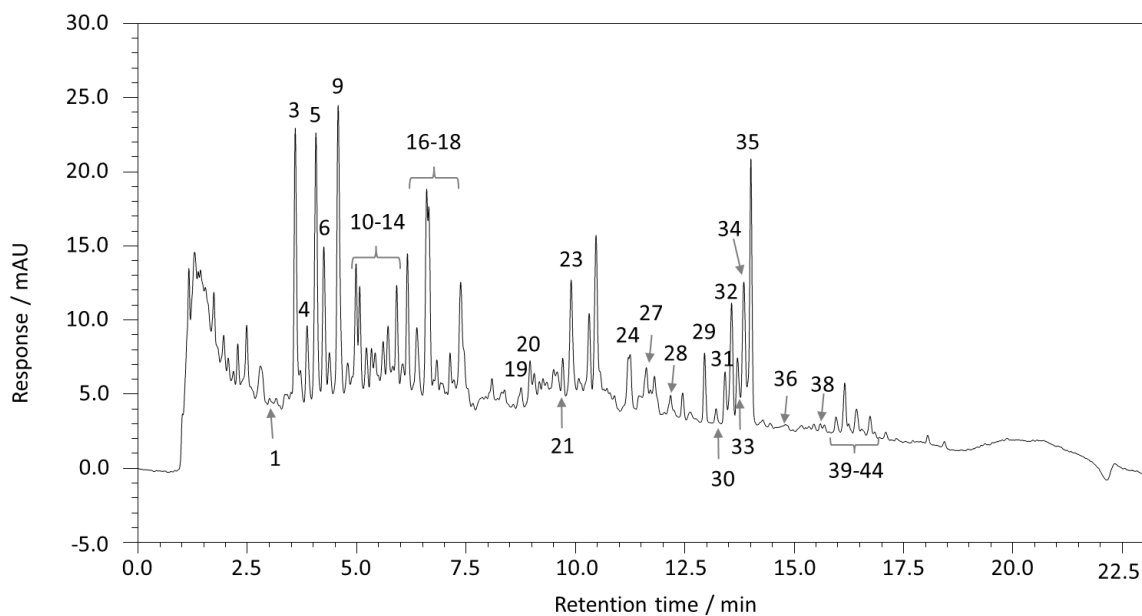


Figure A4.1. UHPLC-DAD chromatogram (300-800 nm) of Horse Fen 13-1 pigments sample -2.26 m OD (9.96 m depth). For peak assignments see Table A4.1

Table A4.1. Assignments of pigments and carotenoids in Horse Fen 13-1 sediments (continued over).

Peak no.	t _R / min	Main UV/vis absorption / nm	[M+H] ⁺ / m/z	Prominent fragment ions / m/z	Assignment	Samples found / m OD
1	3.2	357, 745	533		Unidentified chlorin	-2.26, -2.20
2	3.4	410, 665			Unidentified chlorin	-2.33
3	3.6	387, 406, 431			Carotenoid P7	All
4	3.7	406, 652			Unidentified chlorin	From -2.26 to -0.57
5	3.8	406, 663			Chlorophyllone <i>a</i>	From -2.29 to -0.57
6	4.0	406, 668			Chlorophyllone <i>a</i> epimer	From -2.26 to -0.57
7	4.2	406, 664			Phaeophorbide <i>a</i> methyl ester	-3.03, -2.33, -2.29
8	4.3	409, 665			Phaeophorbide <i>a</i> methyl ester epimer	-3.03, -2.33, -2.29
9	4.6	416, 440, 468			Carotenoid	From -2.26 to -0.57
10	5.1	420, 443, 469			Carotenoid	-2.26, -2.20, -0.57
11	5.3	421, 443, 469			Carotenoid	-2.26, -2.20, -0.57
12	5.7	420, 440, 469			Carotenoid	From -2.26 to -0.57
13	5.9	410, 434, 461			Carotenoid	-2.26, -2.20, -0.57
14	6.2	420, 444, 473			Carotenoid	From -2.26 to -0.57
15	6.6	409, 665			Pyropheophorbide <i>a</i> methyl ester	-3.03, -2.29
16	6.7	445, 471			Carotenoid	From -2.26 to -0.57
17	6.8	442, 464			Carotenoid	-2.26, -2.20

Table A4.1. (continued) Assignments of pigments and carotenoids in Horse Fen 13-1 sediments (continued over).

Peak no.	t _R / min	Main UV/vis absorption / nm	[M+H] ⁺ / m/z	Prominent fragment ions / m/z	Assignment	Samples found / m OD
18	7.1	444, 469			Carotenoid	-2.26, -2.20, -0.57
19	8.9	421, 443, 471			Carotenoid	-2.26, -2.20, -0.57
20	9.1	441, 466			Carotenoid	-2.26, -2.20
21	9.5	357, 748			Pyrobacteriopheophytin <i>a</i>	-2.26, -2.20
22	9.7	418, 438, 469			Carotenoid	-0.57
23	9.9	358, 424, 682			Unidentified chlorin	-3.03, -2.56, from -2.33 to -2.20
24	11.2	357, 746	889	611, 551	Bacteriopheophytin <i>a</i>	From -3.03 to -0.57
25	11.4	359, 747	889	611, 551	Bacteriopheophytin <i>a</i> epimer	-2.20, -0.57
26	11.6	403, 424, 448			Carotenoid	-2.20, -0.57
27	11.7	442, 470			Carotenoid	-2.26
28	12.2	375, 416, 680	887	609, 549	Bacterioviridin <i>a</i>	-2.26
29	12.4	420, 436, 654			Pyropheophytin <i>b</i>	-3.03, from -2.40 to -0.57
30	12.9	408, 664	871		Phaeophytin <i>a</i>	-3.03, -2.56, -2.26, -2.20, -0.57
31	13.4	419, 434, 462			Carotenoid	-2.26, -2.20, -0.57
32	13.6	415, 438, 467			Carotenoid	From -2.26 to -0.57
33	13.7	442, 470			Carotenoid	-2.26, -2.20, -0.57

Table A4.1. (continued) Assignments of pigments and carotenoids in Horse Fen 13-1 sediments.

Peak no.	t _R / min	Main UV/vis absorption / nm	[M+H] ⁺ / m/z	Prominent fragment ions / m/z	Assignment	Samples found / m OD
34	13.8	448, 472	813 917	549	Carotenoid	-2.26, -2.20, -0.57
35	14.0	410, 665			Pyropheophytin <i>a</i>	All
36	14.8	434, 652			Pyropheophorbide <i>b</i> SCE (C _{27:1} sterol)	-2.26, -2.20
37	15.6	410, 665			Pyropheophorbide <i>a</i> SCE	-2.20
38	15.7	409, 665			Pyropheophorbide <i>a</i> SCE	-2.26, -2.20
39	16.0	410, 665			Pyropheophorbide <i>a</i> SCE	-2.26
40	16.2	406, 665			Pyropheophorbide <i>a</i> SCE	From -2.33 to 1.95
41	16.3	410, 665			Pyropheophorbide <i>a</i> SCE	-2.26, -2.20
42	16.5	406, 665			Pyropheophorbide <i>a</i> SCE	From -2.33 to -2.20, -0.57
43	16.6	409, 665			Pyropheophorbide <i>a</i> SCE	-2.26, -2.20
44	16.7	405, 665			Pyropheophorbide <i>a</i> SCE	From -2.33 to -2.20, -0.57
45	16.9	410, 665			Pyropheophorbide <i>a</i> SCE	-0.57

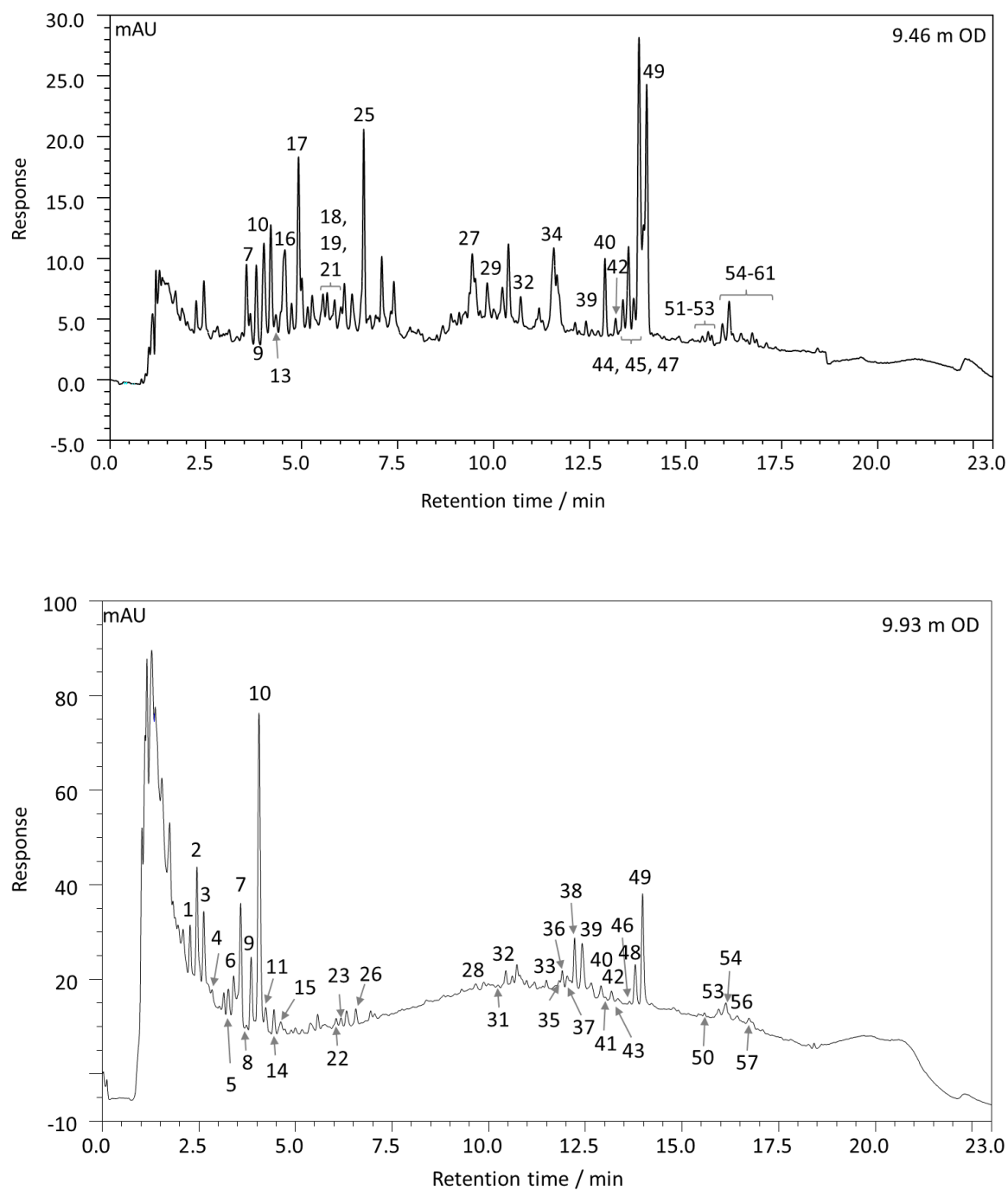
Appendix 4.2. Chromatogram and table of peaks of chlorophyll pigments from Railway Cottage

Figure A4.2. UHPLC-DAD chromatogram (300-800 nm) of Railway Cottage pigments sample 9.46 m OD (5.56 m depth) and 9.93 m OD (5.09 m depth). For peak assignments see Table A4.2.

Table A4.2. Assignments of pigments and carotenoids in Railway Cottage sediments (continued over).

Peak no.	t _R / min	Main UV/vis absorption / nm	[M+H] ⁺ / m/z	Prominent fragment ions / m/z	Assignment	Samples found / m OD
1	2.1	436, 654			Unidentified chlorin <i>b</i>	9.93
2	2.3	421, 666			Unidentified chlorin <i>a</i>	9.93
3	2.5	425, 653			Chlorophyllone <i>b</i>	9.93
4	2.6	434, 649			Chlorophyllone <i>b</i> epimer	9.93
5	3.3	406, 695			Unidentified purpurin	9.93
6	3.4	410, 665			Unidentified chlorin <i>a</i>	9.93
7	3.6	387, 405, 431			Carotenoid P7	All
8	3.7	406, 670			Unidentified chlorin <i>a</i>	8.74
9	3.8	404, 654	535	517, 507, 491	Chlorophyllone without unsaturation?	9.46, 9.93, 10.07
10	4.0	409, 663	535	515, 505, 489	Chlorophyllone <i>a</i>	All
11	4.2	409, 669	535	515, 505, 489	Chlorophyllone <i>a</i> epimer	8.74, 9.93, 10.07
12	4.3	425, 441, 470			Carotenoid	8.74
13	4.3	408, 430, 442			Carotenoid	9.46
14	4.4	409, 664			Phaeophorbide <i>a</i> methyl ester	9.93
15	4.6	435, 649			Unidentified chlorin <i>b</i>	9.93
16	4.6	447, 471			Carotenoid	9.46
17	5.0	420, 442, 469			Carotenoid	9.46

Table A4.2. (continued) Assignments of pigments and carotenoids in Railway Cottage sediments (continued over).

Peak no.	t _R / min	Main UV/vis absorption / nm	[M+H] ⁺ / m/z	Prominent fragment ions / m/z	Assignment	Samples found / m OD
18	5.7	419, 441, 469	889	611, 551	Carotenoid	9.46
19	5.9	434, 460			Carotenoid	9.46
20	6.0	428, 446, 474			Carotenoid	8.74
21	6.1	418, 445, 473			Carotenoid	9.46
22	6.1	410, 670			Unidentified purpurin	9.93
23	6.3	410, 665			Pyropheophorbide <i>a</i> methyl ester	9.93
24	6.5	425, 447, 473			Carotenoid	8.74
25	6.6	418, 447, 472			Carotenoid	9.46
26	6.6	410, 665			Pyropheophorbide <i>a</i> methyl ester epimer	9.93
27	9.4	355, 410, 675			Unidentified chlorin	9.46
28	9.7	357, 752			Pyrobacteriopheophytin <i>a</i>	9.93
29	9.8	359, 424, 685			Unidentified chlorin	9.46
30	10.4	358, 681, 748			Unidentified bacteriochlorin	9.93
31	10.7	411, 663			Unidentified chlorin	9.46
32	10.8	359, 748			Bacteriopheophytin <i>a</i>	All
33	11.5	417, 435, 654			Phaeophytin b	9.93, 10.07

Table A4.2. (continued) Assignments of pigments and carotenoids in Railway Cottage sediments (continued over).

Peak no.	t _R / min	Main UV/vis absorption / nm	[M+H] ⁺ / m/z	Prominent fragment ions / m/z	Assignment	Samples found / m OD
34	11.6	426, 449			Carotenoid	9.46
35	11.8	397, 427, 657			Unidentified chlorin <i>b</i>	9.93
36	11.9	407, 665			Hydroxyphaeophytin <i>a</i>	9.93
37	12.0	436, 655			Unidentified chlorin <i>b</i>	9.93
38	12.2	406, 665			Unidentified chlorin <i>a</i>	9.93
39	12.4	412, 434, 654	827	549, 521	Pyrophaeophytin <i>b</i>	All
40	12.9	408, 664	871	853, 593, 533	Phaeophytin <i>a</i>	All
41	13.0	427, 655			Unidentified chlorin <i>b</i>	9.93
42	13.2	407, 665			Phaeophytin <i>a</i> epimer	9.46, 9.93, 10.07
43	13.3	408, 690			Unidentified purpurin	9.93
44	13.4	412, 434, 463			Carotenoid	8.74, 9.46
45	13.5	415, 438, 467			Carotenoid	8.74, 9.46
46	13.6	410, 663			Unidentified chlorin	9.93
47	13.7	415, 444, 471			Carotenoid	9.46
48	13.8	408, 665	855	839, 589	Unidentified chlorin	9.93
49	14.0	409, 665	813	535	Pyrophaeophytin <i>a</i>	All

Table A4.2. (continued) Assignments of pigments and carotenoids in Railway Cottage sediments.

Peak no.	t _R / min	Main UV/vis absorption / nm	[M+H] ⁺ / m/z	Prominent fragment ions / m/z	Assignment	Samples found / m OD
50	15.4	434, 660			Pyropheophorbide <i>b</i> SCE	9.93
51	15.6	408, 665			Pyropheophorbide <i>a</i> SCE	8.74, 9.46
52	15.7	408, 665			Pyropheophorbide <i>a</i> SCE	8.74, 9.46
53	15.9	411, 665	903	535	Pyropheophorbide <i>a</i> SCE (C _{27:1} sterol)	All
54	16.1	410, 665	929	535	Pyropheophorbide <i>a</i> SCE (C _{29:2} sterol)	All
55	16.2	408, 665			Pyropheophorbide <i>a</i> SCE	9.46, 10.07
56	16.4	406, 665	931	535	Pyropheophorbide <i>a</i> SCE (C _{29:1} sterol)	9.46, 9.93, 10.07
57	16.5	408, 665			Pyropheophorbide <i>a</i> SCE	9.46
58	16.6	403, 665			Pyropheophorbide <i>a</i> SCE	8.74, 9.46
59	16.7	411, 665	933	535	Pyropheophorbide <i>a</i> SCE (C _{29:0} sterol)	8.74, 9.46, 9.93
60	16.8	410, 665	948	535	Pyropheophorbide <i>a</i> SCE (C _{30:0} sterol)	8.74, 9.46
61	17.1	408, 665	946	535	Pyropheophorbide <i>a</i> SCE (C _{30:1} sterol)	8.74, 9.46

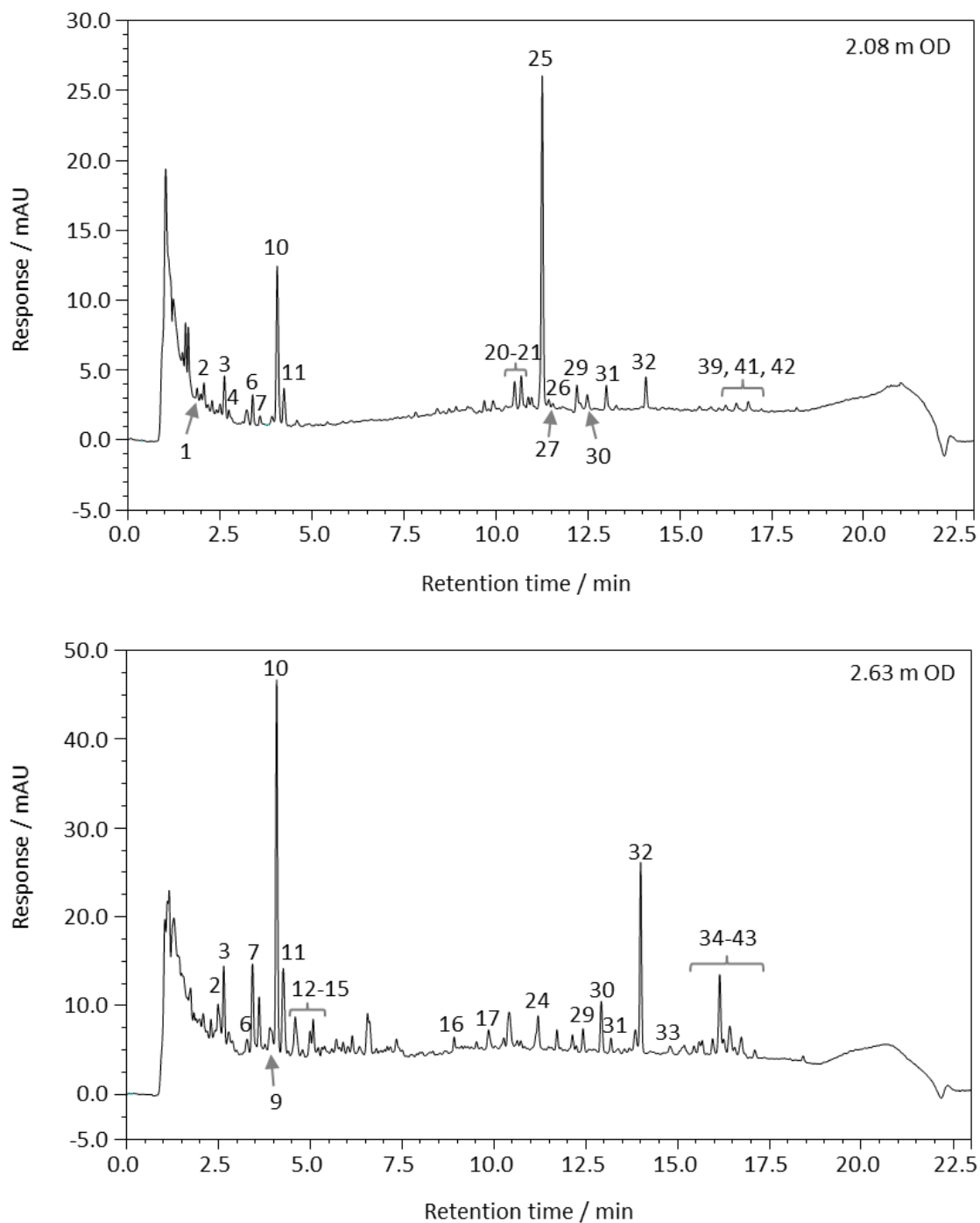
Appendix 4.3. Chromatogram and table of peaks of chlorophyll pigments from Tottenhill Quarry

Figure A4.3. UHPLC-DAD chromatogram (300-800 nm) of Tottenhill Quarry pigments sample 2.08 m OD (0.90 m depth) and 2.63 m OD (0.35 m depth). For peak assignments see Table A4.3.

Table A4.3. Assignments of pigments and carotenoids in Tottenhill Quarry sediments (continued over).

Peak no.	t _R / min	Main UV/vis absorption / nm	[M+H] ⁺ / m/z	Prominent fragment ions / m/z	Assignment	Samples found / m OD
1	1.9	408, 675	600	583, 487	Unidentified chlorin	2.08
2	2.1	437, 655			Unidentified chlorin	2.08, 2.44, 2.63
3	2.7	434, 650	547	529, 519, 503	Chlorophyllone <i>b</i>	2.08, 2.44, 2.63
4	2.8	434, 655			Chlorophyllone <i>b</i> epimer	2.08
5	3.2	405, 675			Unidentified chlorin	2.44
6	3.4	406, 666			Unidentified chlorin	2.08, 2.33, 2.44, 2.63
7	3.6	387, 406, 431			Carotenoid P7	1.95, 2.08, 2.63
8	3.8	414, 653			Unidentified chlorin	2.44
9	3.9	404, 654			Unidentified chlorin	2.63
10	4.1	408, 503, 664	533	515, 505, 489	Chlorophyllone	All
11	4.3	406, 669	533	515, 505, 489	Chlorophyllone epimer	1.95, 2.08, 2.44, 2.63
12	4.4	322			Carotenoid	2.63
13	4.6	444, 468			Carotenoid	2.63
14	5.0	443, 469			Carotenoid	2.63
15	5.1	446, 469			Carotenoid	2.63
16	8.9	418, 444, 469			Carotenoid	2.63
17	9.2	402, 685			Purpurin-7 trimethyl ester	2.33

Table A4.3. (continued) Assignments of pigments and carotenoids in Tottenhill Quarry sediments (continued over).

Peak no.	t _R / min	Main UV/vis absorption / nm	[M+H] ⁺ / m/z	Prominent fragment ions / m/z	Assignment	Samples found / m OD
18	9.9	(358), 424, 684			Unidentified chlorin	2.33, 2.63
19	10.5	410, 665	903	625	Chlorin e ₆ dimethyl phytol ester	2.44
20	10.6	384, 407, 680	695	677, 439	Unidentified bacterioviridin	2.08, 2.33, 2.44
21	10.7	392, 416, 681			Unidentified bacterioviridin	2.08, 2.33
22	11.0	391, 408, 690			Unidentified bacterioviridin	2.33
23	11.1	390, 408, 690			Unidentified bacterioviridin	2.33
24	11.2	360, 748	889	611, 511	Bacteriopheophytin <i>a</i>	2.44, 2.63
25	11.3	385, 409, 680	654	636	Unidentified bacterioviridin	2.08, 2.33
26	11.5	380, 410, 680	698	680	Unidentified bacterioviridin	2.08, 2.33
27	11.6	435, 653			Phaeophytin <i>b</i>	2.08
28	12.2	385, 410, 681			Bacterioviridin <i>a</i>	2.08, 2.33
29	12.4	416, 436, 657	827	549, 521	Pyropheophytin <i>b</i>	2.08, 2.33, 2.44, 2.63
30	12.9	408, 664	871		Phaeophytin <i>a</i>	2.08, 2.33, 2.44, 2.63
31	13.2	408, 665	871		Phaeophytin <i>a</i> epimer	2.63
32	14.0	408, 665	813	535	Pyropheophytin <i>a</i>	2.08, 2.33, 2.44, 2.63
33	14.8	436, 653			Pyropheophorbide <i>b</i> SCE	2.44, 2.63

Table A4.3. (continued) Assignments of pigments and carotenoids in Tottenhill Quarry sediments.

Peak no.	t _R / min	Main UV/vis absorption / nm	[M+H] ⁺ / m/z	Prominent fragment ions / m/z	Assignment	Samples found / m OD
34	15.4	408, 665			Pyropheophorbide <i>a</i> SCE	2.63
35	15.6	408, 666			Pyropheophorbide <i>a</i> SCE	2.44, 2.63
36	15.7	408, 665			Pyropheophorbide <i>a</i> SCE	2.44, 2.63
37	15.9	411, 665	903	535	Pyropheophorbide <i>a</i> SCE (C _{27:1} sterol)	2.44, 2.63
38	16.2	408, 665	929	535	Pyropheophorbide <i>a</i> SCE (C _{29:2} sterol)	2.33, 2.44, 2.63
39	16.3	408, 665			Pyropheophorbide <i>a</i> SCE	2.08, 2.33, 2.63
40	16.4	408, 665	931	535	Pyropheophorbide <i>a</i> SCE (C _{29:1} sterol)	2.33, 2.44, 2.63
41	16.6	412, 665			Pyropheophorbide <i>a</i> SCE	2.08, 2.63
42	16.7	409, 665	933	535	Pyropheophorbide <i>a</i> SCE (C _{29:0} sterol)	2.08, 2.33, 2.44, 2.63
43	17.1	407, 665			Pyropheophorbide <i>a</i> SCE	2.63

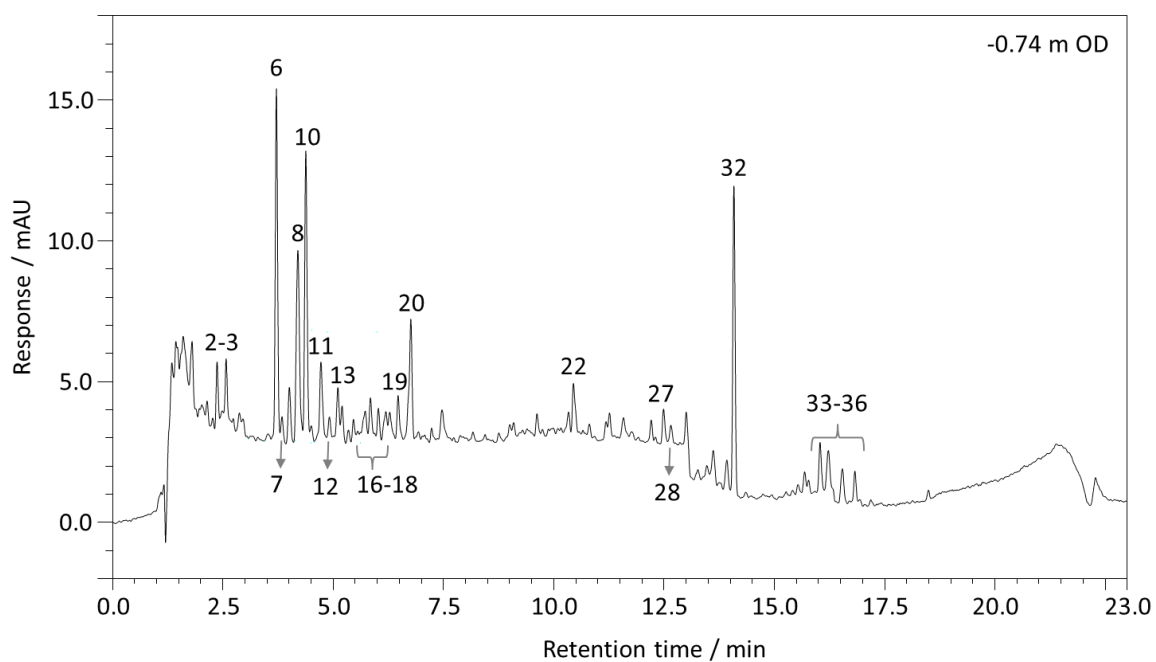
Appendix 4.4. Chromatogram and table of peaks of chlorophyll pigments from Blackborough Quarry

Figure A4.4. UHPLC-DAD chromatogram (300-800 nm) of Blackborough Quarry pigments sample - 0.74 m OD. For peak assignments see Table A4.4.

Table A4.4. Assignments of pigments and carotenoids in Blackborough Quarry sediments (continued over).

Peak no.	t _R / min	Main UV/vis absorption / nm	[M+H] ⁺ / m/z	Prominent fragment ions / m/z	Assignment	Samples found / m OD
1	1.9	392, 416, 440			Carotenoid	-1.05, -0.95
2	2.4	434, 650			Chlorophyllone <i>b</i>	From -1.05 to -0.74
3	2.5	433, 655			Chlorophyllone <i>b</i> epimer	From -1.05 to -0.74
4	2.9	387, 403, 674			Unidentified bacterioviridin <i>a</i>	-1.05, -0.95
5	3.1	408, 666			Unidentified chlorin	-1.05, -0.95
6	3.4	386, 405, 430			Carotenoid P7	All
7	3.6	403, 653			Unidentified chlorin	From -0.95 to -0.54, from -0.14 to 0.47, 1.27
8	3.8	410, 664			Chlorophyllone <i>a</i>	From -1.05 to -0.54, from -0.14 to 3.07
9	3.9	449, 477			Carotenoid	-1.05, -0.54, 1.66, 2.06
10	4.0	406, 669			Chlorophyllone <i>a</i> epimer	From -1.05 to -0.74, from -0.14 to 1.50, 2.06
11	4.2	421, 442, 469			Carotenoid	From -0.95 to -0.54, -0.14, 0.47, 1.27, 1.50, 1.86, 2.06
12	4.6	443, 470			Carotenoid	From -1.05 to -0.74, 0.27, 1.86, 2.06
13	5.1	439, 470			Carotenoid	From -1.05 to -0.74
14	5.7	411, 434, 462			Carotenoid	-0.54, 0.27
15	5.8	472, 492			Carotenoid	0.27

Table A4.4. (continued) Assignments of pigments and carotenoids in Blackborough Quarry sediments (continued over).

Peak no.	t _R / min	Main UV/vis absorption / nm	[M+H] ⁺ / m/z	Prominent fragment ions / m/z	Assignment	Samples found / m OD
16	5.9	420, 444, 473			Carotenoid	From -1.05 to -0.54, from -0.14 to 0.47, 1.27, 1.50
17	6.0	410, 432, 460			Carotenoid	-0.74
18	6.4	445, 472			Carotenoid	From -0.95 to -0.54, 0.27, 0.47, from 1.50 to 2.06
19	6.5	410, 665			Pyropheophorbide <i>a</i> methyl ester	From -1.05 to -0.54, from -0.14 to 0.47, 1.27, 1.50
20	6.9	445, 471	567	549	Carotenoid	From -1.05 to -0.74
21	8.5	442, 468			Carotenoid	-1.05, -0.95
22	10.1	411, 665			Chlorin <i>e</i> ₆ dimethyl phytol ester	-0.74
23	10.7	356, 526, 748	889	611, 551	Bacteriopheophytin <i>a</i>	-1.05, -0.95
24	10.8	360, 754	889	611, 551	Bacteriopheophytin <i>a</i> epimer	-1.05, -0.95
25	10.9	434, 664			Phaeophytin <i>b</i>	0.47, 1.66
26	11.1	411, 438			Carotenoid	2.06
27	12.2	436, 655	827	809, 549	Pyropheophytin <i>b</i>	From -1.05 to -0.74, 1.66

Table A4.4. (continued) Assignments of pigments and carotenoids in Blackborough Quarry sediments.

Peak no.	t _R / min	Main UV/vis absorption / nm	[M+H] ⁺ / m/z	Prominent fragment ions / m/z	Assignment	Samples found / m OD
28	12.3	386, 424, 692			Unidentified chlorin	-0.74, 1.66
29	12.7	406, 664	871	853, 593, 553	Phaeophytin <i>a</i>	-1.05, -0.95, -0.34, from 1.27 to 1.66, 2.06, 2.36
30	13.0	408, 665	871	853, 593, 553	Phaeophytin <i>a</i> epimer	1.66
31	13.3	439, 467			Carotenoid	-1.05, -0.95, 0.07, 0.27, 1.66
32	13.7	409, 665	813	535	Pyropheophytin <i>a</i>	From -1.05 to 2.36
33	15.7	408, 665	915	535, 507	Pyropheophorbide <i>a</i> SCE (C _{28:2} sterol)	From -1.05 to -0.74, 0.27, 1.66, 2.06
34	15.8	410, 665			Pyropheophorbide <i>a</i> SCE	From -1.05 to -0.74, 0.27, from 1.27 to 1.86
35	16.1	409, 665	933	535, 507	Pyropheophorbide <i>a</i> SCE (C _{29:0} sterol)	From -1.05 to -0.74, 0.27, from 1.50 to 1.86
36	16.5	409, 665	948	535	Pyropheophorbide <i>a</i> SCE (C _{30:0} sterol)	From -1.05 to -0.74, 1.50, 1.66
37	20.5	410, 665			Pyropheophorbide <i>a</i> SCE	0.47

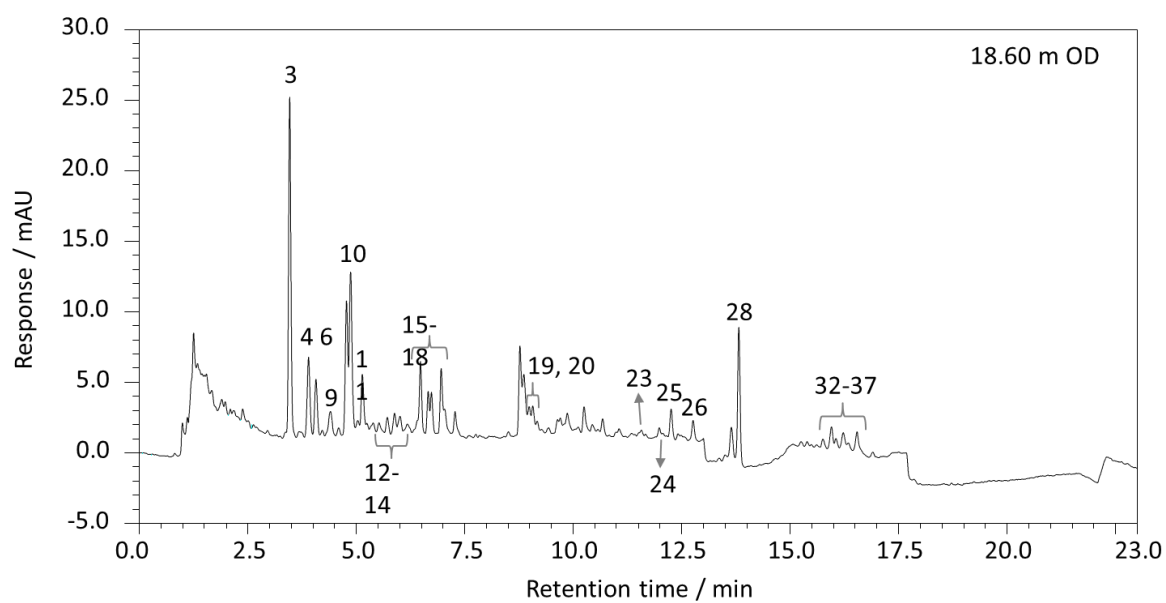
Appendix 4.5. Chromatogram and table of peaks of chlorophyll pigments from Woodston HiB 12-6

Figure A4.5. UHPLC-DAD chromatogram (300-800 nm) of Woodston pigments sample -18.42 m OD. For peak assignments see Table A4.5.

Table A4.5. Assignments of pigments and carotenoids in Woodston sediments (continued over).

Peak no.	t _R / min	Main UV/vis absorption / nm	[M+H] ⁺ / m/z	Prominent fragment ions / m/z	Assignment	Samples found / m OD
1	2.5	413, 435, 655			Chlorophyllone <i>b</i>	-18.32, -18.12
2	2.7	414, 434, 655			Chlorophyllone <i>b</i> epimer	-18.32
3	3.5	387, 406, 431			Carotenoid P7	All
4	3.7	409, 663			Chlorophyllone <i>a</i>	From -18.42 to -18.12
5	3.8	420, 442, 474			Carotenoid	-18.32
6	3.9	404, 669			Chlorophyllone <i>a</i> epimer	-18.42, -18.32, -18.12
7	4.1	407, 658			Unidentified chlorin	-18.22
8	4.2	384, 406, 434			Carotenoid	-17.92
9	4.4	421, 444, 466			Carotenoid	-18.42
10	4.9	419, 443, 471			Carotenoid	From -18.42 to -18.22
11	5.2	420.443, 470			Carotenoid	-18.42, -18.32
12	5.7	410, 438, 463			Carotenoid	-18.42
13	5.9	421, 444, 468			Carotenoid	-18.42
14	6.0	413, 444, 468			Carotenoid	-18.42
15	6.5	422, 445, 473			Carotenoid	-18.42
16	6.7	413, 438, 468			Carotenoid	From -18.42 to -18.22
17	6.8	416, 438, 465			Carotenoid	From -18.42 to -18.22

Table A4.5. (continued) Assignments of pigments and carotenoids in Woodston sediments (continued over).

Peak no.	t _R / min	Main UV/vis absorption / nm	[M+H] ⁺ / m/z	Prominent fragment ions / m/z	Assignment	Samples found / m OD
18	7.0	415, 443, 470			Carotenoid	-18.42, -18.32
19	8.8	421, 443, 471			Carotenoid	From -18.42 to -18.22
20	8.9	423, 446, 472			Carotenoid	From -18.42 to -18.22
21	10.2	409, 446, 666			Carotenoid	-18.22, -18.12
22	11.0	355, 527, 746			Pyrobacteriophageophytin <i>a</i>	-18.32, -18.12
23	11.4	419, 438, 651			Phaeophytin <i>b</i>	-18.42, -18.32
24	12.0	411, 470, 665			Unidentified chlorin	-18.42
25	12.3	415, 438, 655			Pyrophaeophytin <i>b</i>	From -18.42 to -18.02
26	12.8	407, 665			Phaeophytin <i>a</i>	From -18.42 to -18.12
27	13.7	449, 472			Carotenoid	-18.32
28	13.8	409, 665			Pyrophaeophytin <i>a</i>	From -18.42 to -18.02
29	15.3	408, 665			Pyrophaeophorbide <i>a</i> SCE	-18.12
30	15.4	408, 665			Pyrophaeophorbide <i>a</i> SCE	-18.12
31	15.5	408, 665			Pyrophaeophorbide <i>a</i> SCE	-18.12
32	15.8	409, 665			Pyrophaeophorbide <i>a</i> SCE	-18.42, -18.32, -18.12
33	16.0	409, 665			Pyrophaeophorbide <i>a</i> SCE	-18.42, -18.32, -18.12

Table A4.5. (continued) Assignments of pigments and carotenoids in Woodston sediments.

Peak no.	t_R / min	Main UV/vis absorption / nm	$[M+H]^+$ / m/z	Prominent fragment ions / m/z	Assignment	Samples found / m OD
34	16.1	408, 666			Pyropheophorbide <i>a</i> SCE	-18.42, -18.32, -18.12
35	16.3	409, 665			Pyropheophorbide <i>a</i> SCE	-18.42, -18.32, -18.12
36	16.4	406, 665			Pyropheophorbide <i>a</i> SCE	-18.42, -18.12
37	16.6	409, 666			Pyropheophorbide <i>a</i> SCE	-18.42, -18.12
38	16.9	408, 666			Pyropheophorbide <i>a</i> SCE	-18.22, -18.12

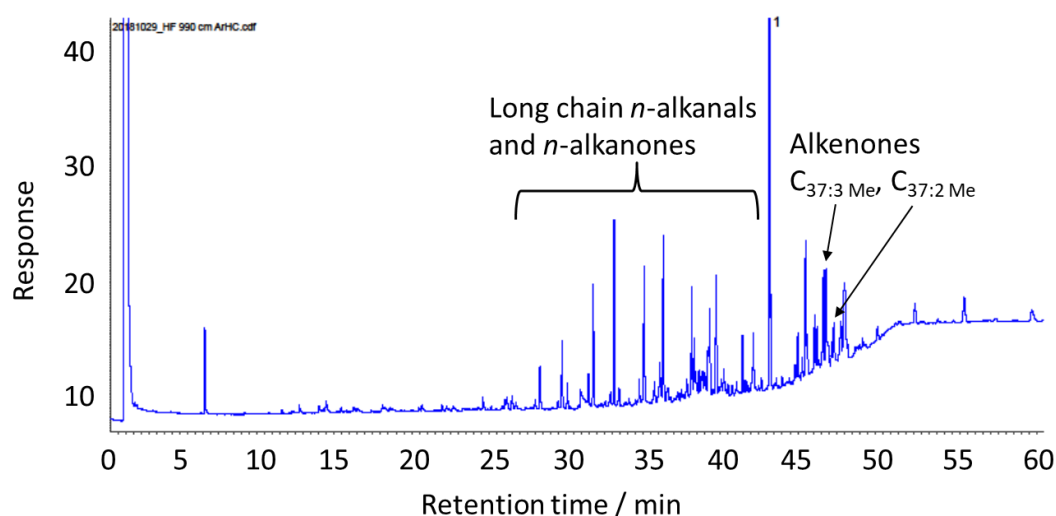
Appendix 4.6. Chromatogram of an aromatic hydrocarbon fraction showing long chain alkenones.

Figure A4.6. GC-FID chromatogram of the aromatic hydrocarbon fraction from Horse Fen 13-1 sample -2.20 m OD showing the retention time of alkenones after long chain *n*-alkanones and *n*-alkanals.

Appendix 5. GC-MS analysis of lipids and interpretation of data

After GC-FID analysis (Section 7.4.1), GC-MS was carried out on selected samples to identify compounds from their mass spectra (Section 7.4.2). The GC-MS spectrum of each component was compared to library data (NIST08 and NIST MS search version 2.3), where available, and literature data. The minimum probability confidence from library results was 80%. Following assignments of peaks from GC-MS, the peaks in GC-FID chromatograms were assigned according to retention time and relative abundance. Quantification was carried out as described in Section 7.5.2

Appendix 6. UHPLC-DAD and UHPLC-DAD-MS analysis of pigments and interpretation of data

The pigments, analysed by UHPLC-DAD (Section 7.4.4), were assigned according to their retention time, UV-vis spectra and comparing the results to previous work (Airs, 2001; Saesaengseerung, 2013). Selected samples were analysed by UHPLC-DAD-MS (Section 7.4.9); the results were interpreted according to their MS and fragmentation pattern and comparison with previous work and literature data. Following final assignments of the peaks, quantification was carried out as described in Section 7.5.1.

Appendix 7. HPLC-MS analysis of GDGTs native lipids and interpretation of data

The GDGT samples were analysed by HPLC-MS (Sections 7.4.3, 7.4.11), assigned according to their retention time and MS spectra and comparing the results to literature data (Weijers *et al.*, 2007; Schouten *et al.*, 2013). For application of the results to proxies (BIT, CBT, TEX₈₆, TEX₈₆^L, lake temperature index), the manually integrated peak areas were used (only if *S/N* was >10), due to the lack of a standard GDGT compound. All proxies, except the lake temperature index, are ratios, thus the results would be identical with or without a standard calibration. The lake water temperature index (Pearson *et al.*, 2011) was calculated by summing all the peak areas of the isoprenoid and branched GDGTs detected in the Loch of Stenness and calculating the fractional percentage of brGDGTs Ib (**G13**), IIa (**G9**) and IIIa (**G6**), used in the proxy (Table A3.2).

Appendix 8. HPLC-MS analysis of derivatised lipids and interpretation of data

The derivatised lipid standards and GDGTs were analysed by HPLC-MS, HPLC-UV and HPLC-FLD (Sections 7.4.5, 7.4.6, 7.4.8, 7.4.10, 7.4.11). The HPLC-UV and HPLC-FLD chromatograms were analysed comparing the retention times to HPLC-MS analysis. Calculation of the yields of reaction by sonication of multiple lipid standards in a rack was carried out as described in Section 2.2.2. The MS and MS/MS spectra (Sections 7.4.10-7.4.12) were analysed and extracted ion chromatograms (EIC) produced calculating the mass of the intact protonated molecule. Fragmentation patterns were derived, also comparing to literature data (Knappy, 2010; Bauersachs and Schwark, 2016; Poplawski, 2017).

Appendix 9. Appendix of structures

Abbreviations:

G: Glycerol dialkyl glycerol tetraether lipids

L: Lipid standards

A: Alkanes, alkanones, alkenones, alkanals, alkanoic acids, alkanols

T: Terpenoids

C: Chlorophyll pigments

B: Bacteriochlorophylls, bacterioviridin pigments

R: Carotenoids

G: Glycerol dialkyl glycerol tetraether lipids (GDGTs)*Table A9.1. List of GDGT structure numbers, name of compounds and m/z. For structures, see Figure A9.1.*

Structure number	Compound name	<i>m/z</i>
G1	Caldarchaeol (or GDGT-0)	1302
G2	GDGT-1	1300
G3	GDGT-2	1298
G4	GDGT-3	1296
G5	Crenarchaeol	1292
G5'	Crenarchaeol stereoisomer	1292
G6	IIIa + IIIa'	1050
G7	IIIb + IIIb'	1048
G8	IIIc + IIIc'	1046
G9	IIa + IIa'	1036
G10	IIb + IIb'	1034
G11	IIc + IIc'	1032
G12	Ia	1022
G13	Ib	1020
G14	Ic	1018

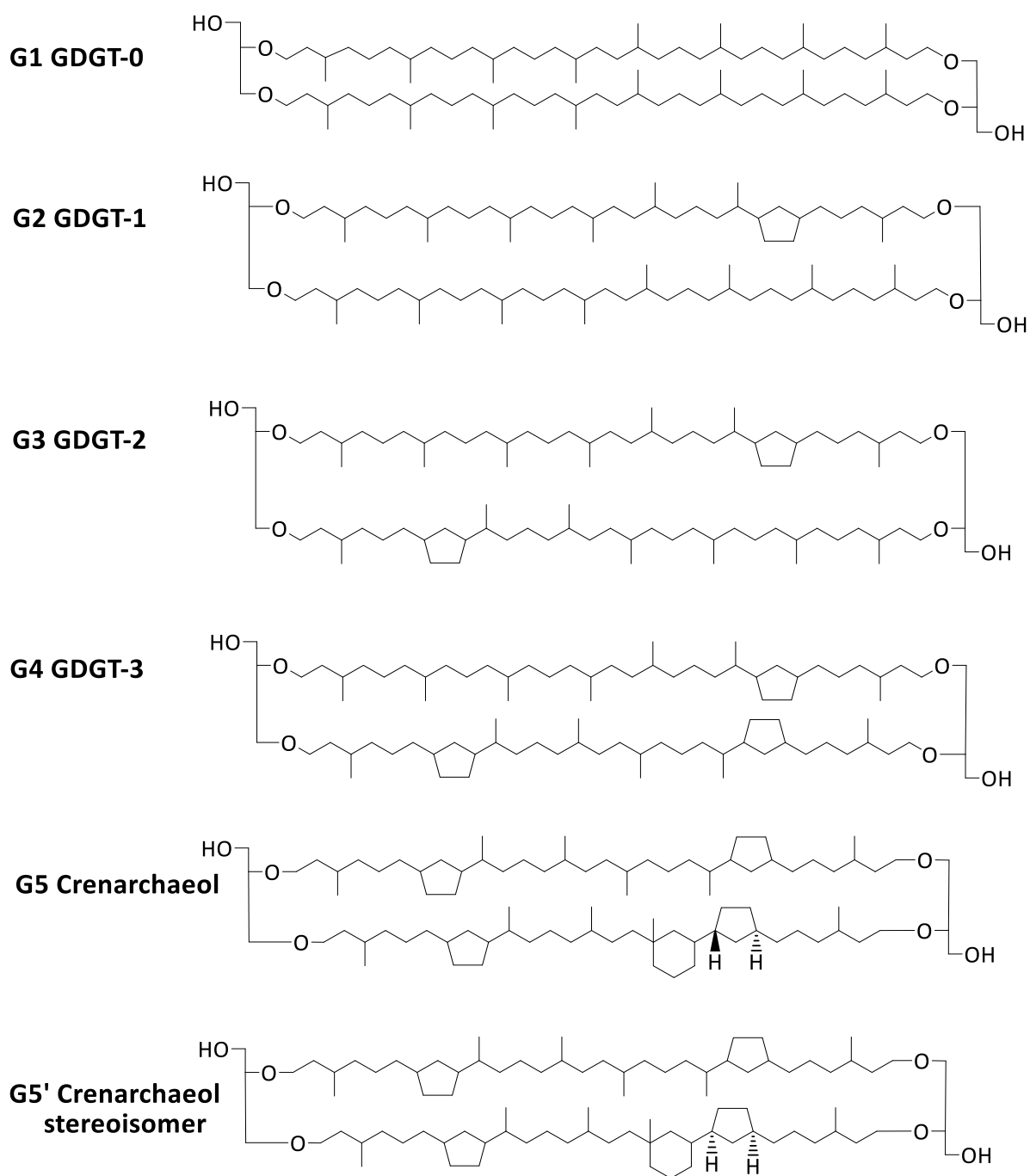
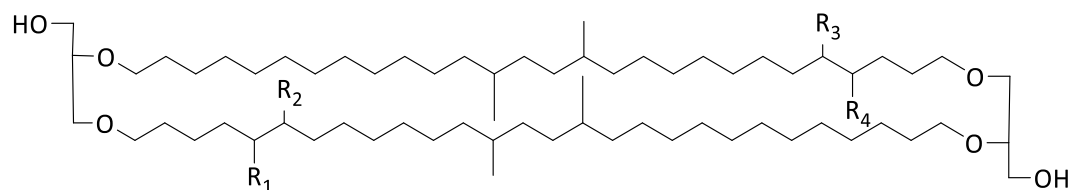
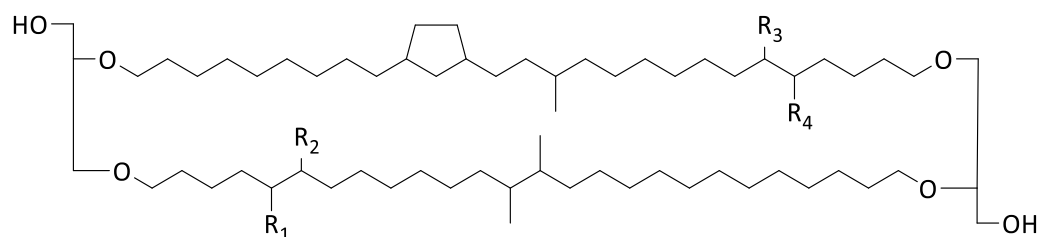


Figure A9.1. Structure of GDGTs (continued over).

G6 IIIa $R_1, R_3 = \text{Me}; R_2, R_4 = \text{H}$; IIIa' $R_2, R_4 = \text{Me}; R_1, R_3 = \text{H}$
G9 IIa $R_1 = \text{Me}; R_2, R_3, R_4 = \text{H}$; IIa' $R_2 = \text{Me}; R_1, R_3, R_4 = \text{H}$
G12 Ia $R_1, R_2, R_3, R_4 = \text{H}$



G7 IIIb $R_1, R_3 = \text{Me}; R_2, R_4 = \text{H}$; IIIb' $R_2, R_4 = \text{Me}; R_1, R_3 = \text{H}$
G10 IIb $R_1 = \text{Me}; R_2, R_3, R_4 = \text{H}$; IIb' $R_2 = \text{Me}; R_1, R_3, R_4 = \text{H}$
G13 Ib $R_1, R_2, R_3, R_4 = \text{H}$



G8 IIIc $R_1, R_3 = \text{Me}; R_2, R_4 = \text{H}$; IIIc' $R_2, R_4 = \text{Me}; R_1, R_3 = \text{H}$
G11 IIc $R_1 = \text{Me}; R_2, R_3, R_4 = \text{H}$; IIc' $R_2 = \text{Me}; R_1, R_3, R_4 = \text{H}$
G14 Ic $R_1, R_2, R_3, R_4 = \text{H}$

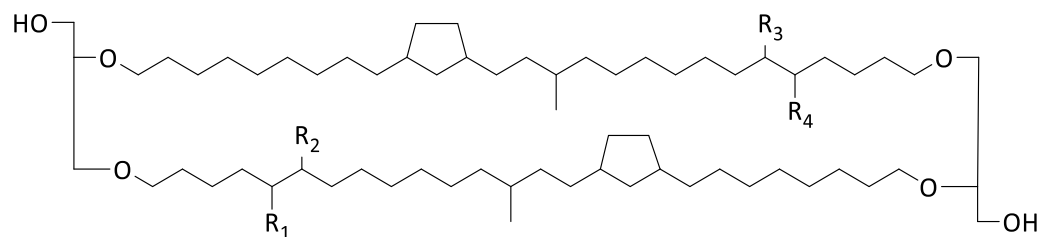


Figure A9.1. (continued) Structures of GDGTs.

L: Lipid standards

Table A9.2. List of lipid standard structure numbers, name of compounds and m/z . For structures, see Figure A9.2.

Structure number	Compound name	m/z
L1	1-octadecanol	270
L2	Cholesterol	386
L3	<i>r</i> -dOG (1,2-di- <i>O</i> -octadecyl- <i>rac</i> -glycerol)	598
L4	1,12-dodecanediol	202

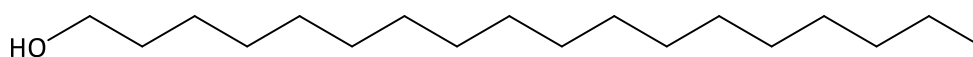
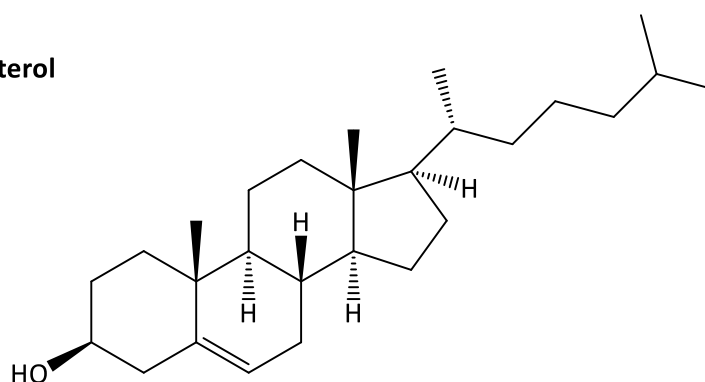
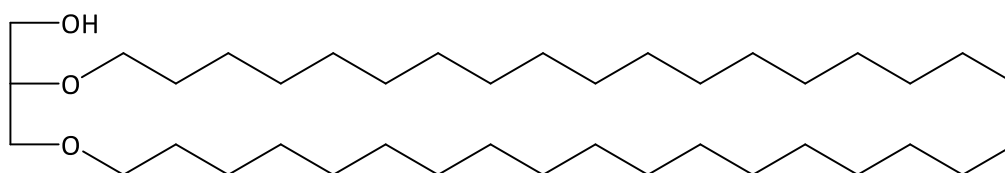
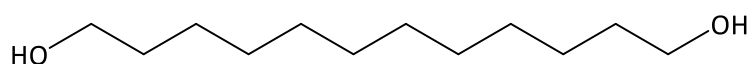
L1 1-octadecanol**L2 Cholesterol****L3 *r*-dOG****L4 1,12-dodecanediol**

Figure A9.2. Structures of lipid standards.

A: Alkanes, alkanones, alkenones, alkanals, alkanolic acids, alkanols

Table A9.3. List of alkanes, alkanones, alkenones, alkanals, alkanolic acids, alkanols structure numbers and name of compounds. For structures, see Figure A9.3.

Structure number	Compound name
A1	Alkane
A2	Alkanone
A3	Alkanals
A4	Alkanolic acids
A5	Alkanols
A6	Alkenone C37:2 methyl
A7	Alkenone C37:3 methyl
A8	Alkenone C38:2 ethyl
A9	Alkenone C37:4 methyl

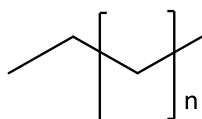
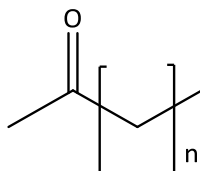
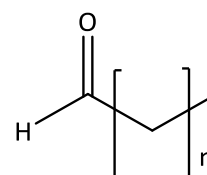
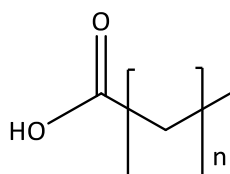
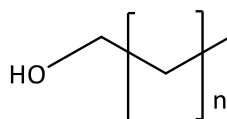
A1 *n*-alkane**A2 *n*-alkanone****A3 *n*-alkanal****A4 *n*-alkanoic acid****A5 *n*-alkanol**

Figure A9.3. Structures of alkanes, alkanones, alkenones, alkanals, alkanolic acids, alkanols (continued over).

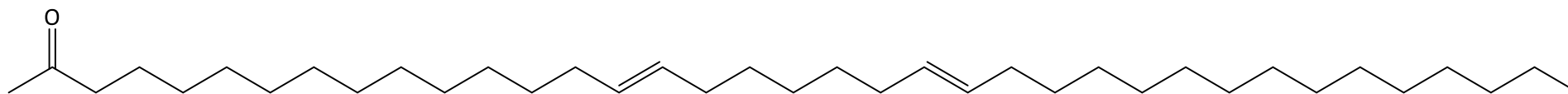
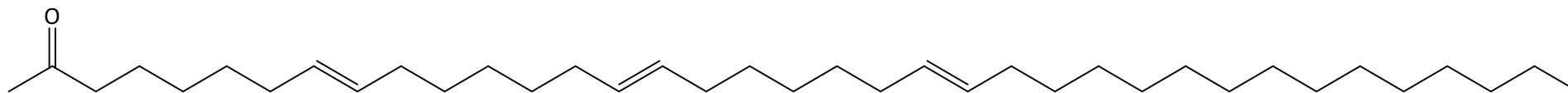
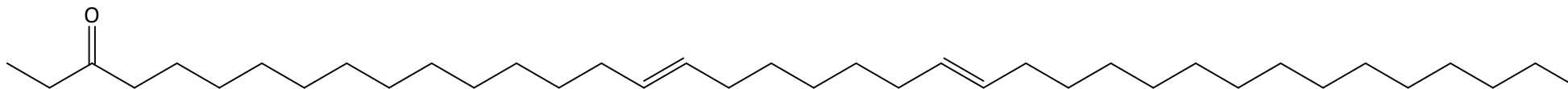
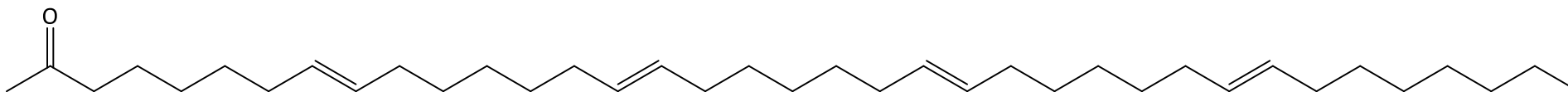
A6 Alkenone C37:2 methyl**A7 Alkenone C37:3 methyl****A8 Alkenone C38:2 ethyl****A9 Alkenone C37:4 methyl**

Figure A9.3. (continued) Structures of alkanes, alkanones, alkenones, alkanals, alkanic acids, alkanols.

T: Terpenoids

Table A9.4. List of terpenoid structure numbers and name of compounds. For structures, see Figure A9.4.

Structure number	Compound name
T1	Kaur-15-ene (Kaur-15-ene, (5 α ,9 α ,10 β))
T2	Kaur-16-ene (Kaur-16-ene, (8 β ,13 β))
T3	Kaurane (Ent-kaurane)
T4	Friedelin (Freidelan-3-one)
T5	Lupan-3-one
T6	Lupenone (lup-20(29)-en-3-one)
T7	γ -sitostenone (Stigmast-4-en-3-one, (24S))
T8	Glutinol (D:B-friedoolean-5-en-3 β -ol)
T9	5 α -stigmastanol ((3 β ,5 α)-stigmastan-3-ol)
T10	Dinosterol (4 α ,23,24-trimethyl 5 α -cholest-22-en-3 β -ol)
T11	β -sitosterol (Stigmast-5-en-3-ol)
T12	Stigmasterol (Stigmasta-5,22E-dien-3 β -ol)
T13	Diatomsterol (24-methylcholesta-5,22E-dien-3 β -ol)
T14	α -tocopherol
T15	Stigmastane
T16	Des-A-lupane
T17	Taraxerone (D-friedoolean-14-en-3-one)
T18	Diploptene (A'-neogammacer-22(29)-ene)

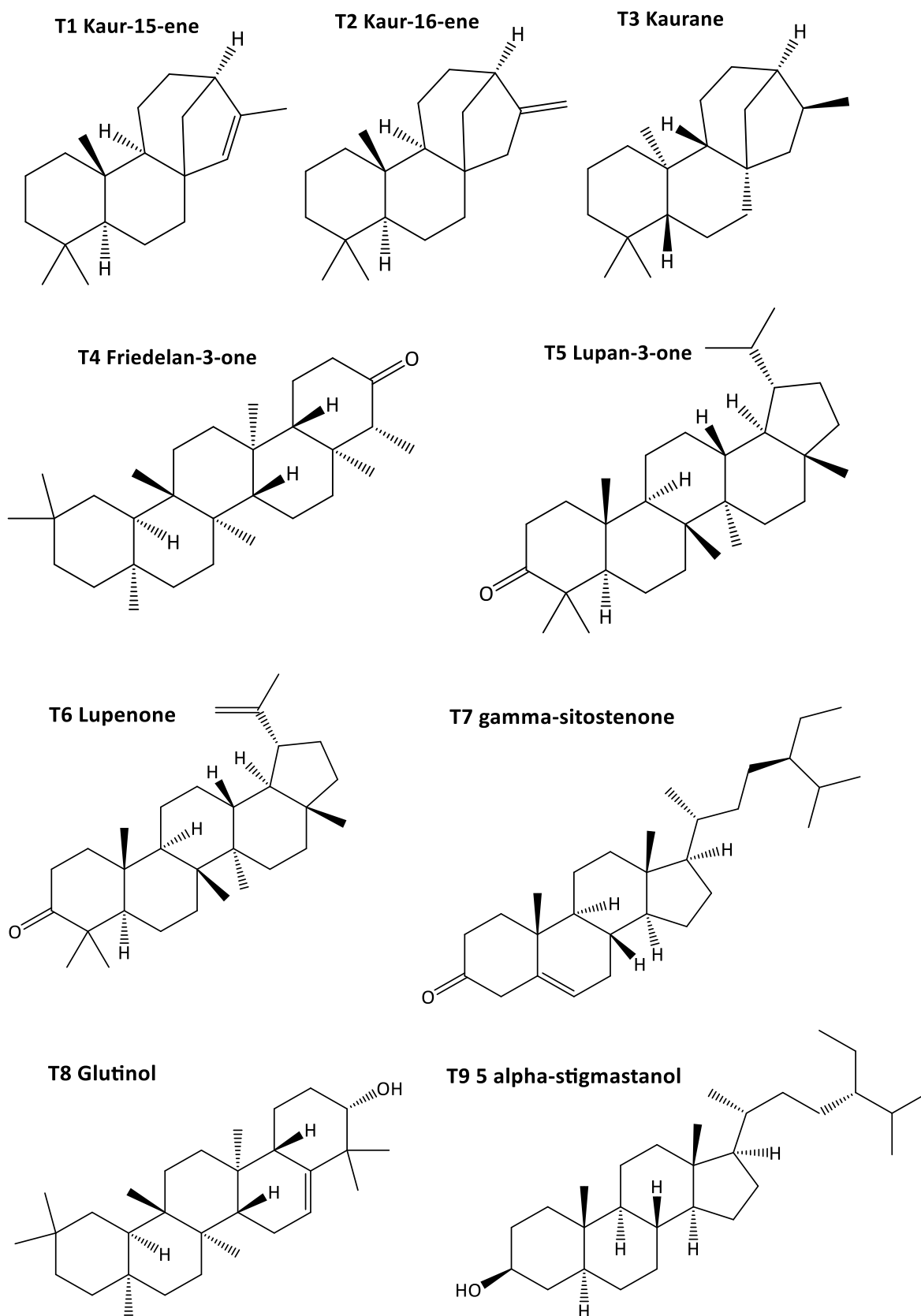


Figure A9.4. Structures of terpenoids (continued over).

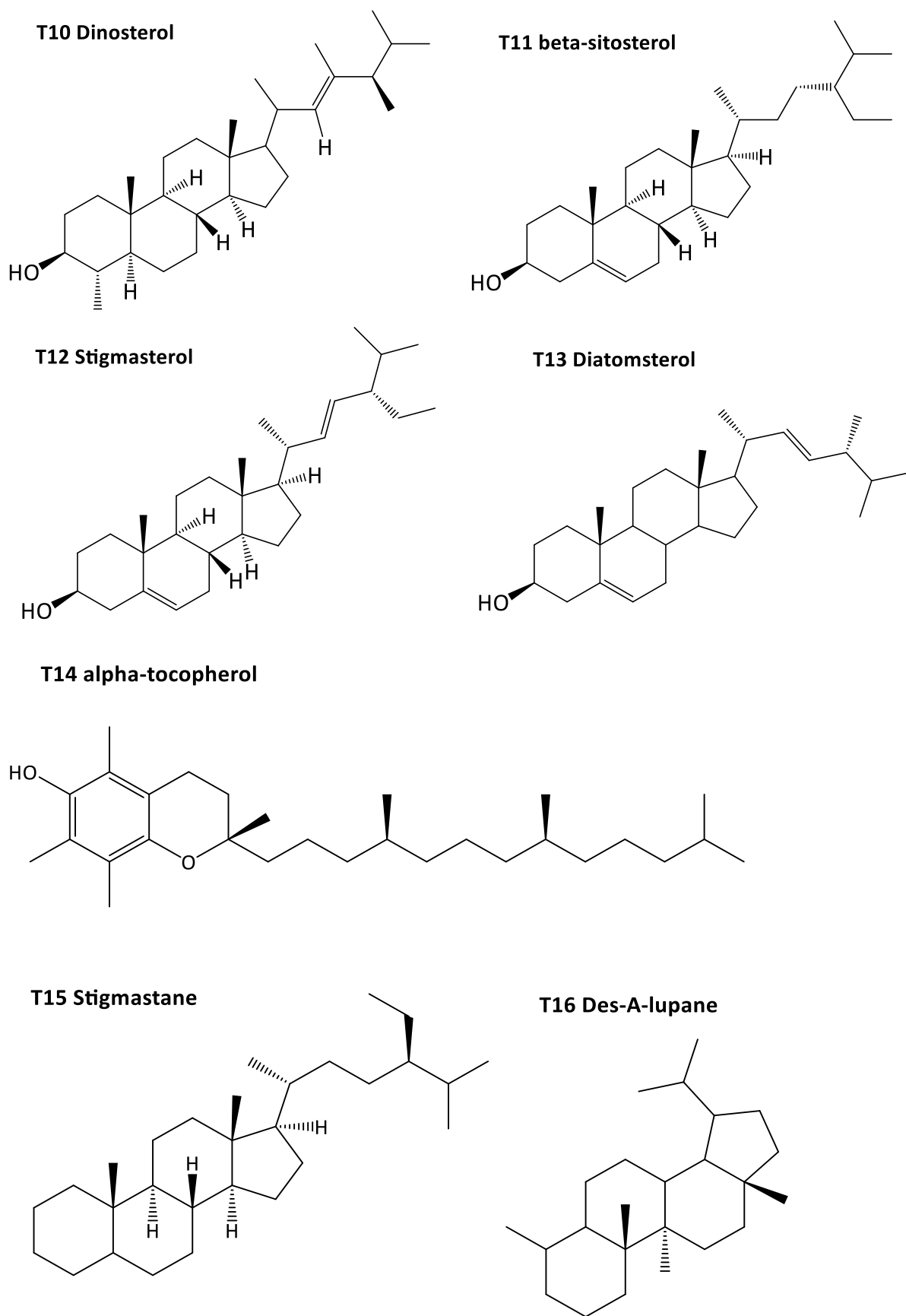


Figure A9.4. (continued) Structures of terpenoids.

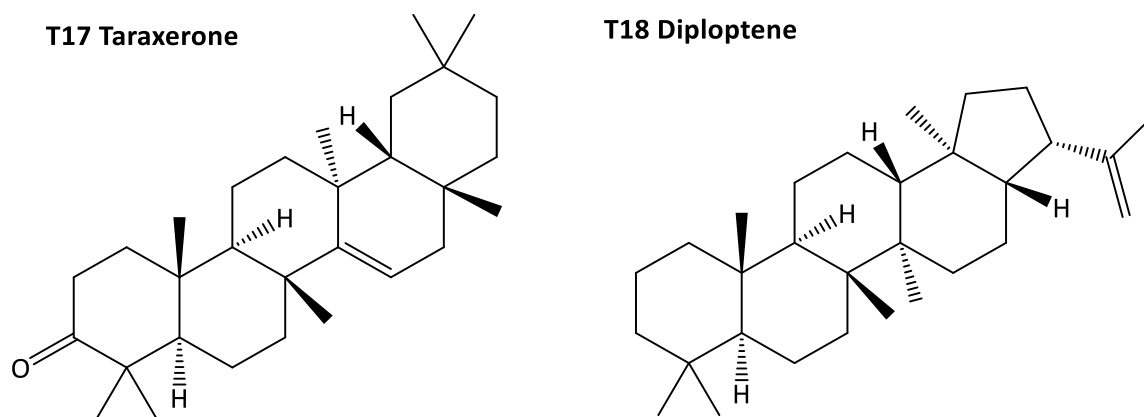


Figure A9.4. (continued) Structures of terpenoids.

C: Chlorophyll pigments

Table A9.5. List of chlorophyll pigment structure numbers and name of compounds. For structures, see Figure A9.5.

Structure number	Compound name
C1	Chlorophyll <i>a</i>
C2	Chlorophyll <i>b</i>
C3	Chlorophyllone <i>a</i> (chlone <i>a</i>)
C4	Chlorophyllone <i>b</i> (chlone <i>b</i>)
C5	Hydroxyphaeophytin <i>a</i> (hphe <i>a</i>)
C6	Phaeophytin <i>a</i> (phe <i>a</i>)
C7	Phaeophytin <i>b</i> (phe <i>b</i>)
C8	Pyrophaeophytin <i>a</i> (phe <i>a</i>)
C9	Pyrophaeophytin <i>b</i> (phe <i>b</i>)
C10	Phaeophorbide <i>a</i> methyl ester (pphorb <i>a</i> ME)
C11	Pyrophaeophorbide <i>a</i> methyl ester (pphorb <i>a</i> ME)
C12	Pyrophaeophorbide <i>a</i> steryl chlorin ester (pphorb <i>a</i> SCE)
C13	Chlorophyll <i>c</i>
C14	Chlorophyll <i>d</i>
C15	Chlorophyll <i>f</i>

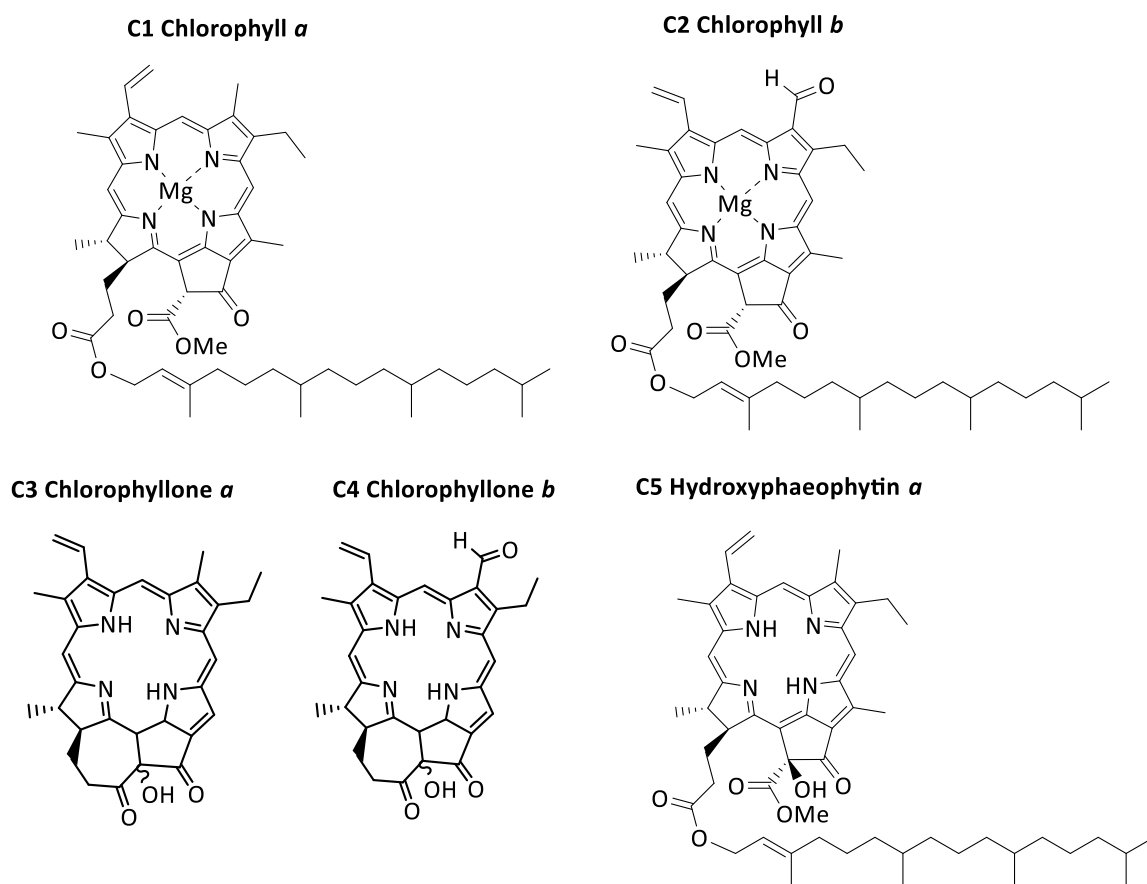


Figure A9.5. Structures of chlorophyll pigments (continued over).

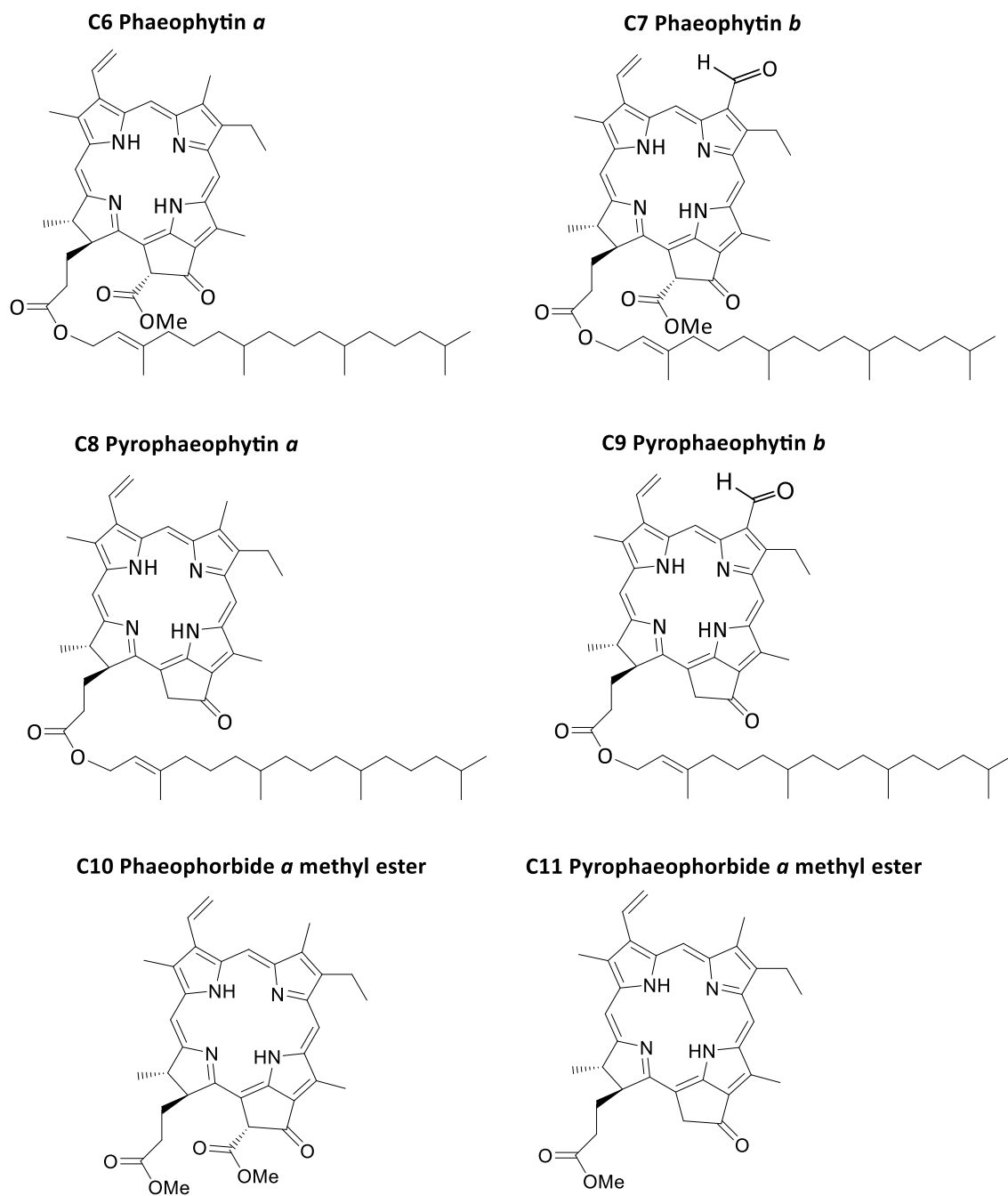
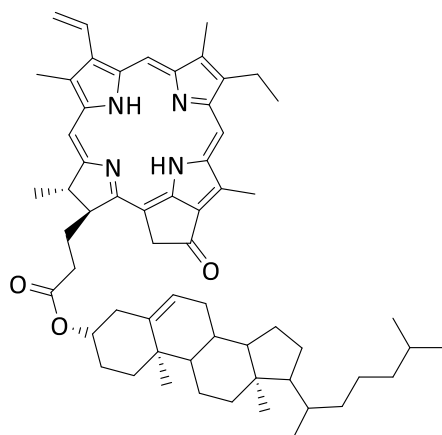
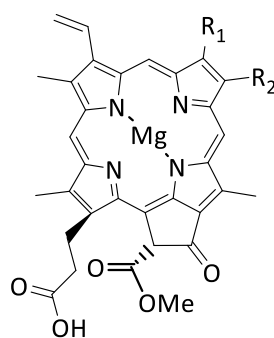


Figure A9.5. (continued) Structures of chlorophyll pigments (continued over).

C12 Pyropheophorbide *a* steryl ester

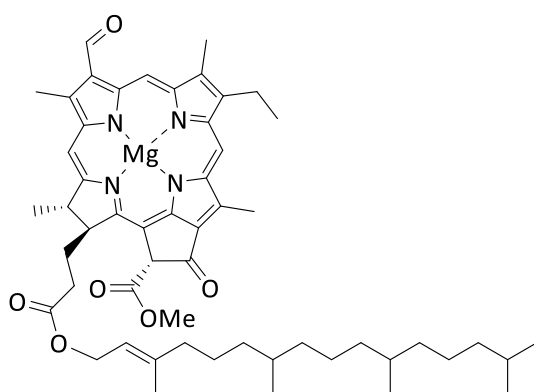


C13 Chlorophyll *c*



c_1 : R1 = Me, R2 = Et
 c_2 : R1 = Me; R2 = Vinyl
 c_3 : R1 = CO₂Me; R2 = Vinyl

C14 Chlorophyll *d*



C15 Chlorophyll *f*

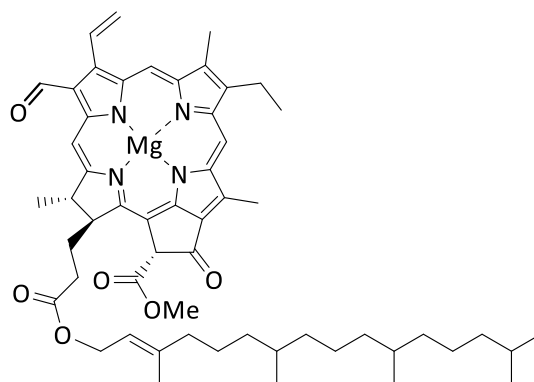


Figure A9.5. (continued) Structures of chlorophyll pigments.

B: Bacteriochlorophylls, bacterioviridin pigments

Table A9.6. List of bacteriochlorophyll and bacterioviridin pigment structure numbers and name of compounds. For structures, see Figure A9.6.

Structure number	Compound name
B1	Bacteriochlorophyll <i>a</i> (bchl <i>a</i>)
B2	Bacteriopheophytin <i>a</i> (bphe <i>a</i>)
B3	Bacteriopyropheophytin <i>a</i> (bpphe <i>a</i>)
B4	Bacterioviridin <i>a</i> (bvir <i>a</i>)
B5	Bacteriochlorophyll <i>c</i> (bchl <i>c</i>)
B6	Bacteriochlorophyll <i>d</i> (bchl <i>d</i>)
B7	Bacteriochlorophyll <i>e</i> (bchl <i>e</i>)

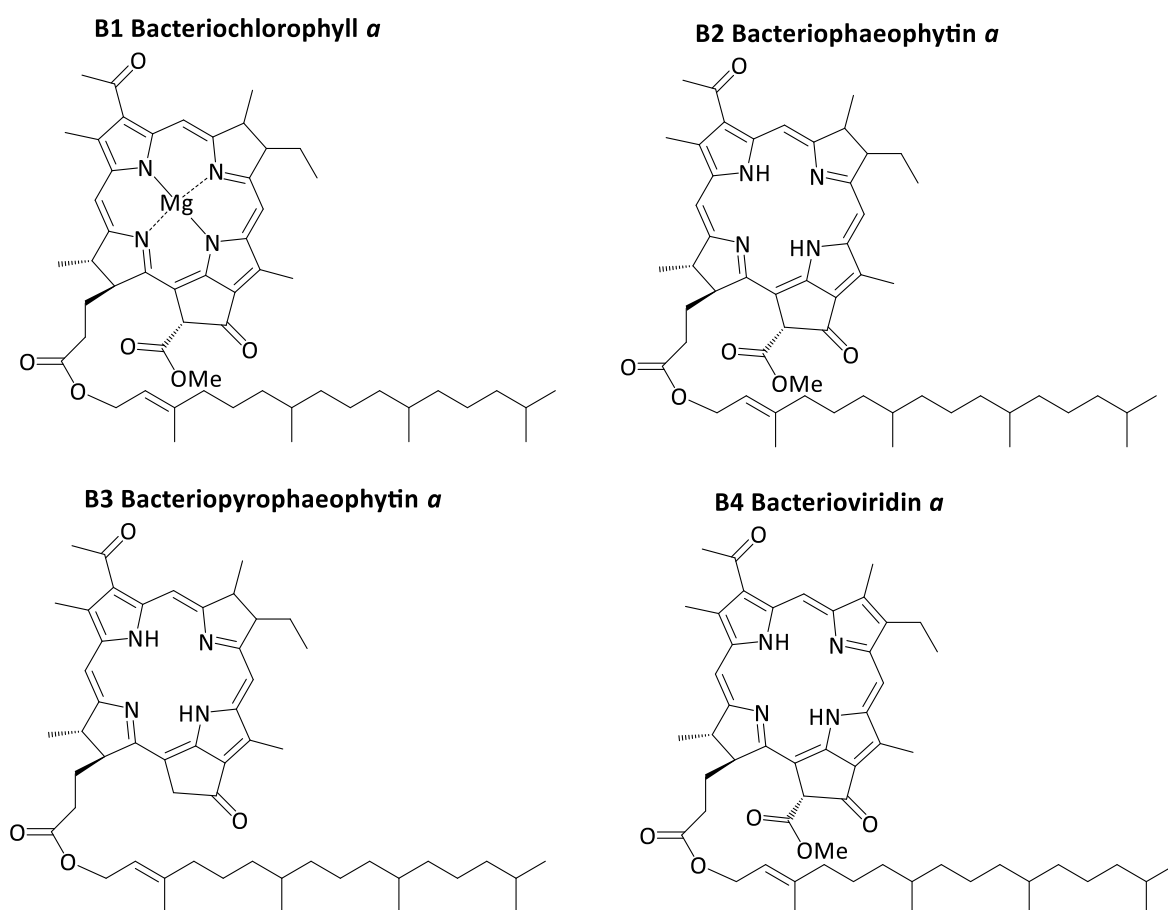
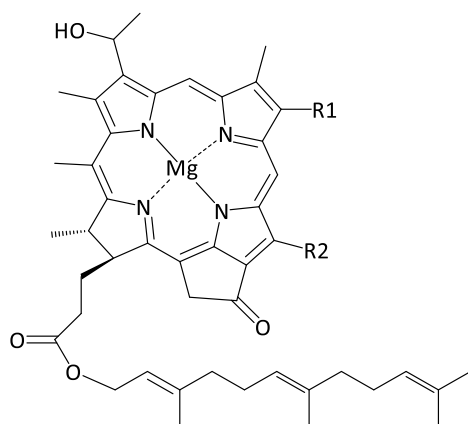


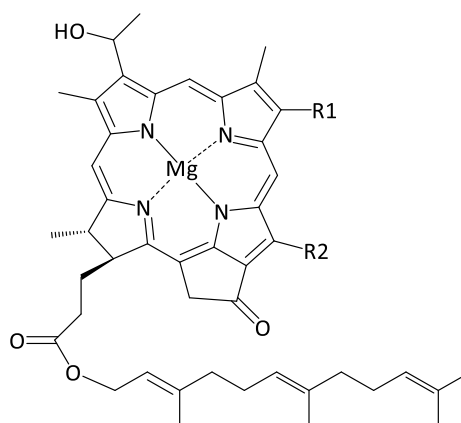
Figure A9.6. Structures of bacteriochlorophyll and bacterioviridin pigments (continued over)

B5 Bacteriochlorophyll *c*



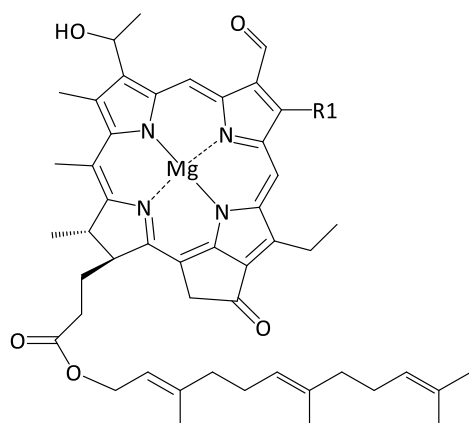
R1 = Et, *n*-Pr or *i*-Bu
R2 = Et or Me

B6 Bacteriochlorophyll *d*



R1 = Et, *n*-Pr, *i*-Bu or *neo*-pent
R2 = Et or Me

B7 Bacteriochlorophyll *e*



R1 = Et, *n*-Pr or *i*-Bu

Figure A9.6. (continued) Structures of bacteriochlorophyll and bacterioviridin pigments.

R: Carotenoids

Table A9.7. List of carotenoid structure numbers and name of compounds. For structures, see Figure A9.7.

Structure number	Compound name
R1	α -carotene
R2	β -carotene
R3	Lutein
R4	Violaxanthin
R5	Diadinoxanthin
R6	Diatoxanthin

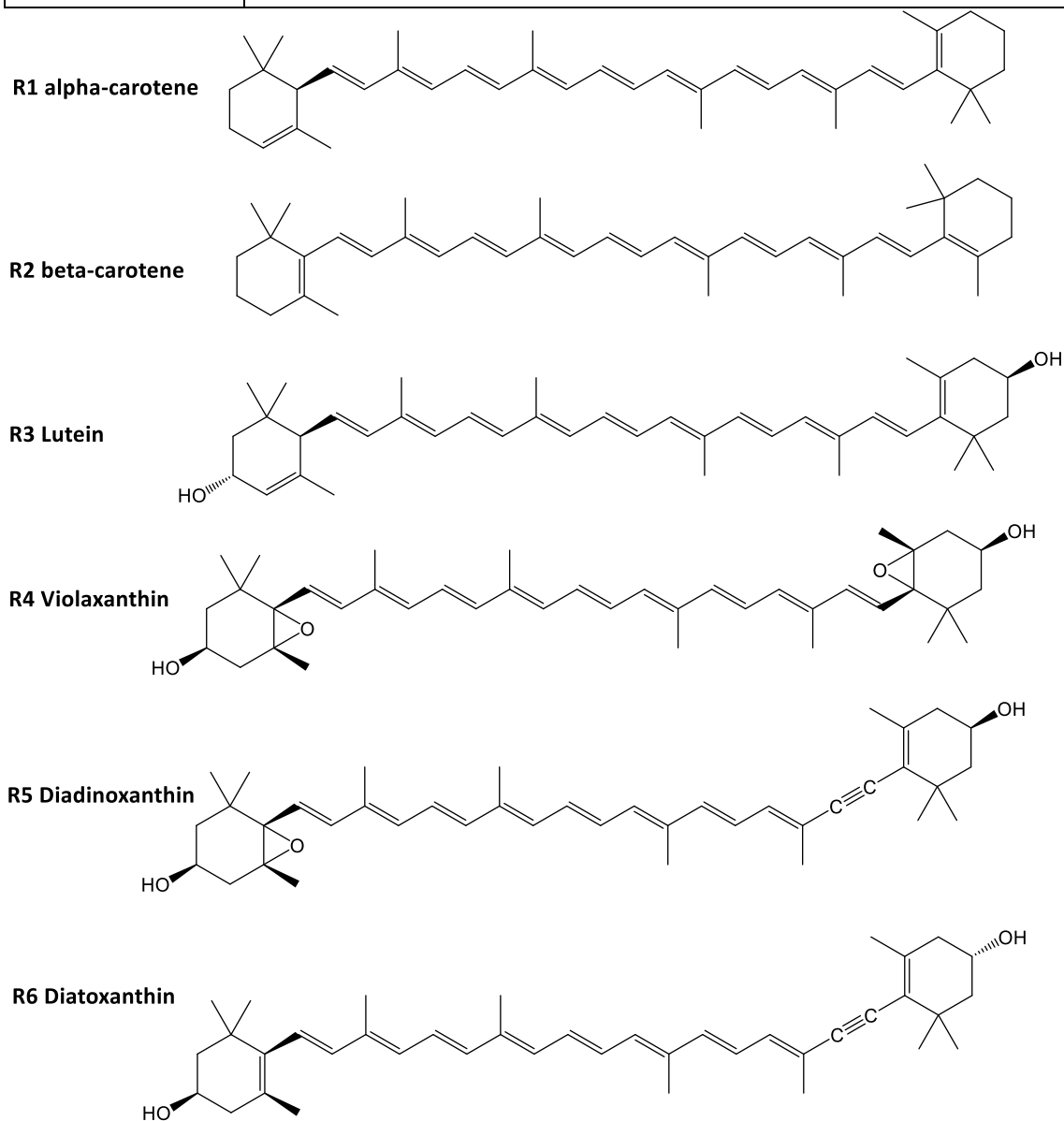


Figure A9.7. Structures of carotenoids.

Abbreviations

ACL	Average chain length index
APCI	Atmospheric pressure chemical ionisation
ASE	Accelerated solvent extraction
Bchl	Bacteriochlorophyll
BIT	Branched and isoprenoid tetraether index
Boc	Tert-butyloxycarbonyl
BPC	Base peak chromatogram
Bphe	Bacteriopheophytin
Bpphe	Pyrobacteriopheophytin
brGDGT	Branched glycerol dialkyl glycerol tetraether
c.	Circa (approximately)
CBT	Cyclisation of branched tetraether index
Chl	Chlorophyll
Chlone	Chlorophyllone
CID	Collision-induced dissociation
CPI	Carbon preference index
cv	Column volume
DAD	Diode array detector
DCM	Dichloromethane
DMAP	4-dimethylaminopyridine
EDC	<i>N</i> '-ethylcarbodiimide hydrochloride
EI	Electron ionisation
EIC	Extracted ion chromatogram
Eq.	Molar equivalents
ESI	Electrospray ionisation
FID	Flame ionisation detector
FLB	Fmoc-lysine(Boc)
FLB-GDGT	Fmoc-Lys(Boc)-glycerol dialkyl glycerol tetraether
FLB-o	Fmoc-Lys(Boc)-1-octadecanol
FLD	Fluorescence detector
Fmoc	Fluorenylmethyloxycarbonyl
GC	Gas chromatography

Abbreviations

GC-FID	Gas chromatography flame ionisation detector
GC-MS	Gas chromatography mass spectrometry
GDD	Glycerol dialkyl diether
GDGT	Glycerol dialkyl glycerol tetraether
GHz	Gigahertz
Gly	Glycine
GMD	Glycerol monoalkanediol diethers
GMGT	Glycerol monoalkyl glycerol tetraether
GMT	Glycerol monoalkanol triol
GTGT	Glycerol trialkyl glycerol tetraether
h	Hour(s)
HPLC	High-performance liquid chromatography
HPLC-FLD	High-performance liquid chromatography fluorescence detector
HPLC-MS	High-performance liquid chromatography mass spectrometry
HPLC-UV	High-performance liquid chromatography ultraviolet detector
i.d.	Internal diameter
iGDGT	Isoprenoid glycerol dialkyl glycerol tetraether
ka	Thousands of years ago
LOD	Limit of detection
Lys	Lysine
Ma	Million years ago
MAAT	Mean annual air temperature
MBT	Methylation of branched tetraether index
MeOH	Methanol
Min	Minute(s)
MIS	Marine isotope stage
MS	Mass spectrometry
MS/MS or MS ²	Tandem mass spectrometry
MTBE	Methyl tert-butyl ether
<i>m/z</i>	Ratio of mass of an ion over its charge number
NP	Normal phase
m OD	Metres above ordnance datum (the datum is mean sea level)
OH-GDD	Hydroxylated glycerol dialkyl diether
OH-GDGT	Hydroxylated glycerol dialkyl glycerol tetraether

Abbreviations

PFP	Pentafluorophenyl
Phe	Phenylalanine
Phe <i>a/b</i>	Phaeophytin <i>a/b</i>
Phorb	Phaeophorbide
Pphe	Pyrophaeophytin
Pphorb	Pyrophaeophorbide
Pro	Proline
<i>r</i> -dOG	1,2 -di- <i>O</i> -octadecyl- <i>rac</i> -glycerol
RP	Reversed-phase
Rpm	Rotation per minute
r.t.	Room temperature
<i>s</i>	Standard deviation
SCE	Steryl chlorin ester
<i>S/N</i>	Signal-to-noise ratio
SST	Sea-surface temperature
TEX ₈₆	Tetraether index of tetraethers consisting of 86 carbons
TEX ₈₆ ^L	Tetraether index of tetraethers consisting of 86 carbons – low
TLC	Thin-layer chromatography
Trp	Tryptophan
UHPLC	Ultra-high performance liquid chromatography
UHPLC-DAD	Ultra-high performance liquid chromatography diode array detector
U ^k ₃₇ and U ^{k'} ₃₇	Index of C ₃₇ unsaturated alkenones
UV	Ultraviolet
UV-vis	Ultraviolet – visible
<i>v/v</i>	Volume/volume
λ _{em}	Emission wavelength
λ _{ex}	Excitation wavelength

References

- Airs, R. L. Chlorophylls of phototrophic prokaryotes: Analytical developments and significance of natural distributions. PhD thesis, University of York (2001).
- Airs, R. L., Atkinson, J. E. & Keely, B. J. Development and application of a high resolution liquid chromatographic method for the analysis of complex pigment distributions. *J. Chromatogr. A* **917**, 167–177 (2001).
- Airs, R. L. & Keely, B. J. Atmospheric pressure chemical ionisation liquid chromatography/mass spectrometry of bacteriochlorophylls from *Chlorobiaceae*: Characteristic fragmentations. *Rapid Commun. Mass Spectrom.* **16**, 453–461 (2002).
- Airs, R. L., Temperton, B., Sambles, C., Farnham, G., Skill, S. C. & Llewellyn, C. A. Chlorophyll *f* and chlorophyll *d* are produced in the cyanobacterium *Chlorogloeopsis fritschii* when cultured under natural light and near-infrared radiation. *FEBS Lett.* **588**, 3770–3777 (2014).
- Airy, G. B. On the computation of the effect of the attraction of mountain-masses, as disturbing the apparent astronomical latitude of stations in geodetic surveys. *Philos. Trans. R. Soc. London A* **145**, 101–104 (1855).
- Antonioli, F., Bard, E., Potter, E. K., Silenzi, S. & Imbrota, S. 215-ka history of sea-level oscillations from marine and continental layers in Argentarola Cave speleothems (Italy). *Glob. Planet. Change* **43**, 57–78 (2004).
- Arthur, M. A., Schlanger, S. O. & Jenkyns, H. C. The Cenomanian-Turonian oceanic anoxic event, II. Palaeoceanographic controls on organic-matter production and preservation. *Geol. Soc. Spec. Publ.* **26**, 401–420 (1987).
- Arthur, M. A. & Dean, W. E. Organic-matter production and preservation and evolution of anoxia in the Holocene Black Sea. *Paleoceanography* **13**, 395–411 (1998).
- Ashton, N., Lewis, S., Parfitt, S., Candy, I., Keen, D., Kemp, R., Penkman, K., Thomas, G., Whittaker, J. & White, M. Excavations at the Lower Palaeolithic site at Elveden, Suffolk. *Proc. Prehist. Soc.* **71**, 1–61 (2005).
- Ashton, N., Lewis, S. G., Parfitt, S. A., Penkman, K. E. H. & Russell Coope, G. New evidence for complex climate change in MIS 11 from Hoxne, Suffolk, UK. *Quat. Sci. Rev.* **27**, 652–668 (2008).

References

- Aydin, N., Daher, S. & Gülaçar, F. O. On the sedimentary occurrence of chlorophyllone *a*. *Chemosphere* **52**, 937–942 (2003).
- Bai, Q. Y. & Zelles, L. A method for determination of archaeal ether-linked glycerolipids by high performance liquid chromatography with fluorescence detection as their 9-anthroyl derivatives. *Chemosphere* **35**, 263–274 (1997).
- Ballantyne, C. K. Extent and deglacial chronology of the last British-Irish Ice Sheet: Implications of exposure dating using cosmogenic isotopes. *J. Quat. Sci.* **25**, 515–534 (2010).
- Banerjee, S. & Mazumdar, S. Electrospray ionization mass spectrometry: A technique to access the information beyond the molecular weight of the analyte. *Int. J. Anal. Chem.* **2012**, 1–40 (2012).
- Barlow, N. L. M., Long, A. J., Gehrels, W. R., Saher, M. H., Scaife, R. G., Davies, H. J., Penkman, K. E. H., Bridgland, D. R., Sparkes, A., Smart, C. W. & Taylor, S. Relative sea-level variability during the late Middle Pleistocene: New evidence from eastern England. *Quat. Sci. Rev.* **173**, 20–39 (2017).
- Basse, A., Zhu, C., Versteegh, G. J. M., Fischer, G., Hinrichs, K-U. & Mollenhauer, G. Distribution of intact and core tetraether lipids in water column profiles of suspended particulate matter off Cape Blanc, NW Africa. *Org. Geochem.* **72**, 1–13 (2014).
- Bates, M. R., Parfitt, S. A. & Roberts, M. B. The chronology, palaeogeography and archaeological significance of the marine Quaternary record of the West Sussex Coastal Plain, Southern England, U.K. *Quat. Sci. Rev.* **16**, 1227–1252 (1997).
- Bates, M. R. & Bates, C. R. Multidisciplinary approaches to the geoarchaeological evaluation of deeply stratified sedimentary sequences: Examples from Pleistocene and Holocene deposits in Southern England, United Kingdom. *J. Archaeol. Sci.* **27**, 845–858 (2000).
- Bates, M. R., Keen, D. H. & Lautridou, J. P. Pleistocene marine and periglacial deposits of the English Channel. *J. Quat. Sci.* **18**, 319–337 (2003).
- Bates, M.R. & Stafford, E. *Thames Holocene: A geoarchaeological approach to the investigation of the river floodplain for High Speed 1, 1994-2004* (Wessex Archaeology: Salisbury, 2013).
- Bates, C. R., Bates, M. R., Dawson, S., Huws, D., Whittaker, J. E. & Wickham-Jones, C. R. The environmental context of the Neolithic monuments on the Brodgar Isthmus, Mainland, Orkney. *J. Archaeol. Sci. Rep.* **7**, 394–407 (2016).
- Bauersachs, T., Compaoré, J., Hopmans, E. C., Stal, L. J., Schouten, S. & Damsté, J. S. S. Distribution of heterocyst glycolipids in cyanobacteria. *Phytochemistry* **70**, 2034–2039 (2009a).

References

- Bauersachs, T., Hopmans, E. C., Compaoré, J., Stal, L. J., Schouten, S. & Damsté, J. S. S. Rapid analysis of long-chain glycolipids in heterocystous cyanobacteria using high-performance liquid chromatography coupled with electrospray ionization tandem mass spectrometry. *Rapid Commun. Mass Spectrom.* **23**, 1387–1394 (2009b).
- Bauersachs, T., Mudimu, O., Schulz, R. & Schwark, L. Distribution of long chain heterocyst glycolipids in N₂-fixing cyanobacteria of the order Stigonematales. *Phytochemistry* **98**, 145–150 (2014).
- Bauersachs, T., Rochelmeier, J. & Schwark, L. Seasonal lake surface water temperature trends reflected by heterocyst glycolipid-based molecular thermometers. *Biogeosciences* **12**, 3741–3751 (2015a).
- Bauersachs, T., Weidenbach, K., Schmitz, R. A. & Schwark, L. Distribution of glycerol ether lipids in halophilic, methanogenic and hyperthermophilic Archaea. *Org. Geochem.* **83–84**, 101–108 (2015b).
- Bauersachs, T. & Schwark, L. Glycerol monoalkanediol diethers: A novel series of archaeal lipids detected in hydrothermal environments. *Rapid Commun. Mass Spectrom.* **30**, 54–60 (2016).
- Baumann, L. M. F., Taubner, R-S., Bauersachs, T., Steiner, M., Schleper, C., Peckmann, J., Rittmann, S. K-M. R. & Birgel, D. Intact polar lipid and core lipid inventory of the hydrothermal vent methanogens *Methanocaldococcus villosus* and *Methanothermococcus okinawensis*. *Org. Geochem.* **126**, 33–42 (2018).
- Bayliss, M. A. J., Homer, R. B. & Shepherd, M. J. Anthracene-9-carbonyl chloride as a fluorescence and ultraviolet derivatising reagent for the high-performance liquid chromatographic analysis of hydroxy compounds. *J. Chromatogr.* **445**, 393–402 (1988).
- Beedham, G. E. *Identification of the British Mollusca* (Hulton Educational Publication Ltd., Raans Road, Amersham, Bucks, 1972).
- Behre, K. E. Coastal development, sea-level change and settlement history during the later Holocene in the Clay District of Lower Saxony (Niedersachsen), northern Germany. *Quat. Int.* **112**, 37–53 (2004).
- Bendle, J. A. P., Rosell-Melé, A., Cox, N. J. & Shennan, I. Alkenones, alkenoates, and organic matter in coastal environments of NW Scotland: Assessment of potential application for sea level reconstruction. *Geochemistry, Geophys. Geosystems* **10**, 1–21 (2009).
- Benjamin, J., Rovere, A., Fontana, A., Furlani S., Vacchi, M., Inglis, R. H., Galili, E., Antonioli, F., Sivan, D., Milko, S., Mourtzas, N., Felja, I., Meredith-Williams, M., Goodman-Tchernov, B., Kolaiti, E.,

References

- Anzidei, M. & Gehrels, R. Late Quaternary sea-level changes and early human societies in the central and eastern Mediterranean Basin: An interdisciplinary review. *Quat. Int.* **449**, 29–57 (2017).
- Bischoff, J., Sparkes, R. B., Doğrul Selver, A., Spencer, R. G. M., Gustafsson, Ö., Semiletov, I. P., Dudarev, O. V., Wagner, D., Rivkina, E., van Dongen, B. E. & Talbot, H. M. Source, transport and fate of soil organic matter inferred from microbial biomarker lipids on the East Siberian Arctic Shelf. *Biogeosciences* **13**, 4899–4914 (2016).
- Brassell, S. C., Eglinton, G., Marlowe, I. T., Pflaumann, U. & Sarnthein, M. Molecular stratigraphy: A new tool for climatic assessment. *Nature* **320**, 129–133 (1986).
- Bray, E. E. & Evans, E. D. Distribution of *n*-paraffins as a clue to recognition of source beds. *Geochim. Cosmochim. Acta* **22**, 2–15 (1961).
- Brendryen J., Hafliðason, H., Yokoyama, Y., Agasøster Haaga, K. & Hannisdal, B. Eurasian ice sheet collapse was a major source of Meltwater Pulse 1A 14,600 years ago. *Nat. Geosci.* **13**, 363–368 (2020).
- Bridgland, D. R., Harding, P., Allen, P., Candy, I., Cherry, C., George, W., Horne, D. J., Keen, D. H., Penkman, K. E. H., Preece, R. C., Rhodes, E. J., Scaife, R., Schreve, D. C., Schwenninger, J.-L., Slipper, I., Ward, G. R., White, M. J., White, T. S. & Whittaker, J. E. An enhanced record of MIS 9 environments, geochronology and geoarchaeology: Data from construction of the High Speed 1 (London-Channel Tunnel) rail-link and other recent investigations at Purfleet, Essex, UK. *Proc. Geol. Assoc.* **124**, 417–476 (2013).
- Bull, W. B. & Cooper, A. F. Uplifted marine terraces along the alpine fault, New Zealand. *Science* **234**, 1225–1228 (1986).
- Bunting, M. J. Vegetation history of Orkney, Scotland; pollen records from two small basins in west Mainland. *New Phytol.* **128**, 771–792 (1994).
- Candy, I., Coope, G. R., Lee, J. R., Parfitt, S. A., Preece, R. C., Rose, J. & Schreve, D. C. Pronounced warmth during early Middle Pleistocene interglacials: Investigating the Mid-Brunhes Event in the British terrestrial sequence. *Earth-Science Rev.* **103**, 183–196 (2010).
- Carr, A. S., Boom, A., Chase, B. M., Meadows, M. E. & Grimes, H. L. Holocene sea level and environmental change on the west coast of South Africa: Evidence from plant biomarkers, stable isotopes and pollen. *J. Paleolimnol.* **53**, 415–432 (2015).

References

- Castañeda, I. S., Schefuß, E., Pätzold, J., Sinninghe Damsté, J. S., Weldeab, S. & Schouten, S. Millennial-scale sea surface temperature changes in the eastern Mediterranean (Nile River Delta region) over the last 27,000 years. *Paleoceanography* **25**, 1–13 (2010).
- Castañeda, I. S. & Schouten, S. A review of molecular organic proxies for examining modern and ancient lacustrine environments. *Quat. Sci. Rev.* **30**, 2851–2891 (2011).
- Cattaneo, A. & Steel, R. J. Transgressive deposits: A review of their variability. *Earth-Science Rev.* **62**, 187–228 (2003).
- Chagué-Goff, C., Szczuciński, W. & Shinozaki, T. Applications of geochemistry in tsunami research: A review. *Earth-Science Rev.* **165**, 203–244 (2017).
- Chappell, J. Diversity and Reef Growth. *Nature* **286**, 249–252 (1980).
- Chikaraishi, Y., Naraoka, H. & Poulson, S. R. Hydrogen and carbon isotopic fractionations of lipid biosynthesis among terrestrial (C3, C4 and CAM) and aquatic plants. *Phytochemistry* **65**, 1369–1381 (2004).
- CHROMacademy_APCI: *Mass Spectrometry - Fundamental LC-MS - Atmospheric Pressure Chemical Ionisation (APCI)*.
- CHROMacademy_GC: *Theory and Instrumentation of GC Introduction*.
- CHROMacademy_HPLC detectors: *Instrumentation of HPLC – Detectors*.
- CHROMacademy_UV-vis: *Basic Lab Skills : UV-Visible Spectroscopy*.
- Church, J. A., White, N. J., Aarup, T., Wilson, W. S., Woodworth, P. L., Domingues, C. M., Hunter, J. R. & Lambeck, K. Understanding global sea levels: Past, present and future. *Sustain. Sci.* **3**, 9–22 (2008).
- Clark, R. C. & Blumer, M. Distribution of *n*-paraffins in marine organisms and sediment. *Limnol. Oceanogr.* **12**, 79–87 (1967).
- Conte, M. H., Sincre, M. A., Rühlemann, C., Weber, J. C., Schulte, S., Schulz-Bull, D. & Blanz, T. Global temperature calibration of the alkenone unsaturation index ($U^{K'}_{37}$) in surface waters and comparison with surface sediments. *Geochemistry, Geophys. Geosystems* **7**, 1–22 (2006).
- Cranwell, P. A. Chain-length distribution of *n*-alkanes from lake sediments in relation to post-glacial environmental change. *Freshw. Biol.* **3**, 259–265 (1973).

References

- Cranwell, P. A. Decomposition of aquatic biota and sediment formation: Lipid components of two blue-green algal species and of detritus resulting from microbial attack. *Freshw. Biol.* **6**, 481–488 (1976).
- Cranwell, P. A. Lipids of aquatic sediments and sedimenting particulates. *Prog. Lipid Res.* **21**, 271–308 (1982).
- Cranwell, P.A. Long-chain unsaturated ketones in recent lacustrine sediments. *Geochim. Cosmochim. Acta* **49**, 1545–1551 (1985).
- Crisp, M., Demarchi, B., Collins, M., Morgan-Williams, M., Pilgrim, E. & Penkman, K. Isolation of the intra-crystalline proteins and kinetic studies in *Struthio camelus* (ostrich) eggshell for amino acid geochronology. *Quat. Geochronol.* **16**, 110–128 (2013).
- Czeczuga, B. Investigations on carotenoids in Embryophyta. I. Bryophyta. *Bryologist* **83**, 21–28 (1980).
- D’Andrea, W. J. & Huang, Y. Long chain alkenones in Greenland lake sediments: Low $\delta^{13}\text{C}$ values and exceptional abundance. *Org. Geochem.* **36**, 1234–1241 (2005).
- da Silva Abranches, P. A., Ferreira de Paiva, W., de Fátima, Â., Terra Martins, F. & Fernandes, S. A. Calix[n]arene-catalyzed three-component Povarov reaction: Microwave-assisted synthesis of julolidines and mechanistic insights. *J. Org. Chem.* **83**, 1761–1771 (2018).
- Dalton, C., Birks, H. J. B., Brooks, S. J., Cameron, N. G., Evershed, R. P., Peglar, S. M., Scott, J. A. & Thompson R. A multi-proxy study of lake-development in response to catchment changes during the Holocene at Lochnagar, north-east Scotland. *Palaeogeogr. Palaeoclimatol. Palaeoecol.* **221**, 175–201 (2005).
- Damsté, J. S. S., Schouten, S., Hopmans, E. C., van Duin, A. C. T. & Geenevasen, J. A. J. Crenarchaeol: The characteristic core glycerol dibiphytanyl glycerol tetraether membrane lipid of cosmopolitan pelagic crenarchaeota. *J. Lipid Res.* **43**, 1641–1651 (2002).
- Damsté, J. S. S., Rijpstra, I. C., Hopmans, E. C., de Uijl, M. J., Weijers, J. W. H. & Schouten, S. The enigmatic structure of the crenarchaeol isomer. *Org. Geochem.* **124**, 22–28 (2018).
- Dang, X., Ding, W., Yang, H., Pancost, R. D., Naafs, B. D. A., Xue, J., Lin, X., Lu, J. & Xie, S. Different temperature dependence of the bacterial brGDGT isomers in 35 Chinese lake sediments compared to that in soils. *Org. Geochem.* **119**, 72–79 (2018).

References

- Davis, B. A. S., Brewer, S., Stevenson, A. C., Guiot, J. & Data contributors. The temperature of Europe during the Holocene reconstructed from pollen data. *Quat. Sci. Rev.* **22**, 1701–1716 (2003).
- De Deckker, P., Munday, C. I., Brocks, J., O’Loingsigh, T., Allison, G. E., Hope, J., Norman, M., Stuut, J-B. W., Tapper, N. J. & van der Kaars, S. Characterisation of the major dust storm that traversed over eastern Australia in September 2009; A multidisciplinary approach. *Aeolian Res.* **15**, 133–149 (2014).
- De Jonge, C., Hopmans, E. C., Zell, C. I., Kim, J-H., Schouten, S. & Damsté, J. S. S. Occurrence and abundance of 6-methyl branched glycerol dialkyl glycerol tetraethers in soils: Implications for palaeoclimate reconstruction. *Geochim. Cosmochim. Acta* **141**, 97–112 (2014).
- De Jonge, C., Stadnitskaia, A., Hopmans, E. C., Cherkashov, G., Fedotov, A., Streletskaia, I. D., Vasiliev, A. A. & Damsté, J. S. S. Drastic changes in the distribution of branched tetraether lipids in suspended matter and sediments from the Yenisei River and Kara Sea (Siberia): Implications for the use of brGDGT-based proxies in coastal marine sediments. *Geochim. Cosmochim. Acta* **165**, 200–225 (2015).
- De Jonge, C., Stadnitskaia, A., Cherkashov, G. & Sinninghe Damsté, J. S. Branched glycerol dialkyl glycerol tetraethers and crenarchaeol record post-glacial sea level rise and shift in source of terrigenous brGDGTs in the Kara Sea (Arctic Ocean). *Org. Geochem.* **92**, 42–54 (2016).
- de la Vega-Leinert, A. C., Smith, D. E. & Jones, R. L. Holocene coastal environmental changes on the periphery of an area of glacio-isostatic uplift: An example from Scapa Bay, Orkney, UK. *J. Quat. Sci.* **22**, 755–772 (2007).
- Del Rio, J. C., Gonzalez-Vila, F. J. & Martin, F. Variation in the content and distribution of biomarkers in two closely situated peat and lignite deposits. *Org. Geochem.* **18**, 67–78 (1992).
- DeLong, E. F. Archaea in coastal marine environments. *PNAS USA* **89**, 5685–5689 (1992).
- DeLong, E. F., Wu, K. Y., Prézelin, B. B. & Jovine, R. V. High abundance of Archaea in Antarctic marine picoplankton. *Nature* **371**, 695–697 (1994).
- Devoy, R. J. N. Flandrian sealevel changes in the Thames Estuary and the implications for land subsidence in England and Wales. *Nature* **270**, 712–715 (1977).
- Dickinson, M. R., Lister, A. M. & Penkman, K. E. H. A new method for enamel amino acid racemization dating: A closed system approach. *Quat. Geochronol.* **50**, 29–46 (2019).

References

- Didyk, B. M., Simoneit, B. R. T., Brassell, S. C. & Eglinton, G. Organic geochemical indicators of palaeoenvironmental conditions of sedimentation. *Nature* **272**, 216–222 (1978).
- Diefendorf, A. F., Leslie, A. B. & Wing, S. L. Leaf wax composition and carbon isotopes vary among major conifer groups. *Geochim. Cosmochim. Acta* **170**, 145–156 (2015).
- Doğrul Selver, A., Talbot, H. M., Gustafsson, Ö., Boulton, S. & van Dongen, B. E. Soil organic matter transport along a sub-Arctic river–sea transect. *Org. Geochem.* **51**, 63–72 (2012).
- Doğrul Selver, A., Sparkes, R. B., Bischoff, J., Talbot, H. M., Gustafsson, Ö., Semiletov, I. P., Dudarev, O. V., Boulton, S. & van Dongen, B. E. Distributions of bacterial and archaeal membrane lipids in surface sediments reflect differences in input and loss of terrestrial organic carbon along a cross-shelf Arctic transect. *Org. Geochem.* **83–84**, 16–26 (2015).
- Donati, D., Morelli, C. & Taddei, M. A rapid microwave-assisted esterification utilizing the Mukaiyama supported reagent. *Tetrahedron Lett.* **46**, 2817–2819 (2005).
- Eglinton, G. & Hamilton, R. J. Leaf epicuticular waxes. *Science* **156**, 1322–1335 (1967).
- Eley, Y. L., Thomson, W., Greene, S. E., Mandel, I., Edgar, K., Bendle, J. A. & Dunkley Jones, T. OPTiMAL: A new machine learning approach for GDGT-based palaeothermometry. *Clim. Past* (under review; <https://doi.org/10.5194/cp-2019-60>).
- Elling, F. J., Könneke, M., Lipp, J., Becker, K. W., Gagen, E. J. & Hinrichs, K.-U. Effects of growth phase on the membrane lipid composition of the thaumarchaeon *Nitrosopumilus maritimus* and their implications for archaeal lipid distributions in the marine environment. *Geochim. Cosmochim. Acta* **141**, 579–597 (2014).
- Ellison, J. C. & Stoddart, D. R. Mangrove ecosystem collapse during predicted sea-level rise: Holocene analogues and implications. *J. Coast. Res.* **7**, 151–165 (1991).
- Elvert, M., Pohlman, J. W., Becker, K. W., Gaglioti, B., Hinrichs, K.-U. & Wooller, M. J. Methane turnover and environmental change from Holocene lipid biomarker records in a thermokarst lake in Arctic Alaska. *The Holocene* **26**, 1766–1777 (2016).
- Emiliani, C. Pleistocene Temperatures. *J. Geol.* **63**, 538–578 (1955).
- Eyley, S. & Thielemans, W. Surface modification of cellulose nanocrystals. *Nanoscale* **6**, 7764–7779 (2014).

References

- Fang, J., Wu, F., Xiong, Y., Li, F., Du., X., An, D. & Wang, L. Source characterization of sedimentary organic matter using molecular and stable carbon isotopic composition of *n*-alkanes and fatty acids in sediment core from Lake Dianchi, China. *Sci. Total Environ.* **473–474**, 410–421 (2014).
- Farrell, M., Bunting, M. J., Lee, D. H. J. & Thomas, A. Neolithic settlement at the woodland's edge: Palynological data and timber architecture in Orkney, Scotland. *J. Archaeol. Sci.* **51**, 225–236 (2014).
- Ficken, K. J. & Farrimond, P. Sedimentary lipid geochemistry of Framvaren: impacts of a changing environment. *Mar. Chem.* **51**, 31–43 (1995).
- Ficken, K. J., Li, B., Swain, D. L. & Eglinton, G. An *n*-alkane proxy for the sedimentary input of submerged/floating freshwater aquatic macrophytes. *Org. Geochem.* **31**, 745–749 (2000).
- Fietz, S., Huguet, C., Bendle, J., Escala, M., Gallacher, C., Herfort, L., Jamieson, R., Martínez-García, A., McClymont, E. L., Peck, V. L., Prahl, F. G., Rossi, S., Rueda, G., Sanson-Barrera, A. & Rosell-Melé, A. Co-variation of crenarchaeol and branched GDGTs in globally-distributed marine and freshwater sedimentary archives. *Glob. Planet. Change* **92–93**, 275–285 (2012).
- Fisher, E., Oldfield, F., Wake, R., Boyle, J., Appleby, P. & Wolff, G. A. Molecular marker records of land use change. *Org. Geochem.* **34**, 105–119 (2003).
- Foster, L. C., Pearson, E. J., Juggins, S., Hodgson, D. A., Saunders, K. M., Verleyen, E. & Roberts, S. J. Development of a regional glycerol dialkyl glycerol tetraether (GDGT)-temperature calibration for Antarctic and sub-Antarctic lakes. *Earth Planet. Sci. Lett.* **433**, 370–379 (2016).
- Fürsich, F. T., Oschmann, W., Jaitly, A. K. & Singh, I. B. Faunal response to transgressive-regressive cycles: example from the Jurassic of western India. *Palaeogeogr. Palaeoclimatol. Palaeoecol.* **85**, 149–159 (1991).
- Gaba, M. & Dhingra, N. Microwave chemistry: General features and applications. *Indian J. Pharm. Educ. Res.* **45**, 175–183 (2011).
- Gaffney, V., Fitch, S. & Smith, D. *Europe's Lost World, the rediscovery of Doggerland* (York: CBA Research Report, 2009).
- Gagosian, R. B., Peltzer, E. T. & Merrill, J. T. Long-range transport of terrestrially derived lipids in aerosols from the south Pacific. *Nature* **325**, 800–803 (1987).
- Gaskell, S. J. & Eglinton, G. Rapid hydrogenation of sterols in a contemporary lacustrine sediment. *Nature* **254**, 209–211 (1975).

References

- Gedye, R. N., Smith, F. E., Westaway, K. C., Ali, H. Baldisera, L., Laberge, L. & Rousell, J. The use of microwave ovens for rapid organic synthesis. *Tetrahedron Lett.* **27**, 279–282 (1986).
- Gedye, R. N., Smith, F. E. & Westaway, K. C. The rapid synthesis of organic compounds in microwave ovens. *Can. J. Chem.* **66**, 17–26 (1988).
- Gehrels, W. R., Roe, H. M. & Charman, D. J. Foraminifera, testate amoebae and diatoms as sea-level indicators in UK saltmarshes: A quantitative multiproxy approach. *J. Quat. Sci.* **16**, 201–220 (2001).
- Gehrels, W. R., Dangendorf, S., Barlow, N. L. M., Saher, M. H., Long, A. J., Woodworth, P. L., Piecuch, C. G. & Berk, K. A preindustrial sea-level rise hotspot along the Atlantic Coast of North America. *Geophys. Res. Lett.* **47**, 1–12 (2020).
- Gervais, F. Ecology of cryptophytes coexisting near a freshwater chemocline. *Freshw. Biol.* **39**, 61–78 (1998).
- Gibbard, P. L. & Head, M. J. IUGS ratification of the Quaternary system/period and the Pleistocene series/epoch with a base at 2.58 Ma. *Quaternaire* **20**, 411–412 (2009).
- Gibbard, P. L., West, R. G. & Hughes, P. D. Pleistocene glaciation of Fenland, England, and its implications for evolution of the region. *R. Soc. Open Sci.* **5**, 1–52 (2018).
- Gonzalez, S., Innes, J., Huddart, D., Davey, P. & Plater, A. Holocene coastal change in the north of the Isle of Man: Stratigraphy, palaeoenvironment and archaeological evidence. *Geol. Soc. Spec. Publ.* **175**, 343–363 (2000).
- Gorham, E. & Sanger, J. E. Plant pigments in woodland soils. *Ecology* **48**, 306–308 (1967).
- Goto, J., Goto, N., Shamsa, F., Saito, M., Komatsu, S., Suzuki, K. & Nambara, T. New sensitive derivatization of hydroxysteroids for high-performance liquid chromatography with fluorescence detection. *Anal. Chim. Acta* **147**, 397–400 (1983).
- Green, K. A. The fate of lipids in archaeological burial soils. PhD thesis, University of York (2013).
- Greenwood, D. R. The taphonomy of plant macrofossils. In *The Process of Fossilization* pp. 141–169 (Columbia University Press, New York, 1991).
- Hanford, M. J. & Peebles, T. L. Archaeal Tetraether Lipids: Unique structures and applications. *Appl. Biochem. Biotechnol.* **97**, 45–62 (2002).
- Harradine, P. J., Harris, P. G., Head, R. N., Harris, R. P. & Maxwell, J. R. Steryl chlorin esters are formed by zooplankton herbivory. *Geochim. Cosmochim. Acta* **60**, 2265–2270 (1996).

References

- Hayes, J. M. Factors controlling ^{13}C contents of sedimentary organic compounds: Principles and evidence. *Mar. Geol.* **113**, 111–125 (1993).
- Hays, J. D., Imbrie, J. & Shackleton, N. J. Variations in the earth's orbit: Pacemaker of the ice ages. *Science* **194**, 1121–1132 (1976).
- Hearty, P. J., O'Leary, M. J., Kaufman, D. S., Page, M. C. & Bright, J. Amino acid geochronology of individual foraminifer (*Pulleniatina obliquiloculata*) tests, north Queensland margin, Australia: A new approach to correlating and dating Quaternary tropical marine sediment cores. *Paleoceanography* **19**, 1–14 (2004).
- Hein, A. S., Marrero, S. M., Woodward, J., Dunning, S. A., Winter, K., Westoby, M. J., Freeman, S. P. H.T., Shanks, R. P. & Sugden, D. E. Mid-Holocene pulse of thinning in the Weddell Sea sector of the West Antarctic ice sheet. *Nat. Commun.* **7**, 1–8 (2016).
- Hendry, G. A. F., Houghton, J. D. & Brown, S. B. The degradation of chlorophyll – A biological enigma. *New Phytol.* **107**, 255–302 (1987).
- Hershberger, K. L., Barns, S. M., Reysenbach, A.-L., Dawson, S. C. & Pace, N. R. Wide diversity of Crenarchaeota. *Nature* **384**, 420 (1996).
- Hillman, G., Hedges, R., Moore, A., Colledge, S. & Pettitt, P. New evidence of lateglacial cereal cultivation at Abu Hureyra on the Euphrates. *Holocene* **11**, 383–393 (2001).
- Hodgson, D. A., Verleyen, E., Vyverman, W., Sabbe, K., Leng, M. J., Pickering, M. D. & Keely, B. J. A geological constraint on relative sea level in Marine Isotope Stage 3 in the Larsemann Hills, Lambert Glacier region, East Antarctica (31 366–33 228 cal yr BP). *Quat. Sci. Rev.* **28**, 2689–2696 (2009).
- Hollerbach, A. Early diagenetic alterations of biogenetic organic compounds. *Naturwissenschaften* **65**, 202–204 (1978).
- Hopmans, E. C., Schouten, S., Pancost, R. D., van der Meer, M. T. J. & Sinninghe Damsté, J. S. Analysis of intact tetraether lipids in archaeal cell material and sediments by high performance liquid chromatography/atmospheric pressure chemical ionization mass spectrometry. *Rapid Commun. Mass Spectrom.* **14**, 585–589 (2000).
- Hopmans, E. C., Wijers, J. W. H., Schefuß, E., Herfort, L., Sinninghe Damsté, J. S. & Schouten S. A novel proxy for terrestrial organic matter in sediments based on branched and isoprenoid tetraether lipids. *Earth Planet. Sci. Lett.* **224**, 107–116 (2004).

References

- Horton, A., Keen, D. H., Field, M. H., Robinson, J. E., Coope, G. R., Currant, A. P., Graham, D. K., Green, C. P. & Phillips, L. M. The Hoxnian interglacial deposits at Woodston, Peterborough. *Philos. Trans. R. Soc. B Biol. Sci.* **338**, 131–164 (1992).
- Hughes, P. D. M., Mauquoy, D., Barber, K. E. & Langdon, P. G. Mire-development pathways and palaeoclimatic records from a full Holocene peat archive at Walton Moss, Cumbria, England. *Holocene* **10**, 465–479 (2000).
- Huguet, C., Kim, J. H., Damsté, J. S. S. & Schouten, S. Reconstruction of sea surface temperature variations in the Arabian Sea over the last 23 kyr using organic proxies (TEX₈₆ and U₃₇^K). *Paleoceanography* **21**, 1–13 (2006).
- Huguet, A., Coffinet, S., Roussel, A., Gayraud, F., Anquetil, C., Bergonzini, L., Bonanomi, G., Williamson, D., Majule, A. & Derenne, S. Evaluation of 3-hydroxy fatty acids as a pH and temperature proxy in soils from temperate and tropical altitudinal gradients. *Org. Geochem.* **129**, 1–13 (2019).
- IPCC, 2014: Pachauri, R. K., Meyer, L. & Core writing team. *Climate change 2014 Synthesis Report. Intergovernmental Panel on Climate Change* (2014).
- Ishiwatari, R., Hirakawa, Y., Uzaki, M., Yamada, K. & Yada, T. Organic geochemistry of the Japan Sea sediments – 1: Bulk organic matter and hydrocarbon analyses of Core KH-79-3, C-3 from the Oki Ridge for paleoenvironment assessments. *J. Oceanogr.* **50**, 179–195 (1994).
- IUGS, 2020: International commission on stratigraphy, *International chronostratigraphic chart v2020/01*, (<http://www.stratigraphy.org/index.php/ics-chart-timescale>, accessed 17/02/20).
- Iwasawa, T., Wash, P., Gibson, C. & Rebek, J. J. Reaction of an introverted carboxylic acid with carbodiimide. *Tetrahedron* **63**, 6506–6511 (2007).
- Jablonski, D. Apparent versus real biotic effects of transgressions and regressions. *Paleobiology* **6**, 397–407 (1980).
- Jackson, S. T. & Lyford, M. E. Pollen dispersal models in Quaternary plant ecology: Assumptions, parameters, and prescriptions. *Bot. Rev.* **65**, 39–75 (1999).
- Jetter, R., Schaffer, S. & Riederer, M. Leaf cuticular waxes are arranged in chemically and mechanically distinct layers: Evidence from *Prunus laurocerasus* L. *Plant, Cell Environ.* **23**, 619–628 (2000).

References

- Kandiano, E. S. & Bauch, H. A. Surface ocean temperatures in the north-east Atlantic during the last 500 000 years: Evidence from foraminiferal census data. *Terra Nov.* **15**, 265–271 (2003).
- Kaufman, D. S. Temperature sensitivity of aspartic and glutamic acid racemization in the foraminifera *Pulleniatina*. *Quat. Geochronol.* **1**, 188–207 (2006).
- Kaufman, D. S., Polyak, L., Adler, R., Channell, J. E. T. & Xuan, C. Dating late Quaternary planktonic foraminifer *Neogloboquadrina pachyderma* from the Arctic Ocean using amino acid racemization. *Paleoceanography* **23**, PA3224 (2008).
- Kaur, G., Mountain, B. W., Stott, M. B., Hopmans, E. C. & Pancost, R. D. Temperature and pH control on lipid composition of silica sinters from diverse hot springs in the Taupo Volcanic Zone, New Zealand. *Extremophiles* **19**, 327–44 (2015).
- Keatinge, T. H. & Dickson, J. H. Mid-Flandrian changes in vegetation on Mainland Orkney. *New Phytol.* **82**, 585–612 (1979).
- Keely, B. J., Prowse, W. G. & Maxwell, J. R. The Treibs hypothesis: An evaluation based on structural studies. *Energy & Fuels* **4**, 628–634 (1990).
- Keely B. J. Geochemistry of Chlorophylls. In *Chlorophylls and Bacteriochlorophylls: Biochemistry, biophysics, functions and applications*, **25**, ch. 37, pp. 535–561 (Springer, 2006).
- Keinänen, M. M., Korhonen, L. K., Martikainen, P. J., Vartiainen, T., Miettinen, I. T., Lehtola, M. J., Nenonen, K., Pajunen, H. & Kontro, M. H. Gas chromatographic-mass spectrometric detection of 2- and 3-hydroxy fatty acids as methyl esters from soil, sediment and biofilm. *J. Chromatogr. B* **783**, 443–451 (2003).
- Kellock, E. Alkaline basic igneous rocks in the Orkneys. *Scottish J. Geol.* **5**, 140–153 (1969).
- Killops, S. D. & Killops, V. J. *An introduction to organic geochemistry* (Longman geochemistry, 1993).
- Kim, J-H., van der Meer, J., Schouten, S., Helmke, P., Willmott, V., Sangiorgi, F., Koç, N., Hopmans, E. C. & Sinninghe Damsté, J. S. New indices and calibrations derived from the distribution of crenarchaeal isoprenoid tetraether lipids: Implications for past sea surface temperature reconstructions. *Geochim. Cosmochim. Acta* **74**, 4639–4654 (2010).
- Kjemperud, A. Diatom changes in sediments of basins possessing marine/lacustrine transitions in Frosta, Nord-Trøndelag, Norway. *Boreas* **10**, 27–38 (1981).

References

- Klages, J. P., Salzmann, U., Bickert, T., Hillenbrand, C., Gohl, K., Kuhn, G., Bohaty, S. M., Titschack, J., Müller, J., Frederichs, T., Bauersachs, T., Ehrmann, W., van de Flierdt, T., Simões Pereira, P., Larter, R. D., Lohmann, G., Niezgodzki, I., Uenzelmann-Neben, G., Zundel, M., Spiegel, C., Mark, C., Chew, D., Francis, J. E., Nehrke, G., Schwarz, F., Smith, J. A., Freudenthal, T., Esper, O., Pälike, H., Ronge, T. A., Dziadek, R. & the Science Team of Expedition PS104. Temperate rainforests near the South Pole during peak Cretaceous warmth. *Nature* **580**, 81–86 (2020).
- Knappy, C. S. Mass spectrometric studies of ether lipids in Archaea and sediments. PhD thesis, University of York (2010).
- Knappy, C. S., Nunn, C. E. M., Morgan, H. W. & Keely, B. J. The major lipid cores of the archaeon *Ignisphaera aggregans*: Implications for the phylogeny and biosynthesis of glycerol monoalkyl glycerol tetraether isoprenoid lipids. *Extremophiles* **15**, 517–528 (2011).
- Knappy, C. S., Barillà, D., de Blanquiere, J. P. A., Morgan, H. W., Nunn, C. E. M., Suleman, M., Tan, C. H. W. & Keely, B. J. Structural complexity in isoprenoid glycerol dialkyl glycerol tetraether lipid cores of *Sulfolobus* and other archaea revealed by liquid chromatography-tandem mass spectrometry. *Chem. Phys. Lipids* **165**, 648–655 (2012).
- Knappy, C. S., Yao, P., Pickering, M. D. & Keely, B. J. Identification of homoglycerol- and dihomoglycerol-containing isoprenoid tetraether lipid cores in aquatic sediments and a soil. *Org. Geochem.* **76**, 146–156 (2014).
- Koga, Y., Nishihara, M., Morii, H. & Akagawa-Matsushita, M. Ether polar lipids of methanogenic bacteria: Structures, comparative aspects, and biosyntheses. *Microbiol. Rev.* **57**, 164–182 (1993).
- Kuczynska, P., Jemiola-Rzeminska, M. & Strzalka, K. Photosynthetic pigments in diatoms. *Mar. Drugs* **13**, 5847–5881 (2015).
- Lambeck, K., Rouby, H., Purcell, A., Sun, Y. & Sambridge, M. Sea level and global ice volumes from the Last Glacial Maximum to the Holocene. *Proc. Natl. Acad. Sci. U.S.A.* **111**, 15296–15303 (2014).
- Lane, P., Donnelly, J. P., Woodruff, J. D. & Hawkes, A. D. A decadal-resolved paleohurricane record archived in the late Holocene sediments of a Florida sinkhole. *Mar. Geol.* **287**, 14–30 (2011).
- Leavitt, P. R. Experimental determination of carotenoid degradation. *J. Paleolimnol.* **1**, 215–227 (1988).
- Leavitt, P. R. A review of factors that regulate carotenoid and chlorophyll deposition and fossil pigment abundance. *J. Paleolimnol.* **9**, 109–127 (1993).

References

- Lewin, R. A. Prochlorophyta as a proposed new division of algae. *Nature* **261**, 697–698 (1976).
- Li, L., Li, Q., He, J., Wang, H., Ruan, Y. & Li, J. Biomarker-derived phytoplankton community for summer monsoon reconstruction in the western South China Sea over the past 450ka. *Deep. Res. Part II Top. Stud. Oceanogr.* **122**, 118–130 (2015).
- Li, X., Zong, Y., Zheng, Z., Huang, G. & Xiong, H. Marine deposition and sea surface temperature changes during the last and present interglacials in the west coast of Taiwan Strait. *Quat. Int.* **440**, 91–101 (2017).
- Li, X., Anderson, B. J., Vogeler, I. & Schwendenmann, L. Long-chain *n*-alkane and *n*-fatty acid characteristics in plants and soil – Potential to separate plant growth forms, primary and secondary grasslands. *Sci. Total Environ.* **645**, 1567–1578 (2018).
- Li, C., Yu, S., Yao, S., Shen, J., Ji, M., Chen, R., Sun, W. & Ling, C. Response of alpine vegetation to climate changes in the Nanling Mountains during the second half of the Holocene. *Quat. Int.* **522**, 12–22 (2019).
- Lim, K. L. H., Pancost, R. D., Hornibrook, E. R. C., Maxfield, P. J. & Evershed, R. P. Archaeol: An indicator of methanogenesis in water-saturated soils. *Archaea* **896727**, 1–9 (2012).
- Lisiecki, L. E. & Raymo, M. E. A Pliocene-Pleistocene stack of 57 globally distributed benthic $\delta^{18}\text{O}$ records. *Paleoceanography* **20**, 1–17 (2005).
- Liu, X. L., Summons, R. E. & Hinrichs, K. U. Extending the known range of glycerol ether lipids in the environment: Structural assignments based on tandem mass spectral fragmentation patterns. *Rapid Commun. Mass Spectrom.* **26**, 2295–2302 (2012a).
- Liu, X. L., Lipp, J. S., Schröder, J. M., Summons, R. E. & Hinrichs, K-U. Mono- and dihydroxyl glycerol dibiphytanyl glycerol tetraethers in marine sediments: Identification of both core and intact polar lipid forms. *Geochim. Cosmochim. Acta* **89**, 102–115 (2012b).
- Liu, H. & Liu, W. Concentration and distributions of fatty acids in algae, submerged plants and terrestrial plants from the northeastern Tibetan Plateau. *Org. Geochem.* **113**, 17–26 (2017).
- Long, A. J., Scaife, R. G. & Edwards, R. J. Stratigraphic architecture, relative sea-level, and models of estuary development in southern England: New data from Southampton Water. *Geol. Soc. Spec. Publ.* **175**, 253–279 (2000).

References

- Long, A. J., Barlow, N. L. M., Busschers, F. S., Cohen, K. M., Gehrels, W. R. & Wake, L. M. Near-field sea-level variability in northwest Europe and ice sheet stability during the last interglacial. *Quat. Sci. Rev.* **126**, 26–40 (2015).
- Long, A. J., Barlow, N. M. L., Dawson S., Hill, S., Innes, J. B., Kelham, C., Milne, F. D. & Dawson, A. Lateglacial and Holocene relative sea-level changes and first evidence for the Storegga tsunami in Sutherland, Scotland. *J. Quat. Sci.* **31**, 239–255 (2016).
- Longo, W. M., Dillon, J. T., Tarozo, R., Salacup, J. M. & Huang, Y. Unprecedented separation of long chain alkenones from gas chromatography with a poly(trifluoropropylmethylsiloxane) stationary phase. *Org. Geochem.* **65**, 94–102 (2013).
- Lowe, J. & Walker, M. *Reconstructing Quaternary Environments* (Routledge, 3rd ed., 2015).
- Luche, J-L. *Synthetic Organic Sonochemistry* (Plenum Press, New York, 1998).
- Ma, L. & Dolphin, D. Stereoslective synthesis of new chlorophyll *a* related antioxidants isolated from marine organisms. *J. Org. Chem.* **61**, 2501–2510 (1996).
- MacDonald, R. I. Characteristics of self-quenching of the fluorescence of lipid-conjugated rhodamine in membranes. *J. Biol. Chem.* **265**, 13533–13539 (1990).
- Mackenzie, A. S., Brassell, S. C., Eglinton, G. & Maxwell, J. R. Chemical fossils: The geological fate of steroids. *Science* **217**, 491–504 (1982).
- Mackie, E. A. V., Leng, M. J., Lloyd, J. M. & Arrowsmith, C. Bulk organic $\delta^{13}\text{C}$ and C/N ratios as palaeosalinity indicators within a Scottish isolation basin. *J. Quat. Sci.* **20**, 303–312 (2005).
- Maclaren, C. The glacial theory of Prof. Agassiz. *Am. J. Sci. Arts* **42**, 346–365 (1842).
- Madigan, M. T. & Jung, D. O. An overview of purple bacteria: Systematics, physiology, and habitats. In *The Purple Phototrophic Bacteria*, ch. 1, pp. 1–15 (Springer, 2009).
- Marlowe, I. T., Green, J. C., Neal, A. C., Brassell, S. C., Eglinton, G. & Course, P. A. Long chain (*n*-C₃₇–C₃₉) alkenones in the Prymnesiophyceae. Distribution of alkenones and other lipids and their taxonomic significance. *Br. Phycol. J.* **19**, 203–216 (1984).
- Maslin, M. Forty years of linking orbits to Ice Ages. *Nature* **540**, 208–210 (2016).
- Matloubi Moghaddam, F., Doulabi, M. & Saeidian, H. Controlled microwave-assisted synthesis of nanoparticles and their catalytic activity for *O*-acylation of alcohol and phenol in acetic anhydride. *Sci. Iran.* **19**, 1597–1600 (2012).

References

- Mauz, B., Ruggieri, G. & Spada, G. Terminal Antarctic melting inferred from a far-field coastal site. *Quat. Sci. Rev.* **116**, 122–132 (2015).
- Mazzini, I., Anadon, P., Barbieri, M., Castorina, F., Ferreli, L., Gliozzi, E., Mola, M. & Vittori, E. Late Quaternary sea-level changes along the Tyrrhenian coast near Orbetello (Tuscany, central Italy): Palaeoenvironmental reconstruction using ostracods. *Mar. Micropaleontol.* **37**, 289–311 (1999).
- McGuire, W. J., Howarth, R. J., Firth, C. R., Solow, A. R., Pullen, A. D., Saunders, S. J., Stewart, I. S. & Vita-Finzi, C. Correlation between rate of sea-level change and frequency of explosive volcanism in the Mediterranean. *Nature* **389**, 473–476 (1997).
- McManus, J. F., Oppo, D. W. & Cullen, J. L. A 0.5-Million-year record of millennial-scale climate variability in the North Atlantic. *Science*. **283**, 971–975 (1999).
- Meischner, D. Der pliozäne Teich von Willershausen am Harz. In *Europäische Fossilagerstätten*, pp. 223–228 (Springer-Verlag, Berlin Heidelberg, 2000).
- Meyers, P. A. & Ishiwatari, R. Lacustrine organic geochemistry — An overview of indicators of organic matter sources and diagenesis in lake sediments. *Org. Geochem.* **20**, 867–900 (1993).
- Meyers, P. A. Organic geochemical proxies of paleoceanographic, paleolimnologic, and paleoclimatic processes. *Org. Geochem.* **27**, 213–250 (1997).
- Miller, K. G. Sea level change, last 250 million years. *Encycl. Earth Sci. Ser.* 879–887 (2009).
- Mitlehner, A. G. Palaeoenvironments of the Hoxnian Nar Valley Clay, Norfolk, England: Evidence from an integrated study of diatoms and ostracods. *J. Quat. Sci.* **7**, 335–341 (1992).
- Mitrovica, J. X. & Peltier, W. R. On postglacial geoid subsidence over the equatorial oceans. *J. Geophys. Res.* **96**, 20053–20071 (1991).
- Miyashita, H., Ikemoto, H., Kurano, N., Adachi, K., Chihara, M. & Miyachi, S. Chlorophyll *d* as a major pigment. *Nature* **383**, 402 (1996).
- Morii, H., Eguchi, T., Nishihara, M., Kakinuma, K., König, H. & Koga, Y. A novel ether core lipid with H-shaped C₈₀-isoprenoid hydrocarbon chain from the hyperthermophilic methanogen *Methanothermobacter fervidus*. *Biochim. Biophys. Acta - Lipids Lipid Metab.* **1390**, 339–345 (1998).
- Moss, B. Studies on the degradation of chlorophyll *a* and carotenoids in freshwaters. *New Phytol.* **67**, 49–59 (1968).

References

- Müller, P., Kirst, G., Ruhland, G., von Storch, I. & Rosell-Melé, A. Calibration of the alkenone paleotemperature index $U_{37}^{K'}$ based on core-tops from the eastern South Atlantic and the global ocean (60°N-60°S). *Geochim. Cosmochim. Acta* **62**(10), 1757-1772 (1998).
- Müller, A. & Mathesius, U. The palaeoenvironments of coastal lagoons in the southern Baltic Sea, I. The application of sedimentary C_{org}/N ratios as source indicators of organic matter. *Palaeogeogr. Palaeoclimatol. Palaeoecol.* **145**, 1-16 (1999).
- Murray, J. W. *Ecology and applications of benthic foraminifera*. p. 122 (Cambridge University Press, 2006).
- Murray, K. K., Boyd, R. K., Eberlin, M. N., Langley, G. J., Li, L. & Naito, Y. Definitions of terms relating to mass spectrometry (IUPAC Recommendations 2013). *Pure Appl. Chem.* **85**, 1515–1609 (2013).
- Murray-Wallace, C. V. & Woodroffe, C. D. *Quaternary sea-level changes – A global perspective*. (Cambridge University Press, 2014).
- Muto, T. & Steel, R. J. Principles of regression and transgression: The nature of the interplay between accommodation and sediment supply. *J. Sediment. Res.* **67**, 994–1000 (1997).
- Naafs, B. D. A., Inglis, G. N., Zheng, Y., Amesbury, M. J., Biester, H., Bindler, R., Blewett, J., Burrows, M. A., del Castillo Torres, D., Chambers, F. M., Cohen, A. D., Evershed, R. P., Feakins, S. J., Gałka, M., Gallego-Sala, A., Gandois, L., Gray, D. M., Hatcer, P. G., Honorio Coronado, E. N., Hugues, P. D. M., Huguët, A., Könönen, M., Laggoun-Défarge, F., Lähteenoja, O., Lamentowics, M., Marchant, R., McClymont, E., Pontevedra-Pombal, X., Ponton, C., Pourmand, A., Rizzuti, A. M., Rochefort, L., Schellekens, J., De Vleeschouwer, F., Pancost, R. D. Introducing global peat-specific temperature and pH calibrations based on brGDGT bacterial lipids. *Geochim. Cosmochim. Acta* **208**, 285–301 (2017).
- Naafs, B. D. A., Inglis, G. N., Blewett, J., McClymont, E. L., Lauretano, V., Xie, S., Evershed, R. P. & Pancost, R. D. The potential of biomarker proxies to trace climate, vegetation, and biogeochemical processes in peat: A review. *Glob. Planet. Change* **179**, 57–79 (2019).
- Nakakuni, M., Dairiki, C., Kaur, G. & Yamamoto, S. Stanol to sterol ratios in late Quaternary sediments from southern California: An indicator for continuous variability of the oxygen minimum zone. *Org. Geochem.* **111**, 126–135 (2017).
- NASA <https://climate.nasa.gov/vital-signs/sea-level/> (accessed 17/02/2020).

References

- Nascentes, C. C., Korn, M., Sousa, C. S. & Arruda, M. A. Z. Use of ultrasonic baths for analytical applications: A new approach for optimisation conditions. *J. Braz. Chem. Soc.* **12**, 57–63 (2001).
- Naylor, C. C. & Keely, B. J. Sedimentary purpurins: Oxidative transformation products of chlorophylls. *Org. Geochem.* **28**, 417–422 (1998).
- Neises, B. & Steglich, W. Simple method for the esterification of carboxylic acids. *Angew. Chemie Int. Ed. English* **17**, 522–524 (1978).
- Neises, B. & Steglich, W. Esterification of carboxylic acids with dicyclohexylcarbodiimide/4-dimethylaminopyridine: Tert-butyl ethyl fumarate In: *Organic Syntheses*. p. 183 (Wiley Online Library, 1985).
- Nelson, T. J. Fluorescent high-performance liquid chromatography assay for lipophilic alcohols. *Anal. Biochem.* **419**, 40–45 (2011).
- Nicholls, R. J. & Cazenave, A. Sea-level rise and its impact on coastal zones. *Science* **328**, 1517–1520 (2010).
- NIST GC-MS of cholesterol <https://webbook.nist.gov/cgi/cbook.cgi?ID=C57885&Mask=200#Mass-Spec> (accessed 17/9/19).
- O’Leary, M. H. Carbon isotopes in photosynthesis. *Bioscience* **38**, 328–336 (1988).
- Ohtsubo, S., Kanno, M., Miyahara, H., Kohno, S., Koga, Y. & Miura, I. A sensitive method for quantification of acetoclastic methanogens and estimation of total methanogenic cells in natural environments based on an analysis of ether-linked glycerolipids. *FEMS Microbiol Ecol* **12**, 39–50 (1993).
- Olariu, T., Suta, L-M., Popoiu, C., Ledeti, I. V., Simu, G. M., Saviou-Balint, G. & Fulias, A. Alternative synthesis of paracetamol and aspirin under non-conventional conditions. *Rev. Chim.* **65**, 633–635 (2014).
- Ortiz, J. E., Torres, T., Delgado, A., Julià, R., Lucini, M., Llamas, F. J., Reyes, E., Soler, V. & Valle, M. The palaeoenvironmental and palaeohydrological evolution of Padul Peat Bog (Granada, Spain) over one million years, from elemental, isotopic and molecular organic geochemical proxies. *Org. Geochem.* **35**, 1243–1260 (2004).
- Otto, A., Simoneit, B. R. T. & Rember, W. C. Conifer and angiosperm biomarkers in clay sediments and fossil plants from the Miocene Clarkia Formation, Idaho, USA. *Org. Geochem.* **36**, 907–922 (2005).

References

- PAGES, 2016: Past Interglacials Working Group of PAGES. *Rev. Geophys.* **54**, 162–219 (2016).
- Palamakumbura, R. A new palaeogeographic model for the post-glacial marine and estuarine sediments of the Firth of the Forth, Scotland. *British Geological Survey OR/18/016*, 1–49 (2018).
- Parker, J. H., Smith, G. A., Fredrickson, H. L., Vestal, J. R. & White, D. C. Sensitive assay, based on hydroxy fatty acids from lipopolysaccharide lipid A, for gram-negative bacteria in sediments. *Appl. Environ. Microbiol.* **44**, 1170–1177 (1982).
- Pearce, G. E. S., Keely, B. J., Harradine, P. J., Eckardt, C. B. & Maxwell, J. R. Characterization of naturally-occurring sterol esters derived from chlorophyll *a*. *Tetrahedron Lett.* **34**, 2989–2992 (1993).
- Pearson, A., Huang, Z., Ingalls, A. E., Romanek, C. S., Wiegel, J., Freeman, K. H., Smittenberg, R. H. & Zhang, C. L. Nonmarine crenarchaeol in Nevada hot springs. *App. Environ. Microbiol.* **70**, 5229–5237 (2004).
- Pearson, E. J., Juggins, S. & Farrimond, P. Distribution and significance of long-chain alkenones as salinity and temperature indicators in Spanish saline lake sediments. *Geochim. Cosmochim. Acta* **72**, 4035–4046 (2008).
- Pearson, E. J., Juggins, S., Talbot, H. M., Weckström, J., Rosén, P., Ryves, D. B., Roberts, S. J. & Schmidt, R. A lacustrine GDGT-temperature calibration from the Scandinavian Arctic to Antarctic: Renewed potential for the application of GDGT-paleothermometry in lakes. *Geochim. Cosmochim. Acta* **75**, 6225–6238 (2011).
- Pei, H., Wang, C., Wang, Y., Yang, H. & Xie, S. Distribution of microbial lipids at an acid mine drainage site in China: Insights into microbial adaptation to extremely low pH conditions. *Org. Geochem.* **134**, 77–91 (2019).
- Peltier, W. R. Global glacial isostasy and the surface of the ice-age earth: the ICE-5G (VM2) model and GRACE. *Annu. Rev. Earth Planet. Sci.* **32**, 111–149 (2004).
- Penkman, K. E. H., Preece, R. C., Keen, D. H., Maddy, D., Schreve, D. C. & Collins, M. J. Testing the aminostratigraphy of fluvial archives: the evidence from intra-crystalline proteins within freshwater shells. *Quat. Sci. Rev.* **26**, 2958–2969 (2007).
- Penkman, K. E. H., Kaufman, D. S., Maddy, D. & Collins, M. J. Closed-system behaviour of the intra-crystalline fraction of amino acids in mollusc shells. *Quat. Geochronol.* **3**, 2–25 (2008).

References

- Penkman, K. Amino acid geochronology: Its impact on our understanding of the Quaternary stratigraphy of the British Isles. *J. Quat. Sci.* **25**, 501–514 (2010).
- Penkman, K. E. H., Preece, R. C., Bridgland, D. R., Keen, D. H., Meijer, T., Parfitt, S. A., White, T. S. & Collins, M. J. A chronological framework for the British Quaternary based on *Bithynia opercula*. *Lett. to Nat.* **476**, 446–449 (2011).
- Penkman, K. E. H., Preece, R. C., Bridgland, D. R., Keen, D. H., Meijer, T., Parfitt, S. A., White, T. S. & Collins, M. J. An aminostratigraphy for the British Quaternary based on *Bithynia opercula*. *Quat. Sci. Rev.* **61**, 111–134 (2013).
- Permentier, H., Schmidt, K., Kobayashi, M., Akiyama, M., Hager-Braun, C., Neerken, S., Miller, M., Amesz, J. Composition and optical properties of reaction centre core complexes from the green sulfur bacteria *Prosthecochloris aestuarii* and *Chlorobium tepidum*. *Photosynth. Res.* **64**, 27–39 (2000).
- Peterse, F., Kim, J.-H., Schouten, S., Kirstensend, D. K., Koç, N. & Damsté, J. S. S. Constraints on the application of the MBT/CBT palaeothermometer at high latitude environments (Svalbard, Norway). *Org. Geochem.* **40**, 692–699 (2009).
- Peterse, F., van der Meer, J., Schouten, S., Weijers, J. W. H., Fierer, N., Jackson, R. B., Kim, J.-H. & Damsté, J. S. S. Revised calibration of the MBT-CBT paleotemperature proxy based on branched tetraether membrane lipids in surface soils. *Geochim. Cosmochim. Acta* **96**, 215–229 (2012).
- Pfennig, N. Phototrophic green and purple bacteria: A comparative, systematic survey. *Ann. Rev. Microbiol.* **31**, 275–290 (1977).
- Philp, R. P. & Lewis, C. A. Organic geochemistry of biomarkers. *Annu. Rev. Earth Planet. Sci.* **15**, 363–395 (1987).
- Plancq, J., Cavazzin, B., Juggins, S., Haig, H. A., Leavitt, P. R. & Toney, J. L. Assessing environmental controls on the distribution of long-chain alkenones in the Canadian Prairies. *Org. Geochem.* **117**, 43–55 (2018).
- Poplawski, C. Development of a high-throughput technique for screening Archaeal tetraether lipid cores and other alcohols in sediments and microbial cultures. PhD thesis, University of York (2017).
- Powers, L., Werne, J. P., Vanderwoude, A. J., Sinninghe Damsté, J. S., Hopmans, E. C. & Schouten, S. Applicability and calibration of the TEX₈₆ paleothermometer in lakes. *Org. Geochem.* **41**, 404–413 (2010).

References

- Poynter, J. & Eglinton, G. Molecular composition of three sediments from hole 717c: The Bengal Fan. *Proc. Ocean Drill. Proj.* **116**, 155–161 (1990).
- Poynter, J. & Eglinton, G. The biomarker concept – Strengths and weaknesses. *Fresenius. J. Anal. Chem.* **339**, 725–731 (1991).
- Prahl, F. G. & Wakeham, S. G. Calibration of unsaturation patterns in long-chain ketone compositions for palaeotemperature assessment. *Nature* **330**, 367–369 (1987).
- Pratt, J. H. On the attraction of the Himalaya Mountains and of the elevated regions beyond them, upon the Plumb-line in India. *Philos. Trans. R. Soc. A* **145**, 53–100 (1855).
- Preece, R. C., Parfitt, S. A., Bridgland, D. R., Lewis, S. G., Rowe, P. J., Atkinson, T. C., Candy, I., Debenham, N. C., Penkman, K. E. H., Rhodes, E. J., Schwenninger, J-L., Griffiths, H. I., Whittaker, J. E. & Gleed-Owen, C. Terrestrial environments during MIS 11: Evidence from the Palaeolithic site at West Stow, Suffolk, UK. *Quat. Sci. Rev.* **26**, 1236–1300 (2007).
- Railsback, L. B., Gibbard, P. L., Head, M. J., Voarintsoa, N. R. G. & Toucanne, S. An optimized scheme of lettered marine isotope substages for the last 1.0 million years, and the climatostratigraphic nature of isotope stages and substages. *Quat. Sci. Rev.* **111**, 94–106 (2015).
- Rao, K. J., Vaidhyanathan, B., Ganguli, M. & Ramakrishnan, P. A. Synthesis of inorganic solids using microwaves. *Chem. Mater.* **11**, 882–895 (1999).
- Raymann, K., Brochier-Armanet, C. & Gribaldo, S. The two-domain tree of life is linked to a new root for the Archaea. *Proc. Natl. Acad. Sci. U.S.A.* **112**, 6670–6675 (2015).
- Richards, D. A., Smart, P. L. & Edwards, R. L. Maximum sea levels for the last glacial period from U-series ages of submerged speleothems. *Nature* **367**, 357–360 (1994).
- Richey, J. N. & Tierney, J. E. GDGT and alkenone flux in the northern Gulf of Mexico: Implications for the TEX₈₆ and U^{K'}₃₇ paleothermometers. *Paleoceanography* **31**, 1547–1561 (2016).
- Righetti, P. G. & Verzola, B. Folding/unfolding/refolding of proteins: Present methodologies in comparison with capillary zone electrophoresis. *Electrophoresis* **22**, 2359–2374 (2001).
- Rodriguez, D. *A guide to carotenoid analysis in foods* (ILSI Human Nutrition Institute, One Thomas Circle, 2001).
- Rodriguez-Amaya, D. & Kimura, M. *HarvestPlus Handbook for Carotenoid Analysis*. (Harvest. Tech. Monogr, 2004).

References

- Roe, H. M. The Late Middle Pleistocene biostratigraphy of the Thames Valley, England: New data from eastern Essex. *Quat. Sci. Rev.* **20**, 1603–1619 (2001).
- Roe, H. M. & van de Plassche, O. Modern pollen distribution in a Connecticut saltmarsh: Implications for studies of sea-level change. *Quat. Sci. Rev.* **24**, 2030–2049 (2005).
- Roe, H. M., Coope, G. R., Devoy, R. J. N., Harrison, C. J. O., Penkman, K. E. H., Preece, R. C. & Schreve, D. C. Differentiation of MIS 9 and MIS 11 in the continental record: vegetational, faunal, aminostratigraphic and sea-level evidence from coastal sites in Essex, UK. *Quat. Sci. Rev.* **28**, 2342–2373 (2009).
- Rollins, H. B., Carothers, M. & Donahue, J. Transgression, regression and fossil community succession. *Lethaia* **12**, 89–104 (1979).
- Ronkainen, T., McClymont, E. L., Väiliranta, M. & Tuittila, E.-S. The *n*-alkane and sterol composition of living fen plants as a potential tool for palaeoecological studies. *Org. Geochem.* **59**, 1–9 (2013).
- Rontani, J. F. & Volkman, J. K. Lipid characterization of coastal hypersaline cyanobacterial mats from the Camargue (France). *Org. Geochem.* **36**, 251–272 (2005).
- Rontani, J. F., Prahl, F. G. & Volkman, J. K. Characterization of unusual alkenones and alkyl alkenoates by electron ionization gas chromatography/mass spectrometry. *Rapid Commun. Mass Spectrom.* **20**, 583–588 (2006).
- Rovere, A., Stocchi, P. & Vacchi, M. Eustatic and Relative Sea Level Changes. *Curr. Clim. Chang. Reports* **2**, 221–231 (2016).
- Saesaengseerung, N. High-throughput methods for the analysis of pigments in aquatic sediments. PhD thesis, University of York (2013).
- Schanche, J.-S. Microwave synthesis solutions from personal chemistry. *Mol. Divers.* **7**, 293–300 (2003).
- Scheer, H. Structure and occurrence of chlorophylls. In *Chlorophylls*, ch. 1, pp. 3–30 (CRC press, 1991).
- Schellmann, G. & Radtke, U. A revised morpho- and chronostratigraphy of the Late and Middle Pleistocene coral reef terraces on Southern Barbados (West Indies). *Earth-Science Rev.* **64**, 157–187 (2004).

References

- Schemmel, F., Niedermeyer, E. M., Koutsodendris, A., Pross, J., Fiebig, J. & Mulch, A. Paleohydrological changes in the Eastern Mediterranean region during the early to mid-Holocene recorded in plant wax *n*-alkane distributions and $\delta^{13}\text{C}_{\text{TOC}}$ – New data from Tenaghi Philippon, NE Greece. *Org. Geochem.* **110**, 100–109 (2017).
- Schirmer, A., Rude, M. A., Li, X., Popova, E. & del Cardayre, S. B. Microbial biosynthesis of alkanes. *Science* **329**, 559–562 (2010).
- Schnell, G., Schaeffer, P., Tardivon, H., Motsch, E., Connan, J., Ertlen, D., Schwartz, D., Schneider, N. & Adam, P. Contrasting diagenetic pathways of higher plant triterpenoids in buried wood as a function of tree species. *Org. Geochem.* **66**, 107–124 (2014).
- Schouten, S., Hoefs, M. J. L., Koopmans, M. P., Bosch, H. J. & Sinninghe Damsté, J. S. Structural characterization, occurrence and fate of archaeal ether-bound acyclic and cyclic biphytanes and corresponding diols in sediments. *Org. Geochem.* **29**, 1305–1319 (1998).
- Schouten, S., Hopmans, E. C., Pancost, R. D. & Sinninghe Damsté, J. S. Widespread occurrence of structurally diverse tetraether membrane lipids: Evidence for the ubiquitous presence of low-temperature relatives of hyperthermophiles. *Proc. Natl. Acad. Sci. U.S.A.* **97**, 14421–14426 (2000).
- Schouten, S., Hopmans, E. C., Schefuß, E. & Sinninghe Damsté, J. S. Distributional variations in marine crenarchaeol membrane lipids: a new tool for reconstructing ancient sea water temperatures? *Earth Planet. Sci. Lett.* **204**, 265–274 (2002).
- Schouten, S., Huguet, C., Hopmans, E. C., Kienhuis, M. V. M. & Damsté, J. S. S. Analytical methodology for TEX₈₆ paleothermometry by high-performance liquid chromatography / atmospheric pressure chemical ionization-mass spectrometry. *Anal. Chem.* **79**, 2940–2944 (2007a).
- Schouten, S., van der Meer, M. T. J., Hopmans, E. C., Rijpstra, W. I. C., Reysenbach, A-L. Ward, D. M. & Damsté, J. S. S. Archaeal and bacterial glycerol dialkyl glycerol tetraether lipids in hot springs of Yellowstone National Park. *Appl. Environ. Microbiol.* **73**, 6181–6191 (2007b).
- Schouten, S., Hopmans, E. C., Baas, M., Boumann, H., Standfest, S., Könneke, M., Stahl, D. A. & Sinninghe Damsté, J. S. Intact membrane lipids of ‘*Candidatus Nitrosopumilus maritimus*,’ a cultivated representative of the cosmopolitan mesophilic group I Crenarchaeota. *Appl. Environ. Microbiol.* **74**, 2433–2440 (2008).
- Schouten, S., Hopmans, E. C. & Sinninghe Damsté, J. S. The organic geochemistry of glycerol dialkyl glycerol tetraether lipids: A review. *Org. Geochem.* **54**, 19–61 (2013).

References

- Schreve, D. C. Differentiation of the British late Middle Pleistocene interglacials: The evidence from mammalian biostratigraphy. *Quat. Sci. Rev.* **20**, 1693–1705 (2001).
- Sea temperature_Orkney: <https://www.seatemperature.org/europe/united-kingdom/orkney.htm> (accessed 06/05/2019).
- Sea temperature_Nuuk , Greenland: <https://seatemperature.info/nuuk-water-temperature.html> (accessed 29/01/2020).
- Seki, O., Meyers, P. A., Kawamura, K., Zheng, Y. & Zhou, W. Hydrogen isotopic ratios of plant wax *n*-alkanes in a peat bog deposited in northeast China during the last 16 kyr. *Org. Geochem.* **40**, 671–677 (2009).
- Selby, K. A. & Smith, D. E. Late Devensian and Holocene relative sea-level changes on the Isle of Skye, Scotland, UK. *J. Quat. Sci.* **22**, 119–139 (2007).
- Shackleton, N. J. & Opdyke, N. D. Oxygen isotope and palaeomagnetic stratigraphy of equatorial Pacific core V 28-238: Oxygen isotope temperatures and ice volumes on a 10⁵ year and 10⁶ year scale. *Quat. Res.* **3**, 39–55 (1973).
- Shangguan, D., Zhao, Y., Han, H., Zhao, R. & Liu, G. Derivatization and fluorescence detection of amino acids and peptides with 9-fluorenylmethyl chloroformate on the surface of a solid adsorbent. *Anal. Chem.* **73**, 2054–2057 (2001).
- Shennan, I. Holocene crustal movements and sea-level changes in Great Britain. *J. Quat. Sci.* **4**, 77–89 (1989).
- Shennan, I., Innes, J. B., Long, A. J. & Yongqiang Z. Late Devensian and Holocene relative sea-level changes at Rumach, near Arisaig, northwest Scotland. *Nor. Geol. Tidsskr.* **73**, 161–174 (1993).
- Shennan, I. & Horton, B. Holocene land- and sea-level changes in Great Britain. *J. Quat. Sci.* **17**, 511–526 (2002).
- Shennan, I., Bradley, S., Milne, G., Brooks, A. & Bassett. Relative sea-level changes, glacial isostatic modelling and ice-sheet reconstructions from the British Isles since the Last Glacial Maximum. *J. Quat. Sci.* **21**, 585–599 (2006).
- Shennan, I., Long, A.J. & Horton, B.P. *Handbook of Sea-Level Research*. (Wiley / AGU, 2015).
- Shennan, I., Bradley, S. L. & Edwards, R. Relative sea-level changes and crustal movements in Britain and Ireland since the Last Glacial Maximum. *Quat. Sci. Rev.* **188**, 143–159 (2018).

References

- Shuman, F. R. & Lorenzen, C. J. Quantitative degradation of chlorophyll by a marine herbivore. *Limnol. Oceanogr.* **20**, 580–586 (1975).
- Sidell, E. J. Holocene sea level change and archaeology in the inner Thames estuary, London, UK. PhD Thesis, University of Durham (2003).
- Singer, M. J. & Fine, P. Pedogenic factors affecting magnetic susceptibility of northern California soils. *Soil Sci. Soc. Am. J.* **53**, 1119–1127 (1989).
- Skoog, D. A., West, D. M. & Holler, F. J. *Fundamentals of Analytical Chemistry* (Forth Worth, Saunders College, 7th ed, 1996).
- Skoog, D. A.; Holler, F. J.; Nieman, T. A. *Principles of Instrumental Analysis* (Philadelphia Saunders College, 5th ed, 1998).
- Skoog, D. A., West, D. M., Holler, F. J., Crouch, S. R. *Fundamentals of Analytical Chemistry* (Brooks Cole, 8th ed, 2004).
- Slebioda, M., Wodecki, Z. & Kolodziejczyk, A. M. Formation of optically pure *N*-acyl-*N,N'*-dicyclohexylurea in *N,N'*-dicyclohexylcarbodiimide-mediated peptide synthesis. *Int. J. Pept. Protein Res.* **35**, 539–541 (1990).
- Small, D., Bentley, M. J., Jones, R. S., Pittard, M. L. & Whitehouse, P. L. Antarctic ice sheet palaeo-thinning rates from vertical transects of cosmogenic exposure ages. *Quat. Sci. Rev.* **206**, 65–80 (2019).
- Smart, L.; Moore, E. *Solid State Chemistry – An Introduction* (Stanley-Thornes, 2nd ed, 1995).
- Smith, D. E., Barlow, N. M. L., Bradley, S. L., Firth, C. R., Hall, A. M., Jordan, J. T. & Long, D. Quaternary sea level change in Scotland. *Earth Env. Sci. T. S. So.* **110**, 1–38 (2017).
- Sollai, M., Hopmans, E. C., Bale, N. J., Mets, A., Warden, L., Moros, M. & Damsté, J. S. S. The Holocene sedimentary record of cyanobacterial glycolipids in the Baltic Sea: An evaluation of their application as tracers of past nitrogen fixation. *Biogeosciences* **14**, 5789–5804 (2017).
- Squier, A. H., Hodgson, D. A. & Keely, B. J. Sedimentary pigments as markers for environmental change in an Antarctic lake. *Org. Geochem.* **33**, 1655–1665 (2002).
- SROCC, 2019: Pörtner, H.-O., Roberts, D.C., Masson-Delmotte, V., Zhai, P., Poloczanska, E., Mintenbeck, K., Tignor, M., Alegría, A., Nicolai, M., Okem, A., Petzold, J., Rama, B. & Weyer, N.M. *Special Report on the Ocean and Cryosphere in a Changing Climate – Technical Summary*. (2019).

References

- Stal, L. J. Coastal microbial mats: The physiology of a small-scale ecosystem. *South African J. Bot.* **67**, 399–410 (2001).
- Stevens, L. A. The Interglacial of the Nar Valley, Norfolk. *Quart. J. Geol. Soc.* **3**, 291–315 (1959).
- Stieglmeier, M., Alves, R. J. E. & Schleper, C. The phylum Thaumarchaeota. In *The Prokaryotes - Other Major Lineages of Bacteria and the Archaea*, ch. 26, 347–362 (Springer-Verlag Berlin, 2014).
- Straley, S. C., Parson, W. W., Mauzeral, D. C., Clayton, R. K. Pigment content and molar extinction coefficients of photochemical reaction centers from *Rhodospseudomonas spheroides*. *Biochim. Biophys. Acta* **305**, 597-609 (1973).
- Sturt, H. F., Summons, R. E., Smith, K., Elvert, M. & Hinrichs, K-U. Intact polar membrane lipids in prokaryotes and sediments deciphered by high-performance liquid chromatography / electrospray ionization multistage mass spectrometry — New biomarkers for biogeochemistry and microbial ecology. *Rapid Commun. Mass Spectrom.* **18**, 617–628 (2004).
- Sun, J. & Liu, T. Multiple origins and interpretations of the magnetic susceptibility signal in Chinese wind-blown sediments. *Earth Planet. Sci. Lett.* **180**, 287–296 (2000).
- Sun, Q., Chu, G., Li, S., Lü, C. & Zheng, M. Long-chain alkenones in sulfate lakes and its paleoclimatic implications. *Chinese Sci. Bull.* **49**, 2082–2086 (2004).
- Sun, D., Tan, W., Pei, Y., Zhoum L., Wang, H., Yang, H. & Xu, Y. Late Quaternary environmental change of Yellow River Basin: An organic geochemical record in Bohai Sea (North China). *Org. Geochem.* **42**, 575–585 (2011).
- Swift, D. J. P. Coastal erosion and transgressive stratigraphy. *J. Geol.* **76**, 444–456 (1968).
- Takaichi, S. Carotenoids in algae: Distributions, biosyntheses and functions. *Mar. Drugs* **9**, 1101–1118 (2011).
- Talbot, H. M., Head, R. N., Harris, R. P. & Maxwell, J. R. Distribution and stability of steryl chlorin esters in copepod faecal pellets from diatom grazing. *Org. Geochem.* **30**, 1163–1174 (1999).
- Talbot, H. M., Summons, R., Jahnke, L. & Farrimond, P. Characteristic fragmentation of bacteriohopanepolyols during atmospheric pressure chemical ionisation liquid chromatography/ion trap mass spectrometry. *Rapid Commun. Mass Spectrom.* **17**, 2788–2796 (2003).

References

- Talbot, M. R., Jensen, N. B., Lærdal, T. & Filippi, M. L. Geochemical responses to a major transgression in giant African lakes. *J. Paleolimnol.* **35**, 467–489 (2006).
- Teixell, A., Bertotti, G., de Lamotte, D. F. & Charroud, M. The geology of vertical movements of the lithosphere: An overview. *Tectonophysics* **475**, 1–8 (2009).
- Thiel, V., Jenisch, A., Landmann, G., Reimer, A. & Michaelis, W. Unusual distributions of long-chain alkenones and tetrahymanol from the highly alkaline Lake Van, Turkey. *Geochim. Cosmochim. Acta* **61**, 2053–2064 (1997).
- Thomas, G. N. Late Middle Pleistocene pollen biostratigraphy in Britain: Pitfalls and possibilities in the separation of interglacial sequences. *Quat. Sci. Rev.* **20**, 1621–1630 (2001).
- Tierney, J. E. & Russell, J. M. Distributions of branched GDGTs in a tropical lake system: Implications for lacustrine application of the MBT/CBT paleoproxy. *Org. Geochem.* **40**, 1032–1036 (2009).
- Tierney, J. E., Russell, J. M., Eggermont, H., Hopmans, E. C., Verschuren, D. & Sinninghe Damsté, J. S. Environmental controls on branched tetraether lipid distributions in tropical East African lake sediments. *Geochim. Cosmochim. Acta* **74**, 4902–4918 (2010).
- Tierney, J. E. & Tingley, M. P. A Bayesian, spatially-varying calibration model for the TEX₈₆ proxy. *Geochim. Cosmochim. Acta* **127**, 83–106 (2014).
- Tierney, J. E. & Tingley, M. P. A TEX₈₆ surface sediment database and extended Bayesian calibration. *Sci. Data* **2**, 150029 (2015).
- Tomiak, P. J., Penkman, K. E. H., Hendy, E. J., Demarchi, B., Murrells, S., Davis, S. A., McCullagh, P. & Collins, M. J. Testing the limitations of artificial protein degradation kinetics using known-age massive *Porites* coral skeletons. *Quat. Geochronol.* **16**, 87–109 (2013).
- Toney, J. L., Huang, Y., Fritz, S. C., Baker, P. A., Grimm, E. & Nyren, P. Climatic and environmental controls on the occurrence and distributions of long chain alkenones in lakes of the interior United States. *Geochim. Cosmochim. Acta* **74**, 1563–1578 (2010).
- Trendel, J. M., Lohmann, F., Kintzinger, J. P., Albrecht, P., Chiaroni, A., Riche, C., Casario, M., Guilhem, J. & Pascard, C. Identification of des-A-triterpenoid hydrocarbons occurring in surface sediments. *Tetrahedron* **45**, 4457–4470 (1989).
- Tsakos, M., Schaffert, E. S., Clement, L. L., Villadsen, N. L. & Poulsen, T. B. Ester coupling reactions – An enduring challenge in the chemical synthesis of bioactive natural products. *Nat. Prod. Rep.* **32**, 605–632 (2015).

References

- Turich, C. & Freeman, K. H. Archaeal lipids record paleosalinity in hypersaline systems. *Org. Geochem.* **42**, 1147–1157 (2011).
- Uda, I., Sugai, A., Itoh, Y.H., Itoh, T. Variation in molecular species of core lipids from the order *Thermoplasmatales* strains depends on the growth temperature. *J. Oleo Sci.* **53**, 399–404 (2004).
- Van Bergen, P. F., Bull, I. D., Poulton, P. R. & Evershed, R. P. Organic geochemical studies of soils from the Rothamsted classical experiments – I. Total lipid extracts, solvent insoluble residues and humic acids from Broadbalk Wilderness. *Org. Geochem.* **26**, 117–135 (1997).
- Van Campo, E., Duplessy, J. C. & Rossignol-Strick, M. Climatic conditions deduced from a 150-kyr oxygen isotope-pollen record from the Arabian Sea. *Nature* **296**, 56–59 (1982).
- van der Meer, M. T. J., Sangiorgi, F., Baas, M., Brinkhuis, H., Damsté, J. S. S. & Schouten, S. Molecular isotopic and dinoflagellate evidence for Late Holocene freshening of the Black Sea. *Earth Planet. Sci. Lett.* **267**, 426–434 (2008).
- van Soelen, E. E., Lammertsma, E. I., Cremer, H., Donders, T. H., Sangiorgi, F., Brooks, G. R., Larson, R. A., Damsté, J. S. S., Wagner-Cremer, F. & Reichart, G. J. Late Holocene sea-level rise in Tampa Bay: Integrated reconstruction using biomarkers, pollen, organic-walled dinoflagellate cysts, and diatoms. *Estuar. Coast. Shelf Sci.* **86**, 216–224 (2010).
- Vekariya, R. L. A review of ionic liquids: Applications towards catalytic organic transformations. *J. Mol. Liq.* **227**, 44–60 (2017).
- Ventris, P. A. Hoxnian Interglacial freshwater and marine deposits in Northwest Norfolk, England and their implications for sea-level reconstruction. *Quat. Sci. Rev.* **15**, 437–450 (1996).
- Versteegh, G. J. M., Bosch, H. & De Leeuw, J. W. Potential palaeoenvironmental information of C₂₄ to C₃₆ mid-chain diols, keto-ols and mid-chain hydroxy fatty acids; a critical review. *Org. Geochem.* **27**, 1–13 (1997).
- Versteegh, G. J. M., Jansen, J. H. F., De Leeuw, J. W. & Schneider, R. R. Mid-chain diols and keto-ols in SE Atlantic sediments: A new tool for tracing past sea surface water masses? *Geochim. Cosmochim. Acta* **64**, 1879–1892 (2000).
- Volkman, J. K., Eglinton, G., Corner, E. D. S. & Forsberg, T. E. V. Long-chain alkenes and alkenones in the marine coccolithophorid *Emiliania huxleyi*. *Phytochemistry* **19**, 2619–2622 (1980).
- Volkman, J. K. A review of sterol markers for marine and terrigenous organic matter. *Org. Geochem.* **9**, 83–99 (1986).

References

- Volkman, J. K., Barrett, S. M., Blackburn, S. I., Mansour, M. P., Sikes, E. L. & Gelin, F. Microalgal biomarkers: A review of recent research developments. *Org. Geochem.* **29**, 1163–1179 (1998).
- Volkman, J. K., Barrett, S. M. & Blackburn, S. I. Eustigmatophyte microalgae are potential sources of C₂₉ sterols, C₂₂–C₂₈ *n*-alcohols and C₂₈–C₃₂ *n*-alkyl diols in freshwater environments. *Org. Geochem.* **30**, 307–318 (1999).
- Volkman, J. K., Rohjans, D., Rullkotter, J., Scholz-Bottcher, B. M. & Liebezeit, G. Sources and diagenesis of organic matter in tidal flat sediments from the German Wadden Sea. *Cont. Shelf Res.* **20**, 1139–1158 (2000).
- Volkman, J. K. Sterols in microorganisms. *Appl. Microbiol. Biotechnol.* **60**, 495–506 (2003).
- Volkman, J. K. Sterols and other triterpenoids: Source specificity and evolution of biosynthetic pathways. *Org. Geochem.* **36**, 139–159 (2005).
- Vollmer, M. Physics of the microwave oven. *Phys. Educ.* **39**, 74–81 (2004).
- Wakeham, S. G. Reduction of stenols to stanols in particulate matter at oxic-anoxic boundaries in sea water. *Nature* **342**, 787–790 (1989).
- Wakeham, S. G., Pease, T. K. & Benner, R. Hydroxy fatty acids in marine dissolved organic matter as indicators of bacterial membrane material. *Org. Geochem.* **34**, 857–868 (2003).
- Walker, J. S., Squier, A. H., Hodgson, D. A. & Keely, B. J. Origin and significance of 13²-hydroxychlorophyll derivatives in sediments. *Org. Geochem.* **33**, 1667–1674 (2002).
- Wang, Z. & Liu, W. Carbon chain length distribution in *n*-alkyl lipids: A process for evaluating source inputs to Lake Qinghai. *Org. Geochem.* **50**, 36–43 (2012).
- Wang, M., Zhang, W. & Hou, J. Is average chain length of plant lipids a potential proxy for vegetation, environment and climate changes? *Biogeosciences Discuss.* **12**, 5477–5501 (2015).
- Wang, C., Bendle, J., Yang, Y., Yang, H., Sun, H., Huang, J. & Xie, S. Impacts of pH and temperature on soil bacterial 3-hydroxy fatty acids: Development of novel terrestrial proxies. *Org. Geochem.* **94**, 21–31 (2016).
- Wang, C., Bendle, J. A., Zhang, H., Yang, Y., Liu, D., Huang, J., Cui, J. & Xie, S. Holocene temperature and hydrological changes reconstructed by bacterial 3-hydroxy fatty acids in a stalagmite from central China. *Quat. Sci. Rev.* **192**, 97–105 (2018a).

References

- Wang, J., Axia, E., Xu, Y., Wang, G., Zhou, L., Jia, Y., Chen, Z. & Li, J. Temperature effect on abundance and distribution of leaf wax *n*-alkanes across a temperature gradient along the 400 mm isohyet in China. *Org. Geochem.* **120**, 31–41 (2018b).
- Wang, C., Bendle, J. A., Greene, S. E., Griffiths, M. L., Huang, J., Moossen, H., Zhang, H., Ashley, K. & Xie, S. Speleothem biomarker evidence for a negative terrestrial feedback on climate during Holocene warm periods. *Earth Planet. Sci. Lett.* **525**, 115754 (2019).
- Wanner, H., Beer, J., Bütikofer, J., Crowley, T. J., Cubasch, U., Flückinger, J., Goosse, H., Grosjean, M., Joos, F., Kaplan, J. O., Küttel, M., Müller, S. A., Prentice, I. C., Solomina, O., Stocker, T. F., Tarasov, P., Wagner, M. & Widmann, M. Mid- to Late Holocene climate change: An overview. *Quat. Sci. Rev.* **27**, 1791–1828 (2008).
- Watanabe, T., Hongu, A., Honda, K., Nakazato, M., Konno, M., Saitoh, S. Preparation of chlorophylls and pheophytins by isocratic liquid-chromatography. *Anal. Chem.* **56**, 251–256 (1984).
- Weber, J., Bauersachs, T. & Schwark, L. A multiphasic Younger Dryas cold period recorded in sediments of Lake Steisslingen, SW-Germany: A biomarker perspective. *Quat. Int.* **542**, 121–136 (2020).
- Weijers, J. W. H., Schouten, S., Spaargaren, O. C. & Sinninghe Damsté, J. S. Occurrence and distribution of tetraether membrane lipids in soils: Implications for the use of the TEX₈₆ proxy and the BIT index. *Org. Geochem.* **37**, 1680–1693 (2006a).
- Weijers, J. W. H., Schouten S., Hopmans, E. C., Geenevasen, J. A. J., David, O. R. P., Coleman, J. M., Pancost, R. D. & Damsté, J. S. S. Membrane lipids of mesophilic anaerobic bacteria thriving in peats have typical archaeal traits. *Environ. Microbiol.* **8**, 648–657 (2006b).
- Weijers, J. W. H., Schouten, S., van den Donker, J. C., Hopmans, E. C. & Sinninghe Damsté, J. S. Environmental controls on bacterial tetraether membrane lipid distribution in soils. *Geochim. Cosmochim. Acta* **71**, 703–713 (2007).
- West, R. G. The Quaternary deposits at Hoxne, Suffolk. *Philos. Trans. R. Soc. B, Biol. Sci.* **239**, 265–345 (1956).
- Wilson, M. A., Airs, R. L., Atkinson, J. E. & Keely, B. J. Bacterioviridins: Novel sedimentary chlorins providing evidence for oxidative processes affecting palaeobacterial communities. *Org. Geochem.* **35**, 199–202 (2004).

References

- Wilson, K., Berryman, K., Cochran, U. & Little, T. Early Holocene paleoseismic history at the Pakarae locality, eastern North Island, New Zealand, inferred from transgressive marine sequence architecture. *Tectonics* **26**, 1–18 (2007).
- Woese, C. R., Kandler, O. & Wheelis, M. L. Towards a natural system of organisms: proposal for the domains Archaea, Bacteria, and Eucarya. *Proc. Natl. Acad. Sci.* **87**, 4576–4579 (1990).
- Wollenweber, H. W. & Rietschel, E. T. Analysis of lipopolysaccharide (lipid A) fatty acids. *J. Microbiol. Methods* **11**, 195–211 (1990).
- Woodroffe, C. D. The impact of sea-level rise shorelines. *Prog. Phys. Geogr.* **14**, 483–520 (1990).
- Woodroffe, C. D. & Murray-Wallace, C. V. Sea-level rise and coastal change: The past as a guide to the future. *Quat. Sci. Rev.* **54**, 4–11 (2012).
- WoRMS *Ecrobia ventrosa* <http://www.marinespecies.org/aphia.php?p=taxdetails&id=238104> (accessed 26/01/20).
- WoRMS *Tritia* <http://www.marinespecies.org/aphia.php?p=taxdetails&id=246140> (accessed 26/01/20).
- Wu, W., Ruan, J., Ding, S., Zhao, L., Xu, Y., Yang, H., Ding, W. & Pei, Y. Source and distribution of glycerol dialkyl glycerol tetraethers along lower Yellow River-estuary-coast transect. *Mar. Chem.* **158**, 17–26 (2014).
- Xie, S., Nott, C. J., Avsejs, L. A., Maddy, D., Chambers, F. M. & Evershed, R. P. Molecular and isotopic stratigraphy in an ombrotrophic mire for paleoclimate reconstruction. *Geochim. Cosmochim. Acta* **68**, 2849–2862 (2004).
- Yang, Y., Wang, C., Bendle, J. A., Yu, X., Gao, C., Lü, X., Ruan, X., Wang, R. & Xie, S. A new sea surface temperature proxy based on bacterial 3-hydroxy fatty acids. *Org. Geochem.* **141**, 103975 (2020).
- You, J., Song, C., Yan, T., Sun, Z., Li, Y. & Suo, Y. An improved reagent for determination of aliphatic amines with fluorescence and online atmospheric chemical ionization-mass spectrometry identification. *Anal. Chim. Acta* **658**, 98–105 (2010).
- Young, A. J. The photoprotective role of carotenoids in higher plants. *Physiol. Plant.* **83**, 702–708 (1991).

References

- Zachos, J. C., Berggren, W. A., Aubry, M. P. & Mackensen, A. Isotope and trace element geochemistry of Eocene and Oligocene foraminifers from Site 748, Kerguelen Plateau. *Proc., Sci. results, ODP* **120**, 839–854 (1992).
- Zachos, J., Pagani, H., Sloan, L., Thomas, E. & Billups, K. Trends, rhythms, and aberrations in global climate 65 Ma to present. *Science* **292**, 686–693 (2001).
- Zech, M., Krause, T., Meszner, S. & Faust, D. Incorrect when uncorrected: Reconstructing vegetation history using *n*-alkane biomarkers in loess-paleosol sequences – A case study from the Saxonian loess region, Germany. *Quat. Int.* **296**, 108–116 (2013).
- Zhang, J., Yu, H., Jia, G. & Chen, F. Terrestrial *n*-alkane signatures in the middle Okinawa Trough during the post-glacial transgression: Control by sea level and paleovegetation confounded by offshore transport. *Geo-Marine Lett.* **30**, 143–150 (2010).
- Zhu, C., Yoshinaga, M. Y., Peters, C. A., Liu, X-L., Elvert, M. & Hinrichs, K-U. Identification and significance of unsaturated archaeal tetraether lipids in marine sediments. *Rapid Commun. Mass Spectrom.* **28**, 1144–1152 (2014).
- Zink, K. G., Leythaeuser, D., Melkonian, M. & Schwark, L. Temperature dependency of long-chain alkenone distributions in recent to fossil limnic sediments and in lake waters. *Geochim. Cosmochim. Acta* **65**, 253–265 (2001).
- Zocatelli, R., Jacob, J., Gobo, S., Le Milbeau, C., Rousseau, J. & Laggoun-Défarge, F. Spatial variability of soil lipids reflects vegetation cover in a French peatland. *Org. Geochem.* **76**, 173–183 (2014).